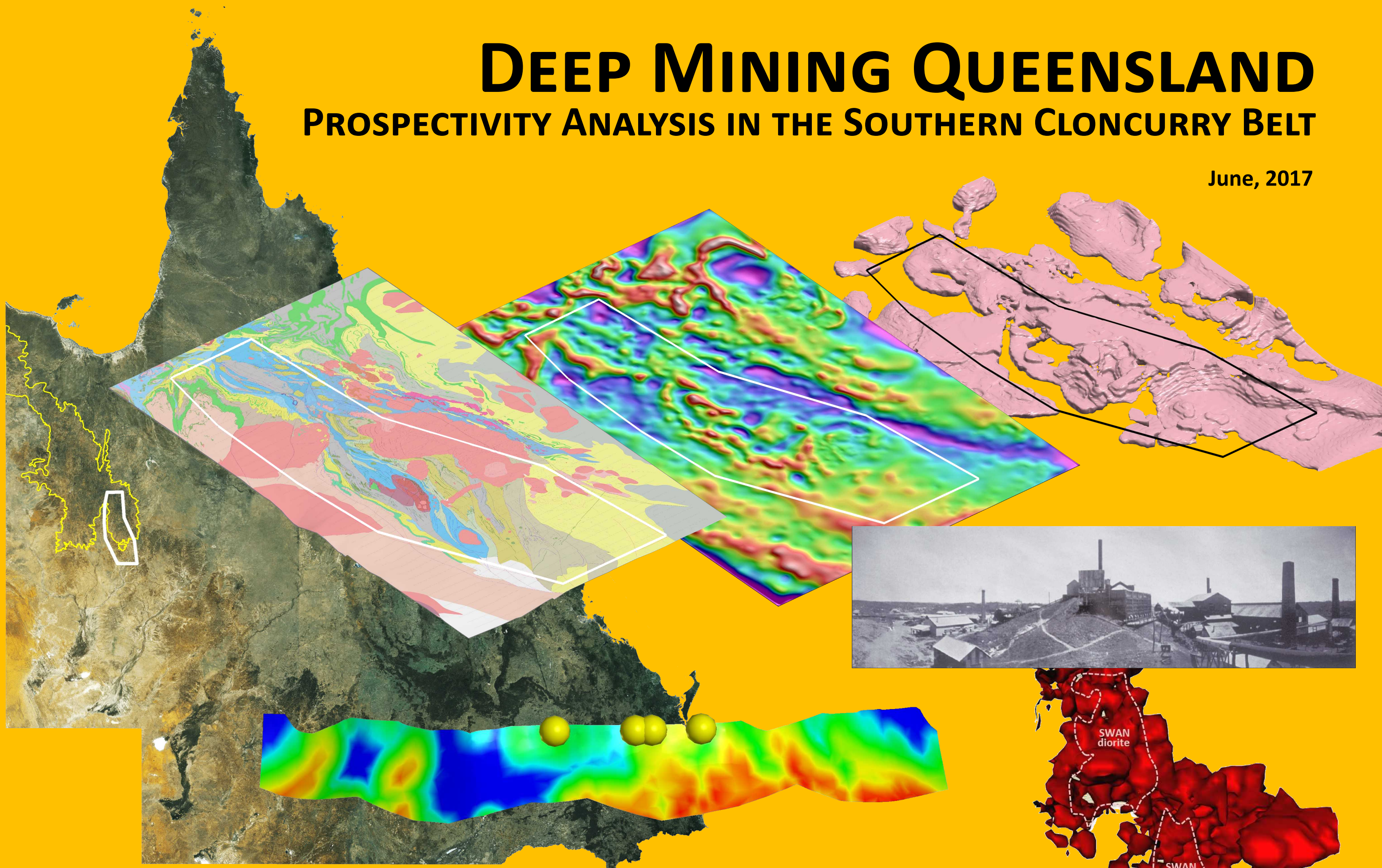


# DEEP MINING QUEENSLAND

## PROSPECTIVITY ANALYSIS IN THE SOUTHERN CLONCURRY BELT

June, 2017



## Deep Mining Queensland: Prospectivity Analysis in the Southern Cloncurry Belt, Queensland, Australia.



# SMIBRC

WH Bryan Mining &  
Geology Research Centre

### Authors:

Travis Murphy  
Mark Hinman  
John Donohue  
Mark Pirlo  
Rick Valenta  
Mark Jones  
Adrian Pratt

### With thanks for contributions:

Paul Donchak  
Mark McGeough  
Margaretha Scott  
Ian Withnall  
Laurie Hutton  
Damian Jungmann  
Jennifer Gunter  
Geoff Phillips  
Tony Baylis  
Peter Fullagar  
Glenn Pears  
Tony Webster  
Theresa Ruatoka  
Dave Crimeen

### With thanks for Software support:



Title Page: Qld Landsat mosaic with Isa Inlier and DMQ Project Area, DMQ Solid Geology; Apparent Density; DMQ Granite Model; historic Mount Elliott Mine & smelter ; SWAN 0.75eqwt%Cu shells with SWAN diorite (diagrammatic only, not in absolute spatial context); Starra Line Propsectivity

Reference: **Murphy, T., Hinman, M., Donohue, J., Pirlo, M., Valenta, R., Jones, M. & Pratt, A., 2017. Deep Mining Queensland: Prospectivity Analysis in the Southern Cloncurry Belt, Queensland, Australia. DNRM-GSQ Commissioned Industry Study.**

## Executive Summary

The Deep Mining Queensland (DMQ) Project comprised a two-year multi-disciplinary research effort aimed at reducing the risk of deep exploration for Cu-Au deposits in the Cloncurry metallogenic province.

The DMQ project was staged as follows:

- Review of characteristics of Iron-Oxide Copper Gold (IOCG) provinces and deposits, globally
- Evaluation and updating of the 2D and 3D geology of the Cloncurry Project area
- Analysis of the geological controls on deposit location and formation in the context of the new geological model
- Development of a 3D prospectivity analysis utilising the interpreted controls on deposit-formation
- Development of an evaluation tool for explorers to assess the potential relative value (future viability) of prospects and targets.

IOCG deposits are characteristically enigmatic, however, at a global-scale, common characteristics are recognized at the camp-scale and deposit-scale; despite different host-rocks and structural history. Synchronicity with voluminous felsic magmatism, regional-scale alteration systems, and localization in sites of late, brittle reactivation of earlier deformation features; are some of the key observations which then focussed analysis of the Cloncurry district.

New insights into the litho-structural development of the Cloncurry mineral-field have been made which place existing deposits into broader geological context, finds commonality between the diverse deposit forms and host-rocks, and have been used to guide 3D prospectivity workflows.

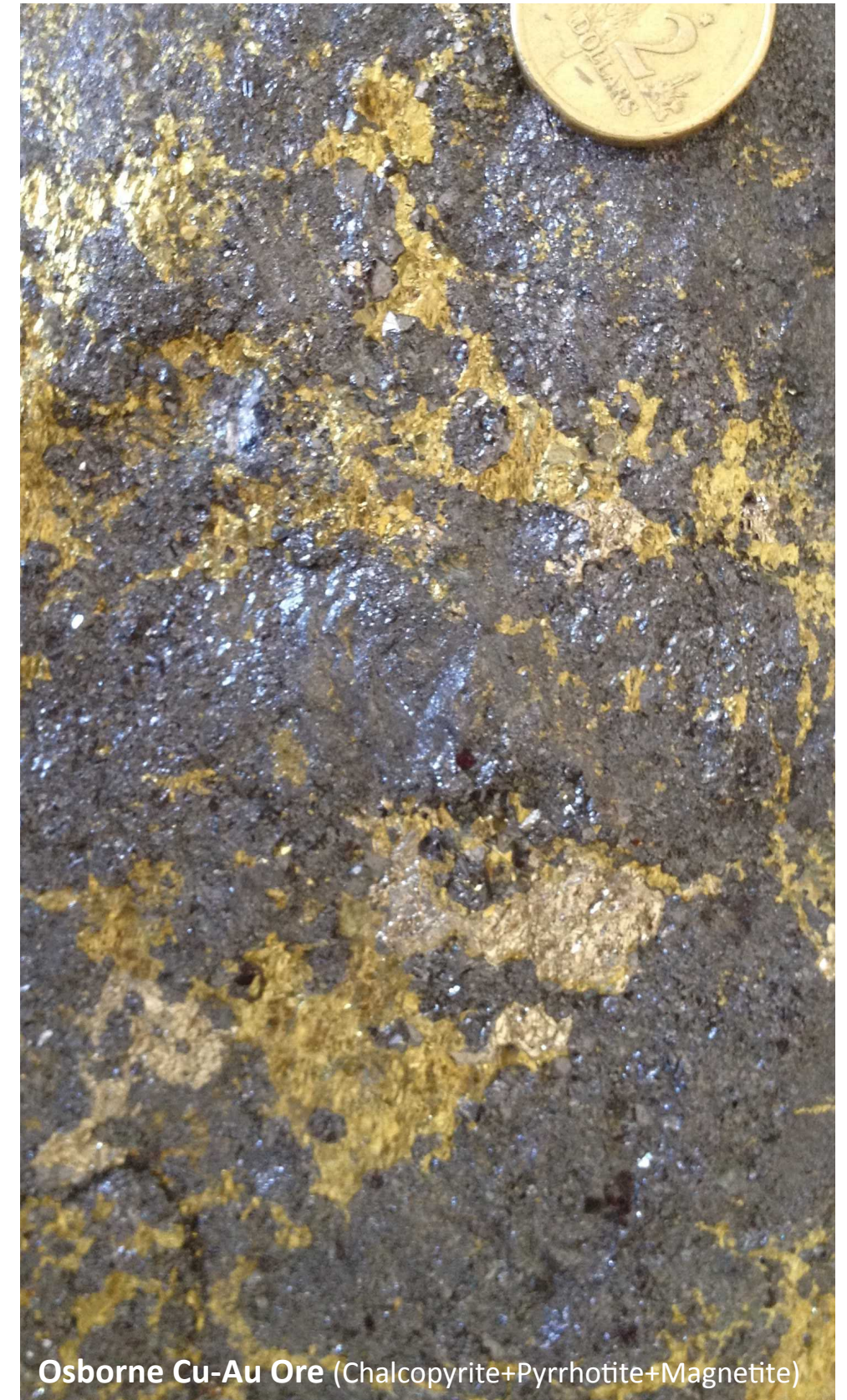
Within the DMQ project area, there is a spectrum of deposit styles and forms; which has previously proved difficult to collate into a cohesive, district-scale understanding of the Cu-Au district. Analysis of existing mines and deposits has revealed the key controls on deposit location, geometry, and tenor; and the unifying essential 'ingredients' have been determined and integrated into the broader litho-structural context.

Innovative modelling of the subsurface granitic intrusions, interpreted to have a specific role in localising deposit formation, has enabled construction of a 3D model of intrusives which differs significantly from previous work. This model provides a common link between camp-scale Cu-Au occurrences and is utilized as a key input into the 3D prospectivity assessment of the mineral field along with the spatial coincidence of structural permeability and reactive host-rocks.

The 3D prospectivity exercise yields domains and tracts of enhanced potential to host Cu-Au mineralization. Parameters for three deposit-types are used, and these broadly correlate with specific mining-related constraints, based on orebody characteristics including geometry, orientation, depth below surface, metal endowment, and both unit and total contained value.

Further to provision of 3D target domains, an interactive spreadsheet tool for rapid relative value assessment has been developed. This is intended to be used by geologists, to apply engineering and minerals-processing criteria to a drilled prospect or conceptual target, as a pre-scoping study level of assessment. The results of the assessments provide understanding of drivers of value, and potential viability; with the aim of enabling ranking of targets within an exploration portfolio and as a stage-gating tool to determine if further investment is warranted on a given prospect.

In summary, the DMQ Project has provided a holistic approach to prospectivity for deeper deposits within the Cloncurry district through enhanced understanding of IOCG systems, improvement to the geological knowledge, provision of tangible geoscience products, and complemented with an assessment tool. The knowledge contained herein, and digital packages which accompany this report; are considered to have a material impact on future exploration of the Cloncurry district, particularly in the deeper search space.



Osborne Cu-Au Ore (Chalcopyrite+Pyrrhotite+Magnetite)

## Table of Contents

<b>Executive Summary</b>	<b>i</b>	<b>Chapter 4: DMQ Southern Cloncurry District 3D Analysis</b>	<b>42</b>
<b>Table of Contents</b>	<b>ii</b>	Introduction	<b>42</b>
<b>List of Figures</b>	<b>iii</b>	Seismic Re-Interpretation	<b>42</b>
<b>List of Tables</b>	<b>iv</b>	Serial Section Interpretation	<b>45</b>
<b>Foreword</b>	<b>v</b>	Southern Cloncurry Granite Morphology: <i>Vp</i> mg Gravity Inversion Modelling	<b>46</b>
		Finalised Section Interpretations	<b>57</b>
<b>Chapter 1: Introduction to the Deep Mining Queensland (DMQ) Project</b>	<b>1</b>	<b>Chapter 5: Prospectivity for Cloncurry-style Cu-Au deposits in the DMQ project area</b>	<b>59</b>
Why the Cloncurry District?	<b>1</b>	Geological criteria determining prospectivity	<b>59</b>
The Case for a Depth Component to Prospectivity	<b>1</b>	Prospectivity Analysis Workflows	<b>60</b>
What Constitutes an Orebody Discovery at Depth?	<b>2</b>	Synthesis of 3D Prospectivity in the Southern Cloncurry Cu-Au district.	<b>64</b>
Application of BRC Expertise to the Issue of Prospectivity at Depth	<b>3</b>		
Parallel Research Work and the Context of the DMQ Project	<b>4</b>	<b>Chapter 6: Quantitative Target and Prospect Evaluation</b>	<b>66</b>
Data Sources	<b>4</b>	Introduction	<b>66</b>
		Early-stage Economic Analysis of Cu-Au Targets and Prospects	<b>66</b>
<b>Chapter 2: Review of Global IOCG Deposits, Characteristics &amp; Processes</b>	<b>5</b>	Orebody Simulations as Input to PEET-UG	<b>68</b>
Characteristics of IOCG style deposits	<b>5</b>	Implications for the DMQ Project Area and Generated Target Domains	<b>71</b>
Fluid Systematics & Diagnostic Geochemistry	<b>8</b>		
IOCG Process Models & Essential Ingredients	<b>9</b>	<b>References &amp; Bibliography</b>	<b>74</b>
<b>Chapter 3: DMQ Southern Cloncurry District Analysis</b>	<b>11</b>	<b>Appendices</b>	<b>79</b>
Introduction	<b>11</b>	1. Eastern Fold Belt Time-Space Chart	
Time-Space Relationships	<b>12</b>	2. Solid Geology Interpretation	
Eastern Fold Belt TIMESLICING	<b>13</b>	3. Detailed District to Local Geology Compilations	
Isan Orogeny Deformation Events	<b>13</b>	4. Eastern Fold Belt Assembly	<b>80</b>
Solid Geology Interpretation	<b>14</b>	5. Serial Sections	
Southern Cloncurry Solid Geology	<b>14</b>	6. Seismic Interpretations	
Tectono-Stratigraphic-Magmatic Assembly of the Eastern Fold Belt	<b>15</b>	7. 3D Models & Prospectivity Analysis	
Pre-Orogenic Architecture & Architectural Inheritance	<b>28</b>	8. DMQ Technical Reports	
Starra-Merlin-Mount Dore	<b>29</b>	9. Geophysical Library	<b>110</b>
Mount Elliott-SWAN	<b>34</b>	10. Global IOCG Database	
Osborne-Kulthor	<b>36</b>	11. Starra ML2733 and ML2745 Data Pack	
Ernest Henry	<b>39</b>	12. PEET-UG	
Essential Ingredients for IOCG/ISCG-style mineralisation	<b>40</b>	13. <i>Vp</i> mg Formatter	

## List of Figures

1.1	DMQ project area, mineral occurrences, mines and the outcropping Mt Isa Inlier.	1	3.22	Detailed Chinova VRMI-2VD over TMI-RTP aeromag of Starra-Merlin-Mount Dore area.	30
1.2	Depth of cover/overburden for discoveries in Australia (1900-2013).	2	3.23	Starra Line long section.	31
1.3	Method of discovery vs depth for Australian gold discoveries (1900-2013).	2	3.24	Starra geodynamic model for Au-Cu mineralisation.	31
1.4	Contained value (USD) of selected mineral deposits and grouped by deposit type.	3	3.25	Detailed geology at Merlin-Mount Dore.	31
1.5	Mining cost estimates (US\$/tonne) and mining rate from various mines.	3	3.26	Detailed drill section at Mount Dore highlighting early D4 Faulting controlling brecciation hosting Cu mineralisation.	32
2.1	Distribution of global IOCG provinces.	5	3.27	Detailed drill section at Merlin highlighting brecciation hosting Mo mineralisation.	33
2.2	Grade-tonnage data for IOCG deposits compared to porphyry Cu deposits.	6	3.28	Merlin Mo-matrix breccias with clasts of albite-altered calc-silicate siltstone fragments.	34
2.3	Plan view aspect ratios for IOCG deposits compared with porphyry Cu deposits.	6	3.29	Mount Elliott-SWAN region DMQ detailed geological interpretation.	34
2.4	Location of major IOCG mineralisation, Na-Ca alteration and Williams Suite granitoids in the Cloncurry Belt.	8	3.30	Detailed Chinova VRMI-2VD over TMI-RTP aeromag over Mount Elliott-SWAN region.	35
2.5	Schematic end-member models of IOCG formation.	9	3.31	Zoomed DMQ interpretation of Mount Elliott-SWAN region.	35
3.1	DMQ project area, extent of Proterozoic outcrop, mineral occurrences, mines and basic infrastructure.	11	3.32	SWAN Level Plan at 2150mRL.	36
3.2	DMQ-EFB updated NWQMP time-space chart.	12	3.33	SWAN mineralisation shell.	36
3.3	Coverages of mapping sources and airborne geophysics used in the DMQ solid geology interpretation.	14	3.34	DMQ geological interpretation of the Osborne-Kulthor region.	36
3.4	Comparison of VRMI-2VD with regional TMI-RTP magnetic data in the central Selwyn region.	14	3.35	Detailed Chinova VRMI-2VD over TMI-RTP aeromag in the Osborne-Kulthor region.	37
3.5	Detailed portion of the DMQ time-space chart.	15	3.36	Kulthor-Osborne geology zoom.	38
3.6	DMQ solid geology interpretation of the southern Cloncurry Belt.	15	3.37	DMQ structural interpretation of Osborne and Kulthor.	38
3.7	~1650Ma end of accumulation.	16	3.38	Kulthor Section 8 geological model.	38
3.8	~1600-1570Ma thin-skinned, Isan D1 folding & faulting.	17	3.39	Merlin molybdenite photomicrograph.	39
3.9	~1555-1535Ma thick-skinned, Isan D2 folding.	18	3.40	Ernest Henry Geology at 1947mRL.	39
3.10	~1555-1535Ma thick-skinned, Isan D2 faulting; ~1555-1535Ma Maramungee magmatism.	19	3.41	Well published N-S section through Ernest Henry.	39
3.11	~1535-1530Ma Isan D2b orogenic collapse; ~1535-1525Ma Saxby magmatism.	20	3.42	1800mRL level plan of EH.	40
3.12	~1525-1520Ma Isan D3 faulting.	21	3.43	1600mRL level plan of EH.	40
3.13	~1515-1500Ma early Isan D4 shortening; ~1515-1500Ma WILLIAMS magmatism ; (Cu-Au, Au-Cu, Mo-Cu).	22	3.44	Oblique section A-A' through EH mineralisation.	40
3.14	~1515-1500Ma early Isan D4 faulting; ~1515-1500Ma WILLIAMS magmatism ; Cu-Au, Au-Cu, Mo-Cu.	23	3.45	Oblique section B-B' through EH mineralisation.	40
3.15	~1515-1500Ma early Isan D4 faulting; ~1515-1500Ma WILLIAMS magmatism ; Cu-Au, Au-Cu, Mo-Cu; QUAMBY.	24	3.46	Modified Surficial ( $\pm$ Formational) IOCG Fluid Model	41
3.16	~1500-1495Ma late Isan D4 faulting; (syn)-late WILLIAMS magmatism.	25	4.1	DMQ solid geology control points for seismic and sectional interpretations.	42
3.17	~1495-1490Ma later Isan D4 faulting; post WILLIAMS.	26	4.2	Seismic line 94MTI-01 interpretation.	43
3.18	~????-????Ma post Isan X-cutting faulting; post WILLIAMS.	27	4.3	Seismic line 06GA-M6 interpretation.	44
3.19	post-Isan, post WILLIAMS X-cutting faulting & potential pre-orogenic Architectures.	28	4.4	Seismic line HiSeis-IVA-1 interpretation.	45
3.20	Areas of detailed geological-geophysical interpretation and tectono-stratigraphic analysis on DMQ solid geology interpretation.	29	4.5	Oblique view of stacked fault and stratigraphic strings from the 47 DMQ section interpretations.	45
3.21	Detailed DMQ tectono-stratigraphic geological-geophysical interpretation of the Starra-Merlin-Mount Dore region.	29	4.6	Six selected section interpretations—Upper Crustal Architecture	46
			4.7	Vpmg apparent density model of GA gravity.	46
			4.8	DMQ solid geology with granite at surface and beneath cover highlighted.	47

## List of Figures

4.9	Fullagar Geophysics Vp <sub>mg</sub> inversion styles.	48
4.10	Cross section example of simple DMQ 3-component, 3 & 2-layer Vp <sub>mg</sub> input model.	48
4.11	Vp <sub>mg</sub> apparent density model and drillcore densities.	48
4.12	Vp <sub>mg</sub> modelling, outcropping 'granite', depth of 'cover' contours, and eastern extent of Cambrian limestone.	49
4.13	Series A geometry inversion starting & output models.	49
4.14	Series B geometry inversion starting & output models.	49
4.15	Series C geometry inversion starting & output models.	49
4.16	Vp <sub>mg</sub> apparent density model and early, un-refined version of DMQ's interpreted extent of significant granite at depth	50
4.17	Vp <sub>mg</sub> inversion modelling and early, un-refined extent of significant granite at depth compared with outcropping granite.	50
4.18	DMQ base-of-granite RL domains.	50
4.19	Percentage misfit of base-of-granite RL domain Vp <sub>mg</sub> inversion model output.	51
4.20	Section 7,609,000N Vp <sub>mg</sub> model starting base-of-granite RL domains; output geometries, and input and output gravity profile.	51
4.21	Modified extent-of-granite to accommodate low density Mitakoodi quartzite and Bulonga felsic volcanics.	52
4.22	Initial mid-granite start depths, 4km buffer zone with assigned start depths, and superimposed cumulative modifications ('tweaks') to the initial start domain.	53
4.23	Version 1 Vp <sub>mg</sub> prism start depths buffered around the extent-of-granite and Vp <sub>mg</sub> output depth-to-granite gridded with colour stretches.	54
4.24	Final version 18 Vp <sub>mg</sub> prism start depths buffered around the extent-of-granite and Vp <sub>mg</sub> output depth-to-granite gridded with colour stretches.	55
4.25	3D view looking NNE of final version 18 granite morphology.	56
4.26	Section 7,609,000N final V18 Vp <sub>mg</sub> mid-granite domained starting model, output granite geometry, and input & output gravity profiles.	57
4.27	A selection of sections from the DMQ section interpretations.	57
4.28	Five section interpretations that coincide with seismic lines and DMQ seismic interpretation.	58
4.29	DMQ solid geology and locations of projected seismic line coincidence with DMQ sectional interpretations.	58
5.1	Excerpt of the time-space chart showing deposit localities relative to stratigraphy.	59
5.2	Schematic cross-section illustrating inferred controls on deposit styles in the DMQ project area.	59
5.3	Schematic cross-section of the asymmetric buffer around the upper Staveley stratigraphic contact.	59
5.4	Schematic cross-section highlighting granite morphology focussing fluid into favourable litho-structural sites.	60
5.5	3D view of the Williams-age felsic intrusions.	61
5.6	Edges of intrusive bodies with higher dip.	61
5.7	Anisotropic buffer applied to the 3D felsic intrusive geometry.	61
5.8	Top of Staveley Formation stratigraphic surface and outcropping Staveley Formation and equivalents.	62

5.9	Asymmetric buffering of the top of Staveley Formation stratigraphic surface.	62
5.10	Modelled faults displayed as coloured surfaces.	62
5.11	Buffered faults where interpreted to predate the latter stages of D4.	62
5.12	Resultant volumes after intersection of structural and stratigraphic buffer domains.	63
5.13	As per Figure 5.12, but coloured by proximity to intrusive buffer zones.	63
5.14	Location of significant deposits and mines relative to the inferred areas of enhanced prospectivity.	63
5.15	Staveley structural juxtaposition targets.	64
5.16	Higher stratigraphy targets—structurally focussed.	64
5.17	Combined view of Starra-type and Mt Dore/SWAN-type prospectivity	64
5.18	Geological map and targets identified in the DMQ project.	65
6.1	Mineral occurrence map, DMQ project area, depth of cover contours, and key mines developed under-cover.	66
6.2	The progress of studies for mineral projects.	67
6.3	Diagrammatic representation of the orebody/mining-block geometries used in the PEET-UG analysis.	68
6.4	Graphical representation of copper equivalence thresholds used in this analysis.	69
6.5	Internal Rate of Return (IRR) vs grade for each of the orebody/mining-block geometries.	69
6.6	Production rate (and mining method) as a function of dip.	69
6.7	Calculating NPV=0 for the 750mx25m mining scenario at 100m depth to the top of the mining block.	70
6.8	Relationship between orebody geometry, depth of cover, and the required CuEq grade to achieve NPV=0.	70
6.9	Contained value of selected mineral deposits.	71
6.10	Unit-value per tonne of ore for Cloncurry Cu-Au deposits grouped by deposit-style.	72
6.11	DMQ-generated target domains in the Southern Cloncurry District, limited to max. of 2.5km below surface	73

## List of Tables

2.1	Summary of structural-kinematic settings and controls of 'IOCG' deposit formation.	7
2.2	Geochronology of 'IOCG' mineralisation & linked magmatism with proximity in plan view.	7
2.3	Fluid systematics for the 3 main stages of IOCG formation	8
3.0	Historical nomenclatures of Isan Orogenic Events.	11
3.1	Historical nomenclatures of Isan orogenic Events in different Isa-Cloncurry terrains	13
4.1	Low, medium and high density contrasts used in trial Vp <sub>mg</sub> inversion modelling before settling on high contrast densities.	49
4.2	Vp <sub>mg</sub> mid-granite 'PERT' inversion modelling start geometry versions, modifications and run details for the final V18 granite model.	53
6.1	Comparative resource and value details for the deposits plotted in Figure 6.10	72

## Foreword

The Deep Mining Queensland (DMQ) project, a 2 year project commencing in April 2015, is part of the Queensland State Government's investment in priority geoscience projects identified by the mining and petroleum industries. This initiative is part of the Geological Survey of Queensland's (GSQ) Future Resources Program.

The DMQ project represents a holistic approach to resource prospectivity, from discovery through to an assessment of 'mineability', and focussed on the highly endowed Cloncurry Cu-Au district from Cloncurry township to south of the Osborne mine (totalling 8,743km<sup>2</sup>).

### Funding Body and Partners:

- Queensland Government (project funded through DNRM-GSQ)
- Chinova Resources (collaborative relationship, in-kind support through data-sharing)

### Research Aim:

Deep exploration is an industry area of focus given depletion of shallow resources and the likely/predicted mineral endowment under-cover adjacent to mature mining fields. The DMQ project aimed to reduce the risk profile of exploring at depth in the Cloncurry field by identifying tracts of ground, through enhanced understanding of the mineral systems architecture, which were:

- Prospective for large, mass-mineable deposits (of IOCG and/or other affinity), and
- Comprise geotechnical, geothermal, geographical conditions which are amenable to mass-mining methods.

The main aims of the project became as follows:

1. Through review of IOCG provinces both in Australia and globally, characterise:
  - (a) the key structural-tectonic, stratigraphic, magmatic and fluid systematic conditions affecting deposit formation, and
  - (b) geophysical responses of known deposits, with the intention of building controls and parameters for prospectivity analysis.
  - (c) IOCG deposit associations as an indicator to what other styles of mineralization may be possible in the Cloncurry district.
2. Where more detailed geological data became available, validate/update the district-scale 3D geological modelling of the project area to facilitate constrained geophysical inversion and identify any responses where the current understanding of the geology does not fully explain the geophysical response. This focussed on sub-regional-scale resolution of intrusive geometries at depth and hitherto-little-emphasised structural

controls and geometries that may have influenced fluid systematics at the time of IOCG mineralisation. This information was used to build a cohesive understanding of the geological controls on Cu-Au mineralization at the deposit/shoot scale. This would occur in tandem with characterisation of each deposit (style) by geochemistry and geophysical response with the aim of establishing useful vectoring toward mineralization systems and characterising the response of near-misses (above/below/off-flank) of drilling targeting IOCG mineralization. These tasks utilise Chinova Resources' mine-lease scale data and represents an opportunity to significantly refine the controls on mineralization/deposit-characteristics/controls-on-system focus and are key to re-evaluation of the 3D prospectivity of the area.

3. Engineering scenarios were undertaken, constrained by knowledge of the geotechnical properties of the host-rocks in the area, stress conditions, geothermal gradient, 'mineability', mining options available etc, to determine what size/footprint of deposit is required by depth; to sustain a deep mass-mineable operation in the area. This is used as a filter on the 'geological' prospectivity such that opportunities/tracts of ground may be identified which have the necessary inputs, and engineering 'potential' to host a mass-mineable deposit. This is not limited to only that which has been mined before, but open to larger, lower grade systems and previously unrecognized potential.

## Introduction to the Deep Mining Queensland (DMQ) Project

### Why the Cloncurry District?

Queensland accounts for 30% of Australia's copper production and 1.5% of the global copper production (DMRM, 2016). The Cloncurry district is globally significant in terms of the metallogenesis and copper (+gold) mining with discovery history dating back to 1867 (Kennedy, 1978). Discovery rate has declined, with the last significant, long-life mine (Ernest Henry) discovered in 1991 (Webb & Rowston, 1991) and other long-lived mines in the Mt Isa Inlier are coming to a close. Incremental discoveries in the near-mine environment (Kulthor at Osborne Mine, SWAN at Mt Elliott-Corbould Mine) indicate greater potential beyond the initial discovery, in these copper-gold systems. Additional modest sized open-cut resources have been developed (E1/Mt Margaret, Rocklands) and advanced projects transitioning to mining include the Roseby copper deposit.

The perception that shallow exploration targets are depleted and that deeper exploration is the future of resource extraction forms the premise of the Deep Mining Queensland (DMQ) Project.

The DMQ Project aims to reduce the risk of exploring at depth in the Cloncurry Copper-gold district by providing a new approach to exploration which is better informed in terms of the key characteristics required to sustain a viable mining operation.

The key activities of the DMQ Project were to:

- Develop an understanding of Iron-oxide Copper-Gold, and their sulphide dominant variants; both at the global scale and focussed on Cloncurry.
- Apply this knowledge within the framework of the revised Cloncurry district geology and, utilising fresh geophysical and geochemical analysis; determine likely domains of enhanced prospectivity at depth and discovery strategies.
- Provide a framework for assessing prospectivity of viability of a given body of mineralization/conceptual target, in terms of value.

Key ingredients for IOCG/ISCG Cu-Au deposit formation will be discussed in Chapter 2, and a discussion of the inferred controls on the range of Cu-Au deposit styles in the Cloncurry district is embodied in Chapter 3.

Prospectivity analysis (Chapter 4) will be assessed in a qualitative, expert-informed process utilizing the three-dimensional spatial distribution of key geological features, their geometries, and their intersections/inter-relationships.

Since discovery and development of the large Ernest Henry Cu-Au deposit (220Mt @ 1.43% CuEq), and application of large tonnage, sub-level caving underground mining; the potential for mining of deeper orebodies in the Cloncurry district is more promising. Discovery of the SWAN deposit by Ivanhoe Australia led to conceptual mining studies around the application of mass-mining methods to extract this resource (Figure 1.1). To date, the metal price environment renders the SWAN underground project as marginal with the most favourable option as mining via a large scale block-cave (AMC, 2012). The DMQ project, for this and other reasons to be explained in further sections of this report, places emphasis on 'mass-mining' methods of orebody extraction.

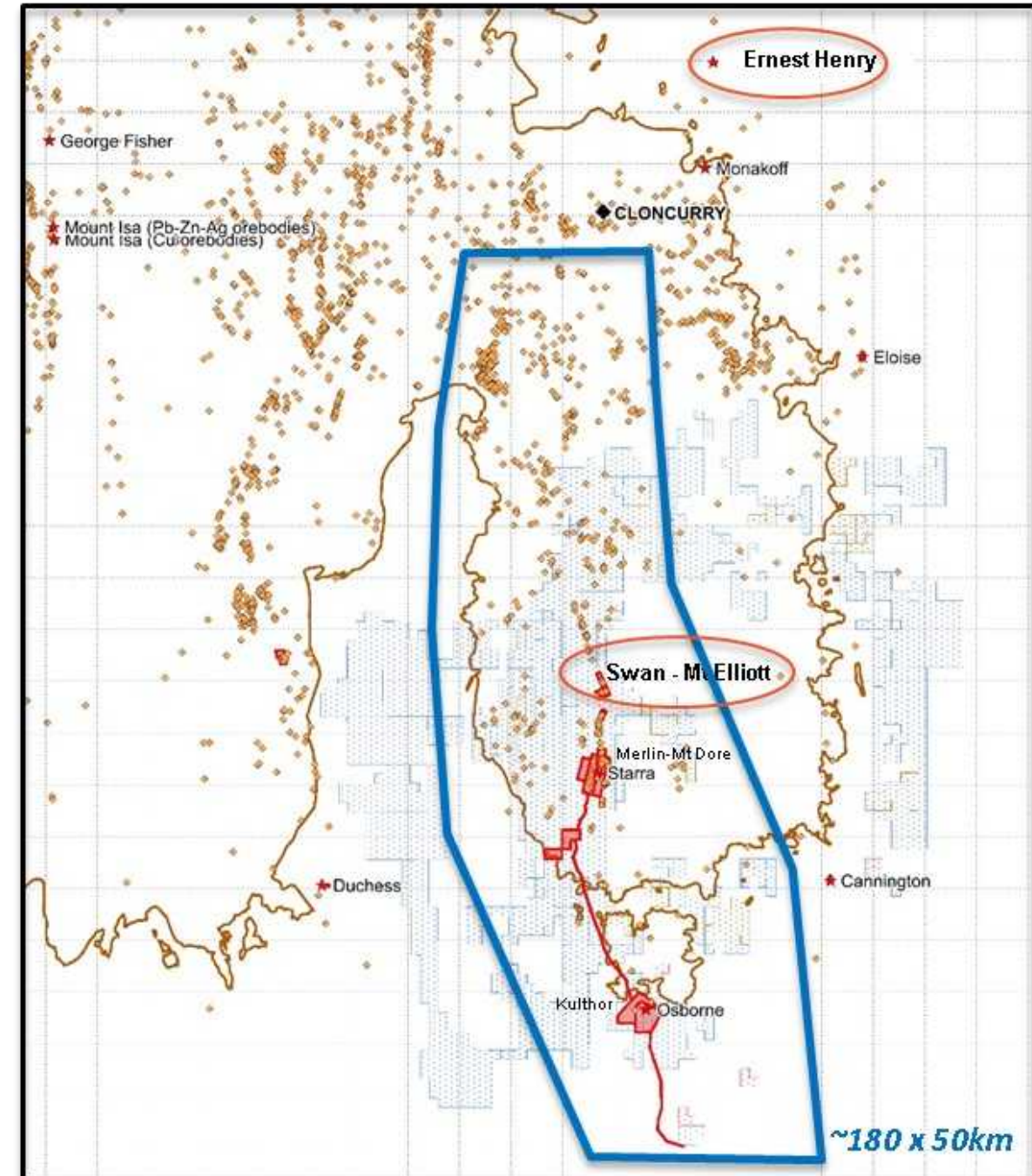
### The Case for a Depth Component to Prospectivity

Exploration and discovery trends indicate that:

- More discoveries are being made at depth (Figure 1.1), and
- Modes of discovery are more model driven at depth (Figure 1.2).

This is coupled with a perception that the opportunity for discovery of significant (>20Mt) ore deposits extending from the shallow sub-surface (0-200m) is significantly diminished. In the Cloncurry district, a wave of discoveries in the 1980's occurred following widespread airborne geophysical surveys. These included Cannington, Ernest Henry, Osborne, and Eloise; and each has at least part of the deposit within the 0-200m below surface region.

Discovery at depth requires a comprehensive understanding of orebody models within a framework of interpreted geology supported/guided by geophysical analysis. At depth, geophysics may not necessarily be the ore-finding tool as employed in the near-surface, but is useful in assisting knowledge-development in the 3D geometry and spatial distribution of geological packages and structure.



	Mt	Cu (%)	Au (g/t)
Ernest Henry <sup>1</sup>	220	1.1	0.5
Swan <sup>2</sup>	375	0.44	0.25

<sup>1</sup> Glencore Reserves & Resources, 2014    <sup>2</sup> AMC – Mt Elliott Scoping Study, 2012

**Figure 1.1** DMQ project area (blue) in the context of mineral occurrences (orange) mines (red) and the boundary of the outcropping Mt Isa Inlier.

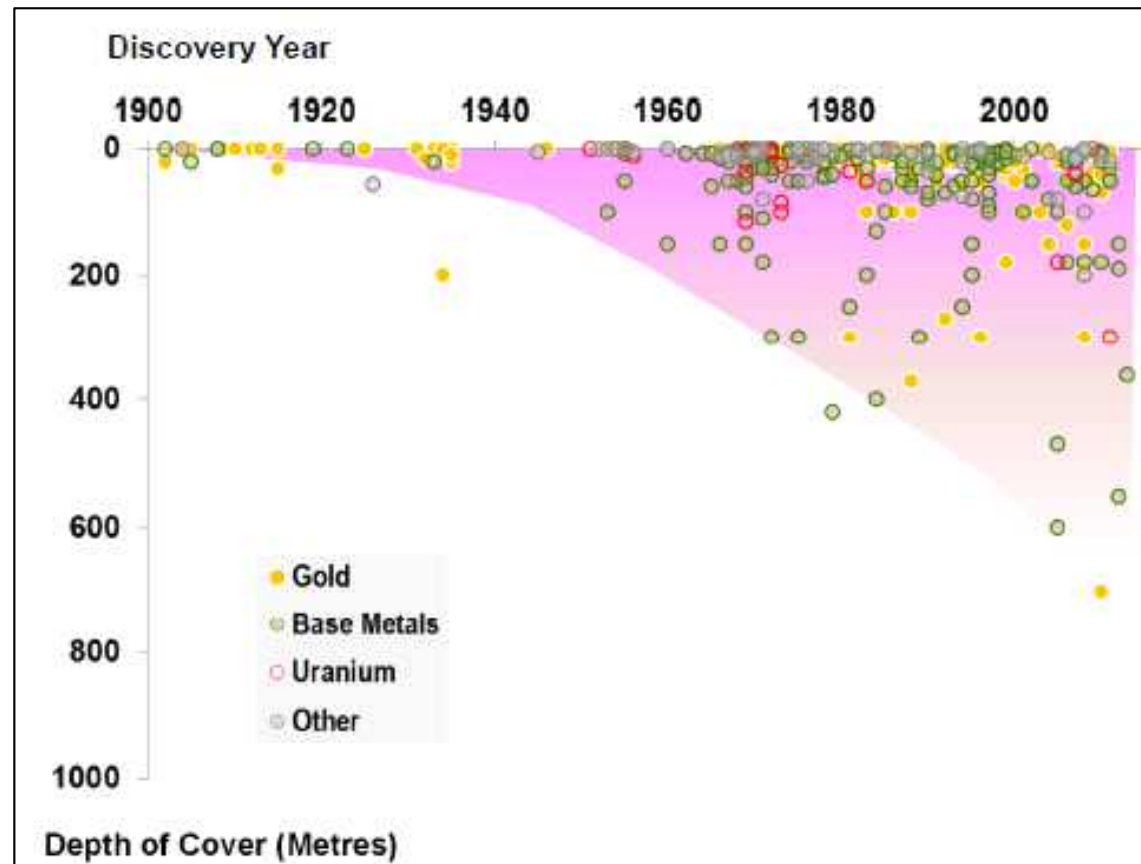


Figure 1.2 Depth of cover/overburden for discoveries in Australia (1900-2013) from Schodde, 2014.

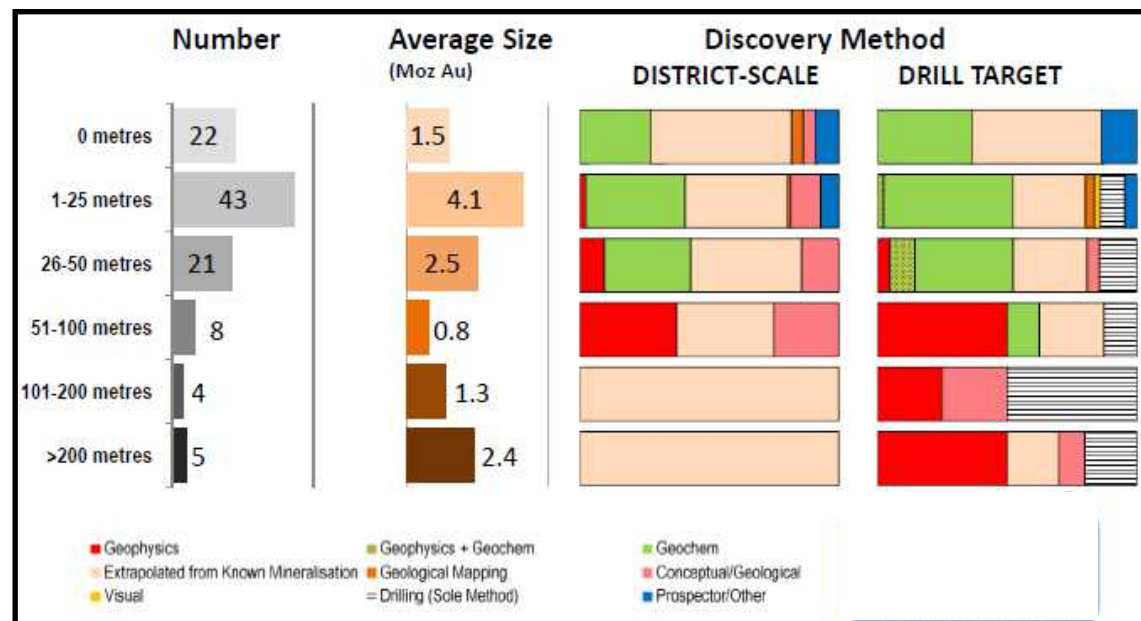


Figure 1.3 Method of discovery vs depth for Australian gold discoveries (1900-2013) from Schodde, 2014.

Other challenges that hinder effective exploration at depth include:

- Conductive overburden
- Density contrasts in overburden
- Drillability of younger cover sequences
- Non-descript geophysical response of mineralization.

Naturally, drilling expenses will increase with depth, putting additional pressure on accurate modelling of the geological architecture. Drilling under cover in a greenfields setting carries additional risk when compared to deep exploration in the brownfields environment. Brownfields exploration has the advantage of enabling extrapolation of known geological features, whereas greenfields undercover relies on geophysical interpretation validated by drilling.

## What Constitutes an Orebody Discovery at Depth?

To determine the viability of any discovered mineralization, value must be included in the prospectivity equation. Mineral deposits are not created equally, and the value of the contained metal per resource tonne varies significantly (Figure 1.3). Having said this, the total value of a deposit will be a product of the tonnage and unit value of the ore. Hence low-grade deposits can be mined if they are very large tonnages and can be extracted at low cost, as demonstrated by the 'Porphyry' and 'IOCG-Gawler' fields in Figure 1.4.

With respect to the Cloncurry district, the known deposits define a field of low to moderate tonnage and generally lower unit value, similar to Western Australian ('Orogenic') gold mines. (Figure 1.4). There is an overlap between the 'IOCG-Cloncurry' and 'IOCG-Gawler' fields (Figure 1.4) which suggests a continuum, however, the x-axis is log-scale and the deposits at the 'smaller' end of the Gawler-IOCG trend (Carapateena & Prominent Hill) are ca. 30% larger than Ernest Henry, the largest Cu-Au mine in the Cloncurry district.

The challenges around discovery of viable Cu-Au resources in the Cloncurry district are largely value driven. As illustrated on Figures 1.3 and 1.4, the Cloncurry deposits occupy a distinct field with relatively low unit value and size.

Potential for long-lived mines at depth will partly rely on low-cost extraction methods. This in turn requires a certain style of orebody, with sufficient geometry and homogeneity to facilitate large scale mining with multiple

extraction points. For example, discovery of a deposit with anticipated 10-20 year mine life, in the order of 20-150Mt total pre-mining resource; will likely be less than ~\$150/tonne ore based on the current spectrum of deposits. The value proposition of building a mine around a deposit like this will be significantly different to a BHT or SHMS (Figure 1.4) type of deposit.

A 'Caving Line' is indicated on Figure 1.3 where deposits are more likely to have, or require, characteristics suited to mass-mining.

Despite deposits containing sufficient value of metal, economic extraction is not guaranteed and relies on multiple factors including but not limited to :

- Orebody geometry
- Metal distribution
- Geotechnical parameters (ore and hangingwall)
- Groundwater
- Geothermal Gradient

The key drivers behind each of the applicable underground mining methods considered in this study are discussed in more detail in Murphy et al. (2015) (Appendix 8). The three mining methods likely to be employed in the deep mining of Cu-Au deposits in the Cloncurry district are:

- Sub-level Open Stopping
- Sub-Level Caving
- Block Caving

Of note are the sequence of mining (top-down vs bottom-up) and capital/operating cost structure.

A collation of mining cost estimates from various mines, globally, is illustrated on Figure 1.5. Note that this chart only displays mining costs, and does not capture processing, administration, geology, transport, smelting etc.

The cost-benefit of larger scale mining, particularly when mining lower value ores, can create significant margin of there is sufficient volume to the deposit. Analyses as to the economic limits in terms of deposit geometry, depth below surface, and grade; are analysed later in Chapter 4 of this report and separately in Murphy et al. (2016).

By comparison, after allowing for capital and operating costs, the estimated net profit per tonne of ore from an Osborne style deposit (approx. \$150/tonne value) is ca. \$27, and from an Ernest Henry sized deposit at the same grade, the profit margin per tonne is approximately \$68. Significantly higher tonnage (throughput and mine life)

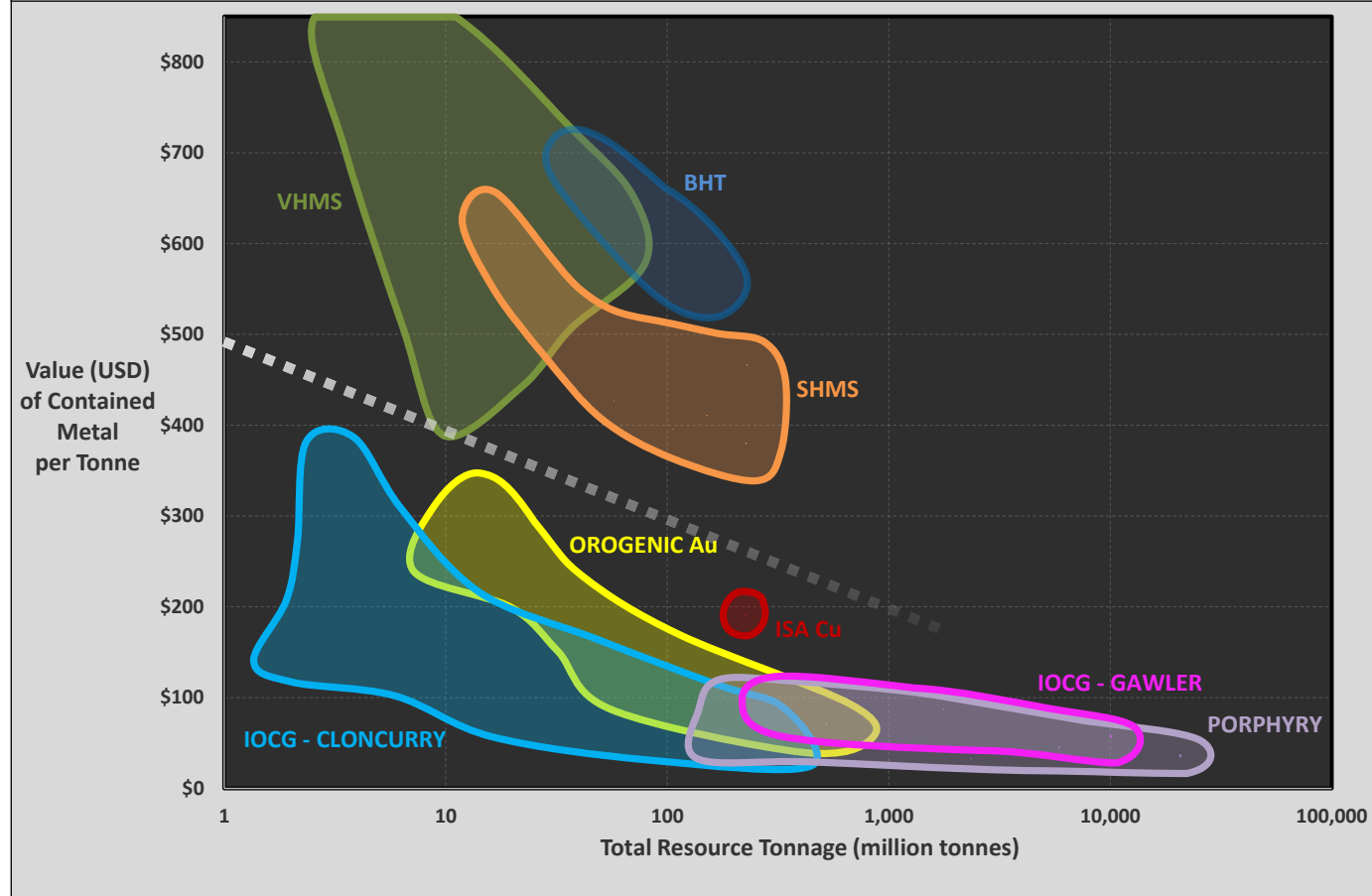
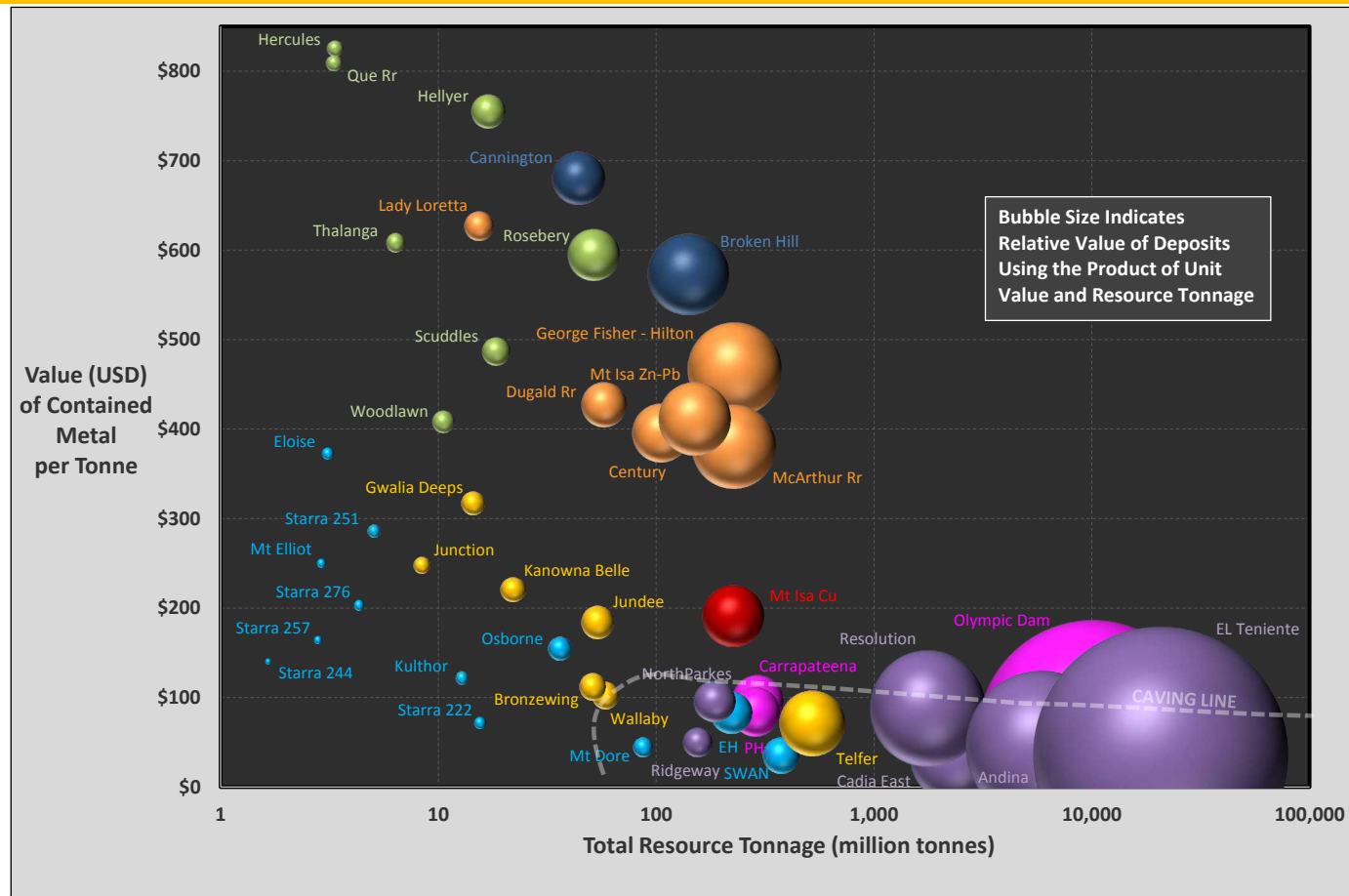


**Figure 1.4** (a) Contained value (USD) of selected mineral deposits. Bubble size indicates relative, pre-mining, total contained value. 'Caving line' indicates a field within which 'mass-mining' methods may be required to facilitate economic extraction. Metal prices and exchange rate as at 14th March, 2017. (b) Grouped by deposit type. Dotted line emphasises the significant value divide between 'massive' ores and disseminated/vein-hosted/discrete-structural deposit styles.

and higher margin ore despite same grade.

The inference is that, to sustain longer mine life and ensure viability of lower value ore, larger deposits amenable to mass-mining should be a priority exploration target. These targets would be situated at the right-hand end of the Cloncurry IOCG field as illustrated on Figure 1.4b.

## Application of BRC Expertise to the issue of Prospectivity at Depth.

The WH Bryan Mining and Geology Research Centre (part of the Sustainable Minerals Institute—'Production Centres') is a unique combination of exploration and mining geoscience with access to mining-technical and minerals-processing expertise.

Previous research projects undertaken in the centre have focused, in the past decade, on mass-mining research in terms of both design and operation. These have included:

- 'International Caving Study'
- 'Mass-Mining Technology 1-3'

- 'Supercaves'
- 'Next Generation Cave Mining'
- 'Geology and Mass Mining'

To complement this history of mining research, the BRC has built capability in the areas of:

- Structural Geology
- Ore deposit analysis
- Geophysics
- Geochemistry

The centre is well-placed to determine the merits of mining-informed exploration in the Cloncurry district with the aim of reducing risk to explorers.

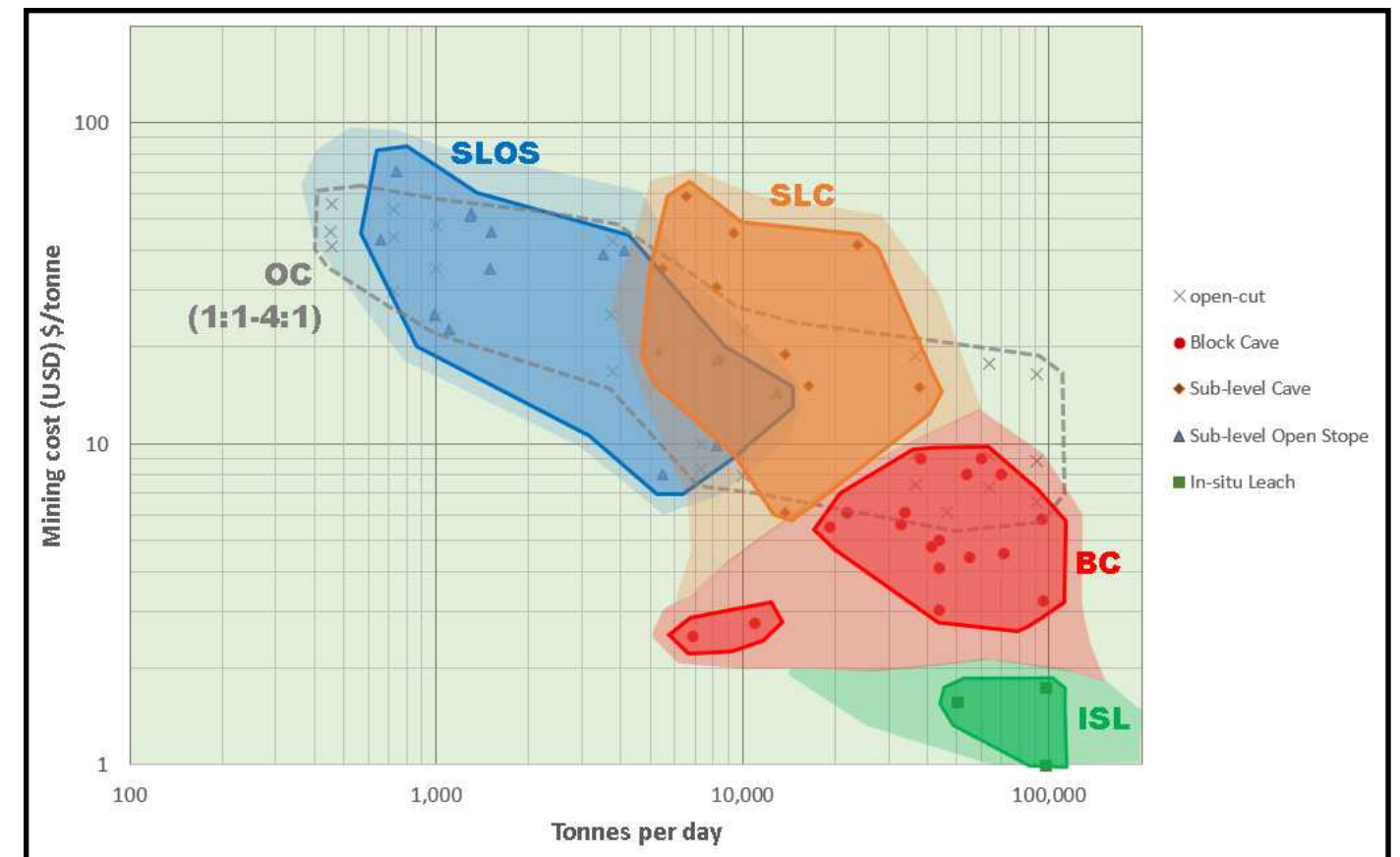


**Figure 1.5** Mining cost estimates (US\$/tonne) and mining rate from various mines globally. Mining costs do not capture processing, administration, geology, transport, smelting etc.

## Parallel Research Work and the Context of the DMQ Project

To maximise the potential of the Future Resources Funded projects, the following summary is provided to place the DMQ project in context of parallel GSQ-funded studies in the Cloncurry district. Each study has a point of difference, but has commonality in the geographical area of interest and deposit-styles under investigation. It is likely that elements of the CSIRO and GMEX-MBC-HCOV projects can be utilised by explorers in conjunction with the enhanced geological and prospectivity understanding provided by the DMQ project. As will be discussed in later parts of this report, there is no singular solution for target generation in the Cloncurry district due to the complex interplay of variable host-rocks or host-positions within the stratigraphy, rheological contrast of lithologies heterogeneously focussing strain, proximity to intrusives of favourable geometry, and deformation features providing fluid-focussing and localised controls on sites for mineralization.

### DMQ Focus

With a focus on the Cloncurry District, the DMQ project has sought to use public domain data (from the Geological Survey of Queensland) together with data held by an exploration company (Chinova Resources), rather than conducting new geological, geophysical or geochemical surveys. The geology of the AOI has been re-interpreted, using geophysical datasets including seismic, aeromagnetic and gravity. The re-interpreted geology has been considered in a temporal context, allowing a time-space plot to be developed that helps to explain the evolution of the belt, and how this relates to the known mineral occurrences.

The geology, geophysical and geochemical response (Appendix 8) of several key deposits in the DMQ AOI have been presented, highlighting that different controls exist for mineralisation at each deposit or within each mineral camp, and that there are no grand targeting silver bullets that exist.

The reinterpreted solid geology, guided by geophysical data allowed a series of sections throughout the DMQ AOI to be produced. These were in turn combined into a 3D model. Geophysical inversion techniques based on apparent density models derived from gravity data have allowed estimates to be made on the geometry of granite bodies, the domains above edges of which tend to be prospective for Cu-Au mineral deposits. This depth

dimension is one of the key features that sets DMQ apart, and the 3D model analysis has allowed a series of prospective tracts and targets to be identified.

Another key output from the DMQ research is an economic evaluation tool, developed specifically for the DMQ AOI, that allows explorers to quickly assess exploration targets in terms of their underground mineability. The assessment is intended to provide fast feedback to explorers, and while it in no way is intended to replace any feasibility studies, it is thought that it will keep mining economics in the forefront of explorer's minds. The assessment tool will help guide explorers as to whether to persist with a target that shows characteristics (including size and grade potential) that will allow it to be mined from underground at a profit, or whether to limit further work and focus exploration resources elsewhere.

### CSIRO Uncover Cloncurry, A Mineral Systems Approach to the Eastern Mount Isa Inlier: Characterization, Processes, Prediction, Detection, and Recovery

Between 2015 and 2016, the CSIRO conducted research that aimed at integrating petrophysical and geochemical/mineralogical micro-characterisation for several deposits across the Cloncurry District. The primary aim was to use the data to better understand processes that led to the formation of the diverse styles of mineralisation in the district.

Much of the work was focussed on correlating magnetite growth and/or recrystallization events, interpreted from measurements of anisotropy of magnetic susceptibility (AMS), to the stress regime of deformation events in the Mt Isa Eastern Succession. An initial goal of the research was aimed at using estimates of pyrrhotite vs. magnetite made from measurements of magnetic remnance vs. magnetic susceptibility, as a proxy for a map of redox gradients. However, the different responses could not easily be separated, due to pyrrhotite usually being overwhelmed by magnetite and multiple overprinting systems confusing the interpretation. Consequently, maps of redox gradient derived from petrophysical measurements were not realised.

SEM (TIMA) was used to create micro-scale mineral maps, showing zoning that is interpreted to relate to gradients in pH, redox and the activity of water. Such gradients are inferred to be primary controls on the mobilisation and precipitation of ore metals, with Cu-S transport interpreted in fluids of relatively low water activity and alkaline pH, and Fe transport in acidic fluids. Andesine-

ilmeneite mineral assemblages identified by the TIMA are thought to indicate relatively reduced and acidic hydrothermal environments, whilst K-feldspar-titanate assemblages indicate relatively oxidised and alkaline environments. Mixing of fluids is suggested as a possible mechanism for ore deposition.

Litho-geochemistry was investigated for typically 1-2 select drillholes in several deposits. These data were obtained from pXRF and acid digest/ICP-MS methods. The immobile trace elements could often be used to highlight composition differences in the host rocks, whilst some pathfinder elements could be used to highlight lithological units, contacts or zones that were considered to be anomalous.

Multi-element geochemistry was also examined using multivariate statistics in an attempt to highlight key differences between mineralised samples from different deposits.

This study operated at a distinct scale-of-observation compared to the DMQ project., with observations and data obtained from meso- to micro-scale analytical techniques. While insights into the micro-textures and fluid chemistry add to the knowledge bank concerned with understanding the Cloncurry Cu-Au systems, the DMQ project suggests information and geological interrelationships effecting discovery occur at scales orders of magnitude greater than these observations.

### GMEX-MBC-HCOV : Advanced Understanding of Structural and Geochemical Controls on Mineralisation in the Eastern Mount Isa Inlier Using Innovative Techniques for Exploration

This study was largely focussed on results derived from 2D geomechanical modelling that was performed using the UDEC software package.

The geomechanical modelling was based on the numerical simulation of the mechanical response of a jointed or fractured rock mass to an imposed stress. The model used inputs of lithological 'blocks', separated by discontinuities (representing faults and rock contacts). The applied stress field used in the simulations was selected from an understanding of the geological evolution of the Mt Isa Eastern Succession; being NE-directed shortening (D3) followed by an ESE-directed shortening (D4) at crustal depths of 7 km. A limitation in this 2D modelling process is that geological contacts, intrusive boundaries, and faults are treated as being vertical. As will be shown in the DMQ project results, the gently dipping stratigraphy and

structure enable inference of target locations in the subsurface that are spatially disparate from the outcropping host-rock position. The simplified 2D geology applied here cannot achieve this.

Outputs from the geomechanical modelling were provided in 2 forms; geotiffs that showed zones of interpreted high and low stress, and also as 'predictor' maps (MapInfo .tab files and geotiffs) that were derived by combining an interpreted 'fluid factor' with an estimate of differential stress, to predict the likelihood and type of failure (shear/extensional shear/tensile).

Interpretation was performed at several scales, however focus was on two different regional scales (covering fifteen 1:100,000 geology sheets and six 1:100,000 geology sheets respectively) as well as three local (prospect-scale) models.

Over a few of the local scale geomechanical interpretations, soil geochemistry data obtained using pXRF was used to highlight areas of Cu anomalism. The soil Cu data was also levelled against litho-geochemical domains, that were themselves developed through a combination of litho-geochemical interpretation and field mapping. The geochemical data was considered to be a potentially useful tool to help verify and rank exploration targets identified through the geomechanical modelling. However the targets tested were all near-surface, with likely shallow residual soil profiles.

### Data Sources

The data sources considered in this project have come from two main sources; the Geological Survey of Queensland (GSQ) data that included a compilation by TerraSearch to form the Mt Isa East data package, and an extensive data set provided by Chinova Resources. Geological, geophysical, geochemical and drilling data is available from each data source.

## Review of Global IOCG Deposits, Characteristics & Processes

### Characteristics of IOCG style deposits

The Iron-Oxide Copper-Gold (IOCG) family of deposits cover a broad variety of deposits, having considerable internal variability, but with some generally-agreed unifying characteristics. DMQ sought to review and analyse IOCG deposits across the globe, to identify a set of ingredients essential to IOCG formation that are also 3D-mappable. At least 38 mines/deposits occurring across 9 major IOCG provinces were reviewed in detail. The entire Global Review can be found in Technical Report No1 in Appendix 8 and the associated database compilation in Appendix 10.

#### Generally agreed IOCG characteristics

- abundant, low-Ti, Fe-oxides: magnetite and/or hematite;
- Cu ± Au at economic grades;
- a distinctive suite of minor elements: (*differing mixes of*) Ag, REE, U, Mo, F, P, Ni, As, Co, & Ba;
- an association with extensive & pervasive alkali alteration – both sodic-calcic, Na-(Ca) and potassic, K;
- formed in shallow crustal environments, in brittle regimes (*in the 2-12km depth range*);
- prominent structural ± lithological control;
- most commonly coeval, but (*usually*) not proximal to magmatism (*in the form of plutons & batholithic complexes*);
- common district association with Cu-Au-barren, Fe-oxide deposits.

#### IOCG characteristics with no agreement

- distinctive tectonic environments of formation;
- distinctive magmatic associations;
- characteristic ages of formation;
- non-magmatic brine involvement: basinal evaporitic and/or formational evaporitic;
- mafic metal-source rocks.

### Spatial & Temporal Associations of IOCG Deposits

IOCG deposits and districts occur on all continents (Figure 2.1). In some places (notable the Central Andean Coastal Belt of Chile and Peru), there is a spatial coincidence of IOCG deposits with porphyry Cu-(Au) deposits. However, this association is not well established elsewhere, suggesting that a critical component for IOCG formation is missing in other porphyry Cu arcs.

Another key difference between IOCG and porphyry Cu-(Au) deposits is that despite some overlap, IOCG deposits

generally have better Cu grades, and a greater spread to lower tonnages, compared to the more clustered grade-tonnage distribution of porphyry systems (Figure 2.2).

Large IOCG deposits in a district also tend to be accompanied by multiple small, non-economic prospects and showings (“smoke”), whilst large porphyry systems tend to be much more focussed, delimited by plutons or intrusions. Consequently, IOCG districts imply massive regional/semi-regional fluid systems that are spatially considerably ‘leaky’ in character.

IOCG deposits are observed to cover an age range from late Archean to the Pliocene, suggesting that their formation is independent of any crustal, hydrosphere or atmospheric stage of Earth development.

### IOCG Dimensions & Mining Methods

When Plan View Aspect Ratios of a sub-set of IOCG deposits are plotted against their tonnage (Figure 2.3), they tend to show a large spread in distribution—from

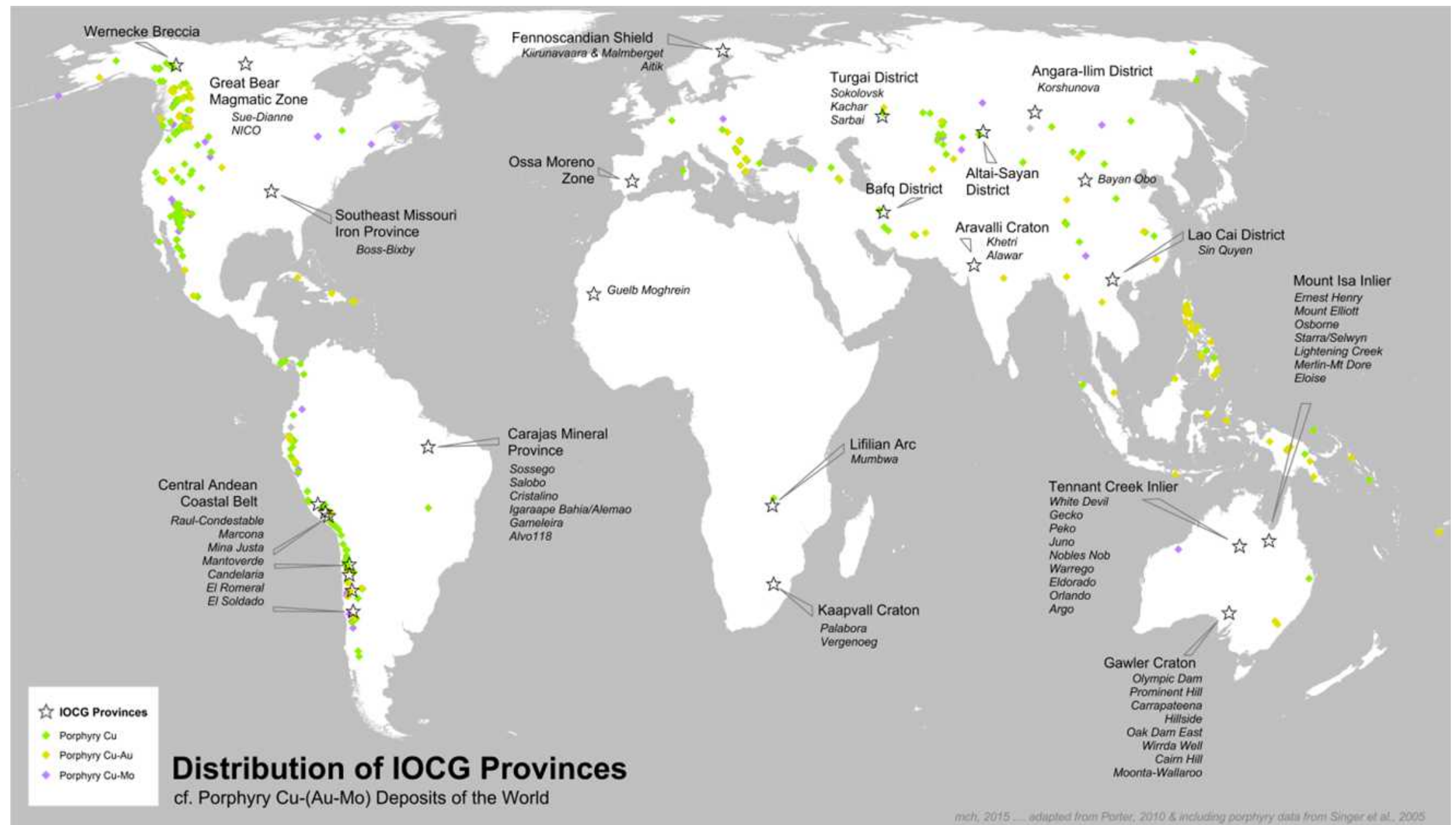


**Figure 2.1:** Distribution of global IOCG provinces. Figure adapted from Porter (2010) and includes data from Singer et al. (2005). Note the coincidence of IOCG province with Andean porphyry Cu belts and absence of IOCG deposits in other porphyry belts.

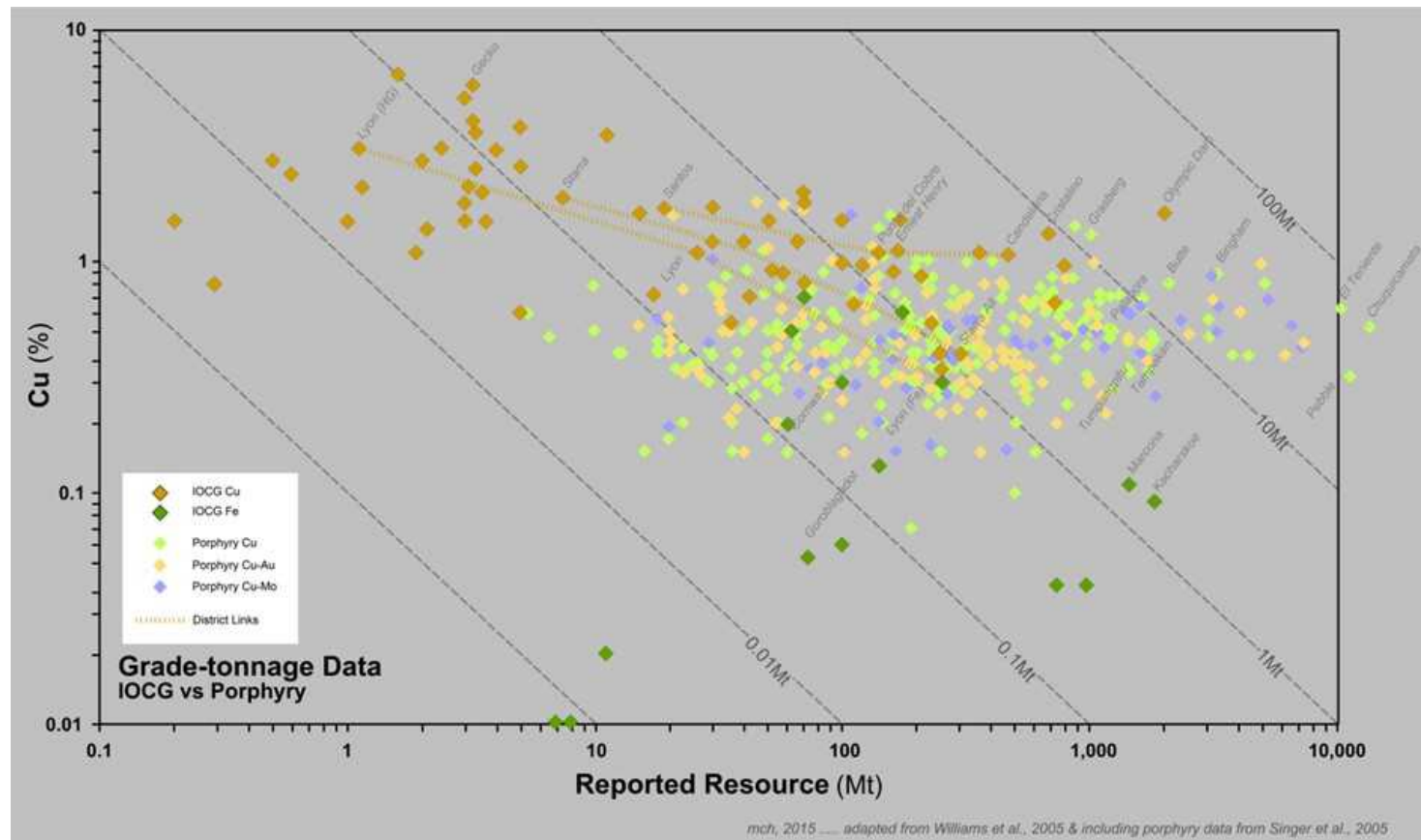


**Figure 2.2:** Grade-tonnage data for IOCG deposits compared to porphyry Cu deposits. Figure adapted from Williams et al. (2005) and includes data from Singer et al. (2005). Tie lines connect deposits within a single district and highlight the spread of deposit tonnages developed with districts. Individual IOCG districts are characterised by a multitude of lower tonnage and lower grade occurrences that are not shown here.

equidimensional to extreme elongation. This contrasts with the much more equidimensional plan view of porphyry Cu deposits. Dimensional variability is considered to be a function of structural control, lithological replacement and host homogeneity.

The vast majority of global IOCG mines compiled by DMQ are, or have been mined in open pits and/or underground using Sub-level Open Stopping (SLOS) mining methods. Only Phalaborwa, a steeply plunging and equidimensional (in plan) deposit in South Africa has been mined using block caving. The Carapateena deposit in South Australia has however had a block cave operation as the favoured mining method following a feasibility study.

Orebody geometry has a major control on underground mass-mining options. The huge variability from plan-view equidimensionality, combined with down-dip complexities (frequently dilution, reflecting wide-spread, stacked-lensoidal geometries) has been a contributing factor in limiting the mass underground mining of many IOCG deposits.

## 'IOCG' System Synthesis

### Structure

Globally, IOCG systems can be contractional or extensional, however individual districts tend to have broadly common kinematics at the time of mineralisation. It is common for a 'late', brittle reactivation of pre-existing ductile or mylonitic structures during mineralisation. IOCG mineralisation is focussed either along, around or closely adjacent to, longer-lived, crustal-penetrative structures that have an extended history with pre-, syn- and (potentially) post-mineralisation re-activations. Whilst IOCG structural control is significant, it also considered to be particularly broad in nature.

Table 2.1 summarises structural-kinematic settings and controls of 'IOCG' deposit formation for a sub-set of deposits where enough published data could be obtained.

### Magmatism—Timing & Proximity

IOCG mineralisation has been shown to be broadly

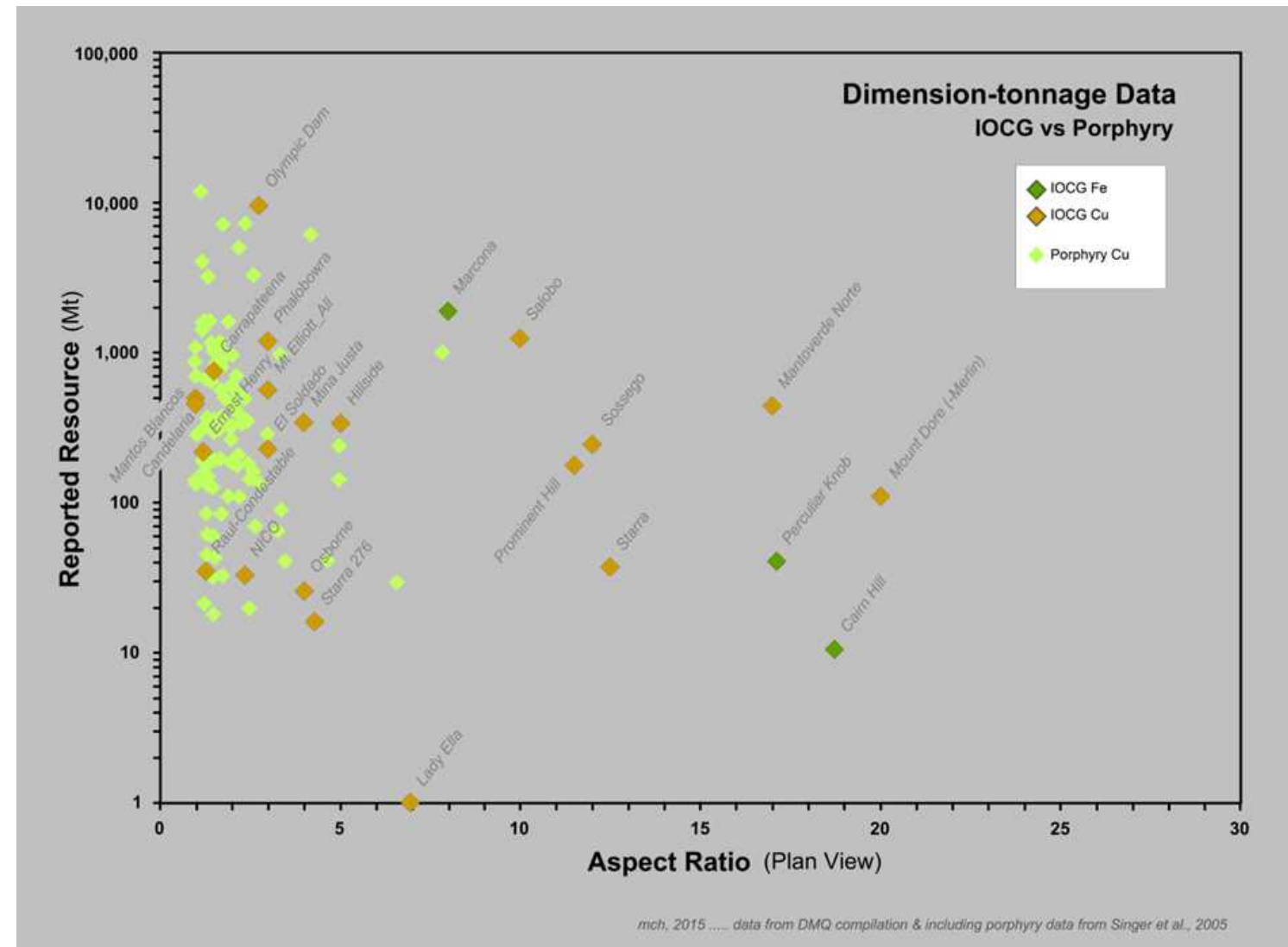


**Figure 2.3:** Plan View Aspect Ratios for IOCG deposits compared with porphyry Cu deposits. IOCG data from DMQ compilation and porphyry data from Singer et al. (2005).

synchronous with crustal magmatism by several workers in numerous review papers: Hitzman (1992, 2000), Williams et al. (2005), Porter (2010), Barton & Johnson (2004, 2015). Magmatism can be regional-scale batholithic granitoid complexes, synchronous mafic-felsic-intermediate volcanism, or synchronous cogenetic mafic(-intermediate) dykes, sills and plugs. Mafic inputs imply a mantle source that has been emplaced into the lower crust. The mafic input also drives higher heat flows, high temperature metamorphism (Rubenach et al., 2008), crustal anatexis, and magmatism (Haywood & Skirrow, 2010; Porter, 2010).

However, particularly when assessed in plan-view, a broad range of distances exists between deposits and significant volumes of outcropping, synchronous magmatism (especially batholithic complexes). A likely reason for this is that plan-view distances do not well account for the likelihood of intrusions having closer proximity to

mineralisation at depth.

Table 2.2 summarises and highlights the synchronicity of mineralisation with crustal magmatism, and also contains an estimate of the plan view distance of the linked magmatism from mineralisation for several deposits.

In the metamorphic terrain-hosted Cloncurry district, there is not an obvious direct or even a close spatial linkage between mineralisation and linked intrusive complexes. Instead, significant crustal-scale structures, acting as fluid conduits appear to be more important. In contrast, the magmatic terrain-hosted districts have a much closer proximity of magmatism linked to mineralisation.

Rather than use empirically-based classification systems, a process-based system should be considered. It needs to recognise that IOCG deposits have highly variable Fe-oxide and Fe-sulphide contents, highly variable Cu, Au and other

District	DEPOSIT	Age	Regional Tectonics		Local Faults		Style	Detail	Note	References
			Regime	Direction		Orient				
Carajas Province	SALOBO	Arch	Transpressional?	(E)NE-(W)	?	WNW	Brittle	Crustal-scale structure; sinistral overprint	nwc	Xavier et al., 2010
Carajas Province	SOSSEGO	Arch	Transpressional?	(E)NE-(W)	?	WNW	Brittle	Crustal-scale FZ, older, contact structure	nwc	Xavier et al., 2010
Carajas Province	ALVO 118	Arch	Transpressional?	(E)NE-(W)	?	WNW	Brittle	Crustal-scale FZ, older, contact structure	nwc	Torresi et al., 2012; Xavier et al., 2010
Andean Belt, Chile	CANDELARIA	Early Cret	Transtensional	?	?	NNW	Brittle	Fault swarm, antiform; HW of crustal-scale Gregorio Fault Zone	nwc	Lundin Mining, 2014; Marschik et al., 2000; Chen, 2010; Sillitoe, 2003
Andean Belt, Chile	SANTOS	Early Cret	Transtensional	?	?	NNW	Brittle	HW of NNW crustal-scale Gregorio Fault Zone	nwc	Lundin Mining, 2014
Andean Belt, Chile	MANTOVERDE	Early Cret	Transtensional	NW-SE?	Normal	NNW	Brittle	HW of crustal scale, sinistral strike-slip Atacama Fault Zone		Sillitoe, 2003; Reiger et al., 2010
Andean Belt, Chile	EL SOLDADO	Early Cret	Transtensional	NW-SE?	Normal	N to NNW	Brittle	Transtensional zone in sinistral strike-slip FZ		Sillitoe, 2003; Boric et al., 2002
Andean Belt, Peru	CONDESTABLE	Early Cret	Extensional	?	Normal	NW, NE	Brittle			Sillitoe, 2003
Andean Belt, Peru	MINA JUSTA	Cret	?	?	Normal	NE	Brittle	Shallow faults		Chen et al., 2010; Sillitoe, 2003
Olympic Dam Domain	OLYMPIC DAM	MesoProt	Extensional	?	Normal	NE, NW	Brittle	HW of NNW crustal-scale Elizabeth Creek Fault Zone		Haywood & Skirrow, 2010
Olympic Dam Domain	PROMINENT HILL	MesoProt	Extensional	?	Normal	NNW	Brittle	HW of NNW crustal-scale Elizabeth Creek Fault Zone		Haywood & Skirrow, 2010
Olympic Dam Domain	WIRDA WELL	MesoProt	Extensional	?	Normal	NNW	Brittle	HW of NNW crustal-scale Elizabeth Creek Fault Zone		Haywood & Skirrow, 2010
Cloncurry Belt	ERNEST HENRY	MesoProt	Compressional	SE>NW	Reverse	NE	Brittle	Bx & Fr networks; ?formational faulting; post-peak meta		Rusk et al., 2010; Mark et al., 2000
Cloncurry Belt	OSBORNE	MesoProt	Transpressive	SE>NW	Transpressive	NW, NNE	Brittle	Reactn of earlier imbricated stratigraphy; post-peak meta	dmq	King, 2001; Adshead, 1995; Rubenach et al., 2001
Cloncurry Belt	KULTHOR	MesoProt	Compressional	SE>NW	Reverse	NNE	Brittle	Reverse reactn of thrust stratigraphy; post-peak meta	dmq	Hinman, 2012, 2013
Cloncurry Belt	SWAN-MT ELLIOTT	MesoProt	Transpressive	SE>NW	Transpressive	NW, (NE)	Brittle	Transpressive reactn of Mt Elliott Fault & NE dipping package; diorite	dmq	Gunter, 2015; Brown & Porter, 2010; Searle, 1952
Cloncurry Belt	STARRA	MesoProt	Transpressive	SE>NW	Transpressive	N	Brittle	Reactn of earlier Starra Shear; post-peak meta	dmq	Sleigh, 2002; Adshead-Bell, 1998; Hinman, 2012
Cloncurry Belt	MERLIN-MT DORE	MesoProt	Compressional	E>W	Transpressive	NNW	Brittle	BX & Fr networks associate with overthrust; post-peak meta	dmq	Ivanhoe, 2009; Hinman, 2013

**Table 2.1:** Summary compilation of structural-kinematic settings and controls of 'IOCG' deposits during main stage mineralisation. Notes: nwc = not well constrained, dmq = DMQ interpretation, E>W = east over west vergent, HW = hangingwall, Bx = breccia, Fr = fracture; FZ = Fault Zone

District	DEPOSIT	GEOCHRONOLOGY		Proximity to linked Intrusives* in PLAN VIEW (km)						References	
		Mineralisation	Intrusives	0km	0-5	5-10	10-20	>20	?		
Carajas Province	SALOBO	2.58Ga	2.57Ga								see DMQ Compilation in Appendices 8 & 10 for References and details of Geochronology
Carajas Province	IGARAPE BAHIA/ALEMAO	2.77-2.57Ga	2.76Ga								
Carajas Province	GAMELAIRA	1.73-1.70Ga	1.87Ga								
Carajas Province	CRISTALINO	2.72Ga	2.74Ga								
Carajas Province	SOSSEGO	2.53-2.61Ga									
Carajas Province	ALVO 118	1.87Ga	2.74Ga								
Andean Belt, Chile	CANDELARIA	112-110Ma	119-97Ma								
Andean Belt, Chile	SANTOS	112-110Ma	119-97Ma								
Andean Belt, Chile	MANTOVERDE	>121Ma	127-120Ma								
Andean Belt, Chile	MANTOS BLANCOS	142-141Ma	142-141Ma	FD							
Andean Belt, Chile	EL SOLDADO	106-101Ma	118-94Ma								
Andean Belt, Peru	RAUL-CONDESTABLE	115Ma	116-115Ma								
Andean Belt, Peru	MARCONA	159-161Ma									
Andean Belt, Peru	MINA JUSTA	103-99Ma	<109-80Ma								
South Africa	PHALABOWRA	2060Ma	2060Ma	FD							
Olympic Dam Domain	OLYMPIC DAM	1595-1590Ma	1595-1575Ma								
Olympic Dam Domain	PROMINENT HILL	1595-1590Ma	1595-1575Ma								
Olympic Dam Domain	WIRDA WELL	1595-1590Ma	1595-1575Ma								
Cloncurry Belt	ERNEST HENRY	1527Ma	1530Ma								
Cloncurry Belt	OSBORNE	1542-1538Ma	1530-1500Ma							?	
Cloncurry Belt	SWAN-MT ELLIOTT	1530-1510Ma	1530-1500Ma								
Cloncurry Belt	STARRA	1503Ma	1530-1500Ma								
Cloncurry Belt	MERLIN-MT DORE	1520-1490Ma	1530-1500Ma								

**Table 2.2:** Geochronology of 'IOCG' mineralisation & linked magmatism together with the proximity of linked magmatism in plan view. Note: FD = 'IOCG' Fringe Dweller. \* Analysis specifically does NOT consider 3D spatial proximity

temporally overlap with intrusive magmatism.

Typical Na-(Ca) alteration minerals include: albite-scapolite-quartz-(magnetite-actinolite)

The map in Figure 2.4 highlights the extent of Na-Ca alteration in the Cloncurry district. It shows the control of crustal-scale structures that show inversion/re-activation during Isan deformation, which is broadly synchronous with Williams Suite batholithic intrusion. Alteration also shows a significant overlap with carbonate (evaporitic) packages of Cover Sequences 2 and 3 (the Corella and Stavely Formations respectively).

Following the early sodic-calcic alteration, evidence of a potassic-iron alteration event exists. Whether the alteration fluids smoothly evolve from Na-Ca to ore-forming, or instead are catastrophically driven remains unclear. However the latter option

may be more likely, due to a much stronger structural control. Fluid systems become significantly more focussed on their evolution towards strong potassic alteration.

Typical K-rich alteration minerals: biotite-K-feldspar-magnetite

Typical Fe, Ca-rich alteration minerals: magnetite-K-feldspar-(actinolite-carbonate-apatite)

Coexisting Cu-Au poor (or absent) magnetite-hematite iron ore accumulations are commonly hosted in the Fe-Ca-rich assemblages. This suggests that either an additional more potassic fluid component drives richer Cu-Au systems, or that primary fluids, traps and sources are significantly different between the Cu-Au and 'barren' systems. In systems where Cu-Au-rich IOCGs coexist with massive Fe-oxide deposits, the Cu-Au mineralisation post-dates the Fe-oxide accumulations (Chen et al. 2010).

In IOCG systems where vertical zonation can be resolved, potassic alteration systems are better preserved at shallow depths. They may not be obvious with increasing depth, since albite-actinolite-magnetite assemblages accompanying the Cu-Au ore may be strongly developed. A spectrum of alteration assemblages, in response to different physico-chemical conditions can exist in the shallow parts of the system. Two significant variants typically exist: **magnetite dominant**, biotite-K-feldspar-

metals, and may be associated with some selected powerful episodes of crustal magmatism and associated potent fluid systems.

### Alteration & Mineralisation

IOCG systems are accompanied by alteration, from deposit-scale through to regional-scale (10 to >1000 km<sup>2</sup>) (Haywood & Skirrow, 2010; Porter, 2010). The alteration systems have been interpreted as extending to at least mid-crustal depths, reflecting the lithospheric scale of the associated magmato-fluid system. Vast fluid circulation cells produce regional-scale alteration systems and are constrained and focussed by intrusion geometry and by pre-existing and re-activating crustal architectures.

Many IOCG districts and deposits show evidence of early, pre-mineralisation fluid circulation, manifesting in sodic-calcic+iron alteration. This alteration event is the broadest and deepest in the system and is thought to reflect deep circulation of high salinity fluids that scavenge solutes and metals from the rocks that they alter (Oliver et al. 2014). Rarely has the timing of this alteration with respect to magmatism been precisely constrained., however it is commonly assumed to be driven by and therefore

actinolite assemblages, and **hematite dominant**, sericite-chlorite assemblages. The hematite variant is sometimes referred to as the 'hydrolytic' assemblage.

The mineralised portion of IOCG systems is generally more tightly focused than the potassic-iron phase of metasomatism, but may itself be characterised by strongly potassic assemblages, generally dominated by K feldspar. In systems where vertical zonation is well understood (eg. southeastern Carajas; Xavier et al., 2010), less intensely mineralised, potassic-iron alteration lies beneath the main body of mineralisation.

Considerable local variation tends to exist in the alteration schemes described above, and this in turn reflects variations in structure, lithology and permeability. Additionally, different spatial and temporal overlaps can further complicate the interpretation of IOCG alteration systems.

## Fluid Systematics & Diagnostic Geochemistry

The fluid systematics of IOCG formation centres have been examined by numerous authors. Fluid inclusion, calculated fluid O & S isotopic compositions, Br/Cl ratios, Cl & Br isotope data and  $^{40}\text{Ar}/^{36}\text{Ar}$  data have been applied to the characterisation of ore forming fluids, and in particular, the relative contributions of magmatic and non-magmatic (surficial- or buried, formational-derived) fluids within IOCG systems. Ratios of Br to Cl and their isotope composition have been effectively used as basinal-component tracers in a handful of better-studied deposits.

Table 2.3 summarises the salient fluid inclusion, isotopic, modelling and geochemical data for the main stages of IOCG formation. Most investigations have focused on the potassic-iron and mineralising stages of ore formation, however some modelling of the conditions of sodic-calcic alteration in the Isa Eastern Succession have been done by Oliver et al. (2004) and are included in Table 2.3.

Fluid physio-chemical characteristics associated with IOCG metasomatism and mineralisation suggest that Cu-Au mineralisation is driven by the 'late' contribution of a distinct, cooler fluid that mixes/ reacts with either an active iron-potassic hydrothermal system, or already precipitated (or precipitating), magnetite-biotite-K feldspar assemblages. This 'late' distinct fluid mixes the system to variable and lower temperatures and salinities and higher oxidation states and is ubiquitously acknowledged in well studied deposits (Olympic Dam, Raul-Condostable, Mina Justa, La Candelaria, Ernest Henry). In these studies, this distinct, 'late', low temperature, oxidised fluid is ascribed

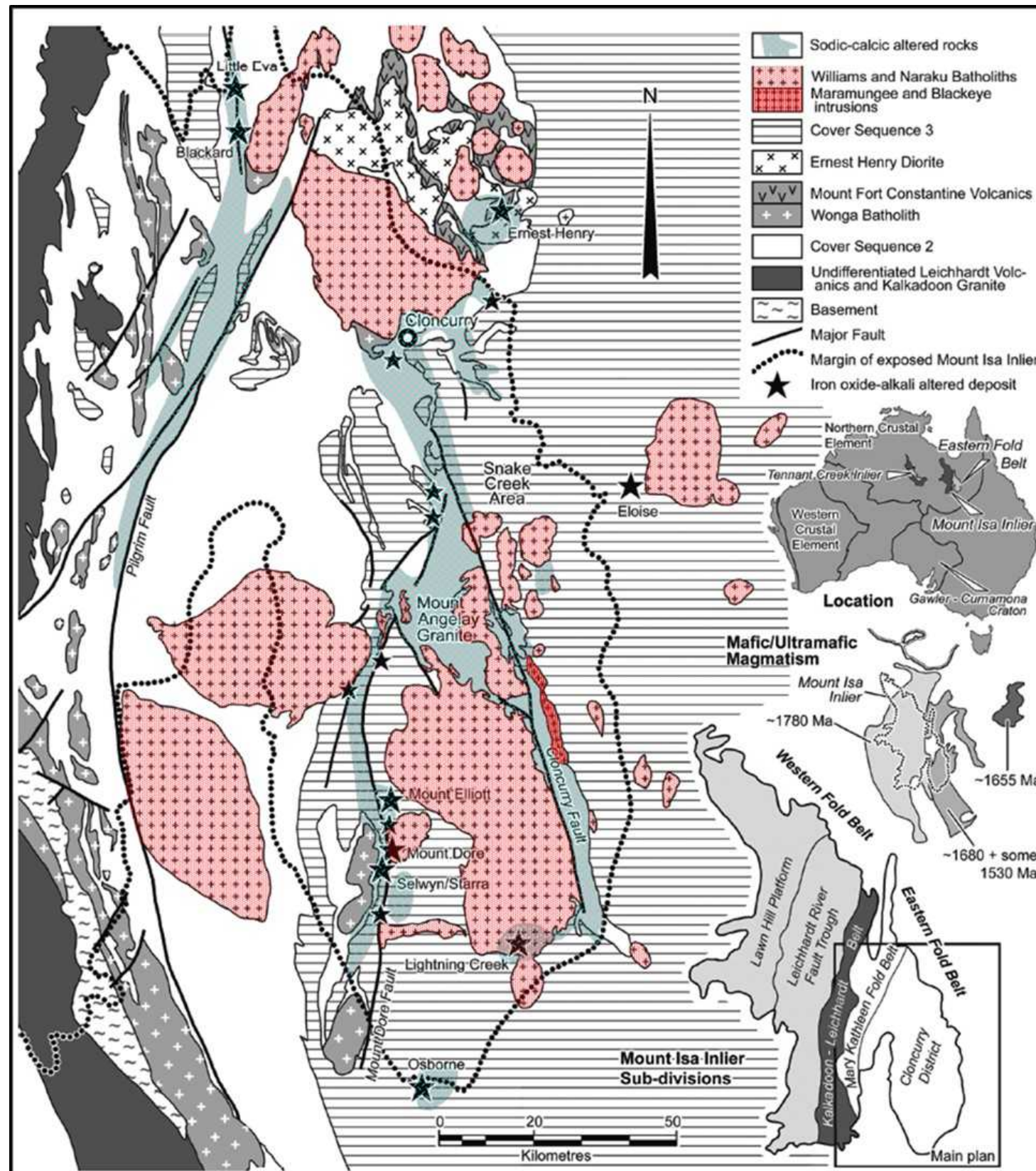


**Figure 2.4:** Location of major IOCG mineralisation, Na-Ca alteration and WILLIAMS Suite granitoids in the Cloncurry Belt. Map adapted from Porter (2010) and includes interpretations from Foster & Austin (2008), Kendrick et al. (2008), Mark et al. (2005) and Oliver (2005)

to surface waters or contemporaneous basinal waters.

Interpretation of the Central Andean IOCG belt (Chen, 2010) highlights the significant changes associated with

the transition from 'barren' iron oxide-potassic assemblages to more oxidised, mineralised assemblages. These include magnetite transitioning to hematite; decreasing temperature; increasing sulphides, increase in

**Table 2.3:** Fluid systematics for the 3 main stages of IOCG formation.

### Regional sodic-calcic alteration

References: Oliver et al. 2004; Porter, 2010; Xavier et al. 2010

Assemblages	albite-scapolite-quartz-(actinolite-apatite-titanite)
Temperature	450-600°C
Salinity	high, Na/K ~10-20
Pressure	200-400MPa
$\delta\text{O}$ , $\delta\text{D}$ fluids	non-discriminatory; overlap with magmatic field

### Potassic-Iron metasomatism

References: Xavier et al. (2010); Haywood & Skirrow (2010); Williams et al. (2005); Porter (2010)

Assemblages	magnetite-biotite-K feldspar-(actinolite-apatite)
Temperature	500-600°C
Salinity	hypersaline brine, >30-70 wt%NaCleq
Br/Cl	variable: magmatic; upper limit of mantle/magmatic to significant bittern brine contribution
$\delta\text{O}$ fluids	variable: often overlaps with magmatic field, to heavy & indicative of basinal/bittern brine contribution
$\delta\text{S}$ fluids	variable: 0 (magmatic), heavy (basinal/bittern brine input), light (local sulphur input)

### Copper-gold mineralisation

References: Chen (2010); Xavier et al. (2008, 2010); Rusk et al. (2010); Haywood & Skirrow (2010); Williams et al. (2005, 2010); Porter (2010)

Assemblages	magnetite-hematite-bornite-chalcopyrite-pyrite-(biotite-K feldspar-sericite-chlorite-pyrrhotite)
Temperature	cooler; 100-300°C
Pressures	130-370MPa (Ernest Henry)
Salinity	variably diluted brine; 1-25 wt% NaCl eq
Br/Cl	variable: mix of magmatic & evaporitic/bittern
$^{40}\text{Ar}/^{36}\text{Ar}$	variable: mix of magmatic & evaporitic
$\delta^{11}\text{B}$	tourmaline; mix of marine evaporate and magmatic
$\delta\text{O}$ fluids	wide range
$\delta\text{S}$ fluids	wide range: dependant on $\text{SO}_4/\text{H}_2\text{S}$ of mixing fluids & host sulphur sources

$\delta S_{\text{fluids}}$ ; increase in  $\delta O_{\text{fluids}}$ .

Chen (2010) ascribes an early, commonly Cu-Au 'barren', magnetite-potassic alteration to magmatic-dominated fluids, and argues that the isotopic data suggests that an oxidised, evaporite-sourced, basinal brine or seawater is likely an important contributor to the 'later' mineralisation phase. Sillitoe (2003) conceded the possibility of "inadvertent" seawater circulation or evaporate dissolution contributions; he favoured a purely magmatic origin for the Andean IOCG deposits ... no doubt prior to significant isotopic investigation.

In some IOCG systems, the 'late', oxidised mineralising fluid is understood. However, less clearly understood is the nature and source of the high temperature, hypersaline brine that scavenges and transports the selective metal suites that ultimately form the IOCG deposit. Two end-members of the hot hypersaline brine origin are thought to have either a magmatic origin, or be formational (surface or buried) / bittern / evaporitic in origin. The reality however, is mixtures of the different deep-seated, end-member, hypersaline components with or without the development (and preservation) of 'late' surficial input. These different fluid mixes, together with different structural and host lithology controls drive the huge diversity of individual members of the 'IOCG' clan.

Five different sources and types of hypersaline brine involved in IOCG formation have been detailed by Porter (2010). Varying levels of support from current research exist for the following brines:

### 1. Fractionating, mantle-derived intrusion exsolution

- At Moho, or in lower-middle crust;
- CO<sub>2</sub>-rich, H, O, C, S-bearing; LREE source (Groves et al. 2010);
- Evidenced by abundant calcite with mantle-like C isotopic signature;
- Phalaborwa, deeply-derived, alkaline magmatism...IOCG fringe dweller?

### 2. Intermediate-felsic batholithic volatile brine exsolution

- Product of anorogenic- and mantle-derived magma mixing;
- Variable mantle contributions...from minor (Hiltaba Suite) to almost entire (Andean IOCG Belt).

### 3. High temperature metamorphism

- Driven by high heat flow regime from mantle-derived intrusion in the lower-middle crust;

- Formational fluids and mineral lattice brine release
  - Largely to accommodate syn-metamorphic origin of Osborne (Gauthier et al. 2001; but see Chapter 4 for dating issues).
- #### 4. Sedimentary evaporitic formation
- Salinity scavenged from buried, formational evaporitic packages by circulating fluids;
  - Low Br/Cl;
  - Dominant process in Cloncurry Na-Ca alteration (Kendrick et al. 2008);
  - Barton & Johnson (2004, 2015) championed model.
- #### 5. Surface-derived, bittern brine
- Surficial evaporitic basin fluids drawn into intrusion-driven fluid circulation cell;
  - Extensional environments, e.g. Andean IOCG Belt with back-arc evaporitic basin(s);
  - Barton & Johnson (2004, 2015) championed model.

## IOCG Process Models & Essential Ingredients

The huge diversity that exists in the 'IOCG' group of deposits has received significant attention from many different researchers. Reflecting the more recent understanding of fluid sources and potential circulation pathways scavenging metals from different crustal sources, Figure 2.5 presents schematic end-member IOCG models. In reality however, blends of end-members and components are likely within single systems. Additionally, IOCG deposits may be formed in hybrid systems with either coeval or superimposed contributions from different deep-seated (hyper-)saline brines.

Williams et al. (2010) highlight the (current) inability of sophisticated geochemistry to resolve the sources of the key ore components in an IOCG system. This is further compounded by the variety of fluid sources and pathways that are represented in different IOCG systems and models. In cases where metal contributions from synchronous and linked magmatism is evident, it is rarely clear whether the metal came from a hypersaline, volatile-rich phase evolved from magma, or was leached from previously consolidated rocks by other circulating hypersaline brines (Williams et al. 2010). This represents a potentially critical uncertainty in compiling regional 3D ingredient requirements for a productive IOCG system.

Nevertheless, several critical features of IOCG systems are

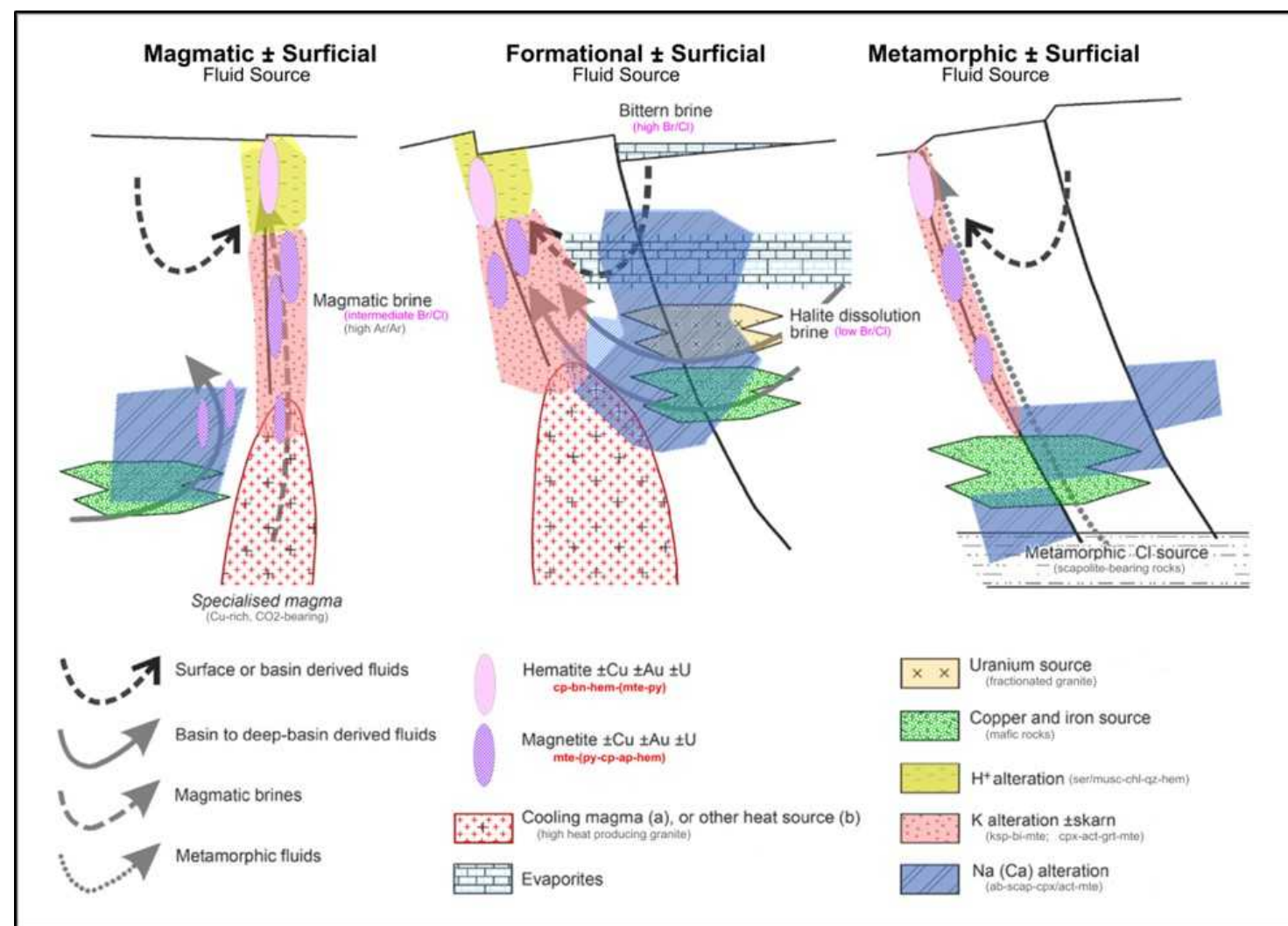


**Figure 2.5:** Schematic end-member models of IOCG formation highlighting the diverse range of fluid system permutations. Figure originally produced by Barton & Johnson (2004) and subsequently modified by Williams et al. (2005) and Williams et al. (2010) incorporating source rock concepts of Hayes et al. (1995), Williams (1994) and Hitzman & Valenta (2005).

becoming clearer, and should be incorporated into a robust targeting and prospectivity analysis:

1. Primary fluid systems that are regional in scale, high temperature and have extreme metal-scavenging ability (i.e. they are hypersaline). The scale and character of the fluid circulation system, combined with the brittle crustal setting of metal deposition causes frequent and widespread 'leakage', resulting in widely-developed, low tonnage mineral occurrence 'smoke' in IOCG districts. If not recognised, this feature in particular can rapidly deplete exploration funds.
2. Cool, oxidised, surficial fluids may have interacted with more deeply-sourced, high temperature, hypersaline fluids, producing high grade ore in many deposits. Deeper systems may not involve cool, surficial fluid interaction. However it is rare for the fluid input to be dominated by a magmatic source. Instead, other non-magmatic fluids play a role. The associated alteration mineral assemblages and oxide/sulphide mixes in IOCG systems can consequently

be highly variable. This diversity needs to be appreciated in geochemical and geophysical exploration planning.

3. The hypersaline IOCG fluids likely have salts contributed by evaporitic sources; either surficial (bitterns, drawn down into circulation), formational (in the path of circulation) or metamorphic (either in the path of circulation or via metamorphic release). The main area of contention is the relative contribution of magmatic components (as a source of minor and trace metals) to evaporite-derived hypersaline fluids. The evaporite or basinal evaporitic fluids are generally considered to be an essential ingredient. However in some older Proterozoic and Archean districts, the evaporitic components are either not readily identifiable or are contentious. In the Cloncurry district, metamorphosed evaporites have been suggested as being able to contribute significant salts to circulating IOCG fluids (Williams, 2014; but see Chapter 4).

4. Metal sources remain contentious. The large, hypersaline, granitic batholith-driven circulation systems provide opportunity for effective metal leaching from a wide variety of crustal rocks. Whilst only circumstantial evidence links economic metals in IOCG deposits to particular sources, mafic rocks are regarded as likely sources of metals, particularly Cu and Au. An older mafic package can be leached by circulating IOCG brines. Alternatively, the mafic input can be a contemporaneous mafic intrusive associated with the granitic batholith or in a thick, mixed mafic-intermediate-(felsic) extrusive volcanic-volcanogenic pile, that is leached by circulating brines.

## DMQ Global IOCG Database

The DMQ Global IOCG Database has been made available as a digital file in Appendix 10.

Major deposits in the following districts have been researched and reviewed: Carajas Province (Brazil); Central Andean Belt (Chile & Peru); Kaapvaal Craton; Gawler Craton; Eastern Fold Belt-Mt Isa Inlier; North America; Southeast Missouri and Tennant Creek Inlier.

The compiled characteristics include:

<b>Deposit</b>	Name; district; ownership; Lat-Long location
<b>Mining</b>	Economic commodities; minor commodities; pre-mining resource; contained metal; initial depth to resource; dimensions; orebody form; mining method; mining history
<b>Geology</b>	Mineralisation style; host sequence; host lithology; structural control; ore mineralogy; ore zonation; alteration mineralogy (paragenesis); alteration extent; metamorphic grade
<b>Geochron</b>	Host rock age; metamorphism age; mineralisation age; linked intrusive age
<b>Discovery</b>	Year of discovery; discovery method; discovery company
<b>Fluids</b>	Salinity; temperature; pressure; Br/Cl; $\delta O$ ;

## DMQ Southern Cloncurry District Analysis

### Introduction

The Deep Mining Queensland Project has focused on a region south of the Cloncurry township to south of Osborne Mine; a region is approximately 8,740sqkm in area (Figure 3.1). The project area is highly endowed with Cu-Au (-Mo) mines and resources and forms part of the richly-endowed Mount Isa Eastern Fold Belt that boasts world class Ag-Pb-Zn deposits (Cannington), Cu-Au deposits (Ernest Henry, Osborne, Rocklands, Starra) and a U deposit (Mary Kathleen) and many smaller resources that have been historically mined or remain in pre-feasibility status awaiting favourable economics and/or brownfields extension.

Deposit	Tonnes	Cu %	Au ppm	Mo %	Re ppm
<b>Ernest Henry</b>	220,000,000	1.1	0.5		
<b>Osborne</b>	36,000,000	2.0	1.0		
<b>Kulthor</b>	12,800,000	1.5	1.0		
<b>SWAN</b> (resource)	375,000,000	0.4	0.3		
<b>Mt Elliott</b>	2,900,000	3.3	1.5		
<b>Mt Dore</b> (resource)	86,500,000	0.6	0.1		
<b>Merlin</b> (resource)	6,400,000			1.5	26
<b>Starra 222</b>	15,500,000	0.6	1.0		
<b>Starra 244</b>	1,650,000	0.7	2.6		
<b>Starra 251</b>	5,040,000	2.3	3.9		
<b>Starra 257</b>	2,800,000	0.7	3.3		
<b>Starra 276</b>	4,300,000	2.7	1.2		
<b>Eloise</b>	3,100,000	5.5	1.4		

**Table 3.0** Historic and current Cu-Au-Mo Resources in the Cloncurry Region

Figure 3.1 highlights the two-fold exploration challenge in the region. Firstly, that existing mined and/or mineable resources were either discovered in the Proterozoic outcropping areas or under relatively shallow cover where the system's geophysical response was substantial and, secondly, that the outcropping Proterozoic is characterised by a multitude of small occurrences ('smoke') that makes focussing on bigger, more robust systems problematic. The region has historically absorbed very significant exploration dollars; much potentially wasted on 'smoke'.

The aim, therefore, of the Deep Mining Queensland Project is to 'sharpen' the targeting tools within the belt. DMQ has taken a two-pronged approach to this 'Prospectivity Analysis' challenge. Firstly the project has endeavoured to developing an understanding of what ingredients characterise the formation of significant resources and to present this 4 dimensionally (3D plus time), in the form of Time-Space tectono-stratigraphic-magmatic understanding, and in detailed 3D geological models that highlight the confluence of mappable essential criteria within the practicably exploreable portions of the near-surface crust.

Secondly, the project has addressed the economic viability issues surrounding mining resources of different grades and geometries discovered at depth whether that be under cover or simply at depth in the exposed Proterozoic terrain. The project seeks to emphasise insightful geometric and process-oriented attributes of significant mineralisation and to provide datasets, geological models and examples that will help explorers focus their activity within the belt towards more highly prospective domains and to increase their understanding of what ingredients and relationships might maximise success.

DMQ's point of difference is its emphasis on process understanding. This applies at a number of levels and scales. At regional scale, a detailed analysis of the geological assembly of the belt highlights important and prospective lithological, package and intrusive relationships, both spatially and temporally; at the camp scale, detailed compilations and interpretations provide insight into the macro-, structural-tectonic and lithological controls on the localisation of mineralisation, and at the mine and resource-scale, detailed (often drillhole-constrained) analyses provide insight into the very local lithological and structural controls that will impact resource domaining and mine design but also highlight what constitutes a drill target.

This Chapter presents many of the above elements of across-scale, process-oriented analysis that underpins the DMQ 4D Geological Model. Chapter 4 extends these relationships into the construction of the DMQ Geological Model on which the Prospectivity Analysis is based.

The major topics covered within Chapter 3 are:

- Updated Time-Space Chart of the Eastern Fold Belt
- Review of Isan Deformation Events and nomenclature
- New DMQ southern Cloncurry Belt Solid Geology
- Tectono-Stratigraphic-Magmatic assembly of the Eastern Fold Belt (full version in Appendix 4) with focus on Cu-Au control
- Pre-orogenic architectures - Origins and Impacts
- Detailed Geology and Controls on Mineralisation at Starra, Merlin-Mount Dore, Mount Elliott-SWAN, Osborne-Kulthor and Ernest Henry
- Essential Ingredients for IOCG/ISCG-style mineralisation

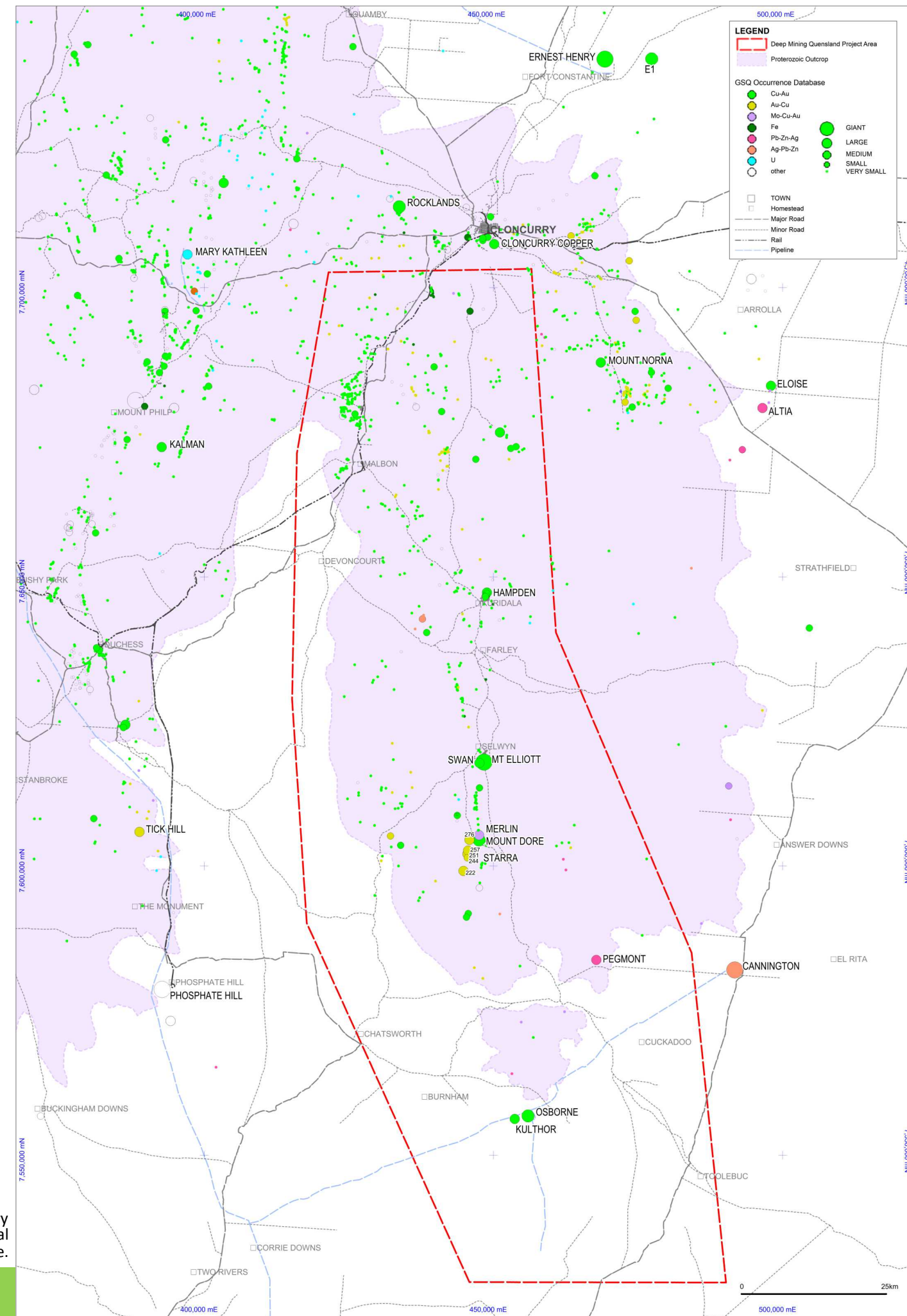
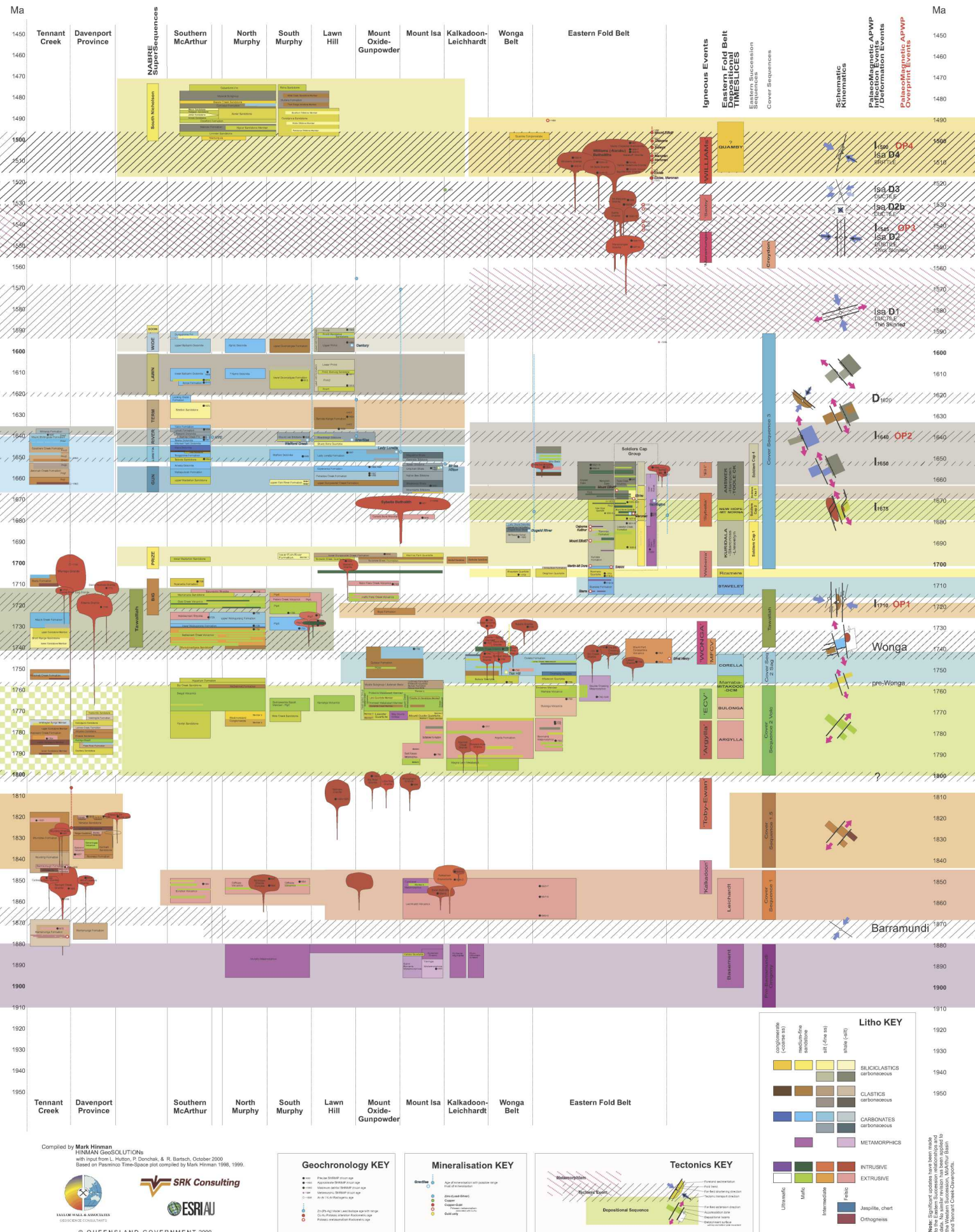


**Figure 3.1** DMQ Project Area in the southern Cloncurry Belt showing extent of Proterozoic outcrop, mineral occurrences and mines, and basic infrastructure.



## Time-Space Relationships

The 2000 NWQMP Time-Space (Tx) Chart has been updated to reflect the current DMQ understanding of package and structural relationships, mineralisation hosts and timing, and the latest geochronology within the Eastern Fold Belt (EFB) where it relates to the DMQ Project area. Data from Withnall & Parsons (2007; 2008), Withnall et al. (2009), Withnall (2016), Duncan et al (2011) and the NWQMEP study (2011) have been invaluable. A GSQ geochronology compilation provided by Ian Withnall has also been very useful.

No attempt has been made to update geochronology beyond the EFB or to refine and update the detailed geochronology pertaining to mineralisation timing (especially IOCG-style mineralisation). Comprehensive compilations of mineralisation timings have been published elsewhere (Duncan et al., 2011). However, the spectrum of mineralisation timings presented in the DMQ-updated NWQMP Tx Chart supports the broad synchronicity of IOCG-style mineralisation with WILLIAMS Suite magmatism. Problems with some past, and much recent, mineralisation timing determinations, especially Re-Os dates, and their significant discord with geological observations will be discussed later in this report (see Osborne-Kulthor section).

The DMQ-EFB updated version of the NWQMP Time-Space (T-x) Chart is presented in Figure 3.2 and accompanies this report in A0 pdf format in Appendix 1. The chart highlights EFB TIMESLICES and Tectonic events and Magmatic episodes that have been used throughout the DMQ analysis and are referred to throughout this report. The DMQ-defined depositional TIMESLICES can incorporate a number of mapped Units/Formations/Members but the available geochronology and/or map relationships support their grouping into particular TIMESLICES. Some mapped Units/Formations have been split between different TIMESLICES on the basis of mapped and interpreted geological relationships (see Solid Geology section in this Chapter and EFB Assembly in Appendix 4). TIMESLICES are referred to in capitals throughout this report (eg. STAVELEY)

Important DMQ modifications and additions made to the EFB Time-Space relationships that contribute to EFB process and evolution understanding are highlighted below ...

- The exhumed higher grade, Double Crossing Metamorphics are time equivalent of the Marraba Volcanics and

**Figure 3.2** DMQ-EFB updated NWQMP Time-Space Chart highlighting package relationships, deformation events, magmatism and their impact on processes of mineralisation

Mitakoodi Quartzite; highlighted by a mafic MARRABA component

- The Doherty Formation and parts of the Corella Formation are excluded from the CORELLA timeslice and are included within the younger STAVELEY package
- The Mount Fort Constantine Volcanics have been removed from CORELLA equivalence and isolated as a potential extrusive volcanic expression of Wonga magmatism in a structurally-isolated basin compartment
- The Staveley Formation is highlighted as a distinct, younger carbonate package (STAVELEY) cf. with the older CORELLA package. No basal STAVELEY has been positively identified and 'basal' STAVELEY appears to be ubiquitously in fault contact with adjacent packages
- The Staveley-Roxmere Quartzite-Kuridala Formations comprise a continuous depositional package. STAVELEY-ROXMERE-KURIDALA transitions are demonstrably in gradational sedimentological contact at Merlin-Mt Dore
- The Roxmere Quartzite (locally 'SQT') at Merlin-Mt Dore (outcrop and drilling) is a cyclically-gradational sedimentary quartzite package which is highly deformed. It is NOT a fault zone .... the so called 'Mount Dore Fault Zone', that has become entrenched in the literature.
- The Roxmere Quartzite, Deighton Quartzite and Knapdale Quartzite at Dugald River are time equivalents and placed in the ROXMERE timeslice
- The Starcross Formation is interpreted to be a broadly time-equivalent variant of the Kuridala Formation and is likely time equivalent with the Llewelyn Creek Formation east of the Cloncurry Fault .... KURIDALA timeslice
- The New Hope Quartzite-Mt Norna Sandstone are time equivalents either side of Cloncurry Fault .... NEW HOPE-MT NORNA timeslice
- The STAVELEY-ROXMERE-KURIDALA-NEW HOPE-MT NORNA succession represents a drowning carbonate system, whose initiation is flagged by the ROXMERE clean clastic inundation, followed by a thick package of turbidites that coarsen and thicken upwards and have an increasing mafic magmatic input in specific domains.

- Coarser NEW HOPE-MT NORNA turbidites flag EFB basin deepening/rifting and are time-equivalent with Sybella intrusion in the Western Fold Belt. Magmatic thermal input into this EFB rift re-activation may flag a 'Hot Rift'

event associated with Ag-Pb-Zn mineralisation at Cannington and Maronan.

- Non-deposition of these STAVELEY-ROXMERE-KURIDALA-NEW HOPE-MT NORNA packages on the exhumed and WONGA-deformed, Double Crossing Metamorphics-Gin Creek Granite (DCM-GCG) block and the MARRABA-MITAKOODI packages further west is indicated.
- Exhumation of the DCM-GCG is hypothesised to result from the little-highlighted, ~1710Ma OP1 Deformation/Orogeny (EW shortening) that, in the Western Fold Belt, also folds the WONGA-extended Eastern Creek Volcanics (tilt blocks) prior to PRIZE and ISA SUPERBASIN deposition (NWQMP, 2000)
- Deep water Answer Slate-Toole Creek Volcanics accumulation reflects post rift, basin foundering perhaps associated with 'hot rift' thermal decay .... ANSWER-TOOLE CREEK timeslice.
- Very significant mafic magmatic input into the TOOLE CREEK package east of the Cloncurry Fault is noted.
- Potential ANSWER-TOOLE CREEK onlap to the west has been suggested but all juxtapositioning with older packages appears to be structural ... both D1 and D2.
- Some felsic magmatism associated with the terminal phases of ANSWER TOOLE CREEK foundering is suggested by the time equivalence of the Ernest Henry Diorite, the Tommy Creek Microgranites and possibly the SWAN diorite (although this may be earlier; Chinova date pending)
- The Quamby Conglomerate may reflect a remnant of an important continental, oxidised, ?evaporitic basin that accumulated at surface during WILLIAMS Suite times. It

may be time equivalent with the South Nicholson Basin to the west.

- The deformation events comprising the Isan Orogeny, their kinematics and their nomenclature have been revised and updated to conform with (1) the DMQ analysis of the EFB transitions from ductile to brittle deformation, (2) the relationships of structuring with evolving EFB magmatism, and (3) to conform with common usage in the current literature (see Table 3.2).

## Eastern Fold Belt TIMESLICING

In order to refine understand of the tectono-stratigraphic assembly of the Eastern Fold Belt, as described above, TIMESLICING of the stratigraphic packaging and EVENT tagging of the deformation and magmatic episodes that impact the belt, and the sequential viewing of their geometries and distributions, offers insights into the important architectures of the belt, critical rock relationships and some of the essential ingredients for mineralisation.

The Eastern Fold Belt portion of the Time-Space Chart presented in Figure 3.2 highlights the stratigraphic TIMESLICING, Magmatic episodes and Deformation events that are integral to the evolution of the belt. The following stratigraphic TIMESLICES and MAGMATIC episodes (in capitals) and Deformation Events (lower case) have been used throughout the DMQ analysis and reporting (from oldest to youngest) :

Pre-BARRAMUNDI, Baramundi Orogeny, LEICHARDT, KALKADOON, ARGYLLA, BULONGA, MARRABA-MITAKOODI, CORELLA, Wonga Extension, OP1 Deformation, STAVELEY, ROXMERE, KURIDALA, NEW HOPE-MOUNT NORNA, ANSWER-TOOLE CREEK, Isan D1, Isan D2, MARAMUNGEE, Isan D2b, SAXBY, Isan D3, WILLIAMS, and Isan D4.

## Isan Orogeny Deformation Events

Understanding and nomenclature for the deformation events that constitute the Isan Orogeny has been various and sometimes confusing since the 1980s when early structural-tectonic work on Isan deformation events began to mature. DMQ had initially adopted a simplified scheme in the southern Cloncurry Belt shown in the second column of the Table below (BRC-DMQ, 2015) which did not recognise ductile D3 deformation prior to brittle deformation synchronous with WILLIAMS Suite intrusion. Apart from the notation, the BRC-DMQ 2017 version of Isan Deformation Events follows that of Rubenach et al., (2008).

We have de-emphasised the syn- to early post-depositional, layer-parallel fabrics (generally microstructurally identified and potentially compactional) and utilised D1 to represent significant, thin-skinned, deformation associated with folding (commonly east-west'ish oriented fold axes when unfolded through D2) and north to north-northwest-directed thrusting and ramping ( $\sigma_1$  north-south'ish).

D2 is the major, east-west shortening, mountain building event ( $\sigma_1$  east-west) producing regional, meridional F2 folds and associated with major reverse faults of significant crustal scale and displacement.

D2b reflects orogenic collapse in the relaxation phase following D2. It results in subhorizontal fabrics and local, minor refolding of earlier folds. Importantly,  $\sigma_1$  is subvertical at this time, and  $\sigma_3$  subhorizontal, significantly influencing the geometry of intrusion within the crust at this time and facilitating equidimensional pluton/batholithic emplacement

D3 appears to reflect renewed east-west'ish  $\sigma_1$  with local-

ised variations producing NNW and NNE-trending folds potentially as a function of local heterogeneities.

D4 is expressed as shallower crustal, more brittle deformation driven by NW-directed, NW-SE shortening in the EFB. D4 is entirely post-peak regional metamorphism, so its local expression is significantly dependant on pre-existing metamorphic mineral assemblages. Ductile platy metamorphic lithologies will accommodate D4 deformation on pre-existing fabrics while more massive brittle lithologies will brecciate and potentially allow focus of Cu-Au-Mo mineralising fluids.

D4 structuring exhibits a significant interplay with crustal magmatism at this late Isan orogenic time. DMQ recognises an evolution of deformation style and patterns through D4 time that relate to the timing of structuring with respect to the intruding, crystallising and solidifying WILLIAMS intrusions. They include syn-WILLIAMS D4 strain partitioning, syn-WILLIAMS early D4 Faulting, (syn)-post WILLIAMS late D4 Faulting and post WILLIAMS later D4 Faulting. This series of deformation styles that may not be precisely synchronous everywhere but relate to the crystallisation of local WILLIAMS Suite intrusions and the partitioning of strain around and ultimately through the fully crystallised granites. This progression of deformation styles are outlined in detail below in the Tectono-Stratigraphic-Magmatic Assembly section and Appendix 4.

In D4 time intrusions take thick, sheet-like forms under the influence of the sub-vertical  $\sigma_3$ .

Note that this Deformational Scheme differs from that presented in the earlier 2016 DMQ Technical Reports and Presentations appended to this Report in its treatment of D3 and D4. Handle with care!

Shortening	BRC-DMQ, 2017	BRC-DMQ, 2015	Rubenach et al., 2008	Austin et al., 2008	Giles et al., 2006 a, b	O'Dea et al., 2006	Rubenach & Lewthwaite, 2003	Laing, 1998	Adshead-Bell, 1998	Bell & Hickey, 1998	Bell, 1983; 1991	Rubenach et al., 2008 Metamorphism
			D <sub>bp</sub>		d <sub>1</sub> (1600Ma)		D <sub>1</sub>		D <sub>1</sub>			M <sub>1</sub>
~N-S	D <sub>1</sub>	D <sub>1</sub>	D <sub>1</sub>		d <sub>2</sub> (1600-1580Ma)	D <sub>1</sub> SSE-NNW	D <sub>2</sub>	D <sub>1</sub>		D <sub>1</sub>	D <sub>1</sub>	M <sub>2</sub> highT-modP
~E-W	D <sub>2</sub>	D <sub>2</sub>	D <sub>2a</sub>	D <sub>2</sub>	d <sub>3</sub>	D <sub>2</sub> ESE-WNW	D <sub>3</sub>	D <sub>2</sub>	D <sub>2</sub>	D <sub>2</sub>	D <sub>2</sub>	M <sub>3</sub> highT-highP
sub-vertical	D <sub>2b</sub>	D <sub>2b</sub>	D <sub>2b</sub> topW				D <sub>4</sub>		D <sub>3</sub> topW	D <sub>2.5</sub> topE&W		M <sub>4</sub>
various (local)	D <sub>3</sub>	D <sub>3-4</sub>	D <sub>3</sub> ENE-WSW	D <sub>3</sub> ENE-WSW	d <sub>4</sub>	D <sub>3</sub> E-W	D <sub>5</sub> ENE-WSW		D <sub>4</sub>	D <sub>3</sub> variable	D <sub>3</sub> ENE-WSW	M <sub>5</sub>
~SE-NW	D <sub>4</sub>	D <sub>3-4</sub>	D <sub>4</sub> SE-NW	D <sub>4</sub> SE-NW			D <sub>6</sub> SE-NW	D <sub>3</sub>	D <sub>5</sub>			M <sub>6</sub> vhighT-lowP
	southern EFB	southern EFB	Snake Creek	Cloncurry Fault	SE EFB-Pegmont, Snake Creek	Mitakoodi Culmination	Snake Creek	southern EFB	Starra-Selwyn	Mt Isa, WFB	Mt Isa, WFB	Snake Creek

Table 3.1 Historical nomenclatures of Isan Orogenic Events in different Isa-Cloncurry terrains. The scheme settled on by DMQ for the southern Cloncurry Belt is in the first column; BRC-DMQ, 2017

## Solid Geology Interpretation

The Deep Mining Queensland Project has produced a detailed re-interpretation of the southern Cloncurry Belt Solid Geology (GIS & pdf, Appendix 3). Ultra-detailed geophysics and prospect-scale geology largely provided by Chinova to the project has enabled resolution of relations under cover and/or the clearer imaging of detailed rock and structural relations in areas of complex geology.

Figure 3.2 outlines the extents of GSQ and AGSO 100K mapping that has formed the basis of the re-interpretation, as well as the excellent and detailed historic mapping (*mostly 1970s-1980s*), journal published mapping and previous company interpretations. Because the DMQ area straddles joins between six GSQ 100K Map-Sheets, less-well-resolved relationships along sheet edges and joins in areas of interest have benefited significantly

from re-working and interpretation of the detailed Chinova geophysical and geological data. In particular the detailed (20K, 10K, 5K and 1K) mapping of John Leishman in the 1970s-1980s along the Starra-Mount Dore-Mount Elliott corridor reflect excellent geological insight and have been invaluable.

Figure 3.3 captures the coverages of detailed airborne geophysics that have formed the basis of the DMQ re-interpretation. Figure 3.4 compares the most recent Geoscience Australia (v6, 2015) magnetic data, of around 80m grid resolution, with ultra-detailed, around 10m grid resolution, Chinova data (2010) within the central DMQ area. This comparison underlines the very significant difference in resolution between the regional and Chinova datasets and highlights the significantly higher fidelity interpretation that the Chinova geophysics has made possible. In particular, interpretation of package continuity, package bounding architecture and both regional & fine fault struc-

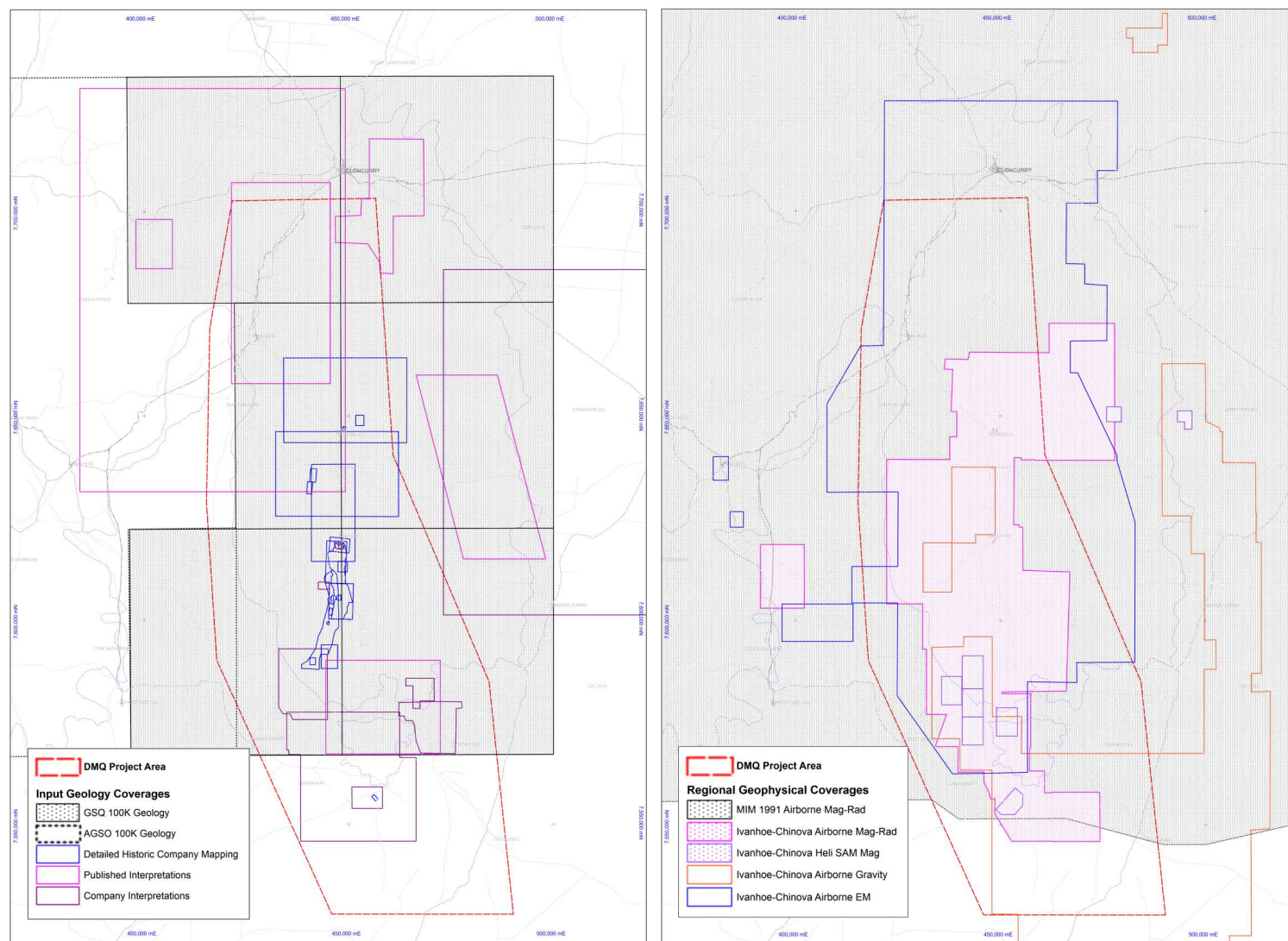


**Figure 3.3** (left) Coverages of government, historic (*mostly 1970s-1980s*) and published mapping as well as previous company interpretations, and (right) coverages of airborne geophysics (Mag-Rad, Heli SAM, Falcon Gravity & AEM) used and incorporated into the DMQ Solid Geology interpretation

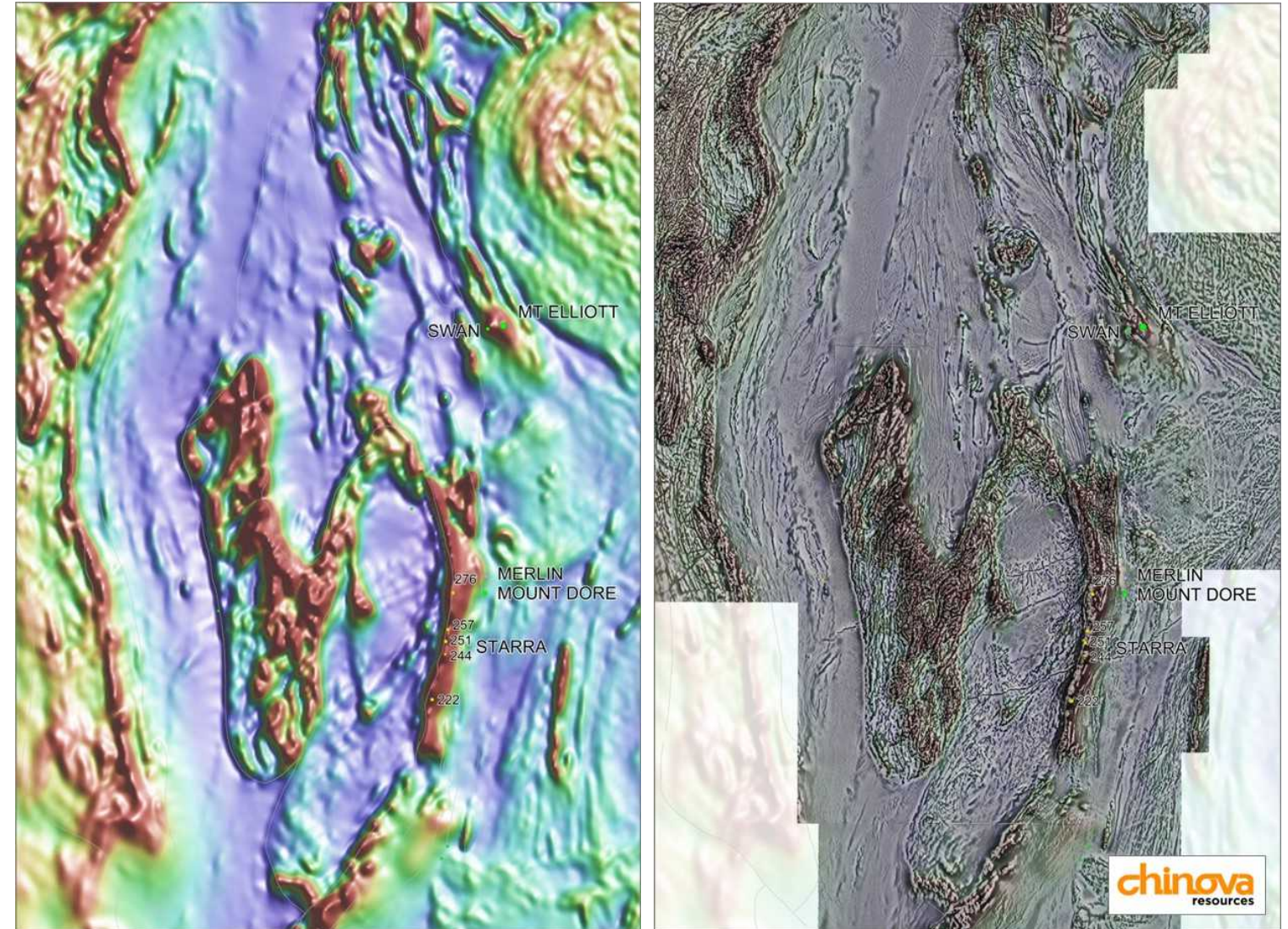


**Figure 3.4** Comparison of 2010 high resolution Chinova vrmi-2vd magnetic data (right) with 2015 GA (v6 grid) Regional tmi-rtp data (left) in the central Selwyn region. Nominal grid resolutions are ~10m and ~80m respectively and highlight how the detailed aero magnetics have enabled a much higher fidelity, tectono-stratigraphic interpretation within the project area.

ture have been significantly enhanced in the DMQ Solid Geology interpretation.

The Proterozoic Solid Geology within the DMQ Project area has been re-interpreted and re-build using the GSQ 100K digital geology maps (including at the time of interpretation in 2015, pre-release coverages for the Selwyn and Mount Angelay areas) as a base. Detailed examples of areas where refined solid geological interpretation have been possible will be presented later in this Chapter. All subsequent maps in this report include all DMQ re-interpretation where the additional Chinova data has allowed significant revision of rock and structural relationships. Areas where additional detailed data was either not available or did not significantly change interpretations remain unrefined from the GSQ 100K interpretation.

## Southern Cloncurry Solid Geology

The finalised DMQ Solid Geology Interpretation is presented in Figure 3.6. A large format (A0) pdf version of the Map is provided in Appendix 3 and Mapinfo digital coverages of the of all the map elements (tectono-stratigraphic TIMESLICES and all of the DMQ structural interpretation and compilations) are provided in Appendix 3 in the form of a Mapinfo Workspace 1Dir which opens the Solid Geology map along with structures, occurrences, detailed compilations, infrastructure, seismic lines, geochronology and the locations of the DMQ cross sections.

This Solid Geology interpretation is well refined within the DMQ Project Area as well as adjacent areas of immediate/critical structural-tectonic-stratigraphic or mineralising importance to the DMQ main game of Prospectivity Analysis in the belt. This interpretation has formed the plan

# Cloncurry District Analysis

view control for forty-seven 4km-spaced serial section interpretations on which the DMQ structural-stratigraphic 4D geological model and Prospectivity Analysis has been built (Chapters 4, 5 and 6). The granite geometries at depth and their morphological interpretation are discussed at length later in Chapter 4.

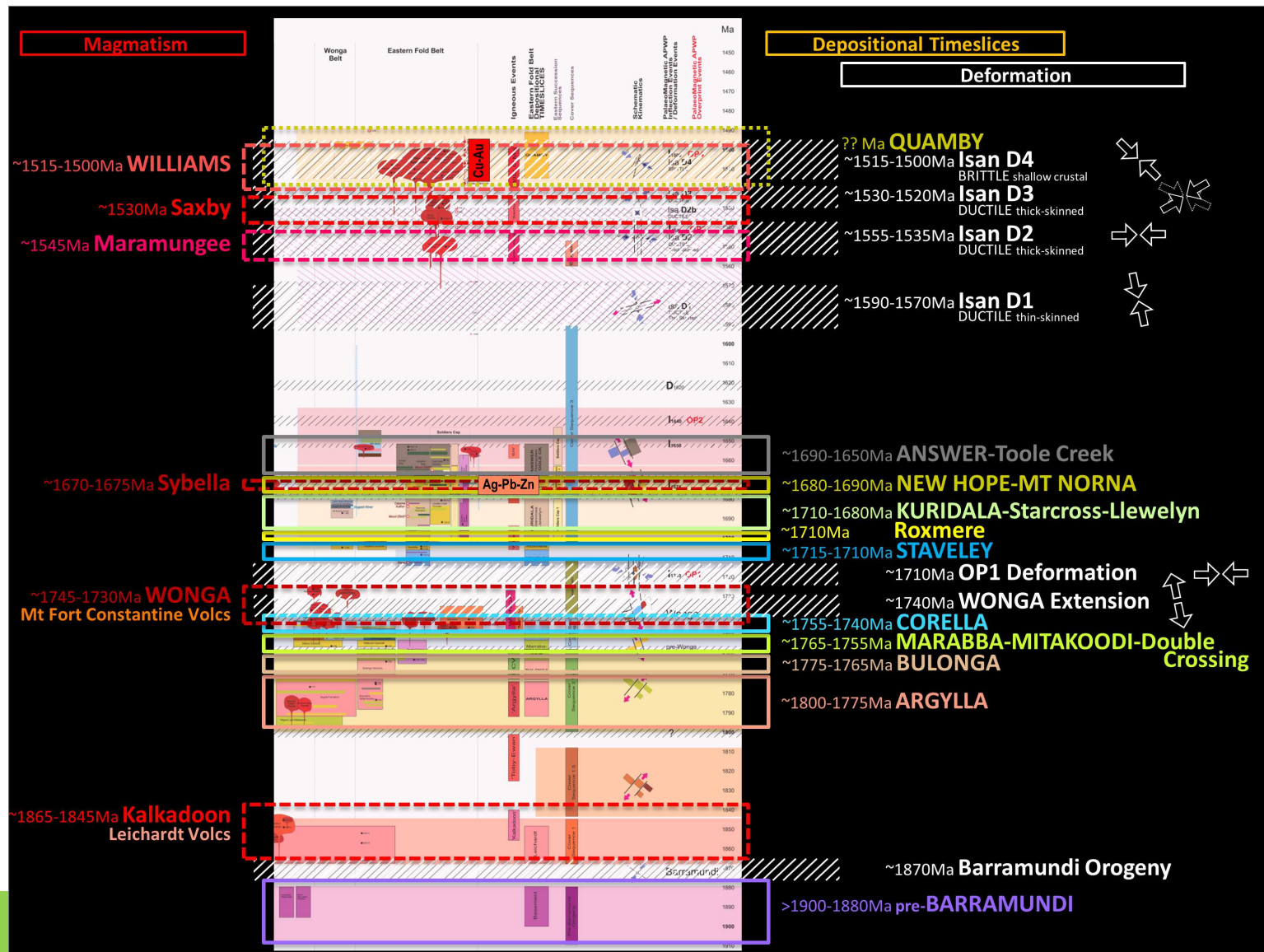
## Tectono-Stratigraphic-Magmatic Assembly of the Eastern Fold Belt

Figure 3.5 is a clipped zoom of the Eastern Fold Belt Time-Space Chart (Figure 3.2) highlighting the TIMESLICES, magmatic episodes and deformation events that are integral to the evolution of the southern Cloncurry Belt. Appendix 4 presents a complete sequence of 29 TIMESLICES and Events from pre-BARRAMUNDI to post-WILLIAMS and post-Isan Orogeny times that encapsulate the tectono-stratigraphic-magmatic and economic mineral development of the belt. Accompanying notes detail stratigraphic units, lithologies and important relationships that speak to

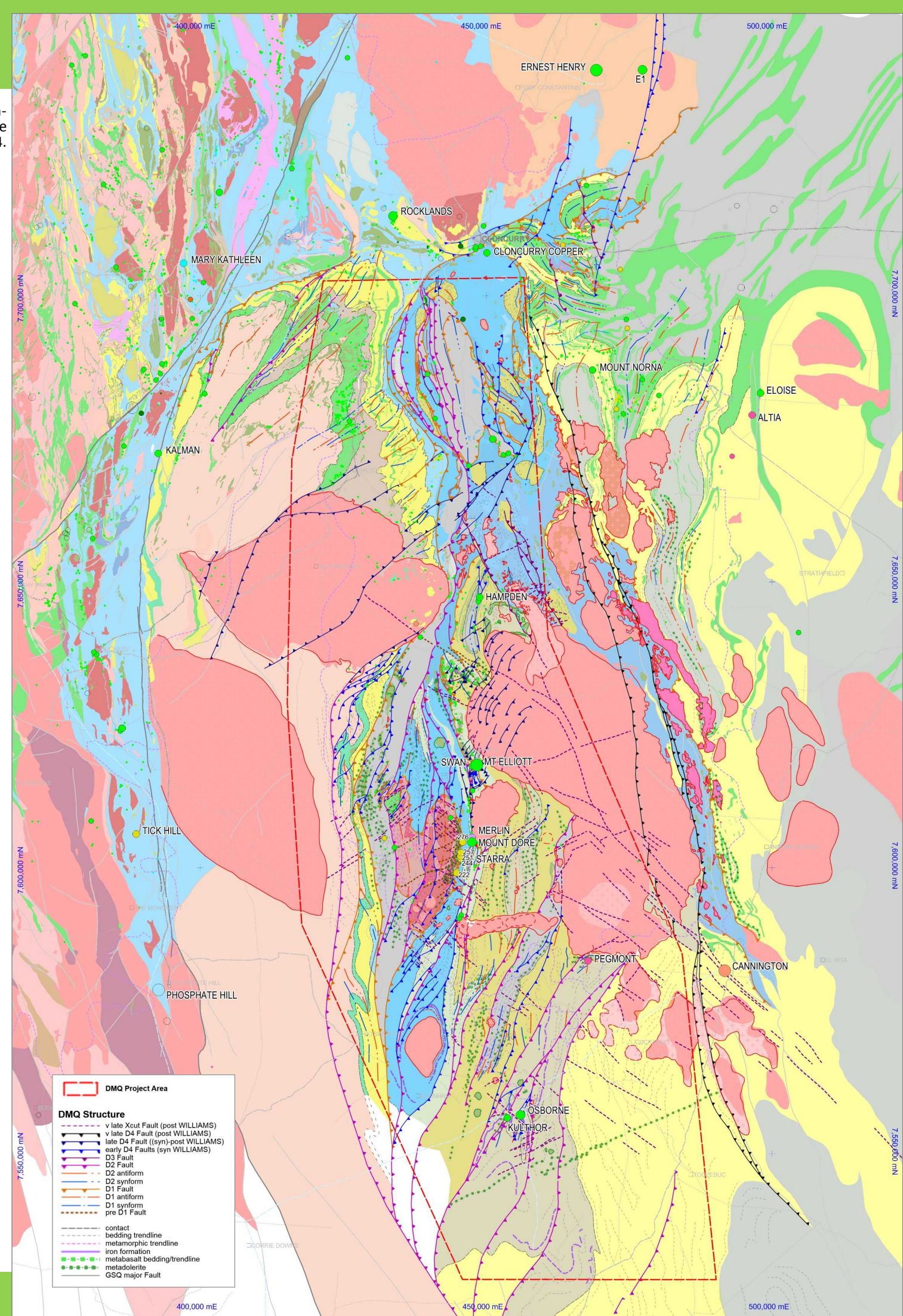
the geodynamic and mineral development within the belt. The sequential integration of these TIMESLICES and Events from ~1900Ma to ~1400Ma produces the rock packaging and structural relationships currently observed and affords considerable insight into the processes implicated in mineralisation of these significantly fertile Palaeo-Meso Proterozoic sequences.

A selection spanning the post-accumulation period after ~1650Ma and the stages of Isan orogeny and magmatism, in particular the WILLIAMS suite intrusion which is integral to IOCG-style Cu-Au-Mo mineralisation within the belt, are reproduced in the following pages along with the clipped EFB Time-Space Chart (Figure 3.5) highlighting the sequential events and their inter-relationships.

**Figure 3.5** Detailed portion of the DMQ Time-Space Chart highlighting the Tectono-Stratigraphic-Magmatic TIMESLICES and Events that are integral to the evolution of the southern Cloncurry Belt.



**Figure 3.6** DMQ Solid Geology Interpretation of the southern Cloncurry Belt. Formational and lithological details of the stratigraphic TIMESLICING is outlined in Appendices 1,2 & 4.



## ~1650Ma End of Accumulation

By around 1650Ma, accumulation in the southern Cloncurry portion of the Eastern Fold Belt had completed. See Appendix 4 for the detailed accumulation, deformation and magmatic history leading up to 1650Ma and associated observations.

Rock relations at 1650Ma incorporated the deformation and magmatic effects of ...

- the **Barramundi Orogeny**, and post-orogenic magmatism
- the **Wonga Extension** including mid-crustal extensional detachments with associated magmatism and possible upper-crustal extensional faulting, tilt blocks and basin compartments (MFCVs and ECVs in WFB)
- significant E-W shortening during the **OP1 Deformation/Orogeny** that in the EFB is implicated in the exhumation of the Double Crossing Metamorphics & Gin Creek Granite to surface or at least to upper crustal levels.

In addition, spatially-focused magmatic input in the form of syn-depositional metadolerite silling is present in the NEW HOPE-MOUNT NORNA and TOOLE CREEK packages.

The following sections of TIMESLICE analysis depicts deformational, magmatic and mineralising events throughout the Isan Orogeny. No structures have been tagged as initiating in Barramundi, Wonga or OP1-time but must necessarily be subtly present.

**In this analysis, faults are highlighted at their interpreted stage of initiation within the Isan Orogeny period.**

Many Isan structures may also have syn-depositional origins which have similarly not been tagged accordingly.

All structures suffer re-activation during subsequent Isan deformational episodes as stress regimes and crustal locations evolve through the orogeny. For simplicity of presentation these reactivations are not explicitly represented but are implicitly assumed to occur.

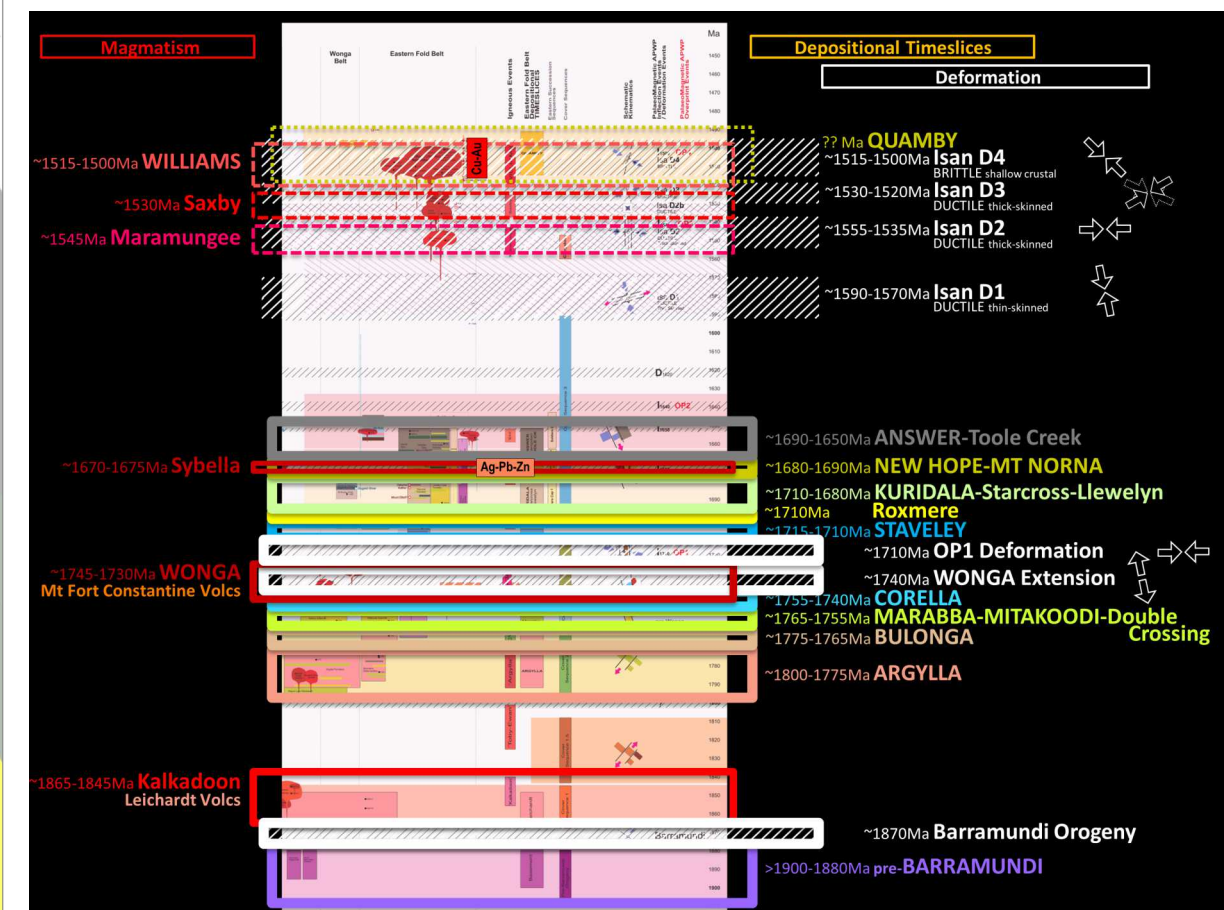
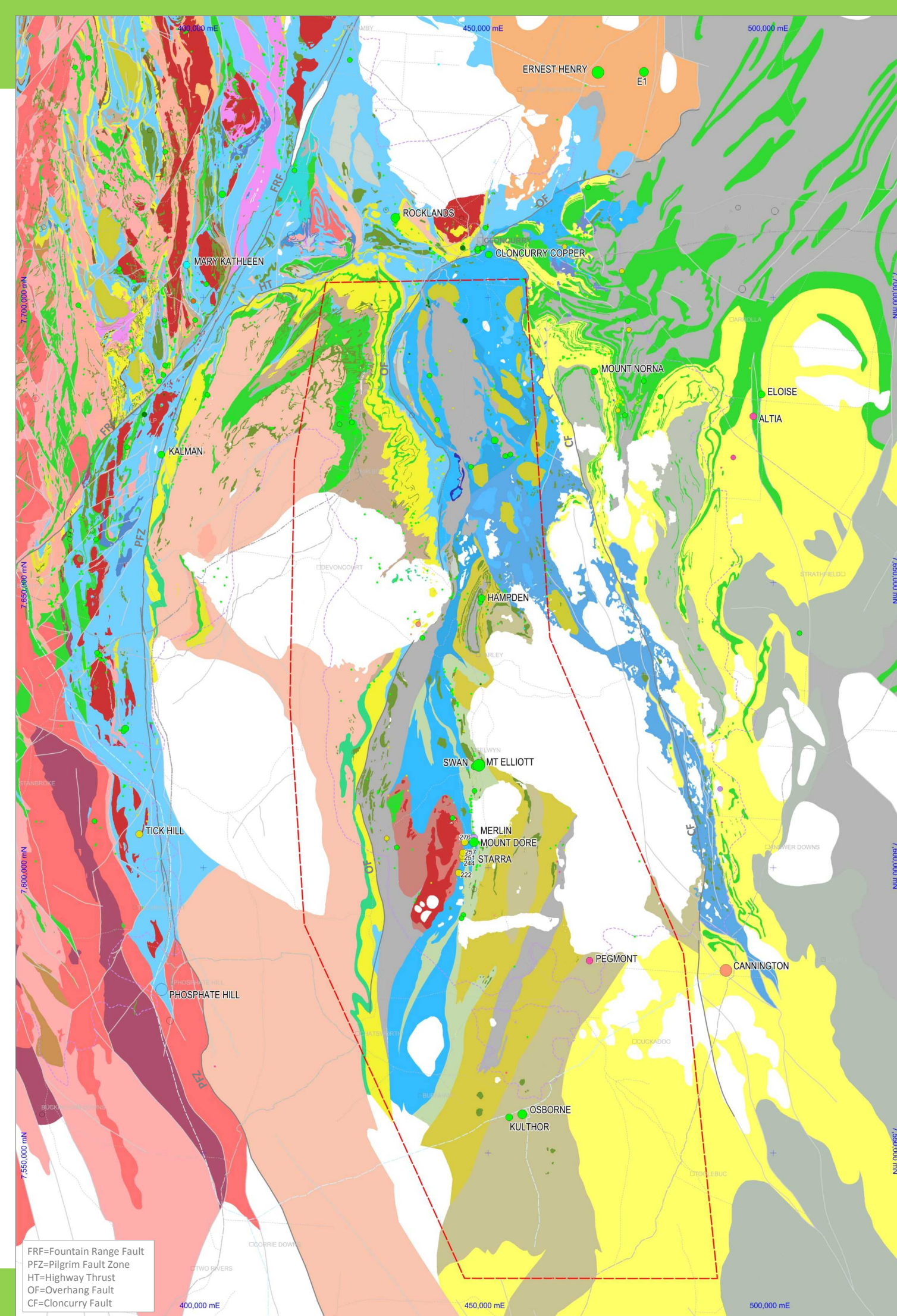


Figure 3.7 ~1650Ma End of Accumulation

## ~1600-1570Ma Thin-skinned, Isan D1 Folding & Thrusting

Thin-skinned Isan D1 characterised by N-S to NNW-SSE shortening with N(NW)-directed movement on major, sub-horizontal thrusts (and potential ramps) and is associated with, locally-preserved and/or identified, significant F1 folding .

- A number of D1 structures have been interpreted by DMQ within the DMQ Project Area: the Overhang Fault including its NE extension, the Starra Shear (following conventional wisdom in the literature, but note alternatives highlighted in STAVELEY timeslice discussion, Appendix 4), the Marimo Thrust and associated structures, and a Mount Elliott-Twiggy Vous-Hampden Fault whose southern extent is obscure.
- In addition the Cloncurry THRUST (as distinct from the Cloncurry FAULT) whose remnants are preserved around later WIL-LIAMS intrusion and are mappable on both sides of the Cloncurry Fault but predominantly to its east in the south, have been assigned to D1. The relationship between D1 folding and a shallow thrust surface north of the Snake Creek Anticline and east of Cloncurry which exposes windows of footwall STAVELEY carbonates suggests this thrust is of D1 timing. East-west'ish D1 folding (folded by D2) is seen to be well developed in this D1 thrust's hanging wall.
- The mapped geometries of thrust discontinuity between footwall STAVELEY and hanging wall TOOLE CREEK east of Cloncurry suggest that the D1 thrust surface may itself be folded in D1 shortening. These geometries may be influenced by their proximity to the NE extension of the Overhang Fault which marks some form of Mount Fort Constantine Volcanic (MFCV) basin margin (perhaps inherited from Barramundi times; see Barramundi & MFCV timeslice discussions, Appendix 4). The MFCV block may act as a buttress in D1-time.
- F1 folding is also well developed in footwall of Overhang Fault (O'Dea et al., 2006) on the west side of the project area.
- Meridional sections of the Cloncurry Thrust to the south as far as Cannington are also now designated D1, in analogous fashion to the D1 Overhang Shear in the west of the belt.
- North-south meridional trends of the southern extensions of the Overhang and Cloncurry Thrusts are rationalised to reflect larger-scale, meridional D2 folding of the earlier flatter-lying D1 structures.
- Many D1 thrusts, folds and linked-ramp structures likely remain unidentified; in particular within highly deformed and metasomatised packages (Marshall, 2003 eg. within the STAVELEY east of the Marimo Syncline).
- Some crustal thickening in D1-time is associated with highTemp-modPress metamorphism (Rubenach et al., 2008)

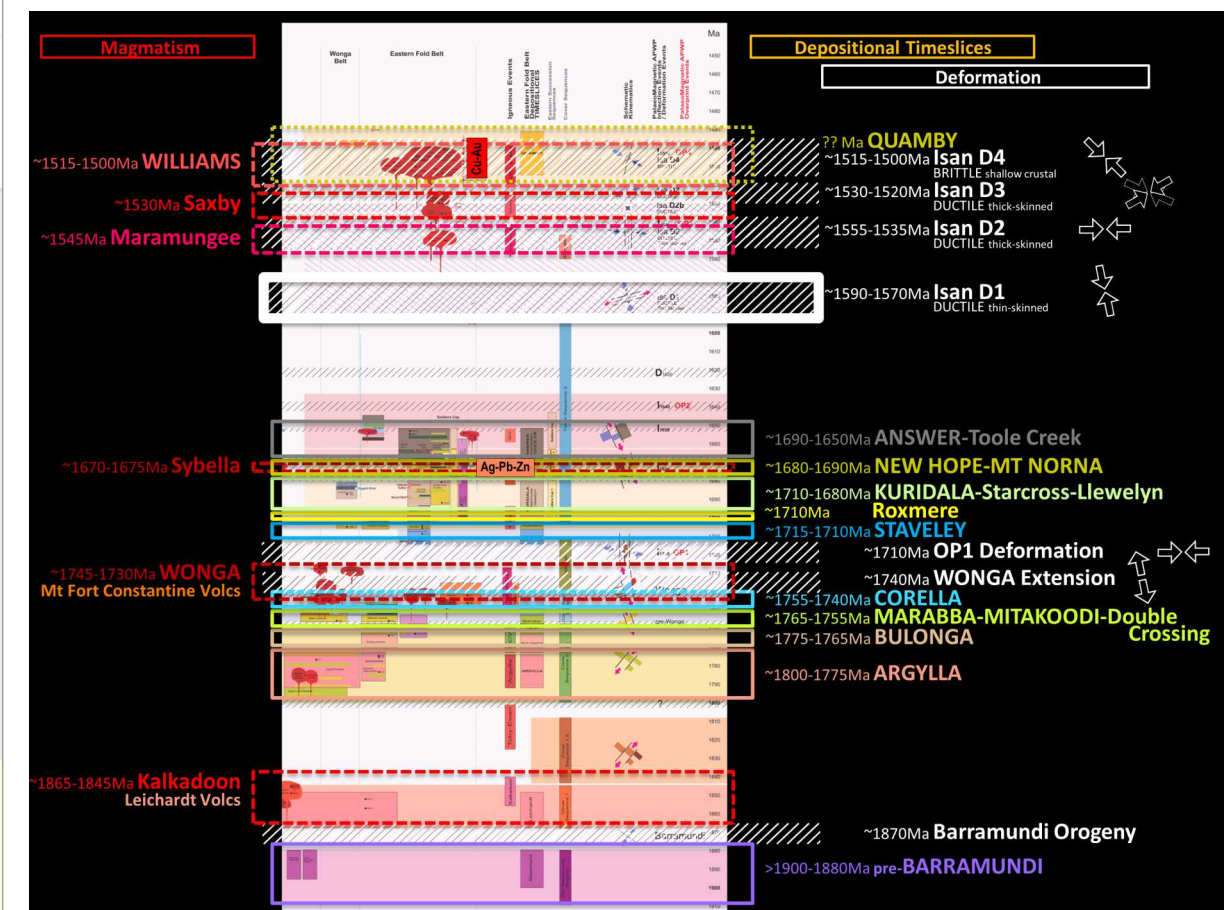
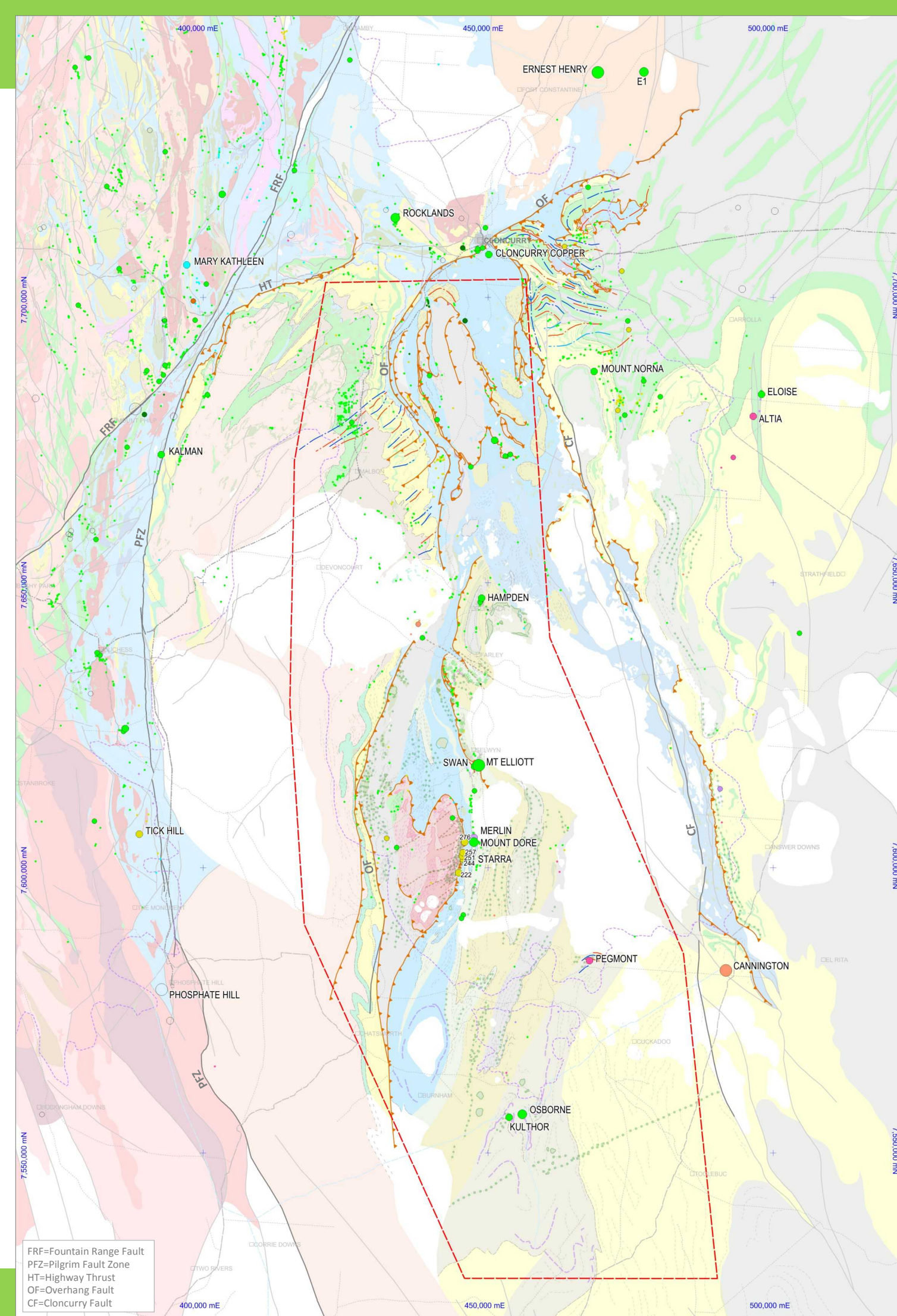


Figure 3.8 ~1600-1570Ma Thin-skinned, Isan D1 Folding & Faulting

## ~1555-1535Ma Thick skinned, Isan D2 Folding

Isan deformation evolves into thick-skinned, mountain-building, D2 orogeny with E-W shortening. Initial Isan D2 folding is characterised by regional-scale, N-S meridional folds of stratigraphy and earlier D1 folds & thrusts.

- Anomalous oriented D2 folding is likely associated with re-activation of older, more fundamental, crustal penetrating and persistent structures. For example, the more NNE-trending Mitakoodi culmination fold axes are likely influenced by a NE-oriented structure which has been multiply re-activated from Barramundi-times (see Isan D1, Wonga-MFCV and Barramundi timeslice discussions).
- Mountain building at D2-time is associated with advancing regional (highTemp-highPress) metamorphism (Rubenach et al., 2008) in a significantly thickening crust.

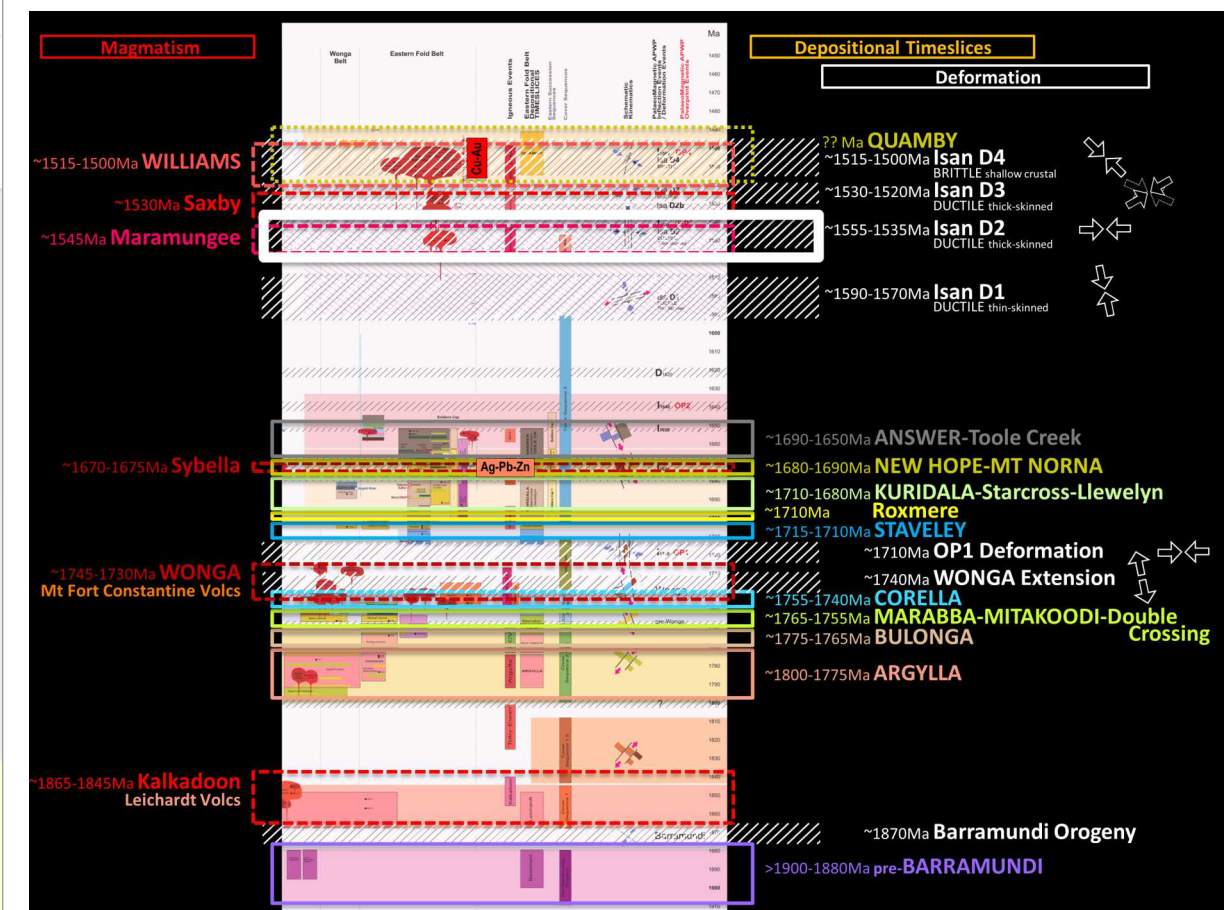
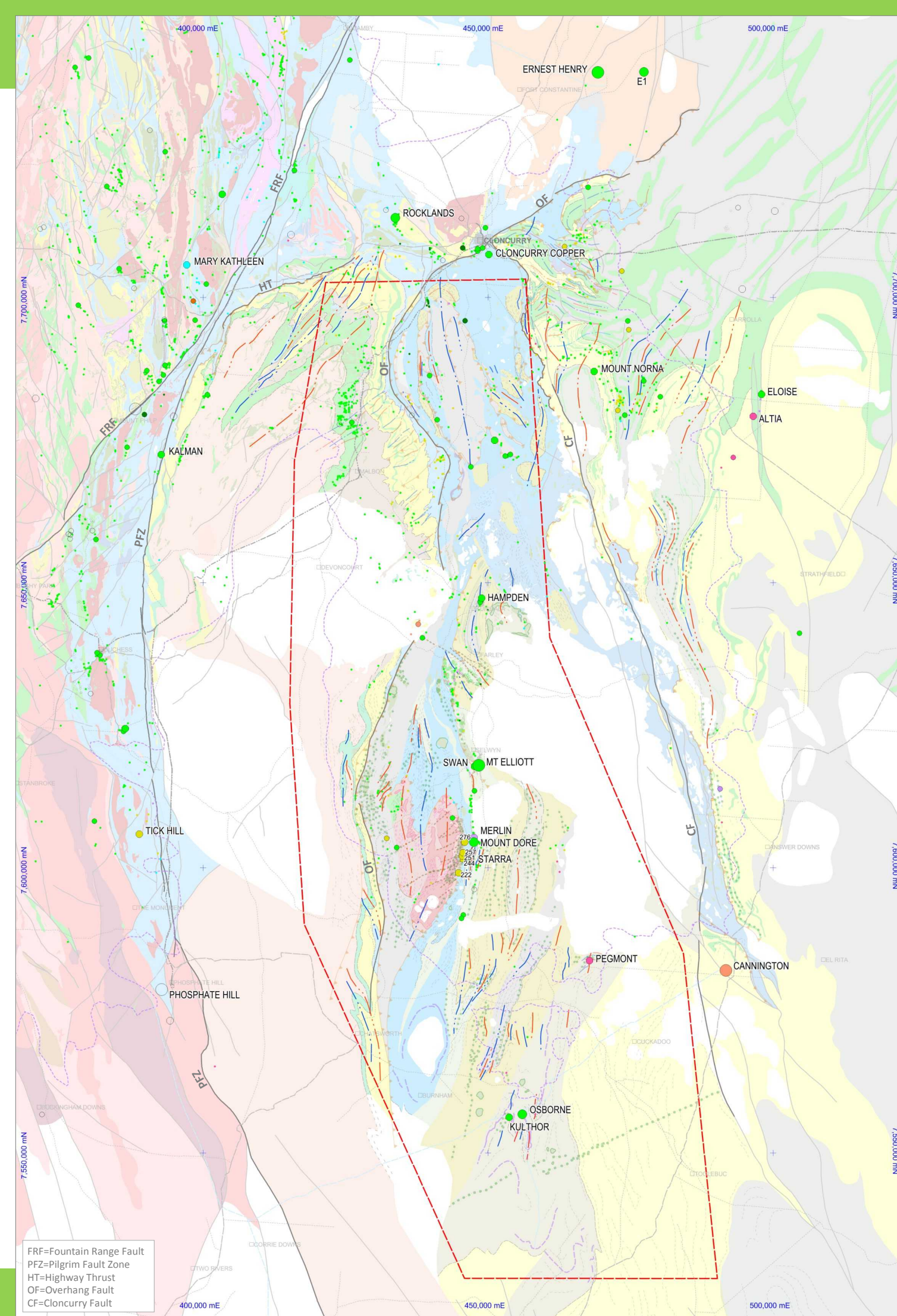


Figure 3.9 ~1555-1535Ma Thick-skinned, Isan D2 Folding

~1555-1535Ma Thick skinned, Isan D2 Faulting  
~1555-1535Ma Maramungee magmatism

Continued D2 shortening is not able to be accommodated by further folding and/or fold tightening and D2 fault failure initiates.

- D2 reverse faults are widespread and are ubiquitously W-vergent (see Sectional interpretations, Appendix 5).
- They have very significant strike lengths and major throws, juxtapositioning packages of contrasting ages and compositions.
- Progressive highTemp-highPress metamorphism at this time yields some syn-deformational intrusives east of the project area ... the Maramungee Suite.

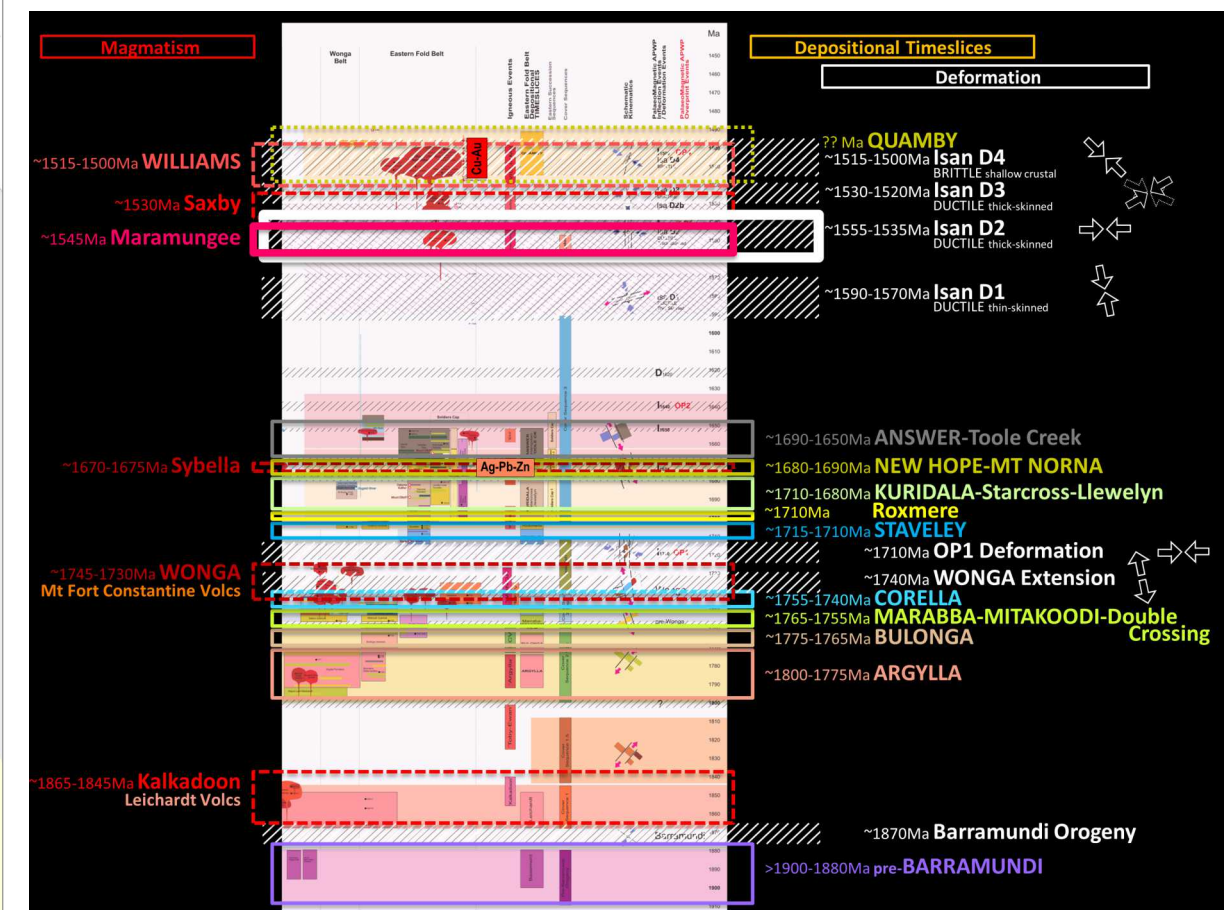
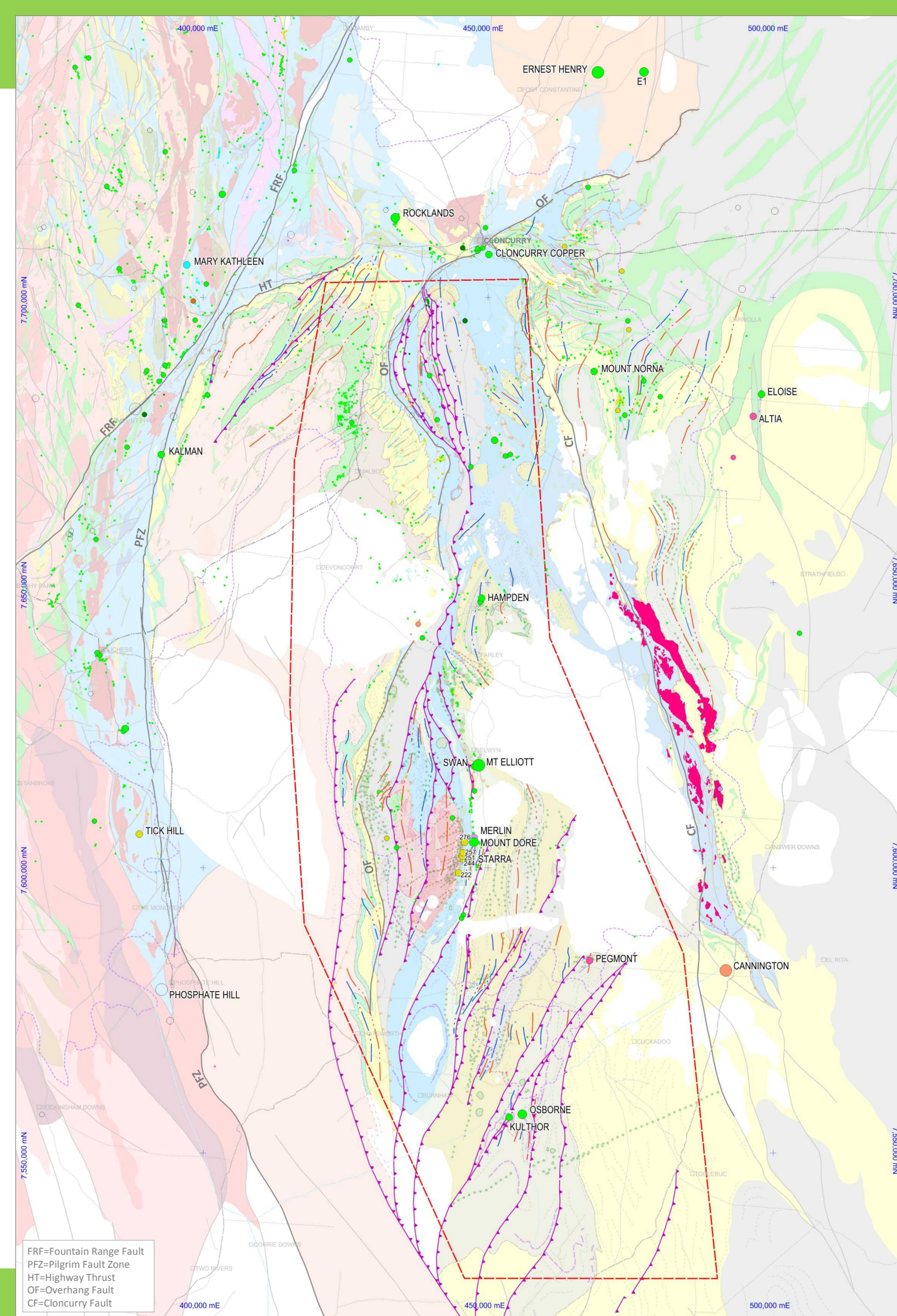


Figure 3.10 ~1555-1535Ma Thick-skinned, Isan D2 Faulting; ~1555-1535Ma Maramungee magmatism

~1535-1530Ma Isan D2b Orogenic Collapse  
~1535-1525Ma Saxby magmatism

In the post-D2 deformation period, orogenic collapse occurs and results in a flip in the regional stress regime to a subvertical  $\sigma_1$  and subhorizontal  $\sigma_3$ .

- This orogenic re-arrangement results in subhorizontal fabrics and localised, minor refolding of earlier folds (Bell & Hickey, 1998; Murphy, 2004). No D2b structures have been identified in the DMQ interpretation.
- Importantly, a subhorizontal  $\sigma_3$  significantly influences the geometry of intrusion within the crust at this time. It facilitates the emplacement of classical, equidimensional, hourglass-shaped, plutons and batholiths. The Saxby and Mount Margaret granites whose geochronology suggests potential synchronicity with D2b, may be plutons intruded under these Isan D2b Orogenic Collapse conditions

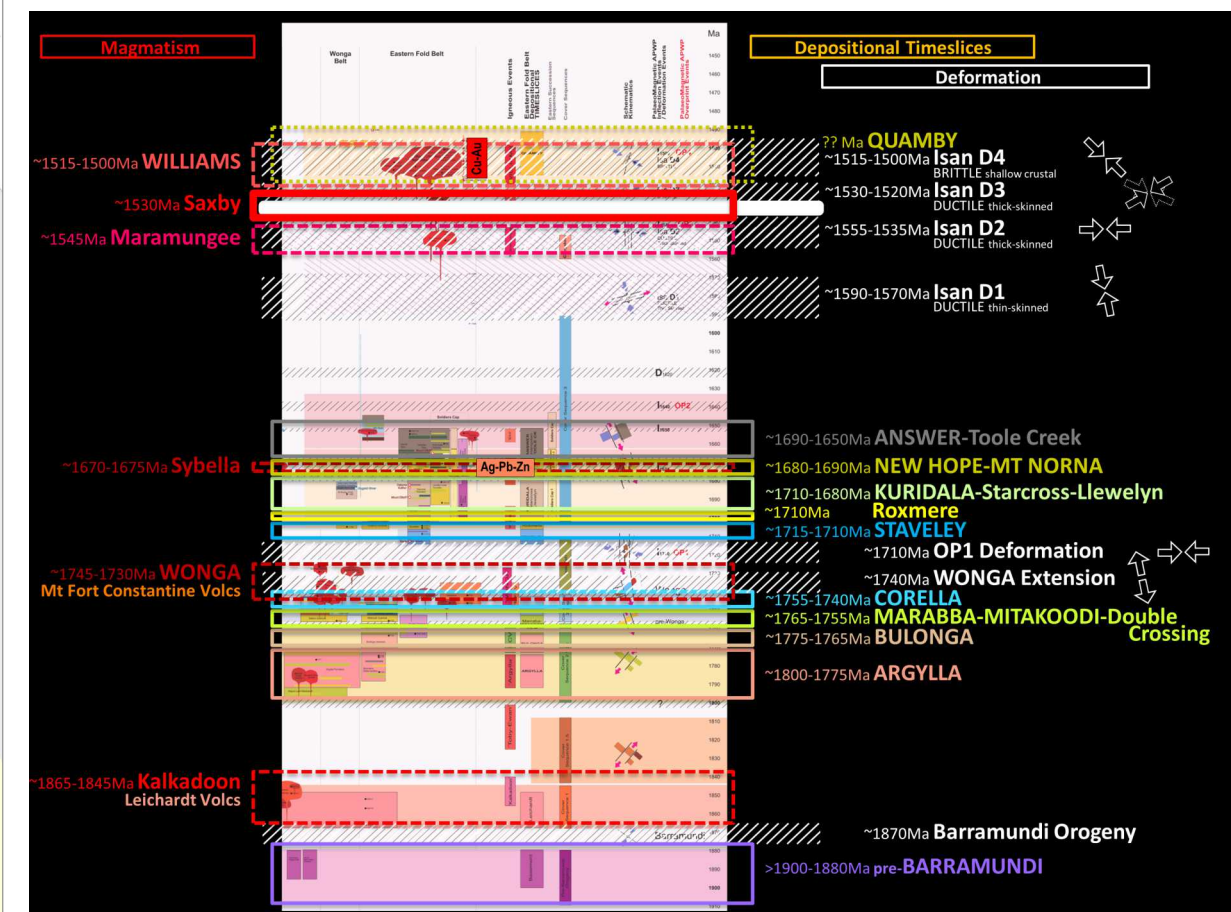
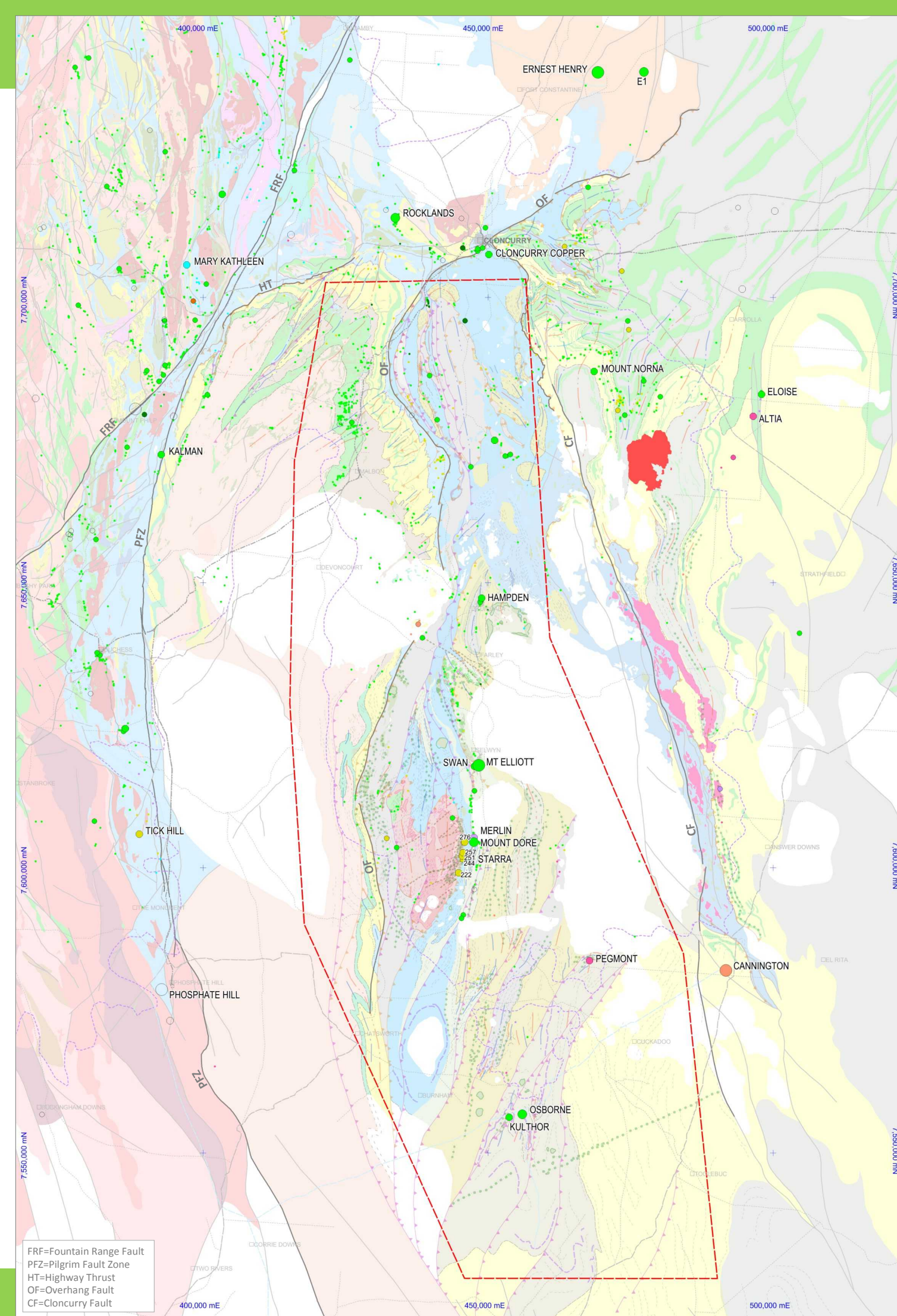


Figure 3.11 ~1535-1530Ma Isan D2b Orogenic Collapse; ~1535-1525Ma Saxby magmatism

## ~1525-1520Ma Isan D3 Faulting

Renewed EW'ish shortening within a significantly thickened crust resulted in continued ductile deformation with significant local variations in structural orientations.

- D3 folding has been identified in detailed mapping exercises in both the Western Succession (Bell, 1983; 1991; Bell & Hickey, 1998; Murphy, 2004) and the EFB (Austin & Blenkinsop, 2008), however, none have been specifically identified in the DMQ regional interpretation.
- D3 fold orientations are variable from NNW to NNE trending. This variation appears to be a result of local heterogeneity during the period of thick crustal shortening resumption in post-D2b time.
- A number of D3 Faults have been identified and tagged in the DMQ interpretation based largely on their cross cutting relationships with D2 folds and their overall orientation. A fault that truncates the northern end of the D2 Hampden Synform (Straight Eight Fault) is pre-Williams and is assign to D3.
- Ongoing metamorphism and partial melting in deep crustal levels at this time generates voluminous magma.

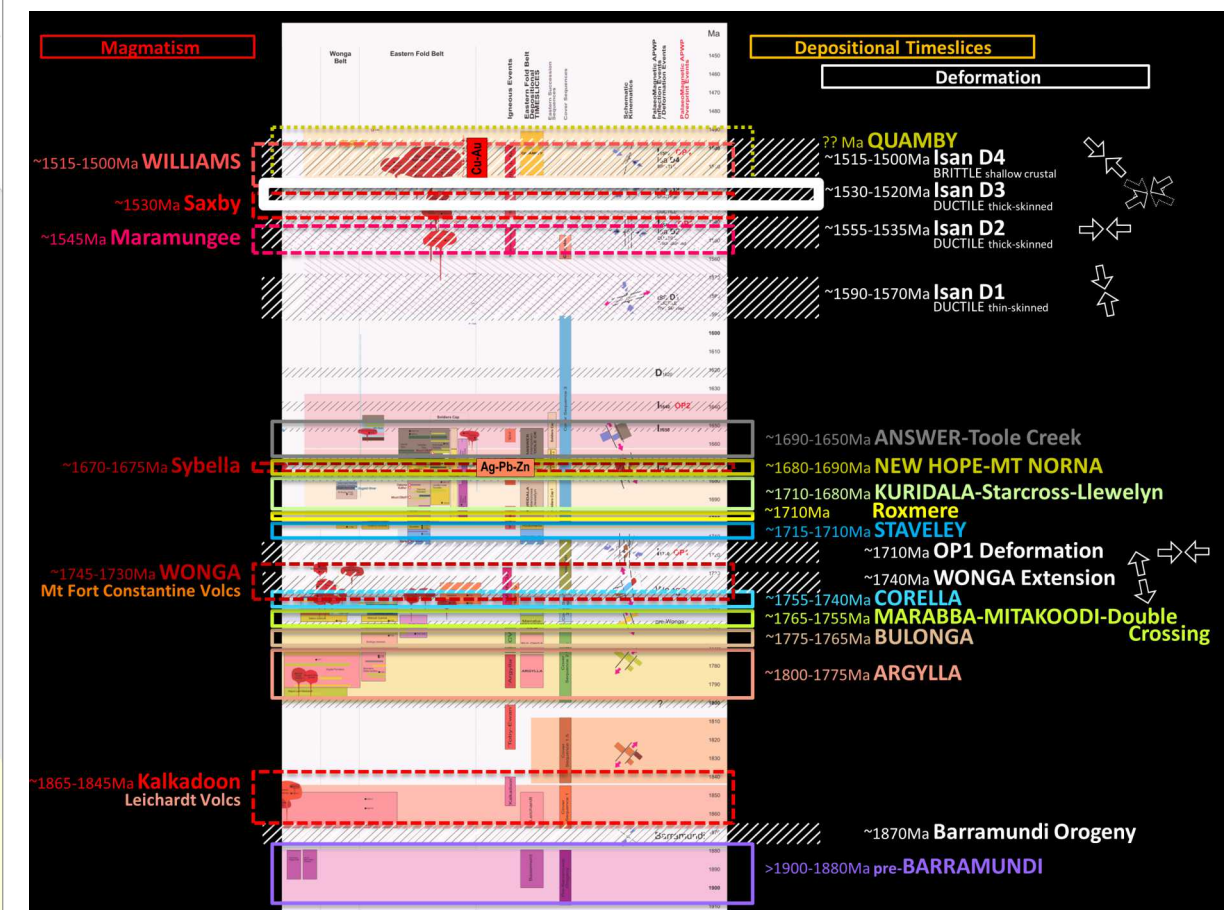
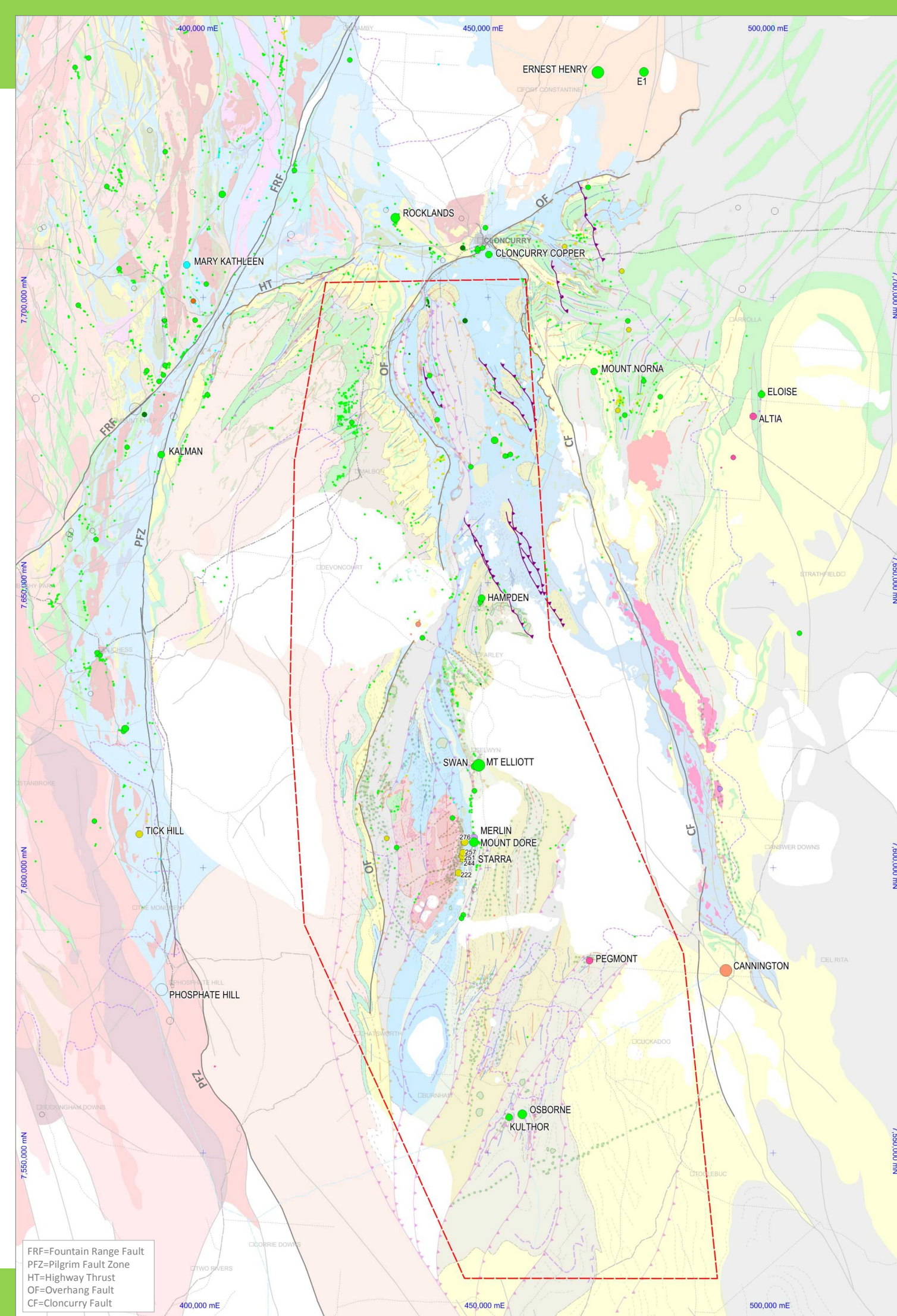


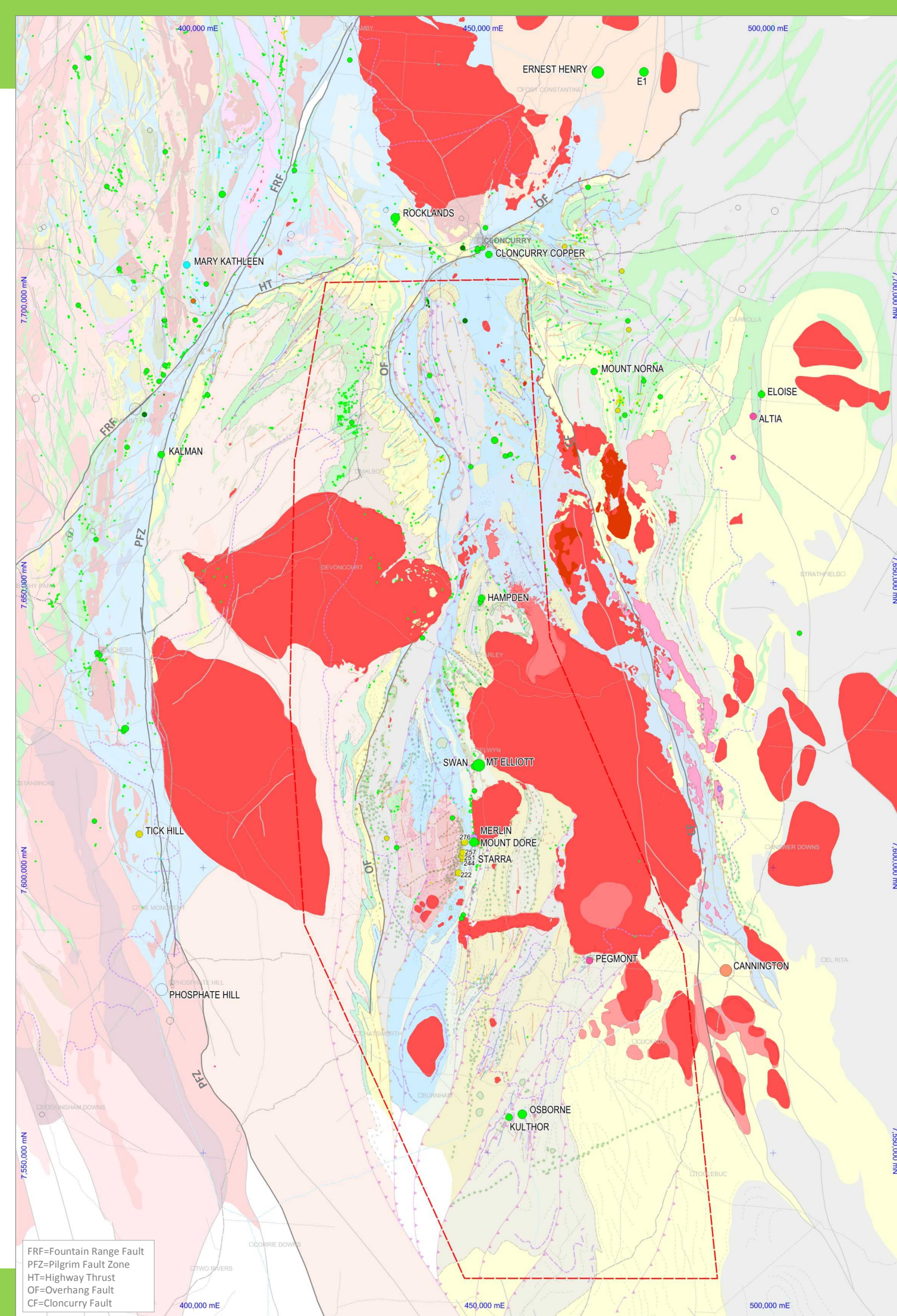
Figure 3.12 ~1525-1520Ma Isan D3 Faulting

~1515-1500Ma early Isan D4 Shortening

~1515-1500Ma **WILLIAMS** magmatism  
(Cu-Au, Au-Cu, Mo-Cu)

By 1510Ma, WILLIAMS Suite intrusion into the middle and upper crust is well advanced under conditions of D4 NW-SE shortening.

- Shallower crustal levels of WILLIAMS intrusion (compared with preceding D2-D3 ductile deformation events) promote brittle deformation where amenable lithologies are present. Strongly foliated, moderate to high grade metamorphic lithologies continue to accommodate D4 deformation by slip on pre-existing fabrics where appropriately oriented with respect to shortening.
- Intrusions take thick, sheet-like forms under the influence of a subvertical  $\sigma_3$  at this time.
- As shortening proceeds, strain partitioning around crystallising granites, results in early fracturing and brecciation in appropriate rock types that potentially focuses early, circulating mineralising fluids forming IOCG-style Cu-Au, Au-Cu, Mo-Cu mineralisation.



FRF=Fountain Range Fault  
PFZ=Pilgrim Fault Zone  
HT=Highway Thrust  
OF=Overhang Fault  
CF=Cloncurry Fault

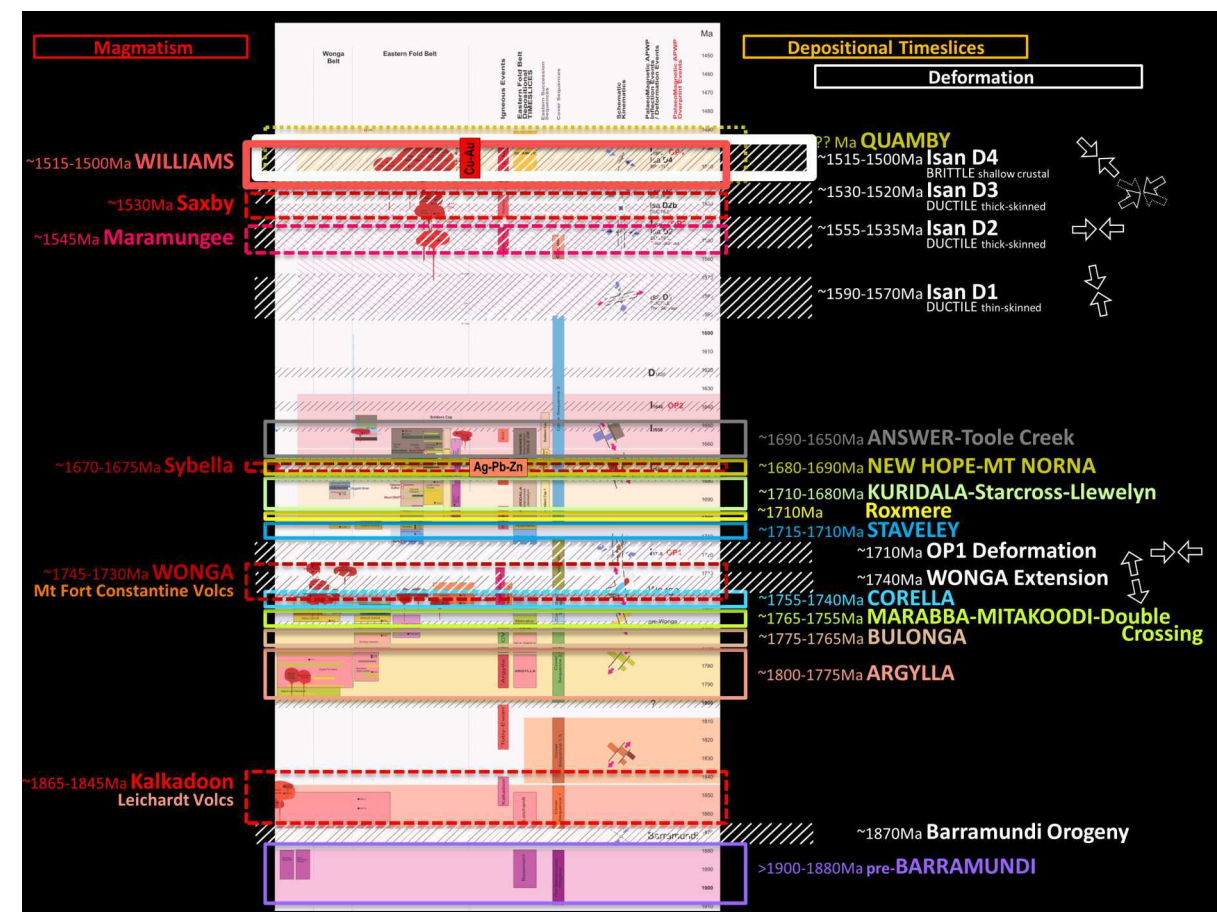
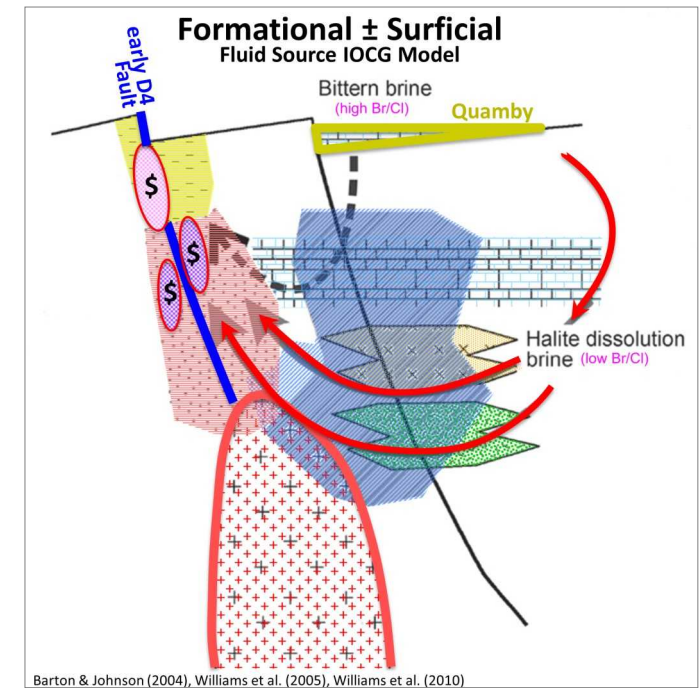


Figure 3.13 ~1515-1500Ma early Isan D4 Shortening; ~1515-1500Ma WILLIAMS magmatism ; (Cu-Au, Au-Cu, Mo-Cu)

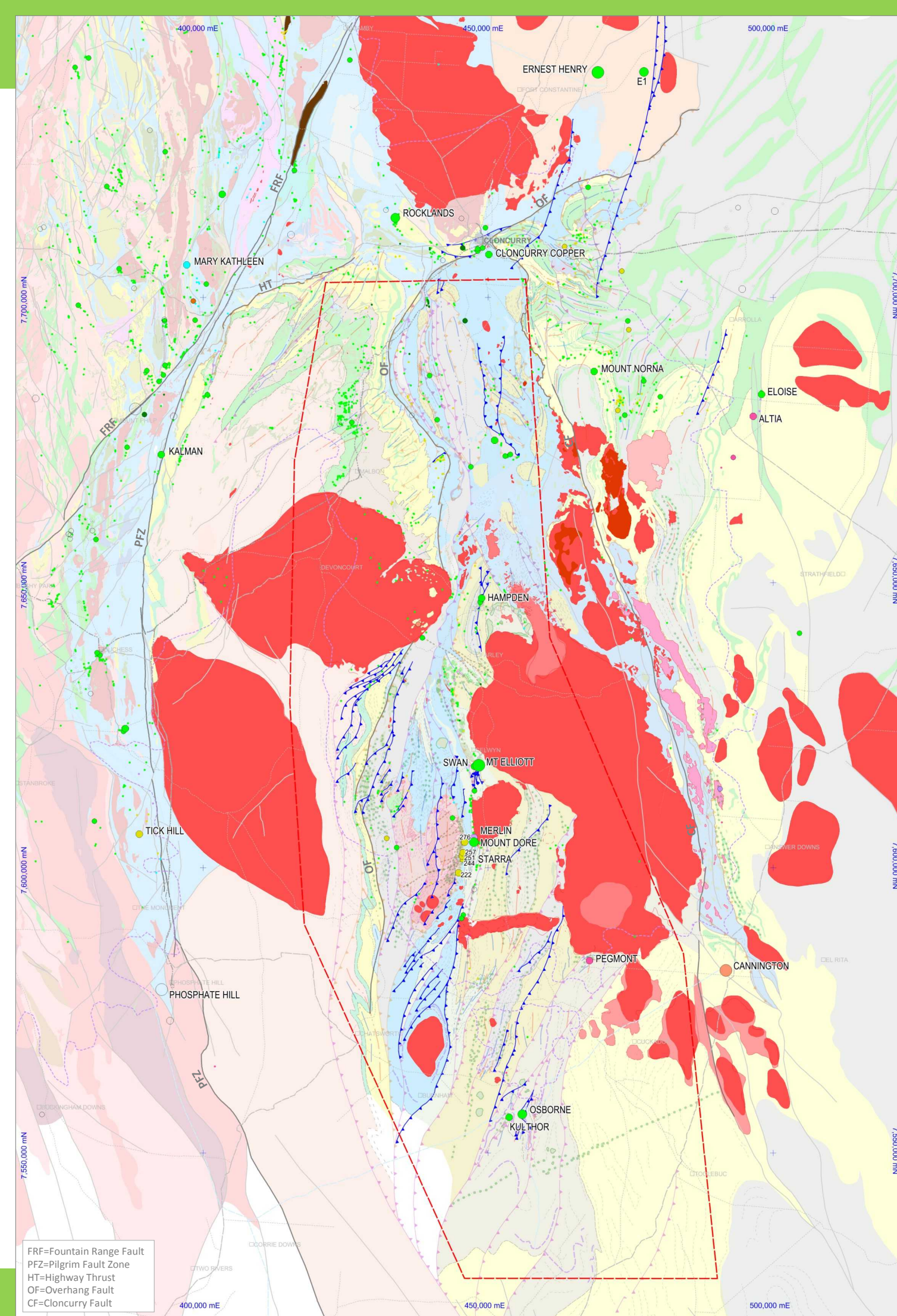


~1515-1500Ma **early Isan D4 Faulting**  
 ~1515-1500Ma **WILLIAMS magmatism**  
**Cu-Au, Au-Cu, Mo-Cu**  
 ~????Ma **QUAMBY**

- Scant geochronology on monazite (Evins et al., 2007) suggests the Quamby Conglomerate may be a remnant of an overlying or sub-adjacent continental clastic basin that is accumulating synchronously with WILLIAMS intrusion at depth in the underlying middle to upper crust.
- As such, the Quamby Basin may potentially contribute an oxidised brine to the IOCG systems in the crust beneath it.
- Formational salinity in the CORELLA & STAVELEY carbonate packages at depth are unlikely to contribute significant salinity to the IOCG systems due to its prior entrainment in peak metamorphic mineral assemblages.
- The Quamby Conglomerate is likely a time equivalent of the South Nicholson Basin formed to the northwest with similar post-Isan orogeny timing.



Barton & Johnson (2004), Williams et al. (2005), Williams et al. (2010)



FRF=Fountain Range Fault  
 PFZ=Pilgrim Fault Zone  
 HT=Highway Thrust  
 OF=Overhang Fault  
 CF=Cloncurry Fault

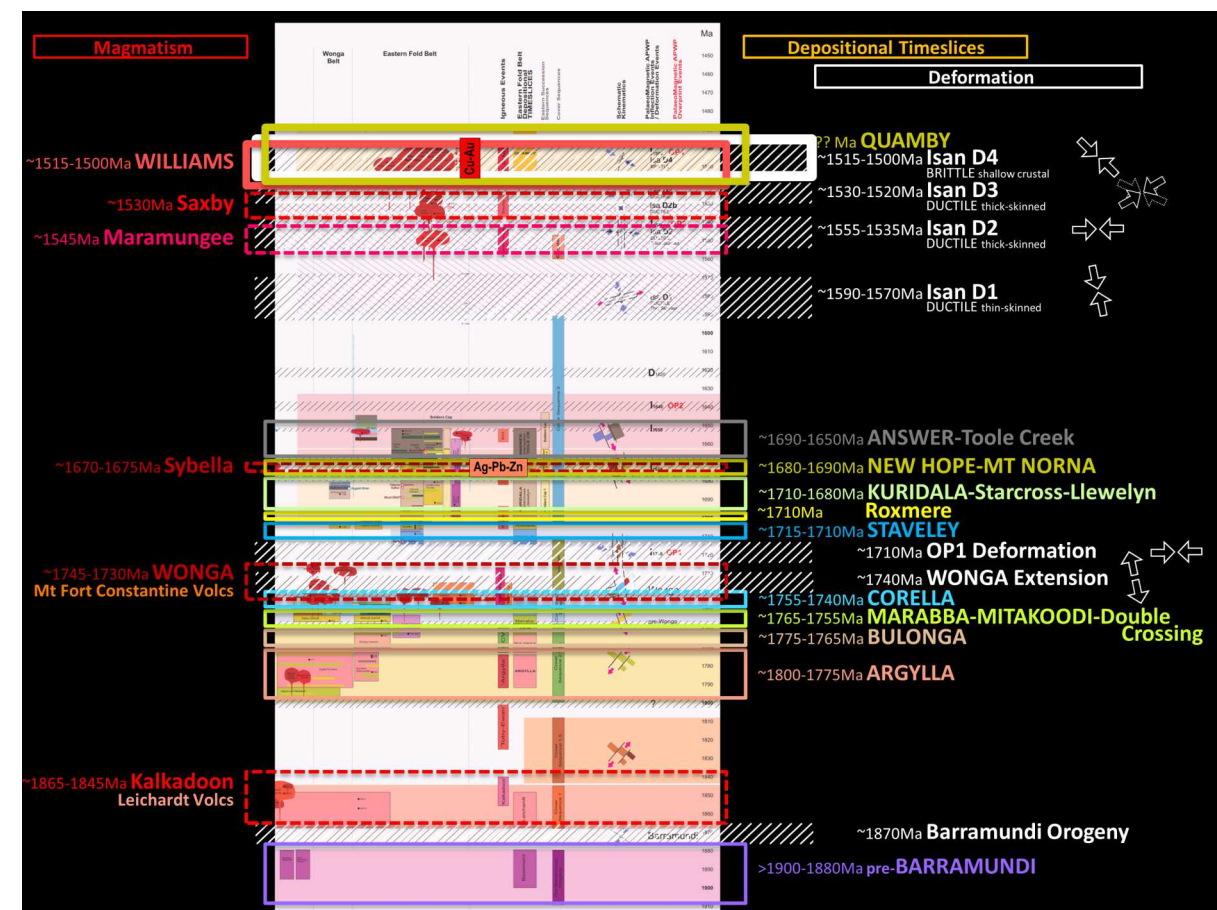


Figure 3.15 ~1515-1500Ma early Isan D4 Faulting; ~1515-1500Ma WILLIAMS magmatism ; Cu-Au, Au-Cu, Mo-Cu; QUAMBY

## ~1500-1495Ma late Isan D4 Faulting (syn)-late WILLIAMS magmatism

When the granites have substantially solidified, either in an ongoing period of D4 shortening, or alternatively, in a post-D4 relaxation phase (as yet unresolved) late D4 Faulting occurs. This phase of faulting demonstrably cuts and deforms previously formed Cu-Au-Mo mineralisation and cuts WILLIAMS-aged granites.

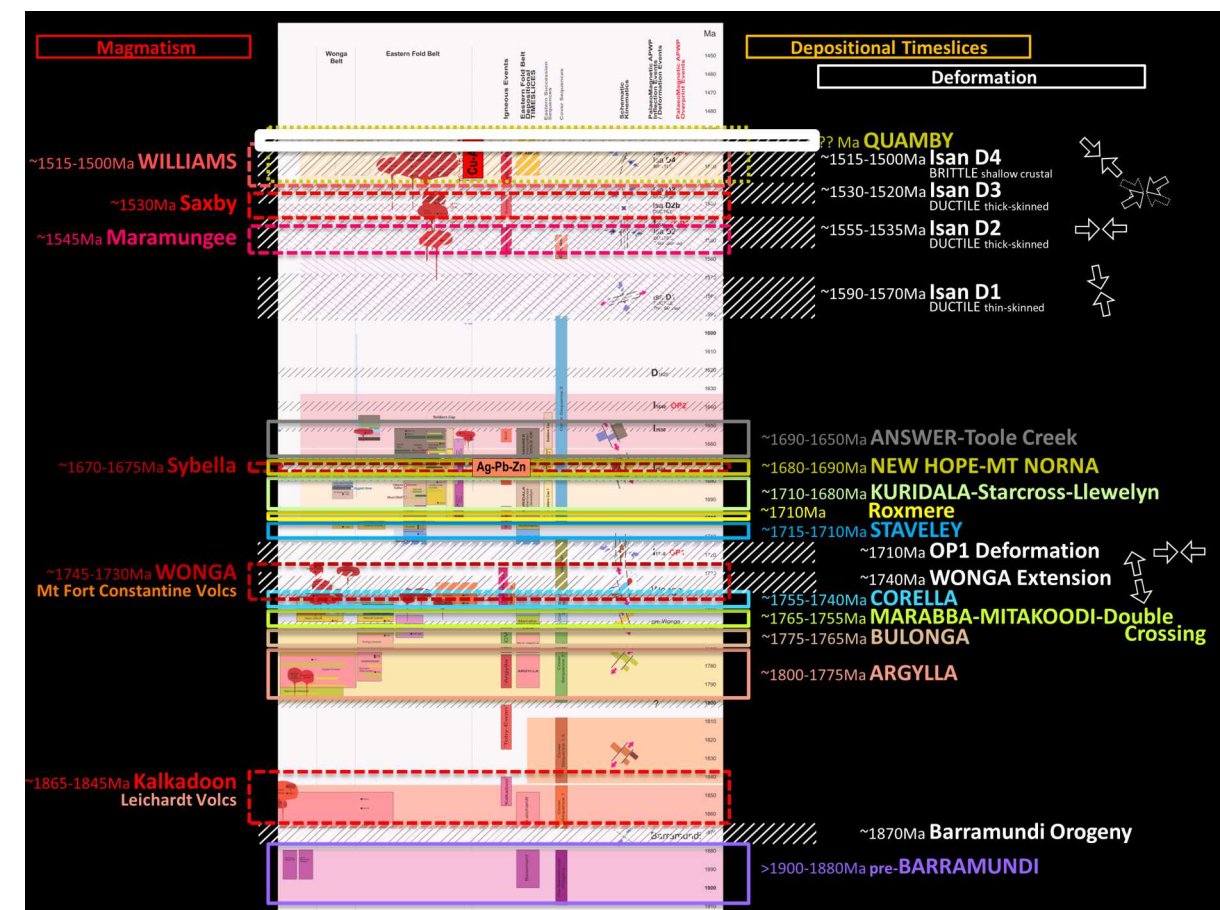
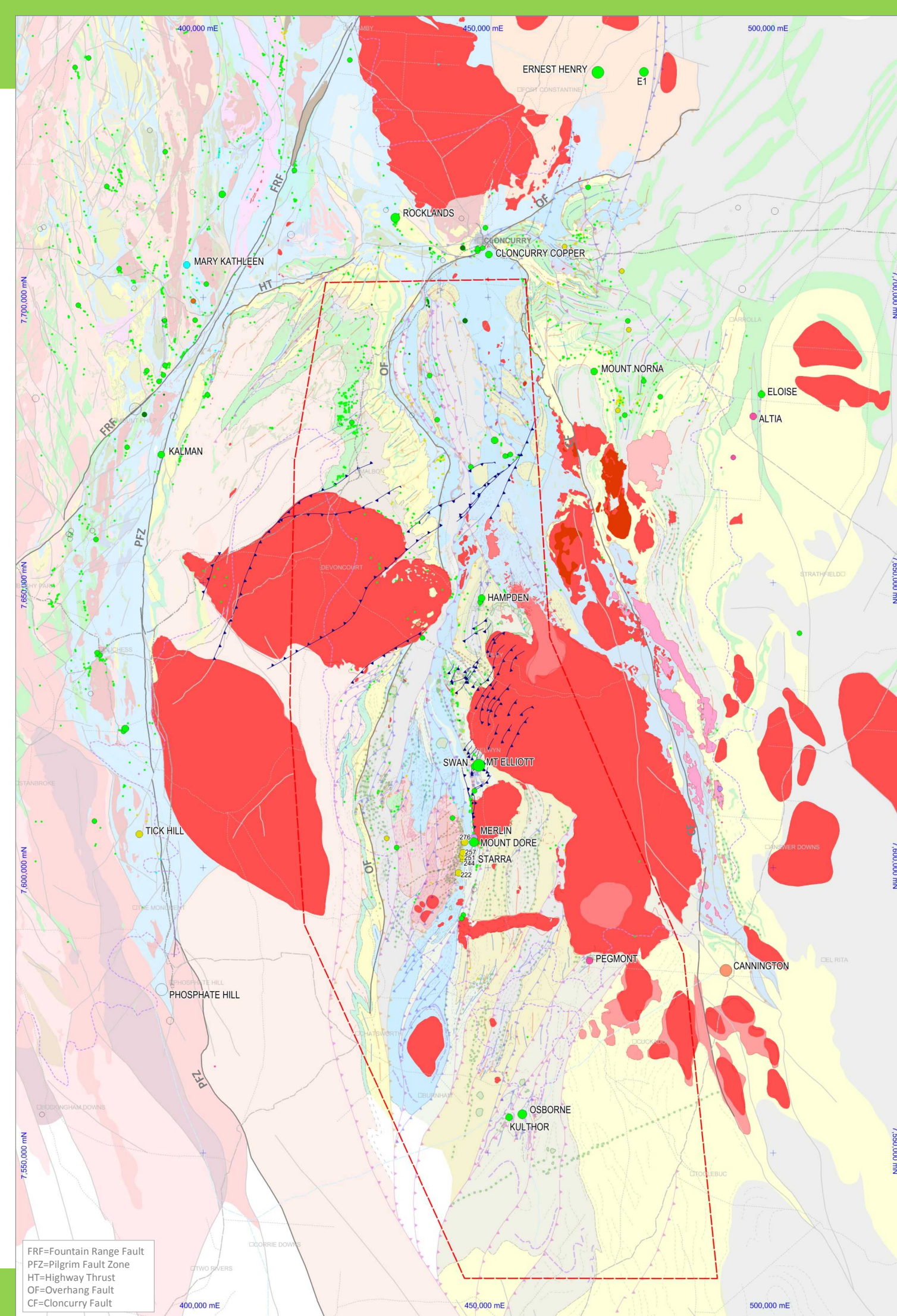
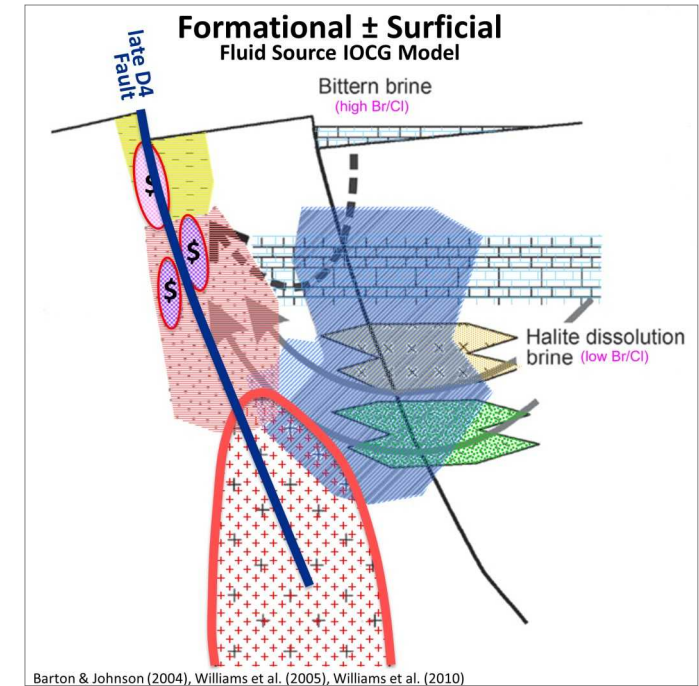


Figure 3.16 ~1500-1495Ma late Isan D4 Faulting; (syn)-late WILLIAMS magmatism

## ~1495-1490Ma later Isan D4 Faulting post WILLIAMS

The Cloncurry (and associated) Faults clearly cut fully solidified WILLIAMS suite intrusions and are a completely distinct set of structures compared with the D1-timed, family of Cloncurry Thrusts.

Other workers (Austin & Blenkinsop, 2008) have argued that within a broadly-defined Cloncurry Fault 'Zone', fabrics and faults formed during ductile D3 deformation and later brittle D4(-D5) sinistral Reidel strike-slip (?transpressive) faulting. DMQ argues that within and around the D1 Cloncurry Thrust domains, D2 and D3 reactivation will naturally be present, but that the mapped traces of the Cloncurry (and associated) Faults are essentially post WILLIAMS (very late D4), brittle transpressive fault systems that express a greater component of reverse movement to the south compared with in the north where displacements are very minor.

The Cloncurry Thrust-Fault domain does appear to mark some sort of depositional divide but the complexity of D1 thrusting within and across the domain makes it difficult to assert that the Cloncurry Fault Zone specifically represents a re-activated basin bounding fault (cf. Austin & Blenkinsop, 2008).

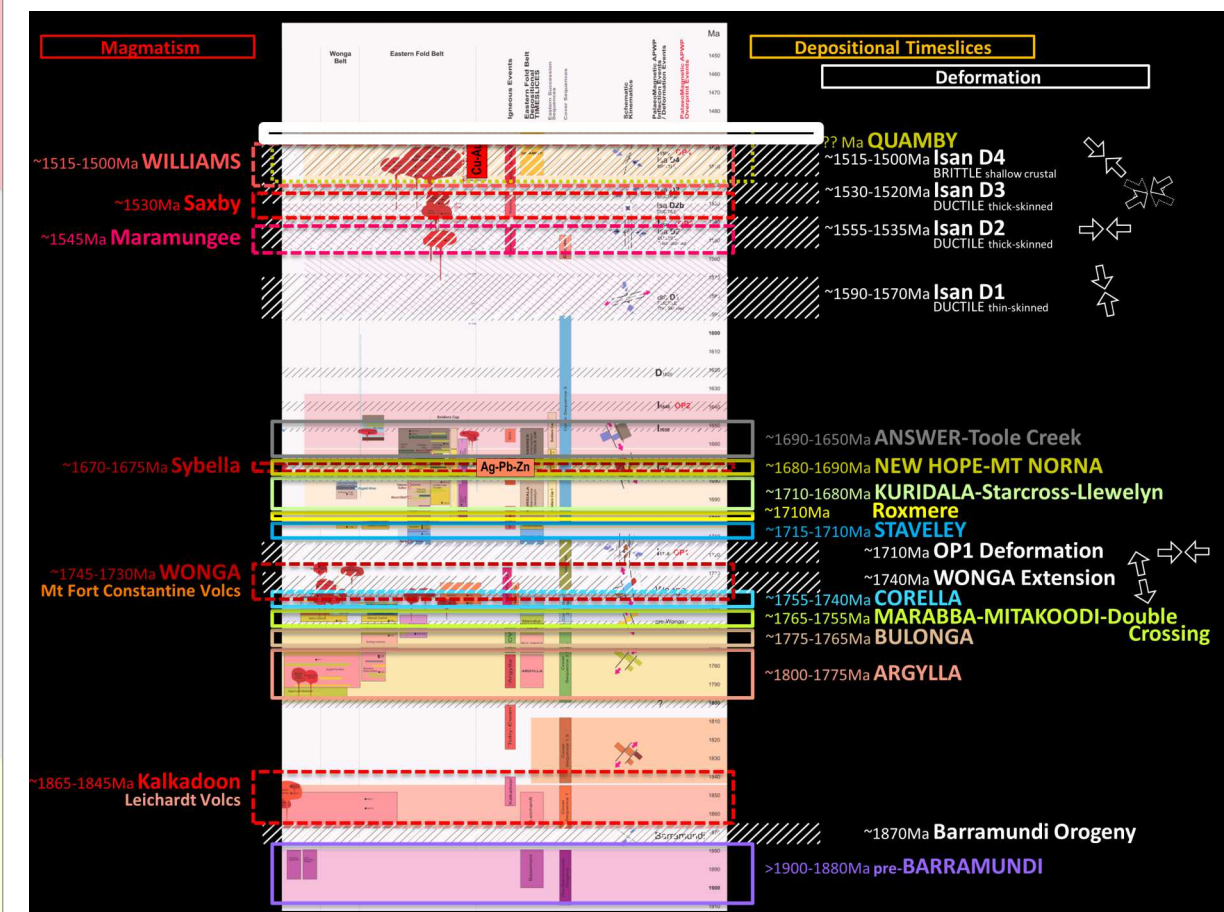
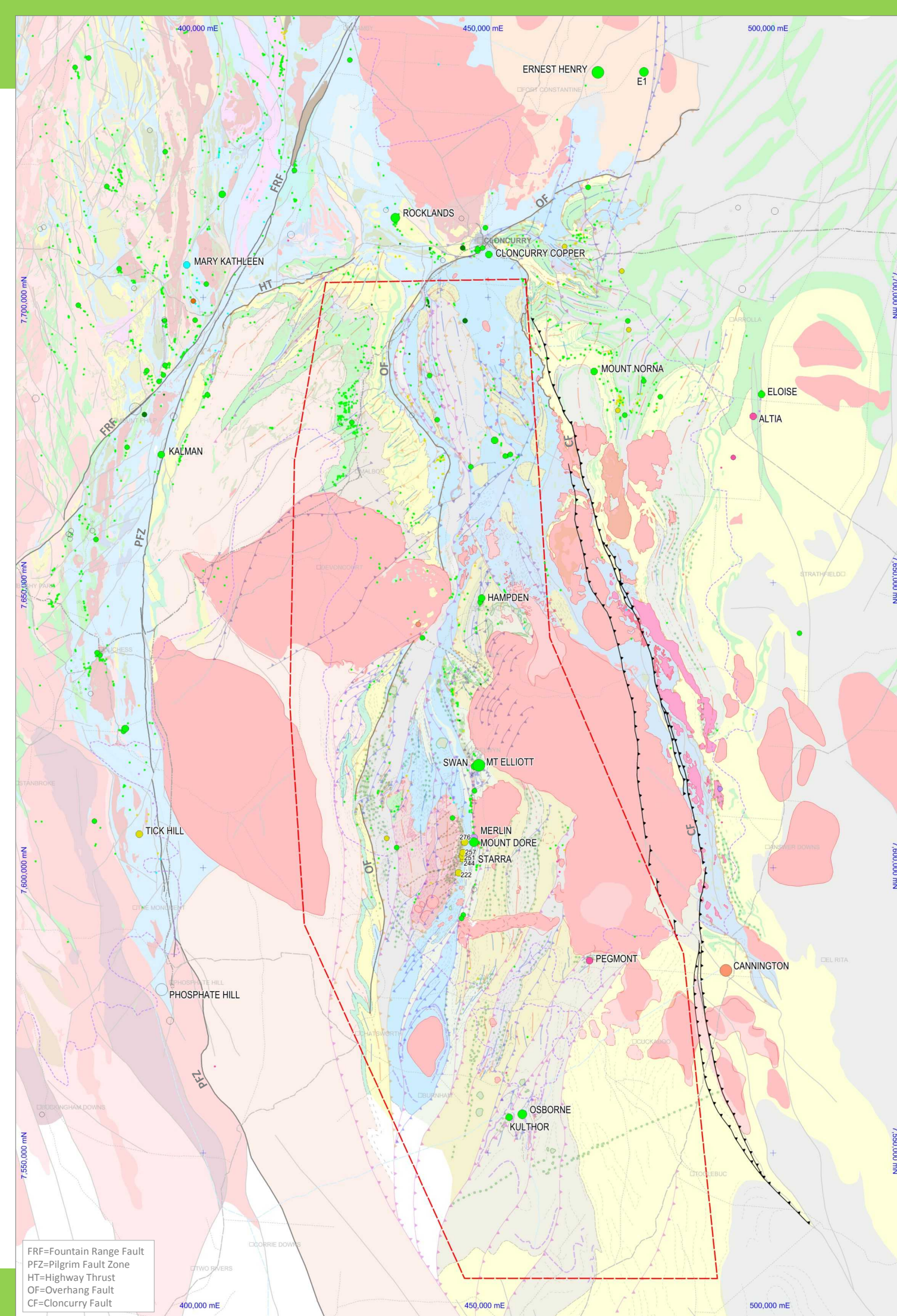


Figure 3.17 ~1495-1490Ma later Isan D4 Faulting; post WILLIAMS

## ~????-????Ma post Isan, X-cutting Faulting post WILLIAMS

Where detailed magnetics allow interpretation and/or prospect-sale mapping has revealed, post orogenic faulting is widespread. It is commonly cross-cutting to the regional trends. It cross-cuts all Isan structuring and falls into three groups: broadly NE-SW, broadly NW-SE and NNW-SSE. In places these orientations form the local joint patterns but fault offsets are interpretable in the detailed Chinova magnetics. Three significant orientations have been identified.

Some domains of post-Isan faulting are hypothesised to reflect old, pre-orogenic architectures (both depositional and inversion) that likely have significant crustal penetration and temporal persistence (see following Pre-Orogenic Architecture section)

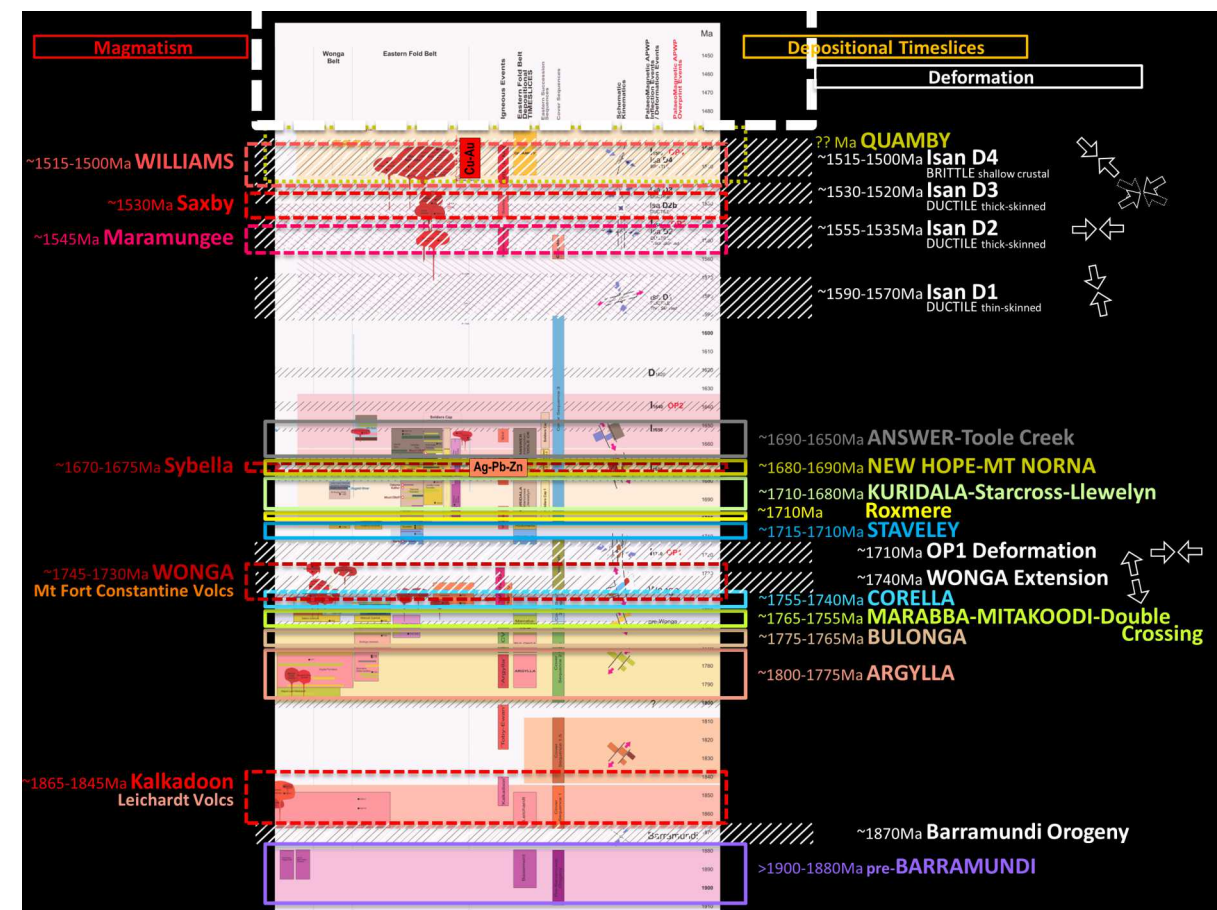
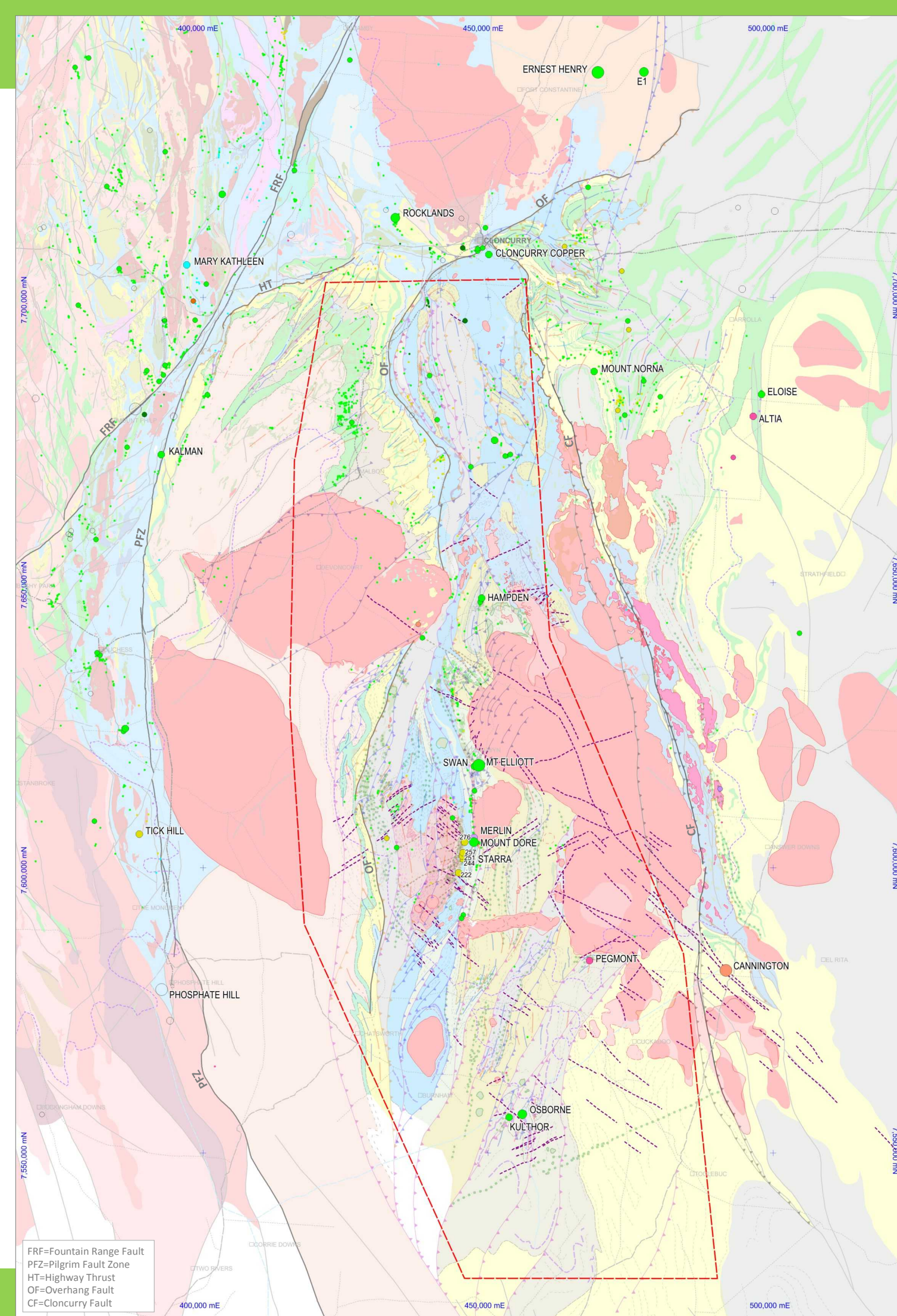


Figure 3.18 ~????-????Ma post Isan X-cutting Faulting; post WILLIAMS

# Cloncurry District Analysis

## Pre-Orogenic Architecture & Architectural Inheritance

The widespread post-Isan faulting, where it can be mapped or interpreted with the available geological and geophysical data, appears to fall into 3 major groupings. In places these structures form the local joint pattern but in particular domains fault offsets are mappable and/or interpretable.

Figure 3.19 highlights three sets of orientations along which late fault offsets are locally interpretable and which potentially reflect older, pre-orogenic architectures that have significant crustal penetration and persistence. These are detailed below.

### NE Architectures

- The northern NE-structural domain trending NE from Cloncurry along the extension of the Overhang Fault Zone and SW beneath the Mitakoodi Culmination potentially has Barramundi-time origins and appears to have 'Wonga'-time re-activation defining the southern margin of MFCV accumulation. Its influence on the atypical orientation of D2 folding within the Mitakoodi Culmination has been noted previously.
- Other NE-structural domains partition compartments of contrasting D1, D2 and D3 deformation. The NE structure between the Marimo and Hampden Synclines separates domains of significantly contrasting structural and magmatic character.
- NE-structural domains have post-WILLIAMS re-activation cutting the northern Wimberu and Mount Dore granites.
- The NE structure at the southern end of Mount Dore Cu mineralisation is demonstrably post Cu-mineralisation, post-Mount Dore granite and marks the southern extremity of Mount Dore Cu mineralisation grade shell (see Merlin-Mount Dore Detailed Geology Section)

### NW Architectures

- NW-structural domains also compartmentalise domains of contrasting structural patterns. The NW-structure at the southern end of the Hampden Syncline marks a complex structural domain of faulting and re-oriented folding that separates the Hampden Syncline from a complexly thrust, faulted and folded package to its south.
- NW-Structural domains also have significant late re-activation cutting WILLIAMS-aged intrusions and they also appear to control some WILLIAMS intrusive margins

### NNW Architectures

- A major NNW-structural domain incorporates the D3 Straight Eight Fault (that truncates the northern end of the Hampden Syncline), shows strong fault re-activation through the Squirrel Hill Granite and may be reflected in a

the major D2 Fault Zone that runs the length of the Marimo Syncline.

### Architectural Inheritance

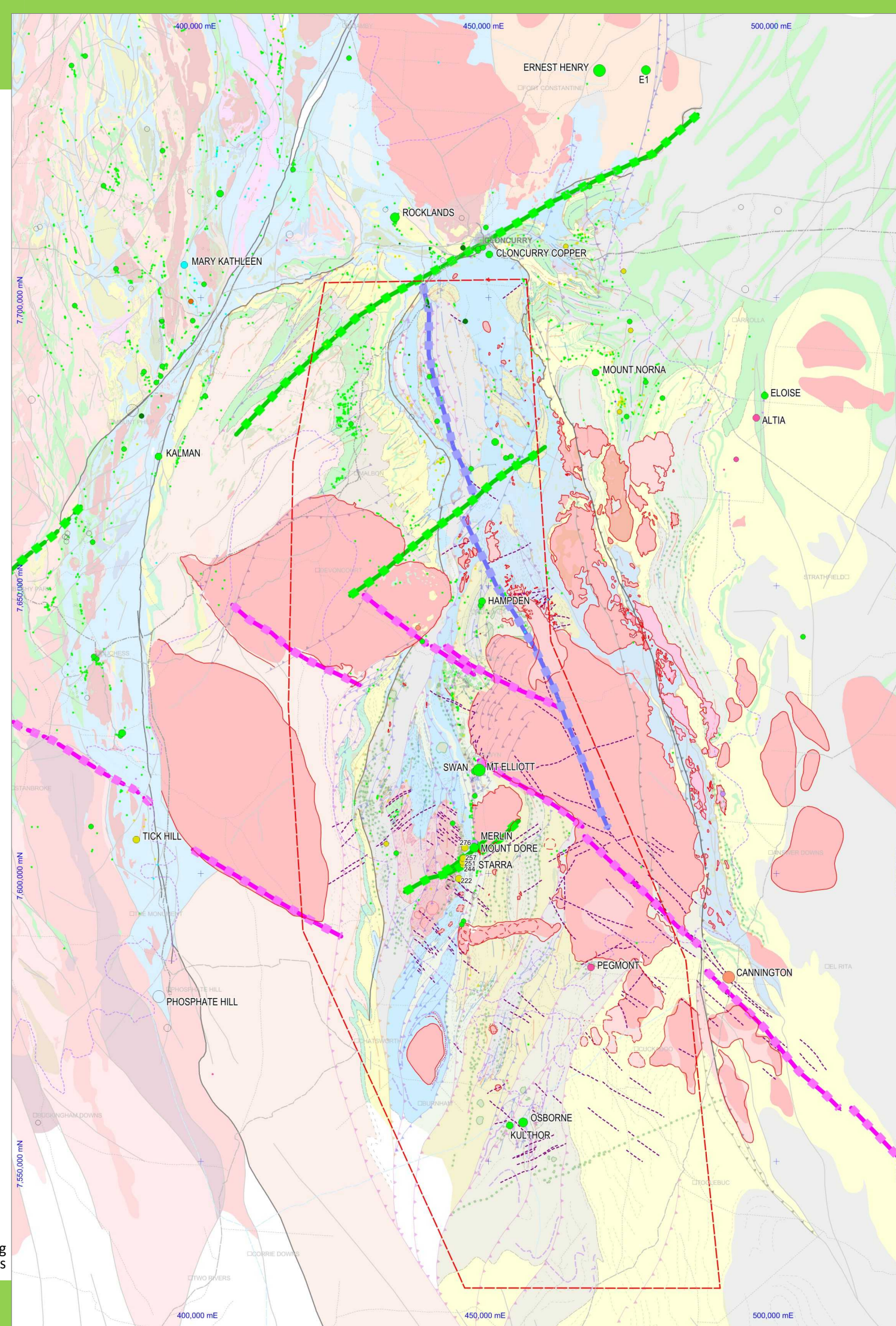
Past compilations and analyses have suggested syn-depositional basin architectural origins for these re-activating architectures, but their origins remain far from certain.

The 2000 NWQMP study suggested, on the basis of isopach and structural work in the Davenport Province by Alastair Stewart (1987), that the NE and NW architectures reflected accommodation/transform/sidewall and normal basin-forming faults respectively (see Davenport column, Figure 3.2) for 1840-1760Ma package accumulation (ARGYLLA-ECV-BULONGA). These orientations have been highlighted in the Western Succession, Lawn Hill Platform and are evident in the under cover interpretations east of the Isa terrain. In the central Isa Belt, the strong N-S architectural grain, enhanced by approximately 50% Isan shortening, has considerably obscured potential NE and NW depositional architectures. Despite this, a significant number of NE to NNE (perhaps D2-shortening rotated?) trending structures are present in Mount Isa major fault compilations and suggests that faults in this orientation also have their origin in significant, crustal-penetrating structures that repeatedly re-activate through all stages of subsequent orogeny and play sidewall/compartmentalisation roles through younger deformations. This is also the possibility that the NE-trending structures may have older origins in BARRAMUNDI-times.

The NNW-reactivation domains in the DMQ Project area are sub-parallel to the very significant regional-scale, meridional architecture of the Isa belt and potentially reflect even more fundamental, older architecture that significantly influenced the belts Isan deformation (Kalkadoon-Leichardt belt, Pilgrim Fault Zone, Cloncurry Fault, Isa Fault *and others*). The 2000 NWQMP study suggested this orientation may reflect Archaean (certainly pre-BARRAMUNDI) architectures and in the EFB may reflect depositional accommodation/sidewall structures during NEW HOPE-MOUNT NORNA rift re-activation and TOOLE CREEK deposition. This orientation is sub-parallel with exhumed Wonga extensional structures.

A propensity to run seismic lines E-W across the inversion grain of the Isa belt has not helped resolve these old, oblique pre-orogenic architectures of very significant crustal persistence.

Figure 3.19 post-Isan, post WILLIAMS X-cutting Faulting & potential pre-orogenic Architectures



## Detailed Geology & Controls on Mineralisation

Four areas of detailed geological analysis, where Chinova (and Glencore) have provided access to previously-presented geological modelling and interpretation, provide significant insight into the timing and controls of IOCG-style mineralisation within the DMQ Project Area.

The following section presents geological and geophysical data on the Starra-Merlin-Mount Dore, Mount Elliott-SWAN, Osborne-Kulthor and Ernest Henry areas as well as DMQ interpretations of the geodynamic controls on ore localisation. Ernest Henry is included in the analysis despite being well outside the project area as it is both the largest IOCG-type deposit in the region and it supports an existing underground mass-mining operation.

The important outcome of these detailed analyses is that significantly different structural controls characterise each of these deposits. In most cases controlling structures are NOT regional-scale structures (with large displacements) that are easily mapped and interpreted in regional data sets, but are rather zones of strain partitioning and small-scale faulting (with small displacements) that are NOT mappable at regional to semi-regional scales (and even locally in many cases) either geologically or geophysically. In DMQ's view, this makes the manipulation of mapped and interpreted major fault networks of little benefit in IOCG-style Cu-Au-Mo targeting. Rather local to semi-regional controls on mineralisation in particular camps should be resolved in the quest for brownfields extensions. Prospective tract analysis for greenfields exploration will be developed later in the DMQ analysis (see Chapter 5).

### Starra-Merlin-Mount Dore

The Starra-Merlin-Mount Dore Solid Geology interpretation is very well resolved by virtue of ultra-detailed aero-Magnetics and heliTEM as well as the invaluable detailed 10K, 5K and 1K mapping of John Leishman completed during the 1970s–1990s for Arimco and Amoco and subsequent work by Ivanhoe-Inova-Chinova. In addition detailed mapping, drillcore logging, interpretation and domaining done by Hinman (2012, 2013) at Merlin, Mount Dore and Starra (minor) under contract to Ivanhoe Australia have contributed to the local understanding. Chinova is gratefully acknowledged for permission to use this material in previous presentations and in this report. Figure 3.21 combines all of the above with detailed DMQ interpretation. Figure 3.22 presents the significantly useful detailed aeroMagnetics that have been used to enhance the DMQ interpretation.

The following points highlight the major geodynamic attributes of this region that impact on mineralisation This analysis should be reviewed in conjunction with the Time-Space Chart (Figure 3.2) and the complete Tectono-Stratigraphic-Magmatic Assembly of the EFB presented in Appendix 4. A complete set of useful geophysical images of the area are assembled in Appendix 9.

Basement to the west comprises the DOUBLE CROSSING METAMORPHICS (DCM) intruded by the syn-deformational, Wonga-aged, GIN CREEK GRANITES (GCG)

- The syn-deformation GCGs are massive in their central domains, but show significant 'thready' syn-tectonic,

**Figure 3.21** Detailed DMQ tectono-stratigraphic geological-geophysical interpretation of the Starra-Merlin-Mount Dore region

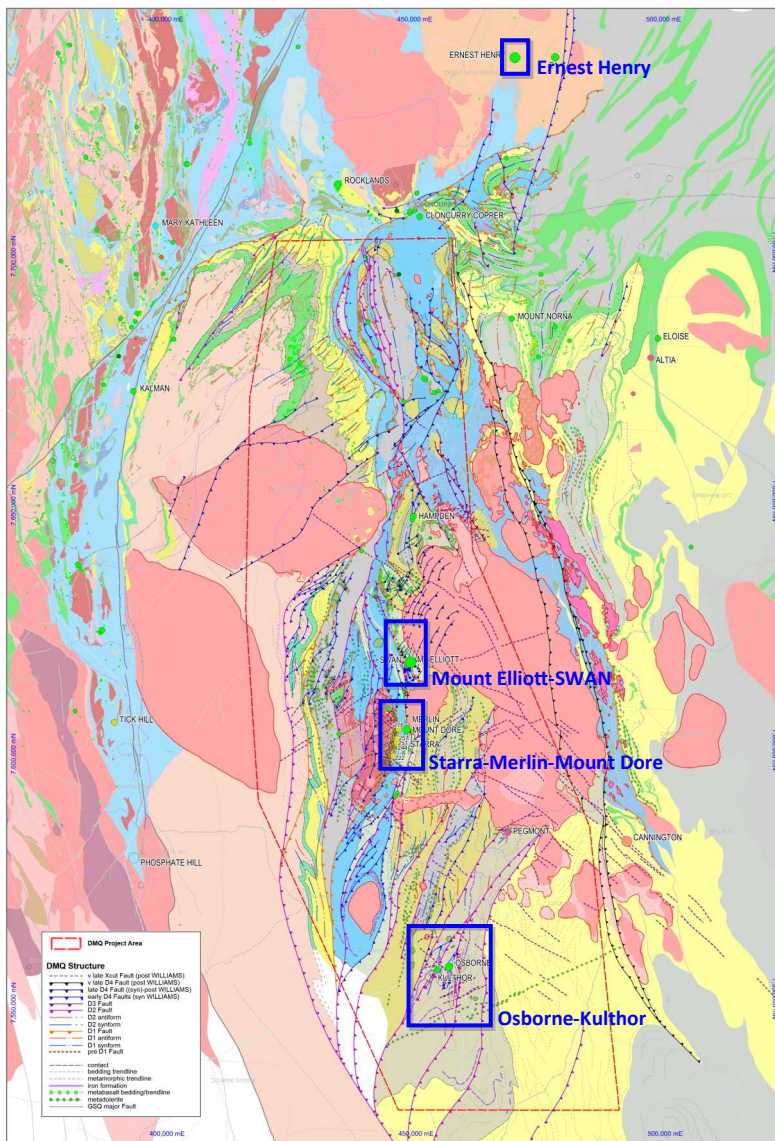
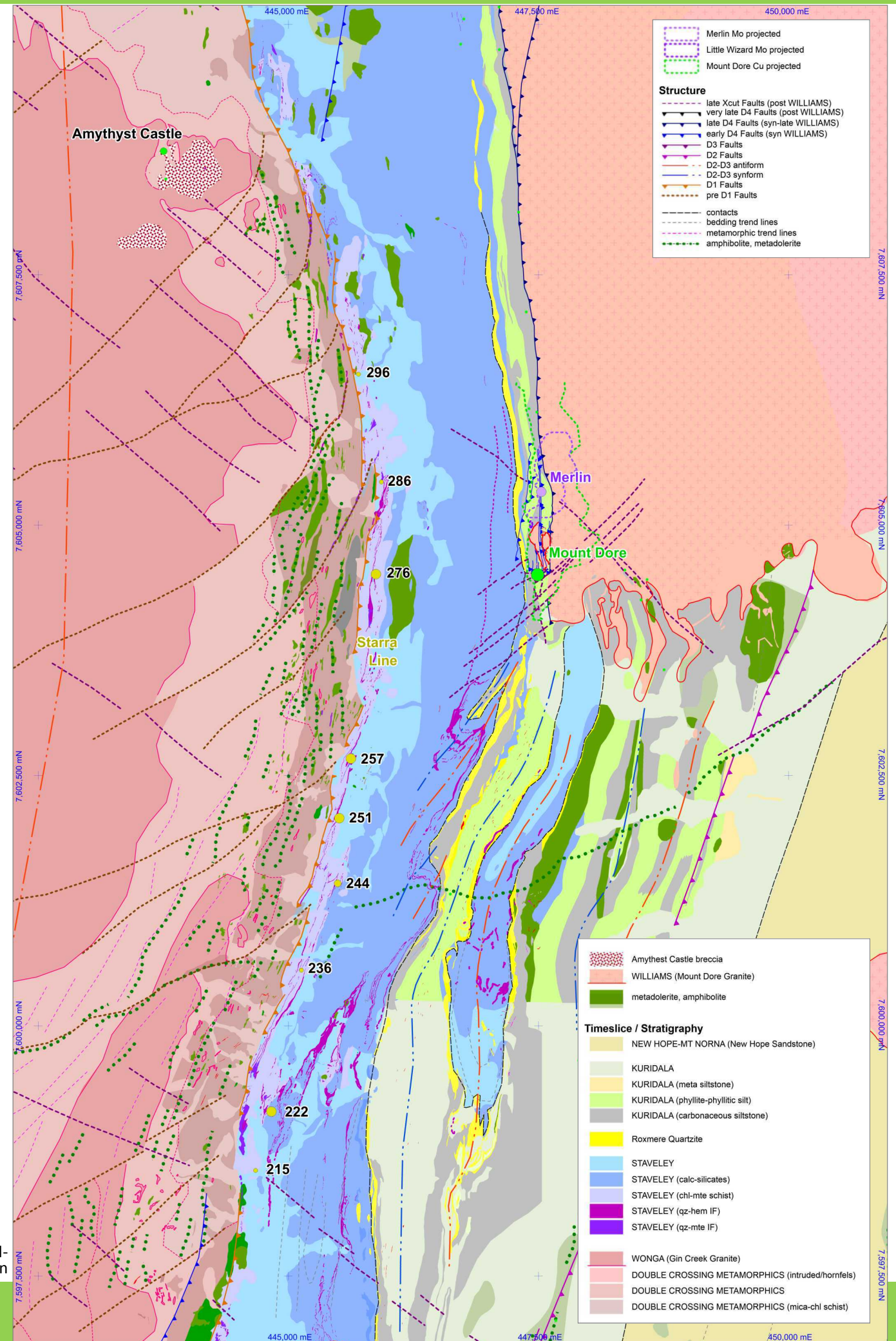


**Figure 3.20** Areas of detailed geological-geophysical interpretation and tectono-stratigraphic analysis that provide insight into the timing and controls of IOCG-style mineralisation in the DMQ Project region ... over the DMQ Solid Geology interpretation.

intrusive relationships with the DCMs over significant volumes. This reflects both significant sheet-like, 'thready' syn-deformational intrusion into the DCM as well as significant xenolith remanence within the intrusive. These relationships are well imaged in the magnetics and radiometrics.

- The DCM-GCG block contains significant NE-oriented discontinuities with large displacements of the DCM-GCG architecture that are NOT duplicated across the D1 Starra Shear/Line (and later) structures. For this reason this basement NE-architecture is tagged pre-D1. Late (post D4) re-activation of these basement structures do dismember the D1 Starra Shear/Line but these late re-activation displacements are small compared to the basement architecture offsets.
- Conventional wisdom (Switzer, 1987; Switzer et al, 1988; Laing, 1998; adopted here by DMQ in the absence of convincing relationships supporting other interpretations) has STAVELY (and younger) packages (to the east) in D1 overthrust relationship with the DCM-GCG (to the west).
- D1 is envisaged to have involved sub-horizontal, thin-skinned thrusting producing ~EW F1 folds and a highly attenuated & folded package of thin iron formations within the D1 Starra Shear. Iron formations (both hematitic and magnetitic) are variously argued to be pre- and/or syn-D1. Some iron formations in the wider region away from intense deformation are strictly formational and likely syn-sedimentary. This does not discount the acknowledged existence of post-depositional formational iron oxide replacement in more local mineralised settings.
- Iron formation folding and attenuation within the D1 Starra Shear produced EW-trending remnant ribbons and fold axes which were rotated into steep orientations during regional D2 shortening when the D1 structures along the Starra Line were folded into steep orientations.
- Regionally (see Figure 3.6) the D1 thrust juxtapositioning of STAVELY over DCM-GCG is interpreted to be folded about NS-trending fold axes to produce the folded map relationships north of the DCM-GCG block. As argued in Appendix 4, STAVELY basal contacts are apparently entirely structural, however, D1-reactivated depositional relationships around the DCM-GCG block (while considered unlikely on the basis of angular discordance) cannot be entirely discounted.
- D2-rotated, steeply plunging D1 folds and ribbons of iron formation along the Starra Line are in stark contrast with the sub-horizontal NS folds in the STAVELY-

KURIDALA packages to the south of the Mount Dore Granite.

- D2 and D3 reverse and transpressive reactivation along the Starra Shear result in complex fold and attenuation relationships along the Starra Line. The resulting geometry comprises remnant lenses and rootless folds of massive iron formation that lie within a wider zone of chlorite-magnetite schist that is itself responsible for the continuous high tmi-rtp response (Figure 3.21 cf 3.22, Appendix 9, & DMQ Presentations) rather than the relatively minor massive iron formation remnants.
- In D4 time, the WILLIAMS-aged, Mount Dore Granite intrudes during NW-directed shortening in post-D2-3 shallower crustal settings. Pre-existing steep NS structures like the Starra Shear suffer sinistral transpressive re-activation and strain partitioning occurs adjacent to and above shoulders of crystallising intrusives (see Merlin-Mount Dore Section below).
- D4 brittle fracture-breccia deformation of appropriate, post-peak metamorphic lithologies focuses circulating fluid flow to form IOCG-type Cu-Au-Mo mineralisation.

The DMQ analysis of host controls on IOCG-style Cu-Au-Mo mineralisation in the southern Cloncurry Belt suggests that lithologies with strong metamorphic fabrics accommodate late Isan D4 re-activation by slip on existing fabrics and exhibit little permeability generation. The presence of a brittle rock type in the zones of focused D4 structuring and re-activation enhances permeability generation and is considered an essential ingredient for IOCG-style mineralisation.

## Starra

Along the Starra Line, known Au-Cu mineralisation shows a significant correlation with the projection of basement, (Starra Shear footwall) NE-trending DCM-GCG pre-D1 structures ... allowing for some D2-3 shortening rotation of them within the DCMs and the broader Starra Shear zone (see Figure 3.21 & 3.22).

The DMQ model for the geodynamic control of Starra Line Au-Cu mineralisation requires the spatial coincidence of (1) a remnant lense of massive iron formation (generally magnetitic, although re-activation along the margins of the tougher hematitic iron formations locally focuses minor mineralisation) within the D4 transpressively re-activated Starra Shear Zone with (2) a footwall (DCM-GCG) pre-D1

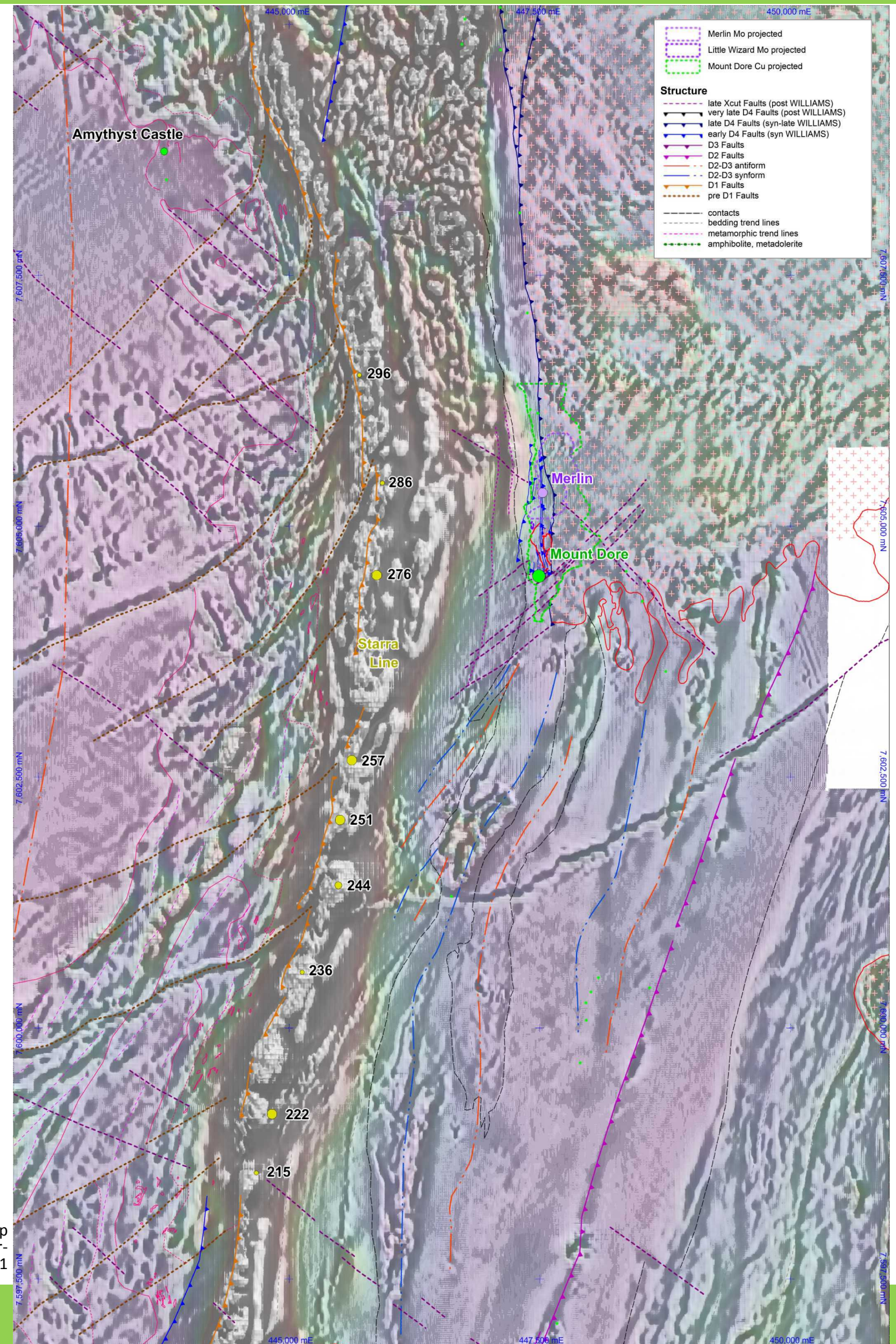


**Figure 3.22** Detailed Chinova vrm1-2vd over tmi-rtp aeroMag of Starra-Merlin-Mount Dore area with overlain DMQ structure framework from Figure 3.21

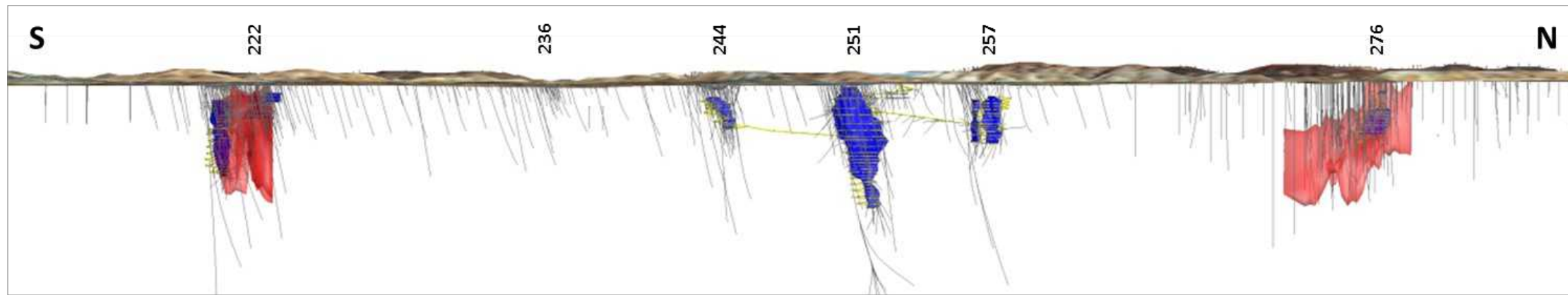


**Figure 3.23** Starra Line Long Section with 2012 mined & probable Resources and drilling from 222 in the south to 276 in the north.

structure (Figures 3.21 & 3.22).

The additional footwall weakness contributes to the focused brittle deformation within the iron formation during D4 NW-directed shortening that drives sinistral transpressive re-activation within the D1 Starra Shear. The plunge of ore systems is hypothesised to reflect the intersection of the footwall structure with the remnant iron formation as presented in Figure 3.24 rather than the plunge of the D1 folds and remnant ribbons of iron formation. Previous interpretations have emphasised pre-D4 fold hinges and ribbon terminations of the iron formations.

Figure 3.23 presents a Long Section of the Starra Line of resources highlighting the steep to moderate plunges of the ore systems. Different plunges are hypothesised to reflect different orientations of the DCM-GCG footwall structures.

Later, post-D4 and post-mineral reactivation of the pre-D1 DCM-GCG NE-trending basement structures cut and weakly displace the Starra Shear and its associated mineralisation. Late NE cross-cutting faults are common in the Starra-Merlin-Mount Dore

area and some are potentially among the families of late faults with potential pre-Isan origin discussed in a previous section.

A full library of geophysical signatures of the Starra-Merlin-Mount Dore region (and the other detailed areas of interest) as well as detailed prospect-scale images around know resources is presented in Appendix 9.

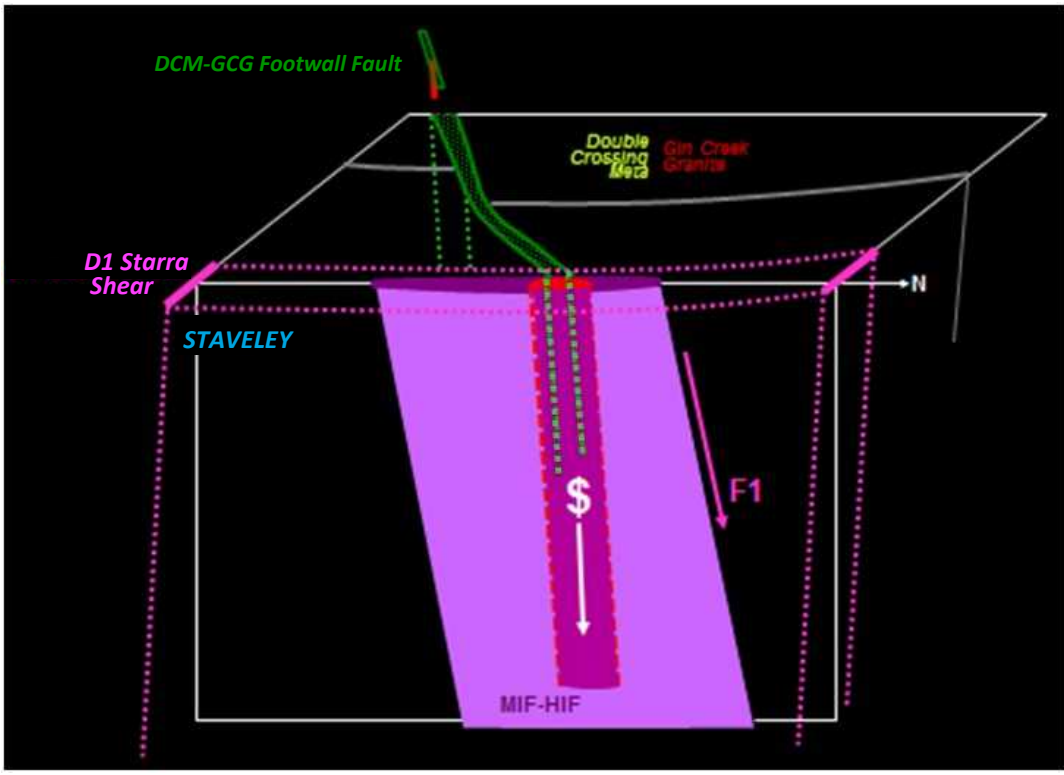
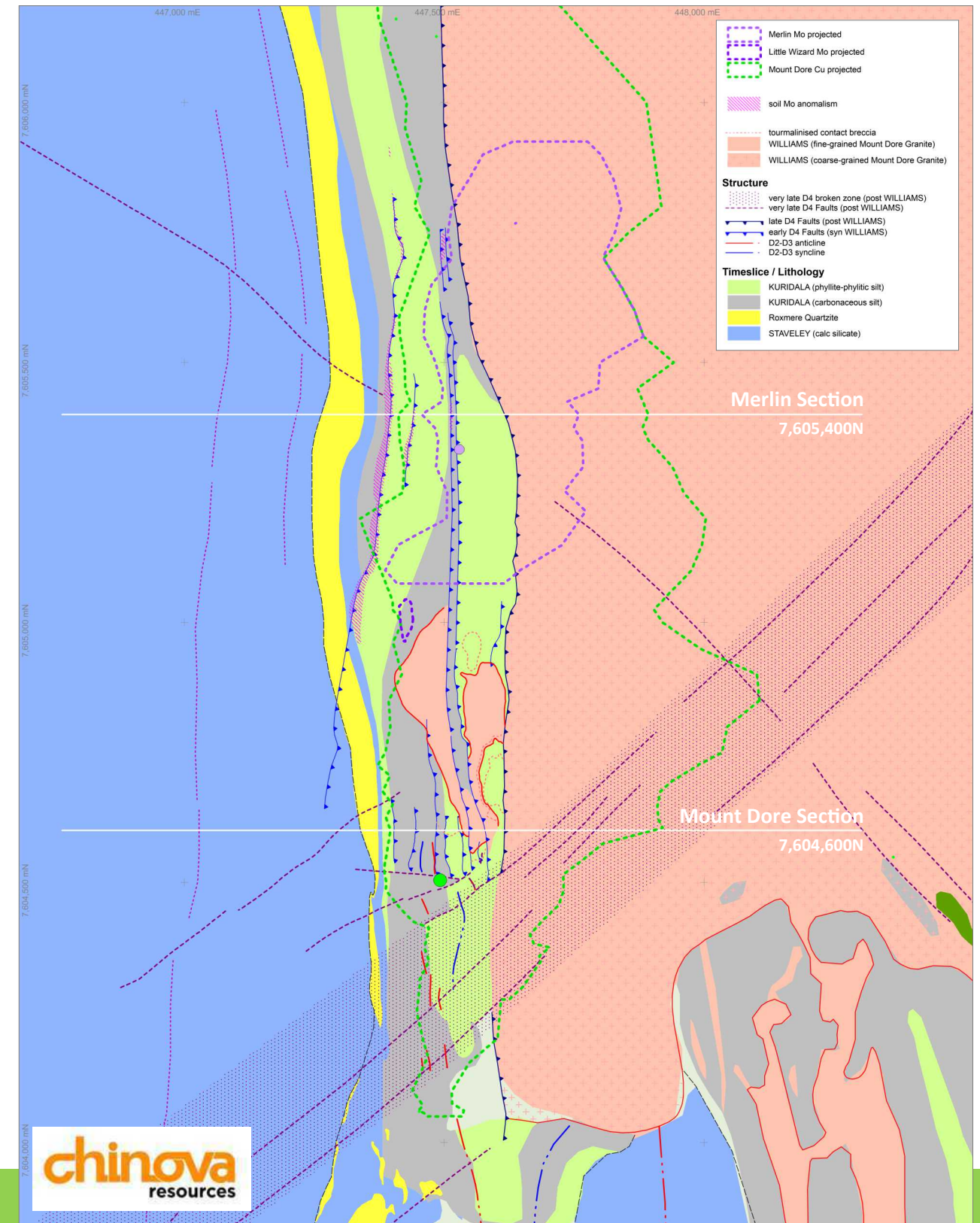
### Merlin-Mount Dore

Merlin and Mount Dore lie 1.6km east of the Starra Line across a largely recessive section of STAVELEY calc-silicates (Figure 3.21 & 3.22). Both the Merlin and Mount Dore resources lie to the east of a siliceous ridge locally known as the 'SQT' but now identified as the rhythmically-cycled ROXMERE Quartzite. Outcrop is sparse between the ROXMERE Quartzite and the Mount Dore Granite (Figure 3.25) but around Merlin-Mount Dore a number of small displacement thrusts have been mapped (Hinman, 2012) which correlate well with drillcore structures. Some of these demonstrably cross cut stratigraphy at very low angles, have tightly-associated Mo soil geochemistry and are the updip expression of mineralisation control at depth. Importantly these control structures are small-scale structures with small displacements that would not (and do not) feature on regional scale structural maps (Figure 3.6). The only significant fault is the Mount Dore Granite overthrust fault which is demonstrably post-mineral and post-WILLIAMS and not related to mineralisation in a process sense.

Both the Merlin and Mount Dore resources lie close to the stratigraphic transition between the STAVELEY and KURIDALA packages. Two sections are presented here through Mount Dore (Figure 3.26) and Merlin (Figure 3.27)

**Figure 3.24** Starra geodynamic model for Au-Cu mineralisation emphasising footwall structural control on enhanced D4 brittle deformation within D1 remnants of magnetite iron formation within the Starra Shear.

**Figure 3.25** Detailed geology at Merlin-Mount Dore (Hinman, 2012) showing the 2 sections in subsequent Figures and the vertical projections of the Merlin, Little Wizard and Mount Dore mineralisation



that were generated utilising detailed drillcore structural analysis (Hinman, 2012). They are accompanied with notes highlighting important structural-stratigraphic and mineralisation control features. Mark Hinman acknowledges Chinova for the use of these sections in previous DMQ presentations and in this report.

## Mount Dore Section 7,604,600N

Significant structural-stratigraphic and process-related relationships in the Mount Dore Section are outlined below.

- The drilling reveals a well-preserved, sedimentologically -gradational stratigraphy from STAVELEY calc-silicates in the west (see also Figure 3.25), up into the ROXMERE Quartzite, through some more calc-silicates, and into KURIDALA phyllites, phyllitic schists and carbonaceous meta-siltstones.
- The Mount Dore KURIDALA section is dominated by carbonaceous meta-siltstones that host most of the Cu-Au mineralisation.
- The early D4 Reverse Faulting, which meshes well with surface-mapped faults (Figure 3.25), is complex, curvilinear and anastomosing. The faulting is in general slightly steeper than bedding and results in small displacements that would only be discernible in 1:500 scale mapping (or better) and detailed drill section analysis .... and would certainly not register in regional scale maps or interpretations.
- Brittle fracture and breccia damage zones around the reverse faults are well developed within the carbonaceous silts and along re-activated contacts, in particular, shallower dipping surfaces and contacts that are well oriented to extend sub-vertically in the transpressive shortening of early D4.
- Better developed mineralisation (higher grade shoots) are likely to have shallowly north-dipping plunges parallel to re-activating (vertically-extending) pre-existing fold plunges and the intersection of bedding and the early D4 faulting.
- The brittle fracture and breccia damage zones host the Cu-Au mineralisation largely within the brittle carbonaceous siltstones. The minor phyllitic volumes at Mt Dore host significantly less mineralisation due their highly schistose nature and ductile (non-brittle) re-activation in D4
- The Mount Dore Granite overthrust Fault starkly contrasts with the early D4 faults. It is highly planar, it is post-mineral deforming both mineralisation and alteration, it juxtaposes internal coarse-grained granite with the Mount Dore package and has a significant, mapp-

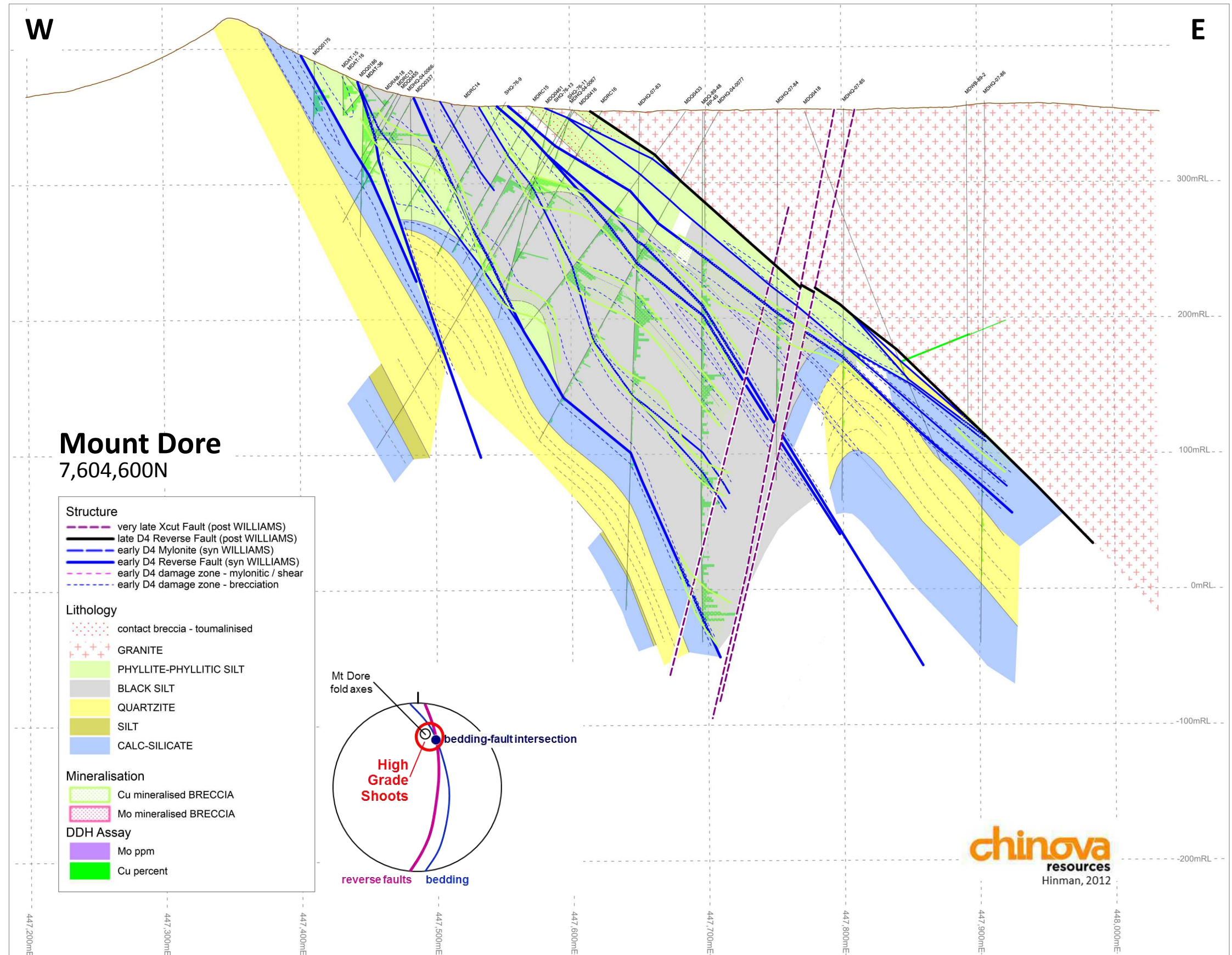


**Figure 3.26** Detailed drill section at Mount Dore (Hinman, 2012) looking north highlighting early D4 Faulting controlling brecciation hosting Cu mineralisation and the post-mineral, late D4 overthrust of the Mount Dore Granite. The stereonet highlights the geometry of potentially better developed brecciation and mineralisation.

ble throw. This fault is the only tangible 'Mount Dore Fault'

- Late (post-granite=post-WILLIAMS) cross-cutting faulting shows minor offsetting of the sectional architecture. This fault zone is parallel to a regional NE-trending joint set at Merlin-Mount Dore and produces a wide zone of late brittle deformation that marks the southern termination of the definable Mount Dore resource (Figure 3.25)

## Merlin Section 7,605,400N

Significant structural-stratigraphic and process-related relationships in the Merlin Section are outlined below.

- The drilling reveals a well-preserved, sedimentologically -gradational stratigraphy from STAVELEY calc-silicates in the west (see also Figure 3.25), up into and out of the ROXMERE Quartzite via some non-calcareous siltstones, through some more calc-silicates, and into KURIDALA phyllites, phyllitic schists and carbonaceous meta-siltstones.
- In contrast with the Mount Dore section, the Merlin KURIDALA section is dominated by phyllites and phyllitic siltstones with only a minor carbonaceous meta-siltstone sequence sitting above the upper STAVELEY calc-silicates. Some other minor carbonaceous siltstones are interbedded within the phyllitic package (see also Figure 3.25)
- The early D4 faulting is again complex, curvilinear and anastomosing and is characterised by brittle fracture and breccia damage zones in the STAVELEY calc-silicates and KURIDALA carbonaceous siltstones, but by ductile (sometimes mylonitic) tight structures within the phyllitic lithologies.
- Brittle fracture and breccia zones host the Mo mineralisation, firstly along a central, early D4 reverse fault along which calc-silicate and carbonaceous siltstone is brecciated, and secondly, along normal calc-silicate-carbonaceous siltstone contacts that are activated during D4 shortening and brecciate in both the footwall and hanging wall of the central mineralised D4 structure.
- Better developed Mo mineralisation (higher grade shoots) likely have shallowly north-dipping plunges parallel to the intersection of bedding and the early D4 faulting. A clear and high grade example is where the footwall brecciated calc-silicate-carbonaceous silt contact converges and merges with the D4 fault damage zone at -50mRL.
- The Mount Dore Granite overthrust Fault is again absolutely planar, is post-mineral and juxtaposes internal

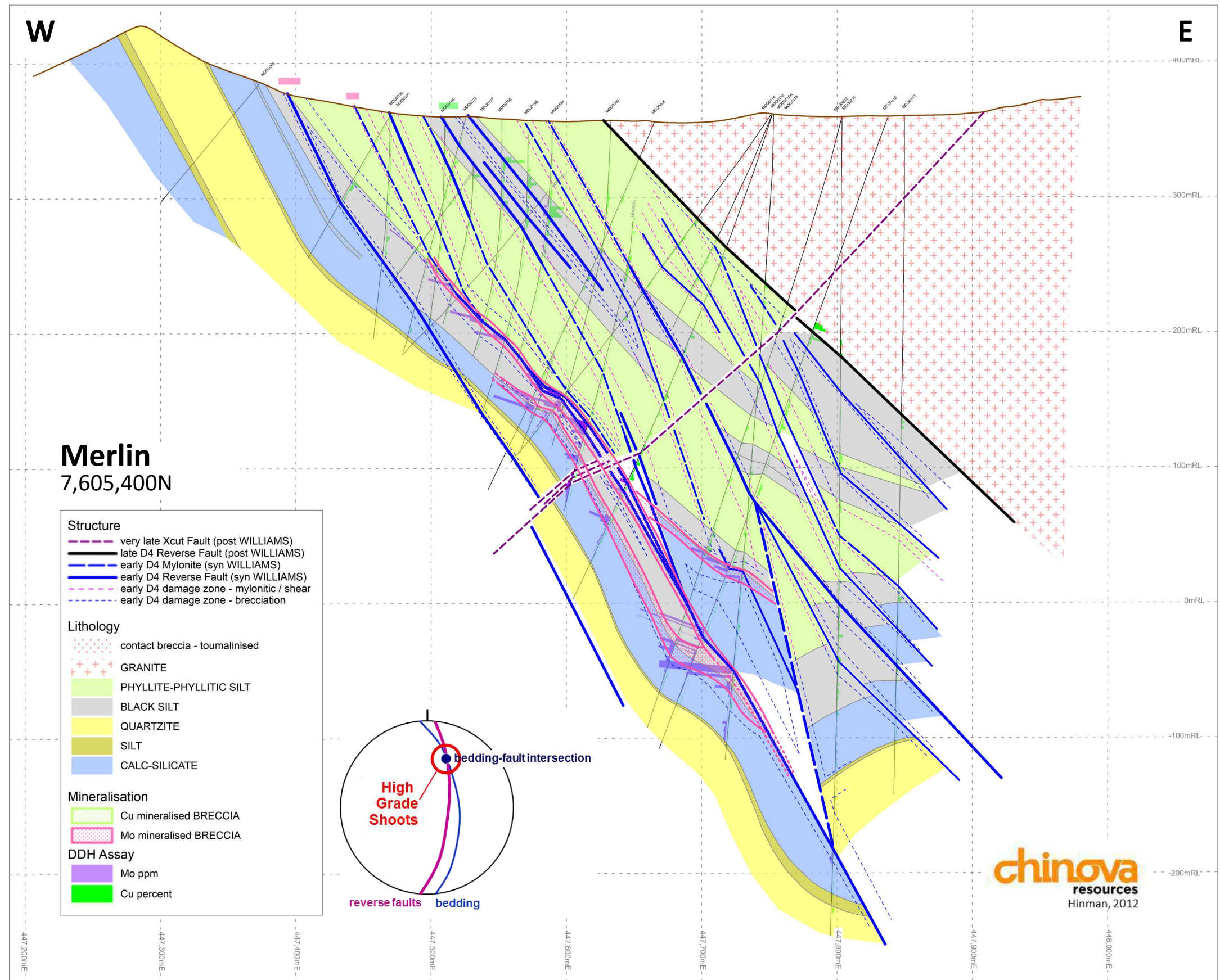


**Figure 3.27** Detailed drill section at Merlin (Hinman, 2012) looking north highlighting brecciation hosting Mo mineralisation controlled by early D4 Faulting and contact re-activation between the brittle STAVELEY calc-silicates and KURIDALA carbonaceous siltstones. The late D4 overthrust of the Mount Dore Granite is planar and post-mineral and is associated re-activation of previously mineralise fracture and breccia zones resulting in the Merlin Mo-matrix breccias (Figure 3.28). The stereoplots highlights the shallow-plunging geometry of potential better developed mineralisation within the Merlin system.

coarse-grained Mount Dore granite with the Merlin package. It alone has a significant, mappable throw but is post-mineral.

- Reactivation of the structures hosting fracture and breccia-controlled Mo mineralisation at this post-Mount Dore granite, post-WILLIAMS, late D4-time, deforms the weak Mo mineralisation to form the Mo-matrix breccias for which Merlin is well known (Figure 3.28)
- Minor Cu mineralisation exists where early D4 faults intersect carbonaceous siltstone higher in the package. This suggests different metal precipitation might simply be a function of different physio-chemical environments and that different timings for Cu-Au and Mo-Cu mineralisation within the Merlin-Mount Dore system might be illusionary.
- Late cross-cutting faults result in minor offsets of the sectional architecture, but do potentially produce offsets of ore that will have mine stope design significance.

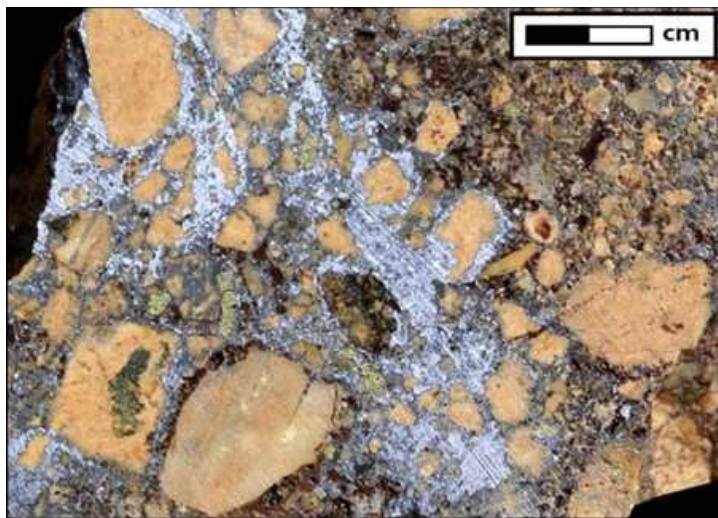


**Figure 3.28** Merlin Mo-matrix breccias with clasts of albite-altered calc-silicate siltstone fragments caused by late D4 re-activation of earlier-formed fracture and breccia-hosted Mo mineralisation. (image from Kirwin, 2009)

## Mount Elliott-SWAN

The DMQ interpretation in the Mount Elliott-SWAN area (Figure 3.29) leverages the detailed Chinova aeromagnetics (Figure 3.30) combined with Leishman 10K mapping between Mount Elliott and Twiggie Voss to the north, Ivanhoe-Chinova detailed prospect-scale mapping by Lazo (2009) and Gari (2013) and superb historic mapping at Mount Elliott by Searl (1952) and geophysical interpretation by Dunnet (19XX).

The DMQ Mount Elliott-SWAN compilation is a crude GIS layering and melding of the various components. It is not a polished GIS interpretation and shows misalignment of magnetically-interpreted faults with mapped package off-

sets. Further refinement is required but the essence of the important structural relationships is captured in the map.

The following points highlight the major tectono-stratigraphic and geodynamic attributes of this region that impact on mineralisation. This analysis should be reviewed in conjunction with the Time-Space Chart (Figure 3.2) and the complete Tectono-Stratigraphic-Magmatic Assembly of the EFB presented in Appendix 4. A fuller set of useful geophysical images of the Mount Elliott-SWAN area are assembled in Appendix 9.

- DMQ's interpretation places Mount Elliott and SWAN in close proximity to an interpreted D1 structure that juxtaposes a magnetic hanging wall package that includes metabasalts & metadolerites within a package dominated by carbonaceous metasediments, WITH relatively magnetically-benign, STAVELEY to KURIDALA packages to its southwest and west (Figures 3.29 & 3.30)
- The magnetic hanging wall package shows significant angular discordance across the D1 fault in both mapped outcrop patterns and in the magnetics (Figures 3.29 & 3.30).
- The timeslice affiliation of the magnetic hanging wall package is uncertain. The presence of significant volumes of metabasalt and metadolerite within metasediments that include significant volumes of carbonaceous lithologies suggests a TOOLE CREEK equivalence (rather than the previously ascribed KURIDALA correspondence) and is the favoured interpretation of DMQ (but is by no means a certainty).
- The interpreted D1 overthrust relationship of the proposed TOOLE CREEK package with STAVELEY is in accord with D1 overthrust relationships mapped and interpreted elsewhere in the project area (specifically east of Cloncurry and in the Snake Creek Anticline region; see Appendix 4)
- At Mount Elliott-SWAN, in the footwall of the D1 Fault (locally called Mount Elliott Fault & Jocks Fault) a steeply north-plunging, potentially F1 fold of the upper STAVELEY-Roxmere Quartzite-KURIDALA sequence is defined from mapping and drilling.
- Significant boudinaging of the metadolerites in the hanging wall package is associated with widespread iron oxide alteration and the relationship with the adjacent WILLIAMS-aged, Squirrel Hills Granite suggests that strain partitioning in this volume of rock has syn-WILLIAMS, D4 timing.
- The DMQ interpretation suggests re-activation and modification of the D1-fold and fault relationships in D2-3 times with a major D2 reverse fault overthrust of the entire D1-juxtaposed TOOLE CREEK-KURIDALA-STAVELEY package westward over structurally-simpler

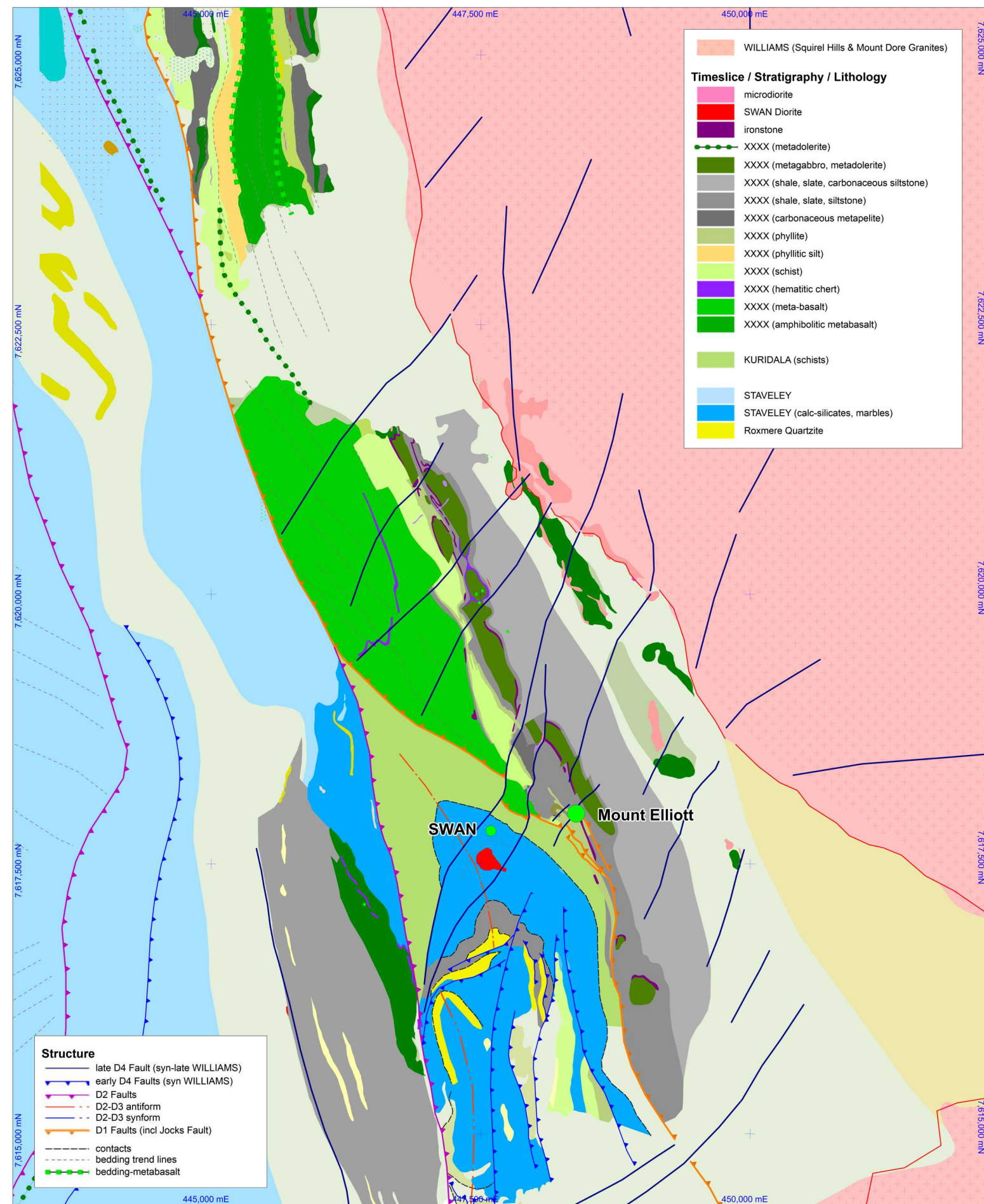


**Figure 3.29** Mount Elliott-SWAN region DMQ detailed geological interpretation highlighting juxtapositioning of a metabasalt, metadolerite-bearing metasedimentary package with STAVELEY-KURIDALA

STAVELEY to the west. This structurally-simpler STAVELEY package includes a thick package of non-calc-silicate metasediments including some siliceous siltstones that have been sometimes ascribed to the Roxmere Quartzite (incorrectly in the view of DMQ).

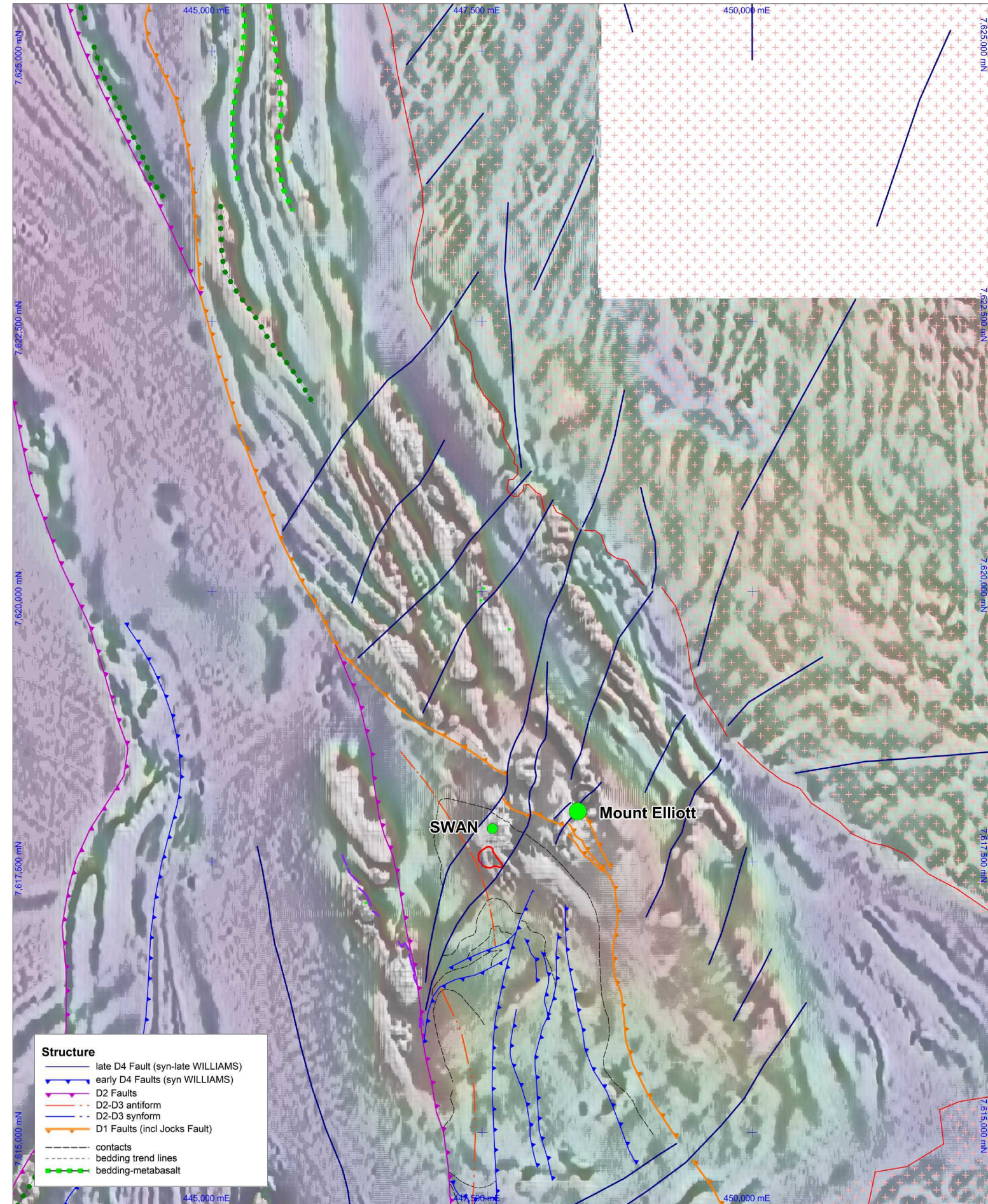
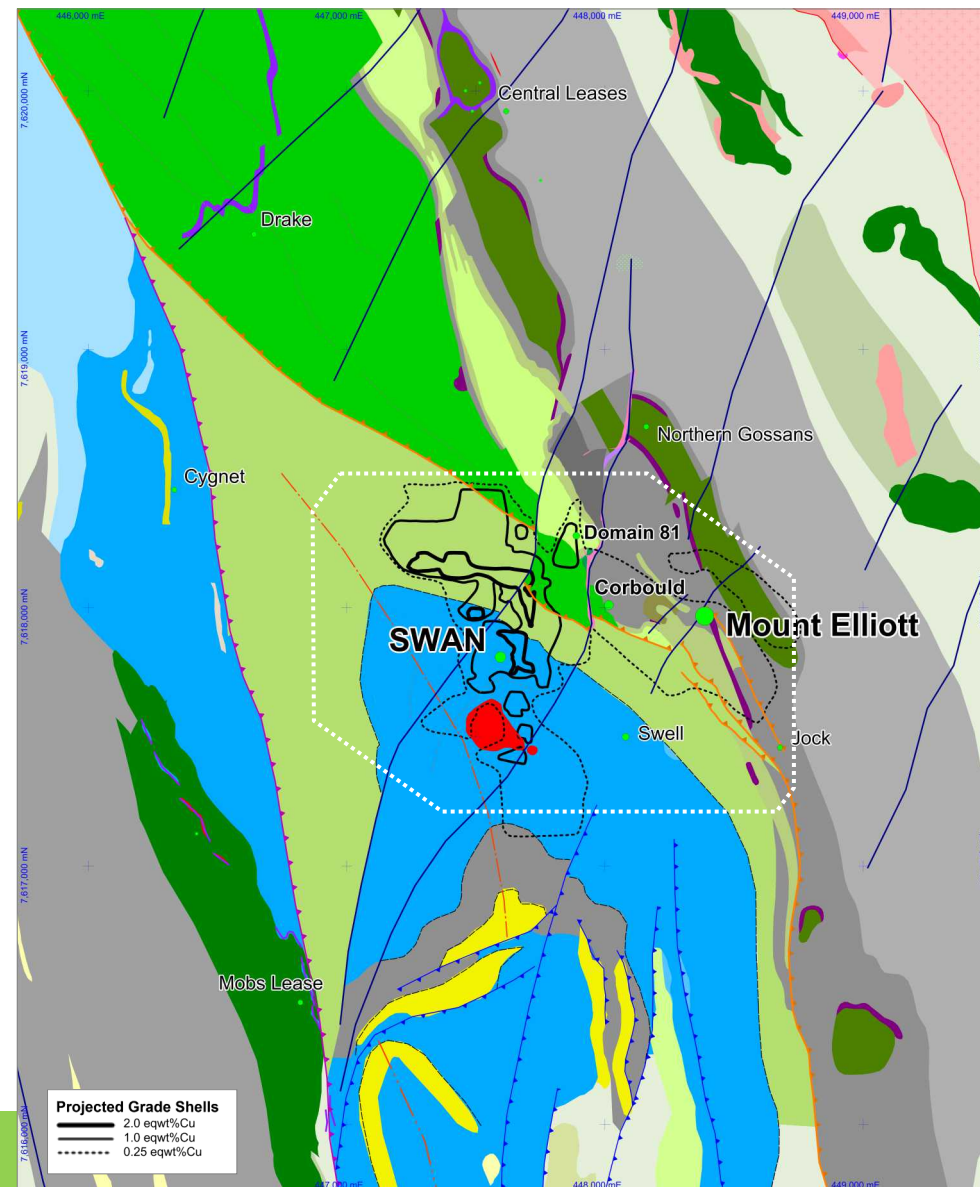
## Mount Elliott-Corbould-SWAN Mineralisation

Figure 3.31 presents eqwt%Cu shells of the SWAN (post mining Mount Elliott-Corbould) vertically projected onto a zoomed view of the Mount Elliott-SWAN DMQ geology. DMQ's interpretation of the controls of Mount Elliott-Corbould-SWAN mineralisation are outlined in the following notes.

- In WILLIAMS, post-peak metamorphic, times at shallow to mid-crustal levels, the Squirrel Hills Granite becomes sufficiently solidified to force strain partitioning during NW-directed D4 shortening in adjoining rock volumes. Existing structures (D1-D3) and schistose metasediments accommodated shortening by transpressive re-activation of existing fabrics and faults.
- However, metadoleritic sills within the D1 hanging wall metasediments and the metabasaltic volumes remained relatively rigid and either deformed in a brittle fashion (block boudinage of the metadoleritic sills) or partitioned strain around themselves. The wedge of D1-truncated metabasalt that terminate just NW of Mount Elliott, and in particular its hanging wall margin, are interpreted to have driven significant strain partitioning and brecciation in the adjacent carbonaceous metasediments to focus fluid flow and control the localisation of the Mount Elliott and Corbould ore zones.

- In the footwall of the D1 Mount Elliott-Jocks Fault, the highly-schistose KURIDALA phyllites and metasediments accommodate D4 transpressive strain by slip on existing schistose fabrics and the partitioning of-strain into the adjacent brittle calc-silicates and marbles of the upper STAVELEY. Brecciation is further localised by the locking effect of the moderately to steeply-plunging SWAN diorite ... resulting in a breccia volume that, in part, wraps (and overprints) the SWAN diorite as well as bridging the gap between the diorite plug and the re-activating KURIDALA schists (see Figures 3.32 & 3.33) and D1 fault. Focused fluid flow

**Figure 3.31** Zoomed DMQ interpretation of Mount Elliott-SWAN region showing projected equivalent Cu% grade shells and NNW steep plunge of SWAN mineralisation sub-parallel with the dip of the STAVELEY-KURIDALA contact. Other legends as for Figure 3.29. Outline of Figure 3.32 at 2150mRL shown in white dashed polygon.



**Figure 3.30** Detailed Chinova vrmi-2vd over tmi-rtp aeroMag over Mount Elliott-SWAN region overlain with the DMQ structure framework from Figure 3.29

within this fracture and breccia volume produced the large tonnage SWAN mineralisation.

- No magmatic link between the SWAN diorite and SWAN mineralisation is implied, however, contact metamorphic pre-conditioning of the STAVELEY calc-silicates prior to brecciation and mineralisation is a possibility.
- Figure 3.32 highlights the tight spatial control of SWAN mineralisation by brecciation at the top of the STAVELEY calc-silicates/marbles between the SWAN diorite and the unmineralised KURIDALA schists. This simplified (Chinova) geological model does not include an interpretation of the D1 fault, the geometry of the metabasalts, nor the post-mineral, late D4 cross-cutting faults.
- The spatial association between the SWAN diorite and SWAN mineralisation is highlighted in Figure 3.33. DMQ interprets them both to be offset by post-mineral faults that also demonstrably cut and displace the WILLIAMS-aged Squirrel Hills Granite (Figures 3.29, 3.30 & 3.31). These late D4 faults potentially do not post date the complete thermal decay of the Squirrel Hills magmatic system. Chinova have drilled Domain 81 mineralisation which appears to be controlled by one of these structures and some of the structures are intruded by potential late-phase WILLIAMS-related microdiorites. DMQ would argue that main stage mineralisation is largely over by the time these structures dislocated the architecture and the already-existing SWAN mineralisation.

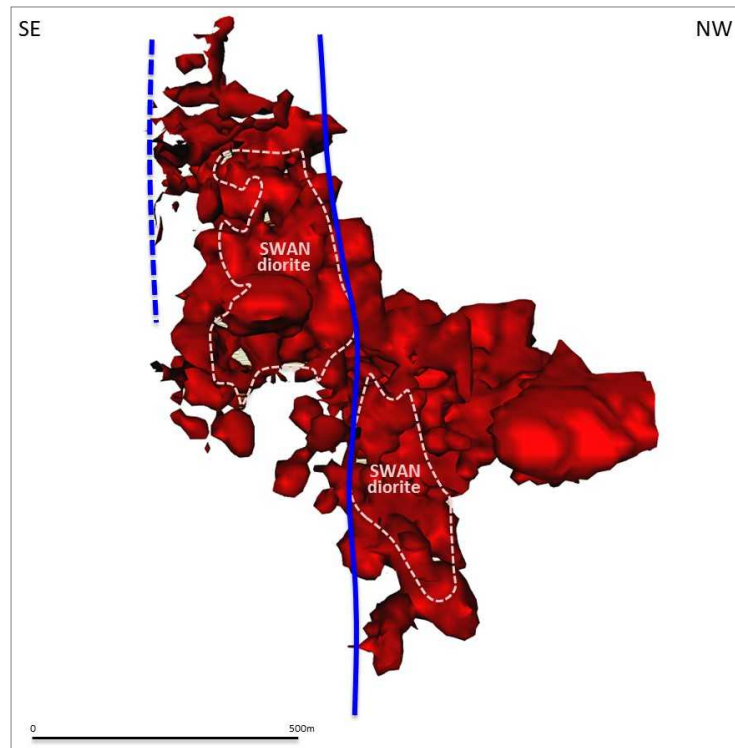


**Figure 3.33** SWAN mineralisation shell at 0.75eqwt%Cu looking SW through the SWAN mineralisation with the ghosted outline of the SWAN diorite and projected post-mineral, late D4 faults that are interpreted by DMQ to offset both the SWAN diorite and mineralisation.

**Figure 3.34** DMQ geological interpretation of the Osborne-Kulthor region that highlights a D2-D4-fault dismembered of a D2-folded package of KURIDALA (Starcross Formation).

## Osborne-Kulthor

Osborne and Kulthor are covered by up to 60m of Cretaceous sediments so the DMQ interpretation (Figures 3.34 & 3.35) is substantially built on Chinova's detailed magnetics augmented with previous company interpretations

from RAB drilling (primarily Morrison, 2002) in the immediate Kulthor-Osborne area and detailed mine-scale work at Osborne (King, 2001) and at Kulthor (Hinman, 2012, 2013).

The Proterozoic geology around Kulthor and Osborne is interpreted to comprise the Starcross Formation which has

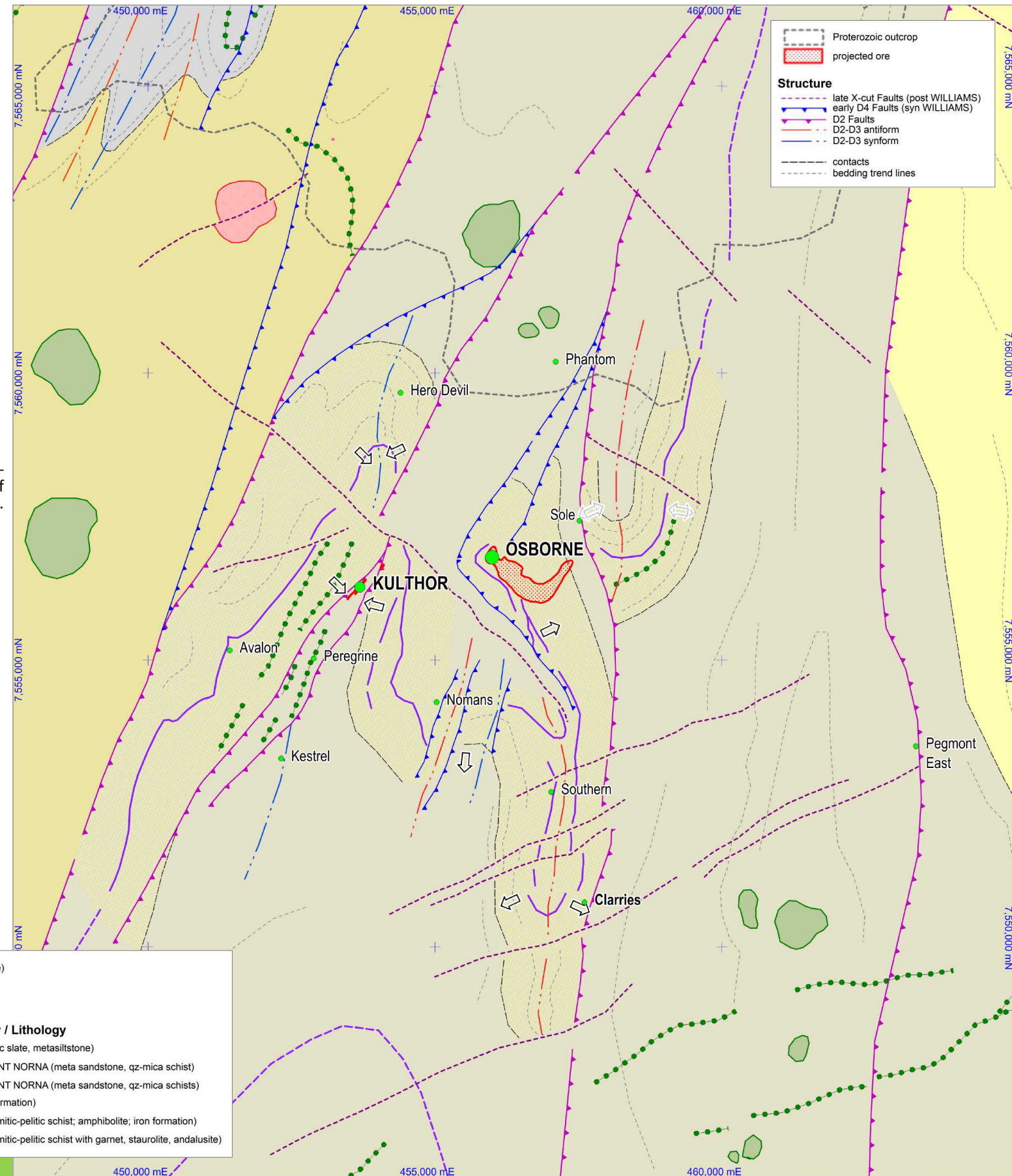
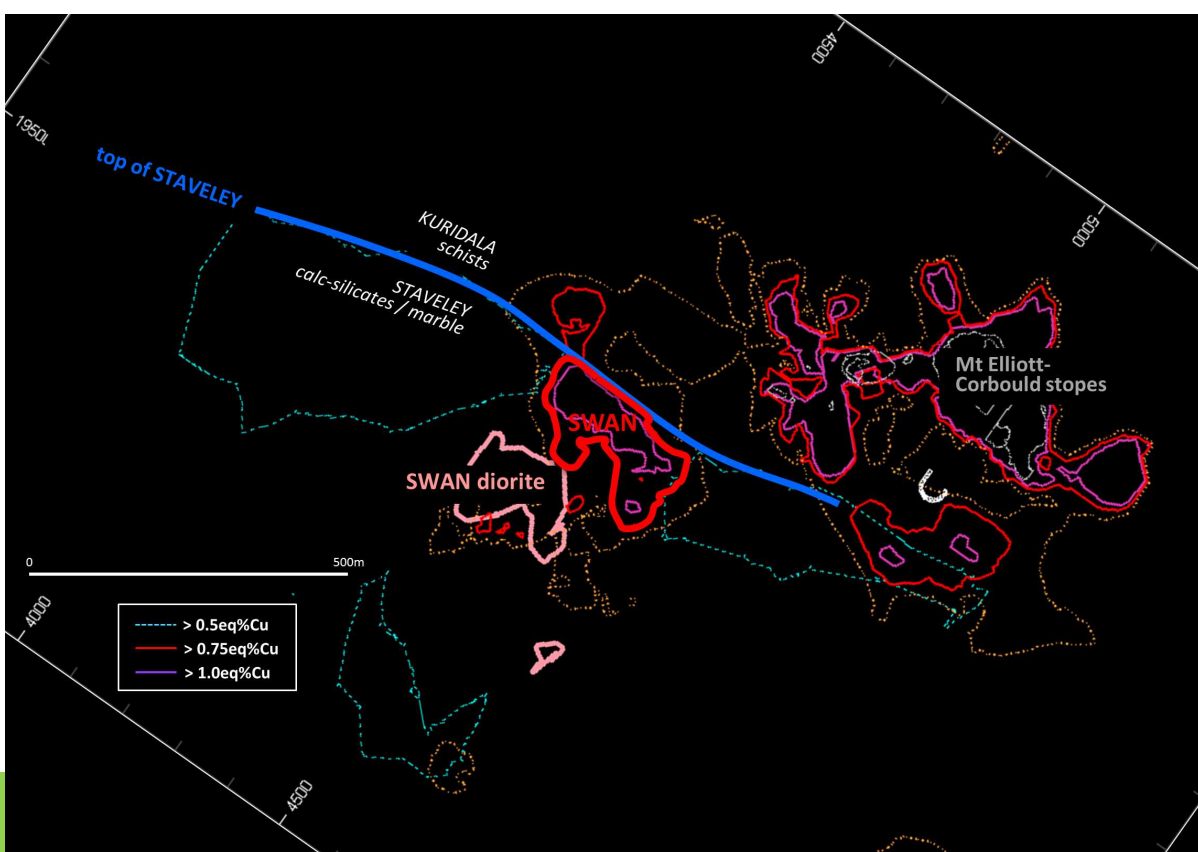


**Figure 3.32** SWAN Level Plan at 2150mRL (250m below surface) showing eqwt%Cu shells and highlighting tight spatial control of SWAN mineralisation by brecciation at the top of the STAVELEY calc-silicates/marbles between the SWAN diorite and the unmineralised KURIDALA schists.



been placed within the KURIDALA timeslice. The following details the major tectono-stratigraphic and geodynamic features of this region that are interpreted to impact on mineralisation. This analysis should be reviewed in conjunction with the Time-Space Chart (Figure 3.2) and the complete Tectono-Stratigraphic-Magmatic Assembly of the EFB presented in Appendix 4. A fuller set of useful geophysical images of the Osborne-Kulthor area are assembled in Appendix 9.

- The local KURIDALA Starcross Formation comprises upper amphibolite-grade, migmatitic metapelitic schists, granoblastic psammites, some magnetite iron formations, amphibolitic metadoleritic sills and locally significant partial melting.
- A particular KURIDALA Starcross psammitic unit (see Figure 3.35) has a distinctive magnetic character and has been used to interpret the structural architecture of the area. It includes magnetite iron formations, formational amphibolitic sills of likely metadoleritic origin and weakly-magnetic, massive psammitic metasedimentary units.
- The KURIDALA Starcross Formation has been folded into a series of disharmonic D2 folds at upper amphibolite grade. These high grade D2 folds contrast with the tight D2 folds developed across the NEW HOPE-MOUNT NORNA-ANSWER transitions to the northwest of Figures 3.34 & 3.35.
- Later D2 shortening results in regional-scale, short-limb, dextral transpressive failure that dismembers the folded metamorphosed packages along regional-scale D2 faults that juxtapose KURIDALA over NEW HOPE-MOUNT NORNA in the west and NEW HOPE-MOUNT NORNA over KURIDALA in the northeast.
- At Kulthor, detailed mine scale analysis (Hinman, 2013) indicates that this D2 faulting has juxtaposed opposite facing packages. An attempt has been made to project this facing throughout the area of detailed interpretation (but it becomes less clear in the major D2-fault block east of Osborne).
- Post D2-D3, at shallower crustal levels in D4 time, these D2 faults are re-activated under NW-directed shortening, some new D4 faults develop with less significant displacements, and where lithology allows, brittle fracture and breccia deformation occurs. High grade meta pelitic schists and other meta-sediments accommodate this shallower crustal deformation via slip on existing fabrics. Like elsewhere in the belt, only lithologies that remain brittle through peak metamorphism, can express fracturing and brecciation to focus mineralising fluid flow at this time.

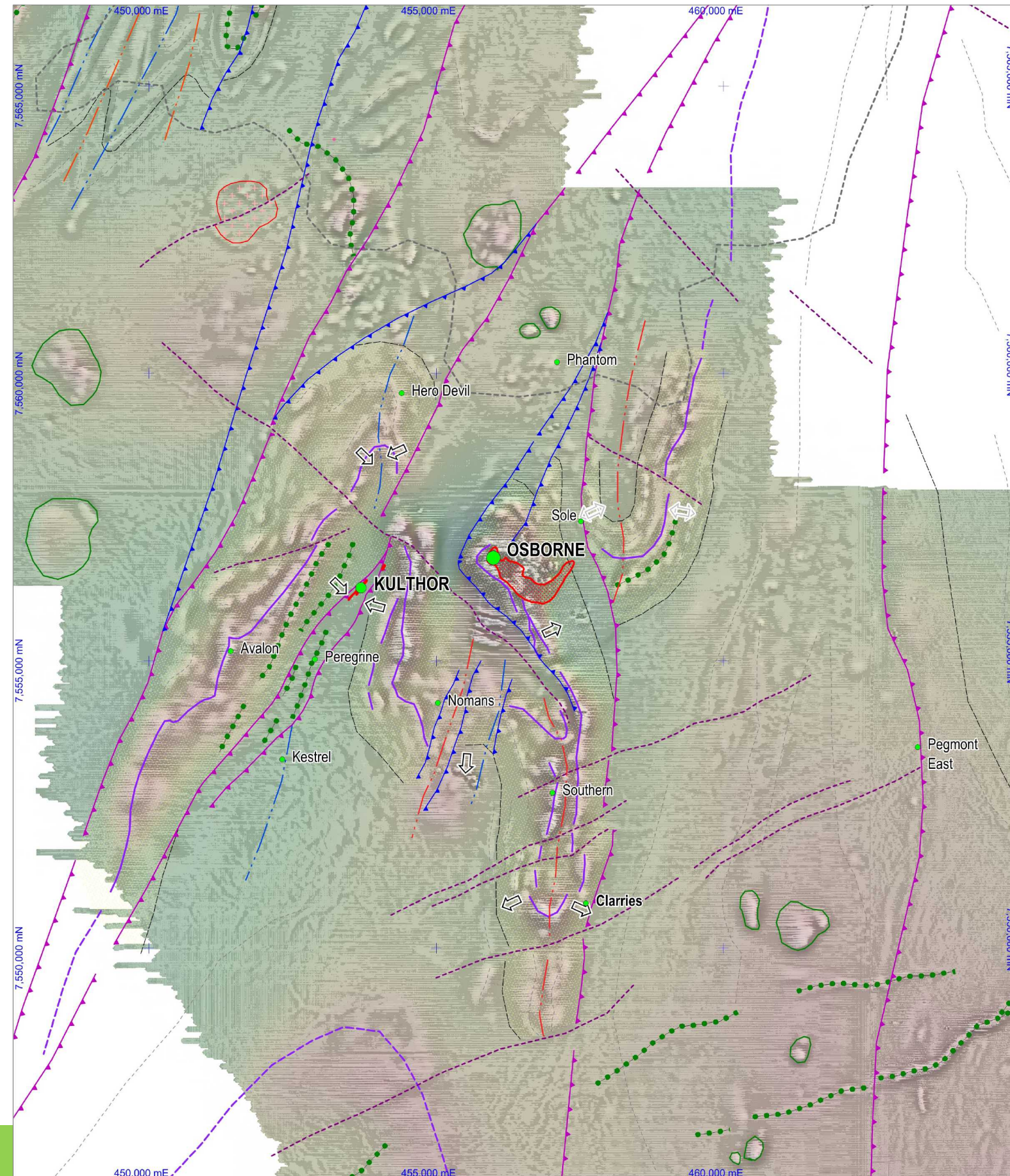
- A complex northwest-trending domain immediately southwest of Osborne shows late cross-cutting fault re-activation but likely reflects an earlier structure that has significantly influenced the iron formation geometries at Osborne and the interpreted distribution of D4 reverse faulting to the zone's north and south. It is hypothesised by DMQ that this pre-existing zone might have acted as a sidewall-style structure during D4 ... accommodating strike-slip-dominated transpressive deformation while the NE-trending D4 structures deformed via reverse-dominated transpressive failure. This is consistent with King's 2001 detailed mine scale work at Osborne.
- King (2001) elegantly documents at Osborne a shift FROM EW-shortening (DMQ D2) associated with fabric development including mylonitic zones around competent blocks (so called 'low-grade', 'Pip' domains), and the vertical imbrication of 'ironstone units' with synchronous partial melting, granoblastic re-crystallisation and sub-horizontal pegmatite formation TO later (DMQ D4) NW-directed shortening which re-activated the grossly NW-trending architecture in strike-slip mode. This re-activation gaped the pre-existing complex structural network, focused silica flooding and drove a brittle fracture-breccia network of the iron formations and silica flooding to host Cu-Au mineralisation. This sequence is in excellent accord with the structural relationships at Kulthor (see below) and elsewhere in the belt.
- Past workers have emphasised apparent lower metamorphic grade assemblages ('low-grade' 'Pip'; sometimes 'SAM' for pSammite-Amphibolite-Magnetite iron formation assemblages) which host mineralisation and appear to have avoided higher grade partial melting and mylonitic deformation. Both Kulthor and Osborne are associated with these unusually siliceous, meta psammitic-siltstone and (at Osborne) magnetite iron formation bearing packages (Figure 3.36). DMQ interprets that these apparently 'low-grade' lithologies are just not compositionally amenable to express amphibolite grade fabrics and mineralogies due to their highly silica-rich and/or magnetite-rich compositions. In post peak-metamorphic, D4-times, in shallower crustal settings they have maintained their brittle character and lie within a sea of highly schistose, high grade migmatitic, granoblastic & pegmatitic, interbedded meta-pelites & psammites. They become the focus of brittle, fracture and breccia deformation, focus fluid flow and host mineralisation where deformation and fluid flow conspire.
- Kulthor mineralisation is controlled by transpressive re-activation of two converging D2 faults and the associated brittle behaviour of amenable lithologies between them (see below). Kulthor mineralisation has not been

convincingly traced north of the aforementioned NW-trending structural domain.

- A string of interpreted metadolerite-granitic plug-like intrusions ring the Osborne-Kulthor area (Figures 3.34 & 3.35) which may reflect co-magmatic mafic magma-

tism and intrusive geometries at depth (see WILLIAMS granite geometry section later).

**Figure 3.35** Detailed Chinova vrmi-2vd over tmi-rtp aeroMag in the Osborne-Kulthor region overlain with the DMQ structure framework from Figure 3.34

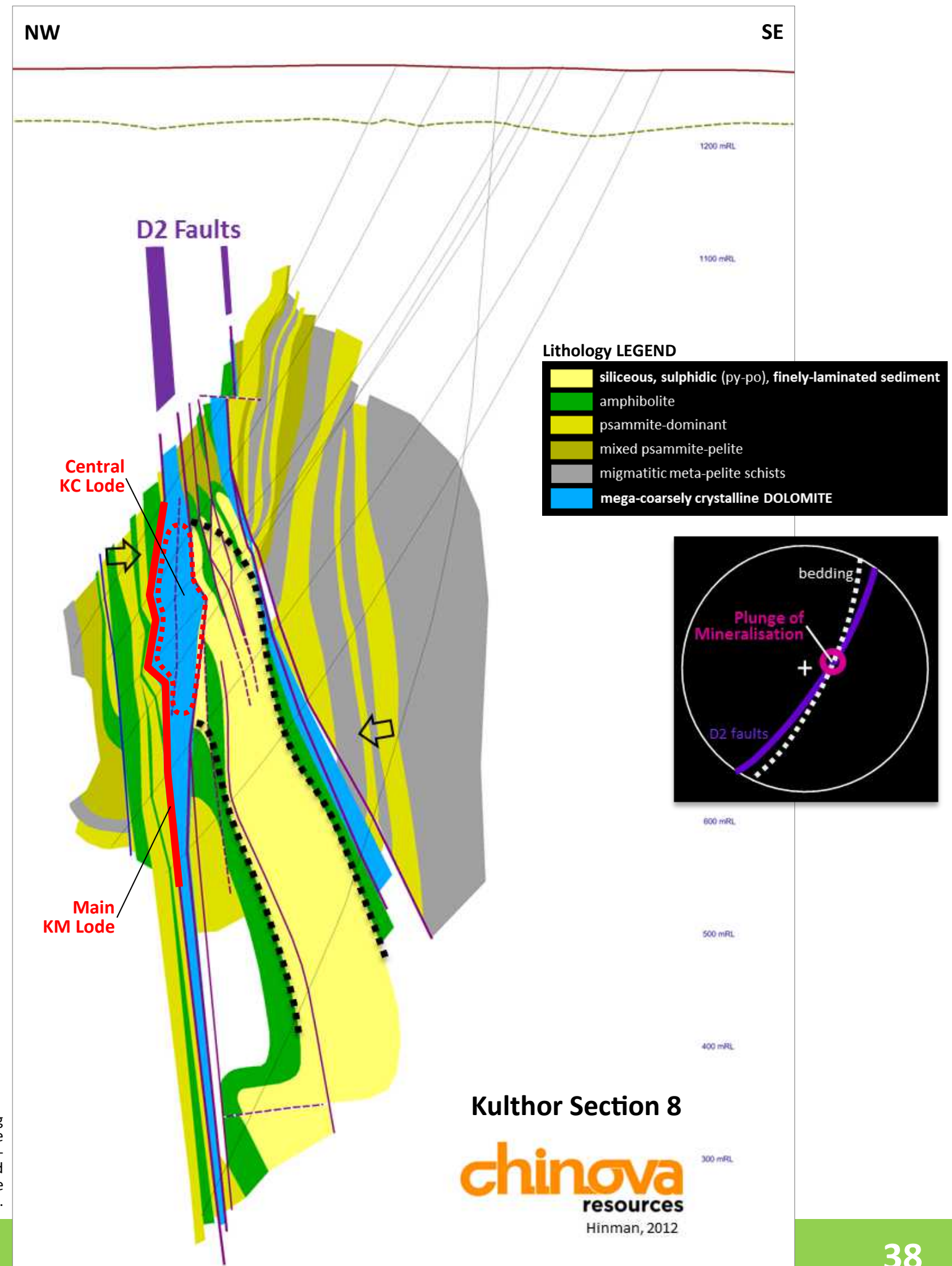


## Kulthor Section 8 Geology - Controls on Mineralisation

A section through the Kulthor system is presented in Figure 3.38. Its location through the centre of the Kulthor orebody is indicated on Figure 3.36. The following highlights the essential features of the Kulthor system and the implications for the control of the sulphide-dominated 'ISCG' mineralisation at Kulthor.

- The Kulthor system is essentially blind to geophysics with mineralisation discovered at depth beneath Cretaceous cover via step-out drilling from a low level aircore geochemical anomaly on the Cretaceous unconformity.
- The two major D2 Faults in the Kulthor system (Figures 3.34 & 3.36) juxtapose opposite facing KULTHOR (Starcross) packages in the KM footwall and the ultimate hanging wall schistose metapelitic package.
- The central block (between the two D2 Faults) includes a thick, finely-laminated, highly siliceous and sulphidic (py-po), fine-grained meta-sandstone-siltstone (part of the 'SAM' package). It is highlighted in both the sectional view (Figure 3.38) and plan view (Figure 3.36). It displays significantly brittle behaviour throughout its deformation history.
- Both the D2 fault zones are filled with mega-coarsely crystalline dolomite which exhibits mega-breccia relationships with the KC lode hanging wall central block 'SAM' lithologies (to the SE). Subsequent 3D DMQ analysis (Chapters 4 & 5) will suggest that STAVELEY packages are present beneath the Kulthor system (potentially within 1km) and that during post D2 time (perhaps during D2b orogenic collapse) but certainly prior to D4 brittle re-activation, dolomite is remobilised from the high metamorphic grade STAVELEY package at depth into the gaping D2 Faults at Kulthor.
- Dolomite precipitation is demonstrably post-peak metamorphism where it forms schistosity-cross-cutting mega breccias with the high grade metamorphics. The mega-crystic dolomite only exhibits brittle fracture and breccia overprint deformation (no ductile deformation) in D4.
- During ongoing D4 shortening (post dolomite), the brittle dolomite and 'SAM' package find themselves within a re-activating D2 fault network and a sea of highly schistose interbedded meta-pelites and psammities. Brecciation

**Figure 3.38** Kulthor Section 8 geological model (looking NE) highlighting Cretaceous cover; coarsely crystalline dolomite within the earlier D2 faults; the siliceous, sulphidic central unit and the location of Main (KM) and Central (KC) 'Lode' Cu-Au mineralisation. Facing in the HW and FW packages is also shown.



**Kulthor Section 8**  
**chinova**  
resources  
Hinman, 2012

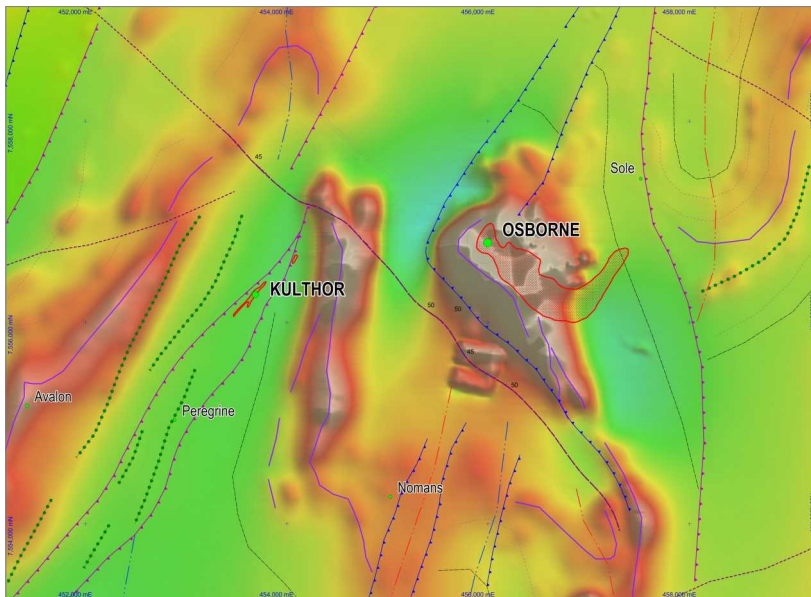
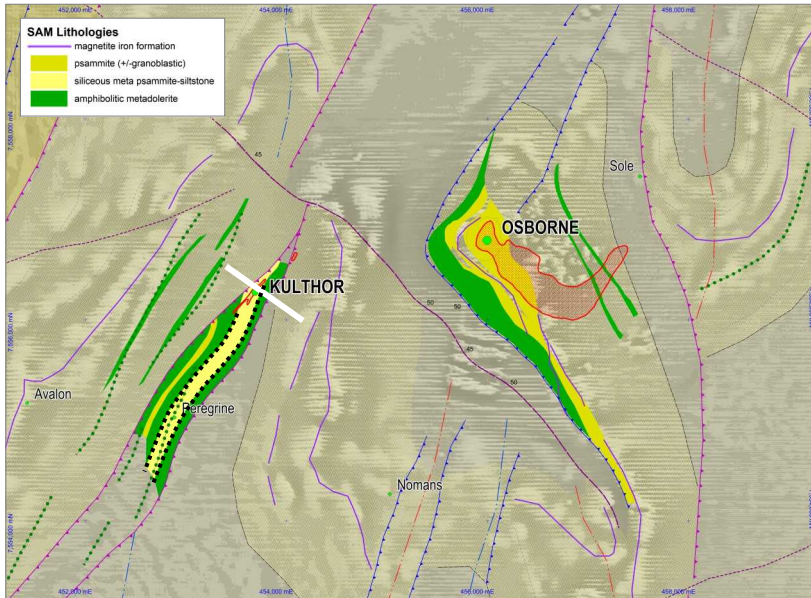


**Figure 3.36** (top) Kulthor-Osborne geology zoom highlighting both systems association with 'SAM' assemblages comprising (±granoblastic) psammities, siliceous (±pyritic) metasediments and amphibolites. **Figure 3.37** (bot) DMQ structural interpretation over Chinova tmi-rtp magnetics highlighting the contrasting 'IOCG' vs 'ISCG' affinities of Osborne and Kulthor respectively.

Figures 3.36 and 3.37 highlight the association of both Osborne and Kulthor with the unusual 'SAM' lithologies that maintain brittle behaviour into post-peak metamorphic times as well as the starkly contrasting magnetic signatures of the two systems that reflects their Fe-oxide and Fe-sulphide dominant associations ('IOCG' vs 'ISCG' respectively).

A full library of geophysical signatures of the Osborne-Kulthor region (and the other detailed areas of interest) as well as detailed prospect-scale images around know resources is presented in Appendix 9.

and fracturing along the re-activated footwall dolomite contact produces the geometrically-planar, KM Main 'Lode' and significantly more geometrically-complex, breccia, fracture and replacement KC Central mineralisation forms within the thickest portions of the dolomite.

- In both plan (Figure 3.35) and section (Figure 3.38) view, these 'Lodes' lie where the central brittle, sulphidic and siliceous 'SAM' package is truncated against the re-activated D2 footwall Fault and the mega-crustic dolomite.
- The abundant local supply of pyrite and pyrrhotite within the central siliceous metasedimentary package is hypothesised to control the Fe sulphide-richness of the Cu-Au Kulthor ore system.
- The geometry of steeply-dipping structure and slightly oblique, shallowly-converging, steeply-dipping stratigraphy produces a steeply-plunging ore system (see stereoplot in Figure 3.38).
- Significant post-mineral, moderately NE-dipping reverse faulting dismembers the steeply-plunging Kulthor system into series of offset fault blocks (the chocolate block fault set). These will not be addressed in further detail here but are critically important to stope design and brownfields exploration (see DMQ Presentations).

## Timing of Osborne-Kulthor mineralisation

Detailed mine-scale work at Osborne and Kulthor have demonstrated the post-peak metamorphic timing, and brittle fracture-breccia control on Cu-Au mineralisation at each of the deposits. The mine-scale structural analyses by Neil Adshead (1995 PhD) and Stephen King (2001) at Osborne and Hinman (2012) at Kulthor have amply demonstrated the post-peak metamorphic and brittle fracture and breccia control on ore in both systems which significantly conflicts with a 1595-1600Ma, so-called 'syn-metamorphic', Re-Os molybdenite age published for Osborne (Gauthier et al., 2001) that has infiltrated the Isan IOCG literature.

This Re-Os molybdenite date contrasts with prior determinations that had Cu-Au mineralisation post dating hydrothermal hornblende and biotite that yielded Ar/Ar ages ca 1540Ma (Perkins & Wyborn, 1998). Due to the potential for Ar loss this ca1540Ma age was considered a maximum age for these alteration minerals and for mineralisation.

This <1540Ma date on Osborne alteration/mineralisation is in considerably better accord with the geological observations and significantly closer to the age of WILLIAMS suite intrusion in the belt (see Tx Chart Appendix 1).

DMQ considers there to be significant problems with Re-Os dating of deformed molybdenite. Recent dating of de-

formed molybdenite from the Merlin Mo resource has returned ages for deformed molybdenite from samples from a single section through the mineralisation (2 adjacent lenses) spanning >50Ma (~1550Ma to ~1500Ma; Babo et al., 2017). Contrary to Babo et al., DMQ regards the younger ages (1521±3Ma) on stylo fracture-controlled molybdenite to potentially better represent the age of original fracture and breccia controlled Mo mineralisation (see Merlin section) and the older Mo-matrix breccia results (1535±6Ma) to reflect disturbed Re-Os systematics within the deformed molybdenite associated with the post-mineral reactivation of the mineralised structures (see details in the Merlin Section discussion).

Little work has been done on the quantitative distributions of Re and Os in deformed molybdenite, but suspect ages abound in the literature (McCandless et al., 1992) in which Re loss results in erroneously older age determinations. Recently published work on Merlin molybdenites by Sharma et al. (2016) highlighted highly significant, inclusion clearing in molybdenite that was deformed, but was unable to identify Re loss (or other systematics) in the cleared, deformed molybdenite. DMQ believes work on the distribution of Re in primary and deformed molybdenites within single systems (like Merlin) requires further work to clarify the perplexing and geologically-not-substantiated ages at Osborne and Merlin. If Re loss is a reality, the Merlin (and Osborne) Re-Os molybdenite ages need to be regarded as maximum ages for mineralisation (cf Babo et al., 2017).

Figure 3.39 reproduces a photomicrograph from Subira Sharma (pers comm, 2015) of Merlin molybdenite highlighting the contrasts between Mo1, which is crowded with inclusions that include carbonaceous matter, and Mo2 which is strongly kinked and inclusion-free.

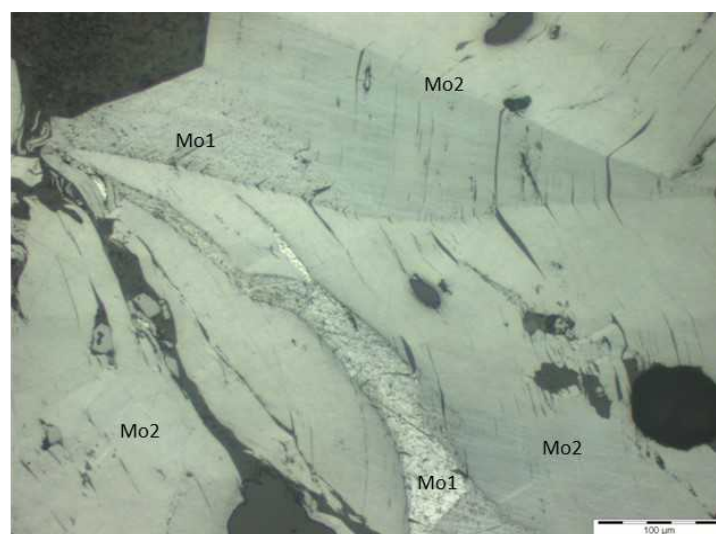


Figure 3.39 Merlin molybdenite photomicrograph showing inclusion-rich Mo1 and clean, kink-deformed, inclusion-free Mo2

## Ernest Henry

Access to mine geological models, previously used in the BRC-Geology and Mass Mining Project (GMM, 2013-2015), was generously approved for use by Trevor Shaw (Glencore MIM) in the DMQ project. Wireframes of geological features, boundaries, and grade shells have allowed

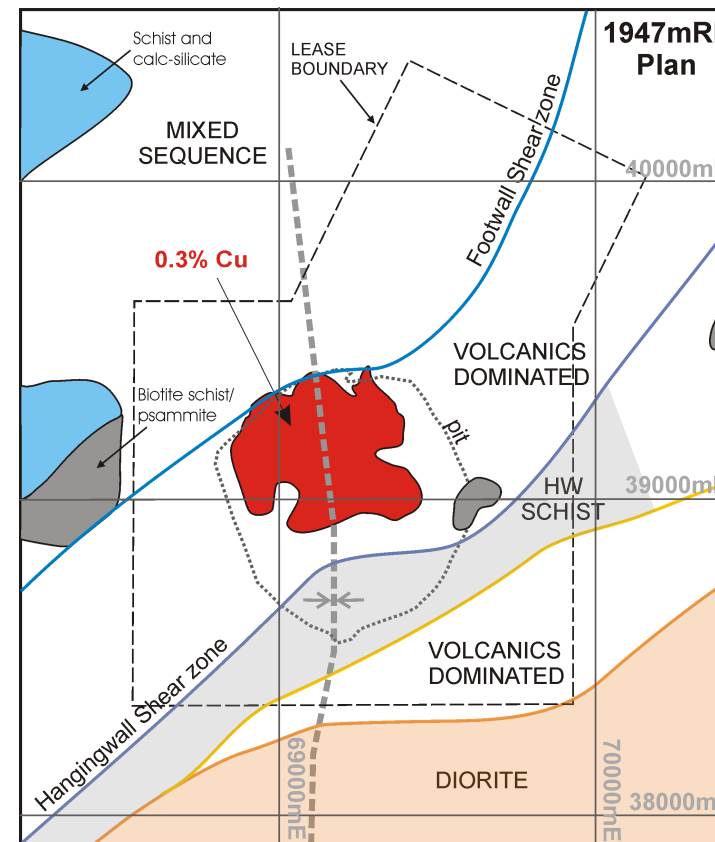


Figure 3.40 Ernest Henry Geology at 1947mRL highlighting the system's location on a NS fold axis. Map modified from Mark et al., 2006.

DMQ to develop an alternative model for the macro-scale controls on the Ernest Henry ore deposit.

The Ernest Henry Cu-Au deposit is hosted within the ~1745-1740Ma Mount Fort Constantine Volcanics (MFCV) which at the mine comprise intermediate volcanics-volcanoclastics, overlain by schists and interbedded volcanics. A medium-grained diorite intruded the MFCV package at ~1657Ma and constitutes a competent body approximately 1km to the SE of the orebody (Figure 3.40). To the immediate NW of the host MFCV package some mixed calc-silicate and metasedimentary packages of possible CORELLA-age are known (Figure 3.40) potentially placing the Ernest Henry orebody close to an either stratigraphic or structural juxtapositioning of MFCVs and CORELLA packages.

The Ernest Henry ore is dominated by magnetite, occurring as matrix to breccia zones and containing lesser amounts of pyrite and chalcopyrite.

The geology of Ernest Henry mine is often portrayed in South-North cross-section through the orebody, with apparent parallelism of geological features and grade boundaries (Figure 3.41). Parallelism of the long axis of the orebody with shear fabrics in adjacent shear zones is commonly inferred to indicate the structural control on the orebody orientation and geometry (Huston, 2016). Three-D geometric observations made during the GMM project suggested a parallelism of the Ernest Henry orebody with the axis of folded stratigraphy in its hanging wall (Webster et al., 2015).

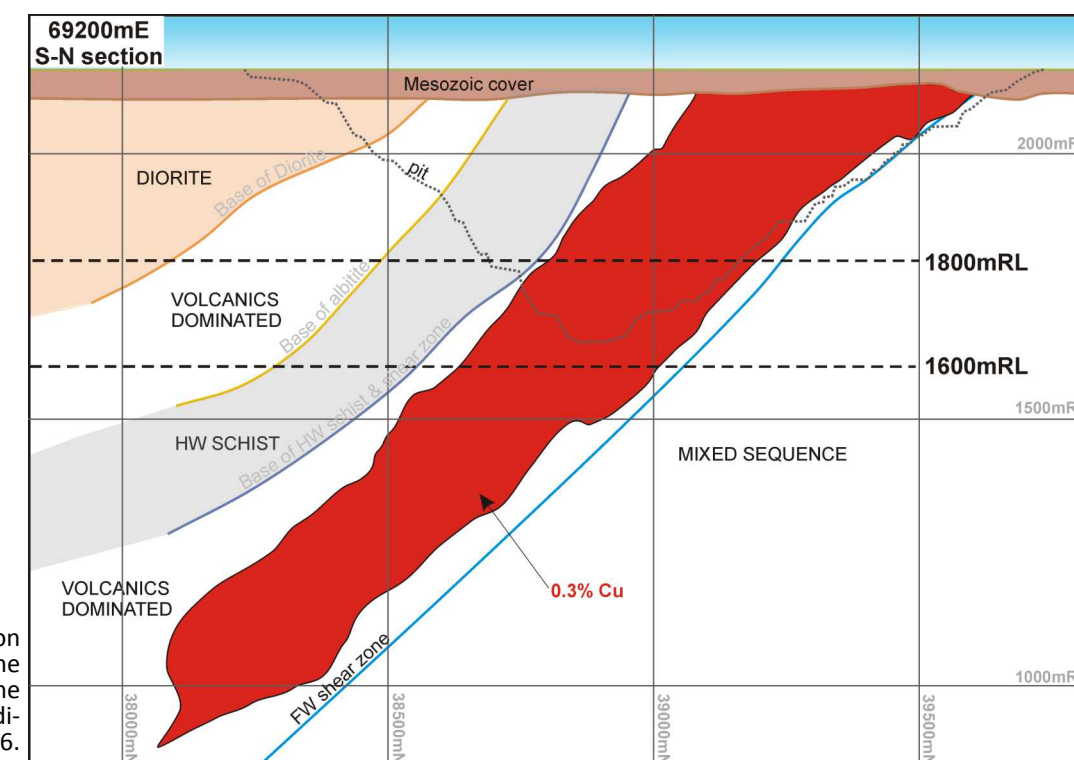
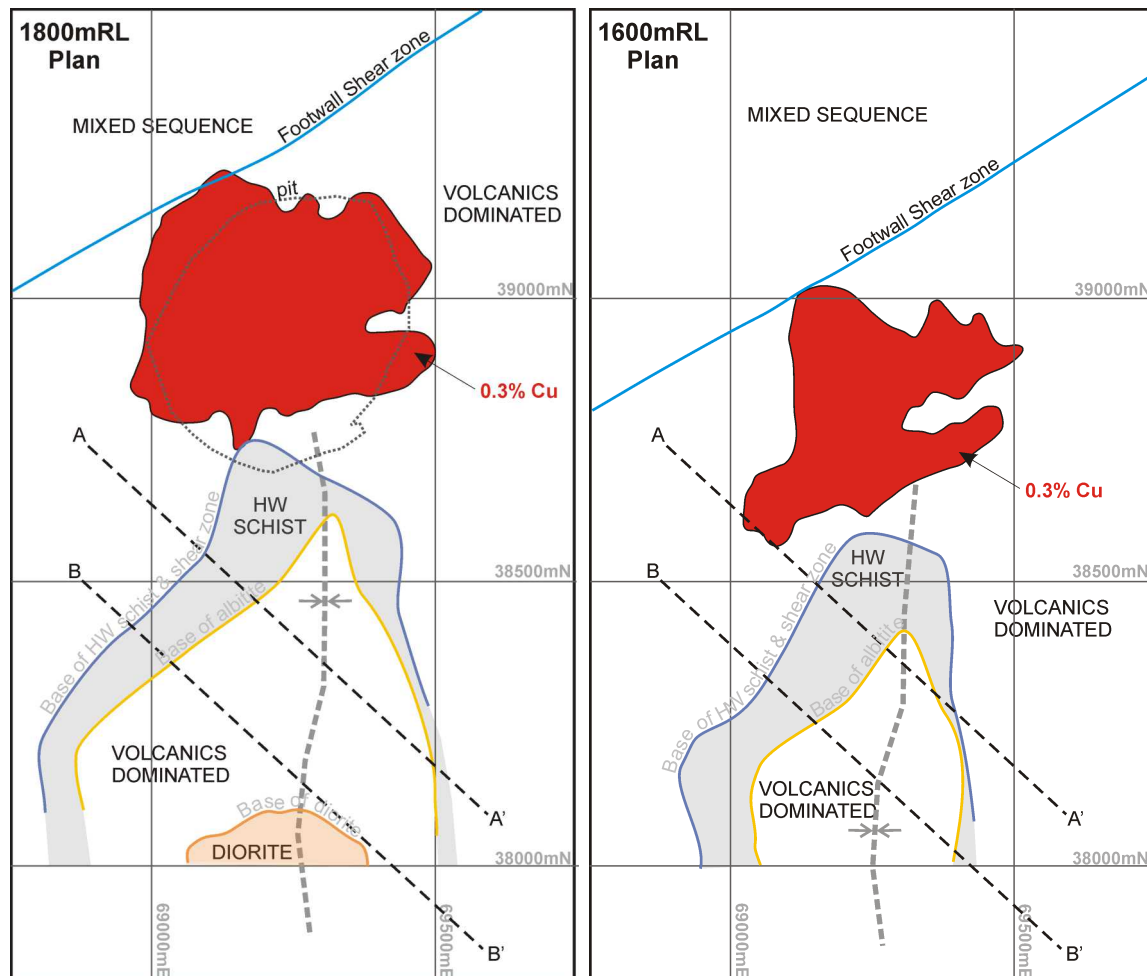


Figure 3.41 Well published N-S section through Ernest Henry emphasising the parallelism of ore with FW shear zone and lithological packaging. Section modified from Mark et al., 2006.

In plan view (Figures 3.40, 3.42 & 3.43), the stratigraphy, and hangingwall shear have a folded geometry modelled as a synform. Folding of the hangingwall shear zone suggests that this feature is controlled by rheological contrast and concentration of strain along the contact of the host volcanics with the overlying schists.

The location of the EH orebody is, broadly speaking, around the intersection of the south-plunging fold axis with the planar SE-dipping Footwall Shear Zone (Figure 3.42). With increasing depth, the modelled grade distribution (outline at 0.3%Cu) indicate northeast trends parallel to the FW Shear Zone which are not folded by the mine-scale synform, suggestive



**Figure 3.42** 1800mRL Level Plan highlighting location of EH ore broadly at the intersection of a south-plunging synform with the FW Shear Zone.

**Figure 3.43** 1600mRL Level Plan highlighting location of EH ore broadly at the intersection of a south-plunging synform with the FW Shear Zone.

that the fold is pre-mineralisation and D2 in timing and consistent with interpretations of later D4 re-activation timing of mineralization (Figure 3.43).

Two cross-sections have been constructed in the D4  $\sigma_1$ - $\sigma_3$  plane and are presented in Figures 3.44 & 3.45. Their locations are indicated in Figures 3.42 & 3.43. This orientation is approximately orthogonal to the apparent tabular zones of mineralization identified in plan view (Figure 3.43). These oblique sections again highlight that mineralization is not folded around the synform; and that the body of mineralization is preferentially located on the western limb of the fold.

In fact, where mineralization projects across the axial trace, as illustrated in Figures 3.44 & 3.45, it changes in shape from a massive amorphous zone, and occurs in narrower, discrete, planar geometries cross-cutting the eastern limb. This geometry would be consistent with west-side-down sense of shear during D4 re-activation, in that brecciation could be focussed in the folded volcanics where the sense of shear of younger deformation is the opposite to

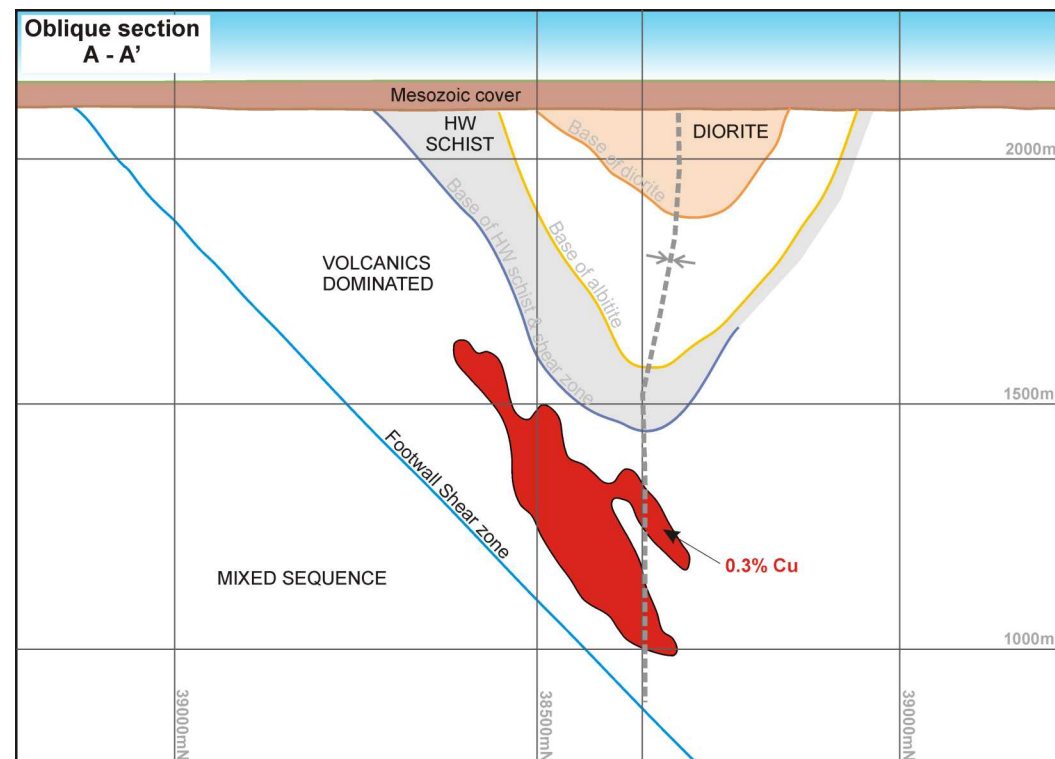


**Figure 3.44** Oblique section A-A' highlighting EH mineralisation's parallelism with the western limb of the south-plunging fold and the Footwall Shear Zone and its discrete planar geometry where it cuts the fold axial plane

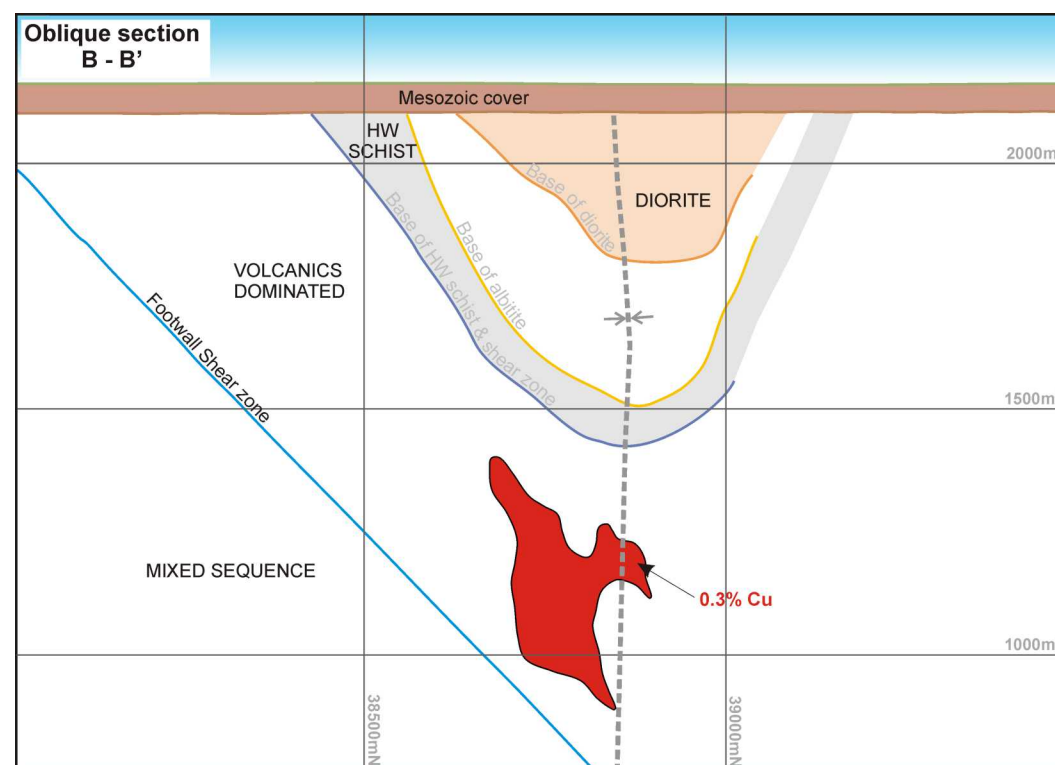


**Figure 3.45** Oblique section B-B' highlighting EH mineralisation's parallelism with the western limb of the south-plunging fold and the Footwall Shear Zone and its discrete planar geometry where it cuts the fold axial plane

that of older deformation fabrics. Localization of brecciation proximal to, but not coincident with, the hinge of the fold may indicate that the juxtaposition of reactivated (eastern limb) and overprinted (western limb) focusses brecciation close to the hinge, with brecciation diminishing with distance away from this zone.

## Essential Ingredients for IOCG/ISCG-style mineralisation

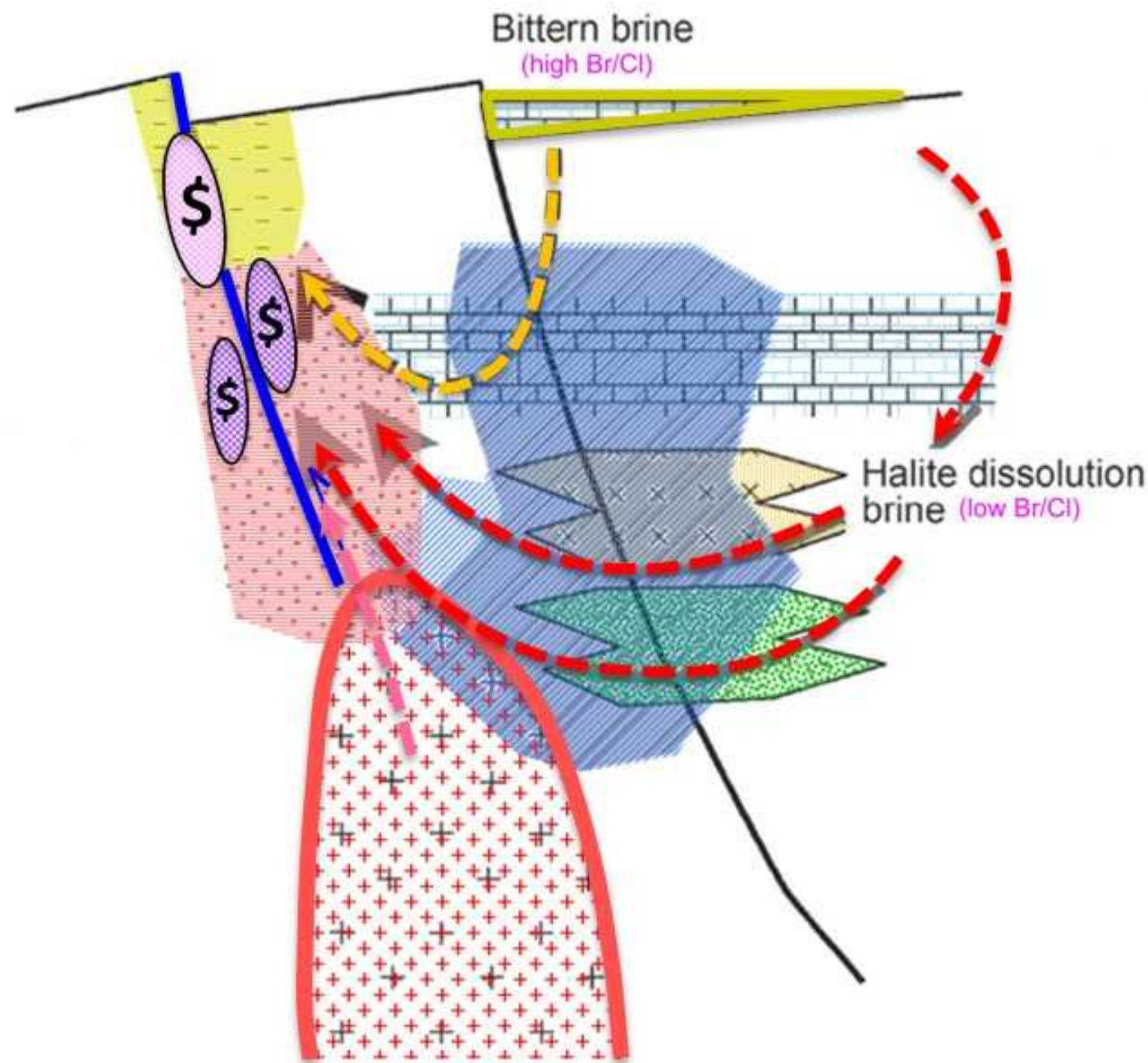
The preceding DMQ Time-Space, Solid Geology, EFB Assembly, detailed geology and mineralisation control analysis highlights a number of essential ingredients that need to conspire to generate IOCG/ISCG-style Cu-Au-Mo mineralisation.

The close temporal association of IOCG/ISCG-style Cu-Au mineralisation with significant crustal magmatism is well understood and well supported in the Eastern Fold Belt (Figure 3.2; Duncan et al., 2011) as well as globally (Chapter 2). The important spatial relationships between intrusion and mineralisation will be developed in Chapter 4. The local structural control on mineralisation is also well established, however, the DMQ analysis has suggested that this control can be significantly more subtle than has previously been suggested and modelled.

The following highlights the insights DMQ believe their analysis suggests to be crucial for syn-WILLIAMS, D4 formation of IOCG/ISCG-style Cu-Au mineralisation in the southern Cloncurry Belt.

- A BRITTLE host lithology in a D4 structural setting that enhances its brecciation to focus fluid flow is critical.
- These D4 structural settings are most commonly NOT major structures but rather (a) domains of D4 strain partitioning, (b) insignificant D4 faults (in the sense that they are not easily mapped or interpreted in geophysics), and/or (c) relatively minor re-activations of older, pre-existing structures. The D4 structuring that focuses mineralising fluid is commonly associated with only small displacements and so can be significantly subtle. A number of D4 scenarios that have produced significant mineralisation have been described here and demonstrate that they have little macroscopic structural geometric control in common.
- Brecciation and fluid flow requires a BRITTLE rock to maintain its BRITTLE nature into post-peak metamorphic D4 times. Calc-silicates, siliceous meta siltstones ( $\pm$  carbonaceous content) and iron formations remain BRITTLE in post-peak metamorphic times and can generate interconnected permeability to focus fluid flow and are common hosts to IOCG/ISCG-style Cu-Au mineralisation. Vast volumes of moderate to high grade metasedimentary schists (-gneisses) of interbedded pelitic-psammitic origin accommodate D4 shortening by slip on well developed, peak metamorphic fabrics. These metasediments do not generally generate an interconnected permeability during D4 and do not focus fluid flow.

# Surficial ± Formational Fluid Source IOCG Model



Barton & Johnson (2004), Williams et al. (2005), Williams et al. (2010)

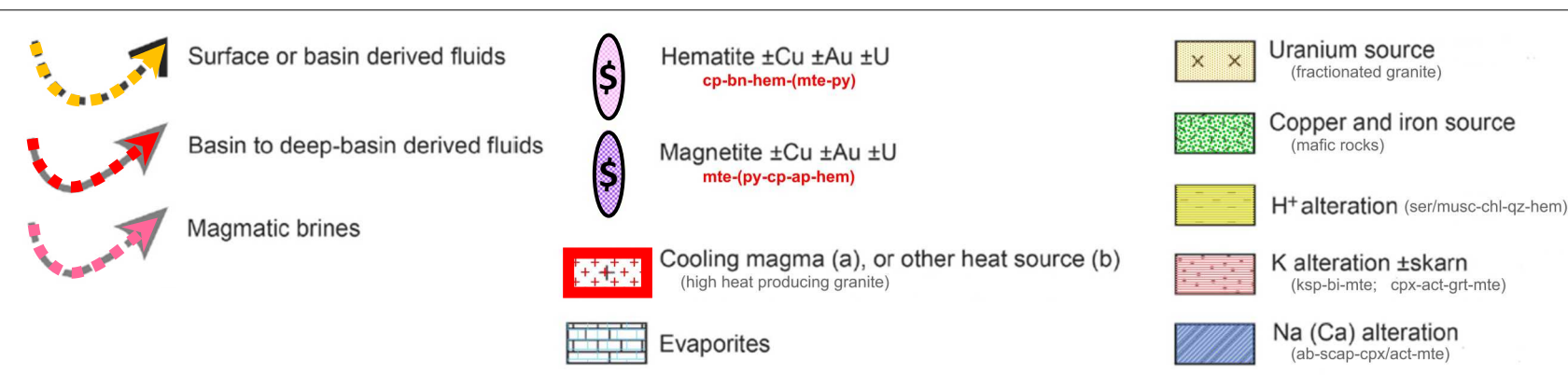


**Figure 3.46** Modified Surficial (± Formational) IOCG Fluid Model of Barton & Johnson (2004), Williams et al. (2005) and Williams et al. (2010) highlighting potential surficial basin oxidised brine source, metal sources, circulation driver, structural control on deposition, Na(-Ca) vs K vs H<sup>+</sup> alteration domains, magnetite vs hematite-rich mineralisation as a function of oxidation state (and depth) of fluid circulation cells and direct magmatic input.

The deposits and resources investigated in more detail by DMQ, suggest significantly different D4 structural geodynamics characterise mineralisation control in each of the different camps.

- At Kulthor: structural abutting of BRITTLE siliceous, sulphidic meta-sandstone-siltstone against D4-reactivating D2 structures. Abundant local sulphide results in ISCG Cu-Au mineralisation.
- At Merlin-Mount Dore: BRITTLE calc-silicates and carbonaceous, siliceous meta-siltstones cut by small-displacement D4 faults control Cu-Au-Mo mineralisation.
- At Starra: BRITTLE D1-remnants of magnetite iron formation coincident with footwall structural weaknesses focus brecciation during D4 re-activation of an old D1 structure to localise Cu-Au mineralisation.
- At Mount Elliott, SWAN and Ernest Henry: BRITTLE calc-silicates, carbonaceous meta-siltstones and intermediate volcanics within D4 strain partitioning domains generate interconnected permeability to localise Cu-Au mineralisation.

Figure 3.46 presents a generalised system model that is a modified version of the Surficial (± Formational) IOCG Fluid Model of Barton & Johnson (2004), Williams et al. (2005) and Williams et al. (2010). DMQ suggests that this model schematically encapsulates potential ingredients of a hypothetical system model that is a good fit with the current DMQ understanding within the southern Cloncurry Belt. Implicit within the model are a number of important elements that require highlighting, explanation and/or discussion but may not be at all critical to Prospectivity Analysis and Targeting within the belt.

- The entrainment of a surficial oxidised brine from a poorly age-constrained QUAMBY basin is entirely speculative. Its suggestion, however, (1) does alleviate the

difficulty in generating large volumes of oxidised brine from post peak metamorphic, evaporitic(?) carbonate sequences (CORELLA & STAVELEY) in which salinity has been tied up in metamorphic minerals and is not readily accessible in D4 time. It (2) also alleviates the need to appeal to an entirely magmatic fluid system for which halide and isotope geochemistry (Williams, 1999; Kendrick et al., 2007) does not provide conclusive support. In addition, DMQ's WILLIAMS granite interpretation and modelling presented in Chapters 4 & 5 strongly suggests that fertile Cu-Au-Mo fluid systems are strongly focussed over the

margins and shoulders of intrusions at depth suggesting a wider, more regional, fluid circulation system (as depicted in Figure 3.46) focuses to form Cu-Au-Mo mineralisation. Known occurrences are NOT in the immediate roof zones of intrusives where purely-magmatic mineralisation might be expected to be found. Lightning Ridge might be the lone exception in the southern Cloncurry Belt over the southern margin of the Squirrel Hills Granite (Pollard, 2000)

- IOCG mineral system models commonly appeal to mafic sources for Cu, Fe, ±Au (Porter, 2010; Figure 3.46 also). Mafic metal sources in the Cloncurry terrain are not specifically defined in the current study but several possibilities exist. Seismic interpretation and serial sectional interpretation by DMQ (Chapter 4; Figure 4.3) suggest MARRABA mafic volcanics are likely present in the footwall of shallow-dipping D1 thrusts in the shallow crust (3-9km) and could lie within the oxidised brine pathways of WILLIAMS-aged thermal brine circulation systems.
- Co-magmatic mafic magmatism at the time of IOCG mineralisation is also commonly implicated in IOCG mineral system models (Porter, 2010). Direct evidence for co-magmatic mafic magmatism at WILLIAMS-time in the Cloncurry Belt is lacking largely due to poor geochronological constraints on mafic rocks and the well-recognised widespread spatial dispersal and broad temporal distribution of mafic extrusion and intrusion within the Isa terrain and in the Eastern Fold Belt (see Time-Space Chart; Figure 3.2; Appendix 1).
- DMQ makes no judgements about the specifics of mafic involvement in the IOCG mineral system while acknowledging the potentially important metal sources mafic rocks may contribute to the IOCG/ISCG systems.
- The high heat-producing, radiogenic nature of the WILLIAMS suite granitoids suggests they themselves may be the source of Uranium commonly associated with the Cloncurry mineral systems.

## DMQ Southern Cloncurry District 3D Analysis

### Introduction

Building on the detailed DMQ Solid Geology and the tectonostratigraphic understanding outlined in the previous chapter, this Chapter outlines the steps taken to build a practical, robust and useful 3D geological model that encapsulates the DMQ 4D understanding of the belt's evolution and that will enable well-constrained Prospectivity Analysis and Targeting to be achieved at realistic, mineable depths. At the current time maximum exploration depths are probably less than 2km but in the interest of achieving a well-constrained prospectivity analysis and acknowledging the critical importance of upper crustal architecture and upper to mid crustal magmatism to IOCG-style mineral systems, DMQ has focused its detailed 3D analysis within a surface to 6-12km-deep volume.

The DMQ depth emphasis is in sharp contrast with previous regional 3D interpretations which have strongly leveraged regional seismic lines with >60km depth profiles and that have tended to weight interpretation towards deep crustal architecture rather than the close-to-surface relationships that would fall within the volume that could be practically explored. In contrast, the DMQ 3D interpretation has focused on projecting the DMQ-refined, Solid Geological interpretation (Figure 3.6 and Appendix 3) into the subsurface using known and well-understood surface and mine 3D relationships combined with DMQ interpretations of 3 seismic lines which have firmly focused the analysis on shallower architectures and rock relationships.

This Chapter presents the work that has formed the basis of DMQ's 3D geological model of the southern Cloncurry Belt. This work includes:

- (1) Three re-interpreted seismic sections across the Project Area that have been robustly constrained by projection from the DMQ surface Solid Geology
- (2) Forty-seven 4km-spaced section interpretations, also tightly constrained by the DMQ surface Solid Geology
- (3) Geologically-constrained, DMQ gravity and density inversion modelling that has been used to define and iteratively refine WILLIAMS-aged granite geometries at depth which DMQ believes are critically important in the localisation of IOCG-style mineralisation within the belt.

Figure 4.1 shows the DMQ Solid Geology interpretation with (1) the 3 seismic lines reinterpreted by DMQ and used to constrain the 3D geological model, (2) the positions of the forth-seven 4km-spaced sections built by DMQ, and (3) all the control points extracted from the Sol-

id Geology interpretation to constrain both the seismic and sectional interpretations.

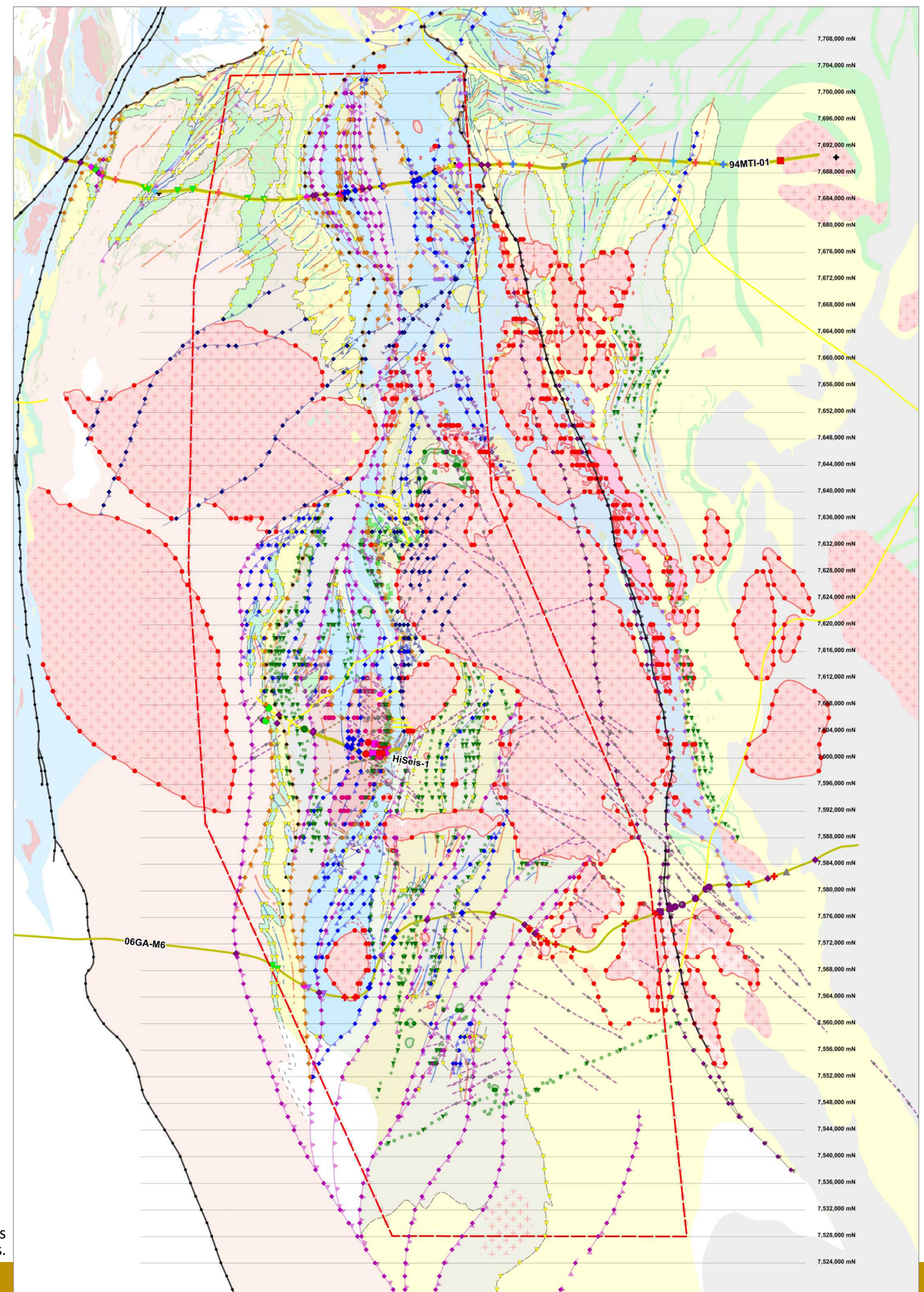
### Seismic Re-Interpretation

Portions of three seismic sections that transect the DMQ Project Area have been re-interpreted by DMQ. Two sections, 94MTI-01 & 06GA-M6, are regional seismic lines shot by AGSO-GA-GSQ in 1994 and 2006 respectively. A third short segment in the central part of the belt is part of a set of 8 lines shot by Ivanhoe in 2008 but which remained un-interpretable due to very poor resolution after previous processing attempts.

DMQ approached Chinova and GSQ to fund some trial re-processing by HiSeis (based in Perth; [www.hiseis.com.au](http://www.hiseis.com.au)) who specialise in hard rock seismic processing and have had considerable success in hard rock terrains using modified processing algorithms developed by them at Curtin University (HiSeis, 2016). Chinova agreed to fund a trial 8km of reprocessing. Subsurface east-dipping reflectors critically hindered resolution at the eastern end of line IVA-1 (fold test failures; see Figure 4.4) but HiSeis generously extended their re-processing westward to complete 16km (for the same money, in the hope of attracting further work in the belt). Figure 4.1 shows the location of the 3 seismic lines re-interpreted in the current study. Detailed shot line locations with respect to DMQ Solid Geology accompany each of the seismic sections (Figures 4.2 to 4.4)

DMQ's seismic interpretations have been depth limited to a subsurface volume where the structural-stratigraphic and intrusive architecture is thought to realistically influence the prospectivity analysis for mass-mineable resources. In practical terms, the depth limitation on mass mineability is perhaps around 2km but the interpretations have been extended into the 6-12km depth zone to provide the architectural context for the prospectivity analysis. The very deep crustal architecture has been ignored. Very significantly conflicting interpretations of the deeper crust on the regional seismic sections already exist (Gibson, 2016; Gibson et al, 2015, MacCready, 2006; Mira, 2010; Paul Donchak, pers. comm.), so depth limiting the DMQ interpretations, combined with the tighter constraints provided by the DMQ re-interpreted Solid Geology, offered greater potential of realising an ultimately sound and useful 3D product in the exploration/mining space.

**Figure 4.1** DMQ Solid Geology showing control points used to constrain seismic and sectional interpretations.



The DMQ interpretations of seismic lines 94MTI-01, 06GA-M6 and IVA HiSeis-1 are presented in Figures 4.2 to 4.4. As in the Solid Geology interpretation, structures have been attributed (and colour coded) by their deformational timing of initiation. All structures are understood to be re-activated during subsequent inversion and deformation where they are suitably oriented with respect to the evolving far-field stress field. The packages interpreted in the seismic section (as in the Solid Geology) correspond to DMQ TIMESLICES that been outlined in Chapter 3.

The following are some of the important highlights of the seismic interpretations (Figures 4.2 to 4.4), made in conjunction with the Solid Geology interpretation (Figure 3.6).

- The vast majority of D1, D2, (D3) and D4 faults dip moderately to the east. At the scale of the shallow crust, they are not vertical as other modelling has assumed.
- Interpreted D1 structures, where they can be extended to depth in the seismic, exhibit significant HW and/or FW discontinuity with juxtaposed packages and are often also D2 folded.
- D2 Faults truncate and displace D2-folded packages & architectures. This relationship is also clear in the Solid Geological interpretation (Figure 3.6) and suggests regional scale D2 faulting post-dates D2 folding.
- Some timeslice packages exhibit distinctive seismic character and, in conjunction with surface control, can be confidently projected to depth (eg. MARRABA, MITAKOODI, STAVELEY, ANSWER-TOOLE CREEK packages).
- Interpreted timeslice package boundaries represent 'form surfaces' in the seismic interpretations and a level of tighter D2 folding mapped at surface is not imaged in the seismic. As a result, inconsistencies between seismic-interpreted, package dips and surface-mapped, package and unit dips will be present in the interpretations.
- A shallowly-dipping 'Cloncurry Thrust' with thin-skinned overthrust geometry swaps sides of the 'Cloncurry Fault' from its west in the north (94MTI-01), to its east in the south (06GA-M6) (see also Solid Geology, Figure 3.6). This family of thrusts are now interpreted to be D1 by virtue of their close spatial association in the north with well-developed D1 folding east of Cloncurry and in the Snake Creek Anticline area often within

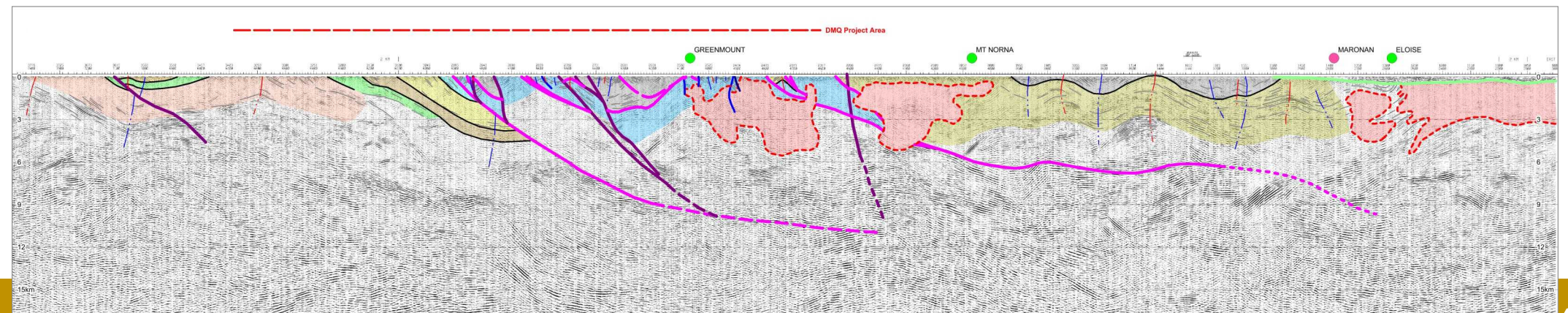
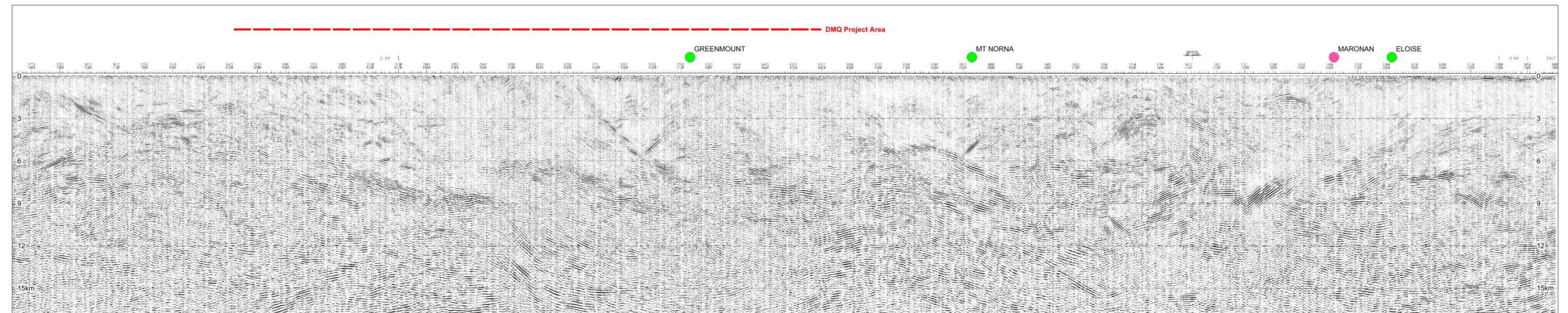
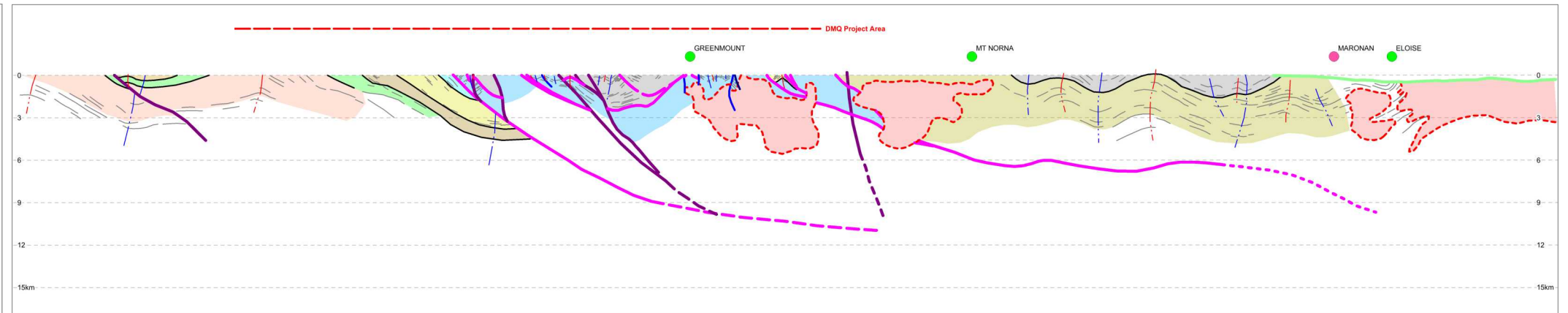
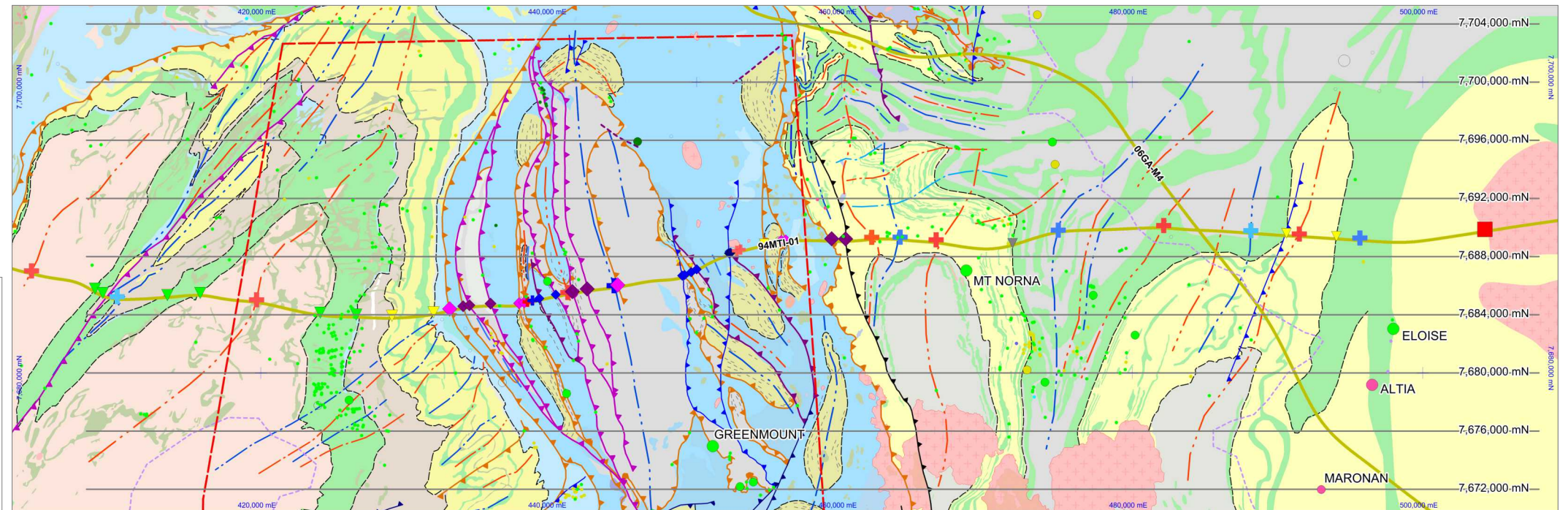
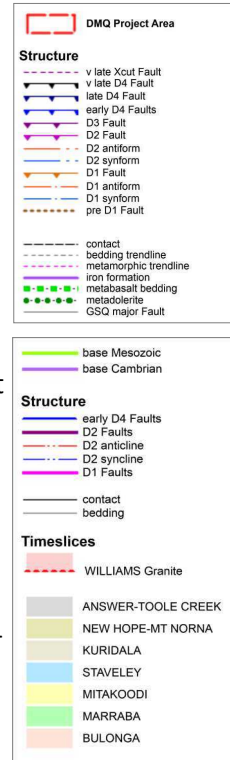


**Figure 4.2** Seismic line 94MTI-01 Interpretation showing seismic line trace and control points over Solid Geology, DMQ interpretation and migrated segy. Caution D1 Fault colour inconsistency between Section & Plan. DMQ Project Area in red.

the immediate hanging wall of the thrust structures that expose footwall STAVELEY calc-silicates (see Figure 3.6 and Appendix 4)

- The late, steep 'Cloncurry Fault' is not well imaged in the seismic but marks a significant discontinuity between domains of east and west-dipping strata on 06GA-M6. Late, steep, relatively tight structures are commonly not well imaged in seismic unless stratigraphic truncations are clear.
- Granites interpreted from quiet homogeneous domains in the seismic extend to at least 5-6km on the 2 regional lines and have bulbous irregular forms ... apart from the thin skin of granite west of the Cloncurry Fault on 06GA-M6 which potentially represents the erosional preservation of the base of a portion of the southern Squirrel Hill granite. Seismic lines have in general been planned to not transect regions of significant granite exposure so seismic constraint on the geometries of major WILLIAMS intrusions at depth does not exist in the southern Cloncurry Belt.
- A number of Cu-Au occurrences subjacent to the seismic lines (Greenmount, Mt Norna, Eloise on 94MTI-01) show some spatial association with WILLIAMS granitic intrusives of significant crustal thicknesses (up to 6km). This important relationship is key to DMQ's process model and will be further developed in this Chapter and subsequent Prospectivity Analysis.
- It remains unclear in both seismic section and plan view what the STAVELEY package sits depositionally above (see also Tx Chart). As discussed in Chapter 3 and in Appendix 4, current conventional wisdom has STAVELEY D1 overthrust over DOUBLE CROSSING METAMORPHICS-GIN CREEK GRANITE and MARRABA-MITAKOODI-CORELLA in the west. This relationship can be projected eastward from the surface expression of the Overhang Shear to depth on 06GA-M6 (Figure 4.3) where HW angular discordance is clear. However, the nature of the packages and their relationships beneath STAVELEY further to the east at relatively shallow depths remains entirely unclear.
- On the HiSeis-IVA-1 seismic section, homogeneous bland zones at the base of the section merge with rotated reflectors that reflect the failure of fold superposition on the eastern end of the section. These bland zones potentially reflect intrusion towards the base and eastern edge of the resolvable part of the seismic section.

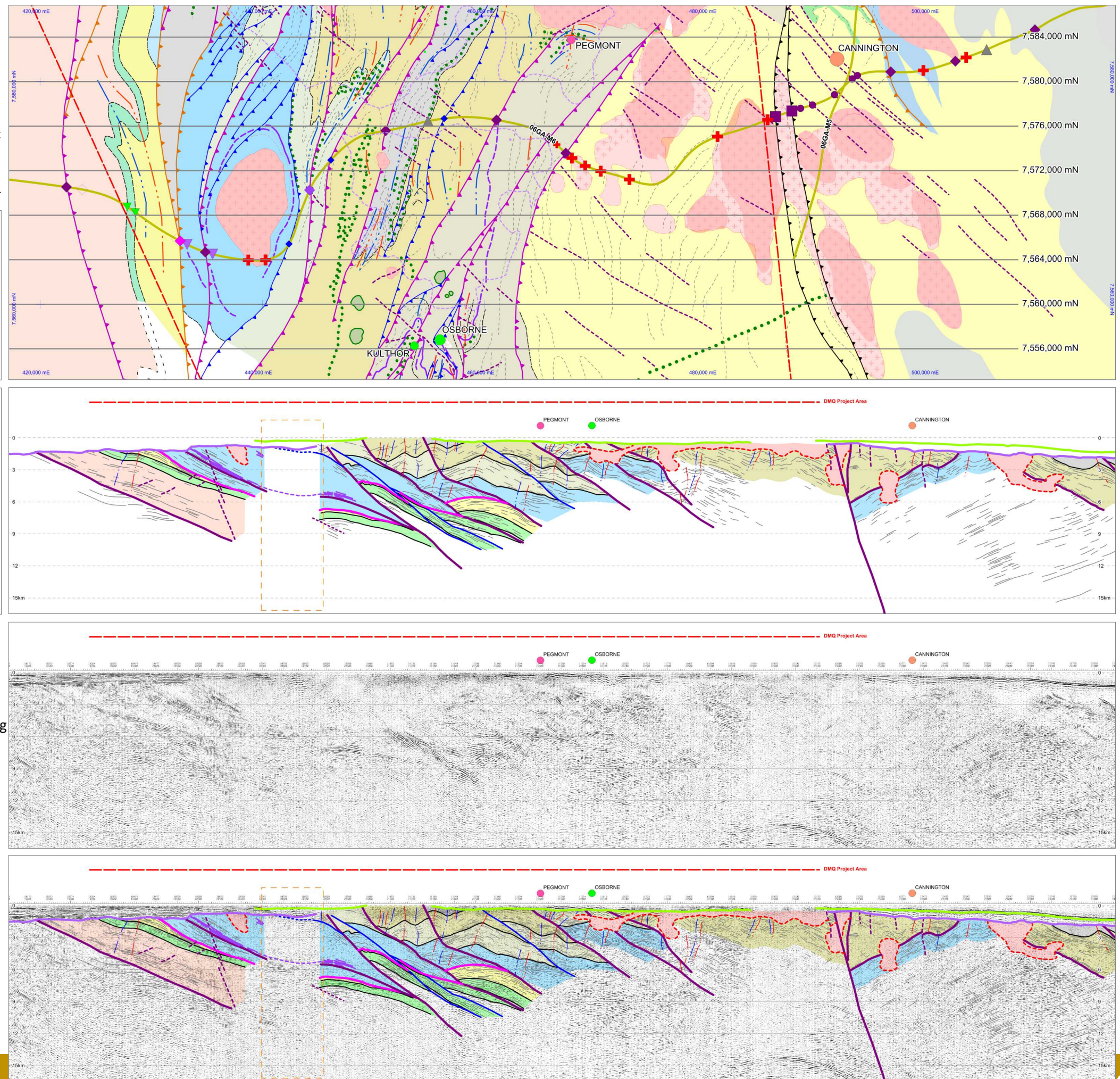
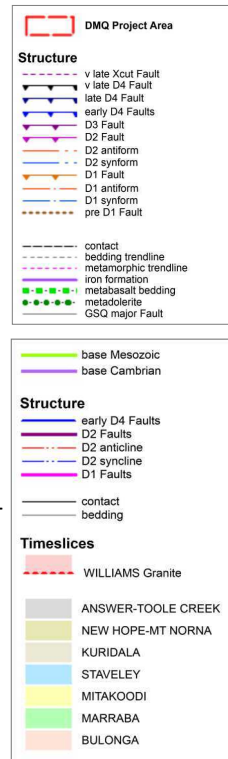
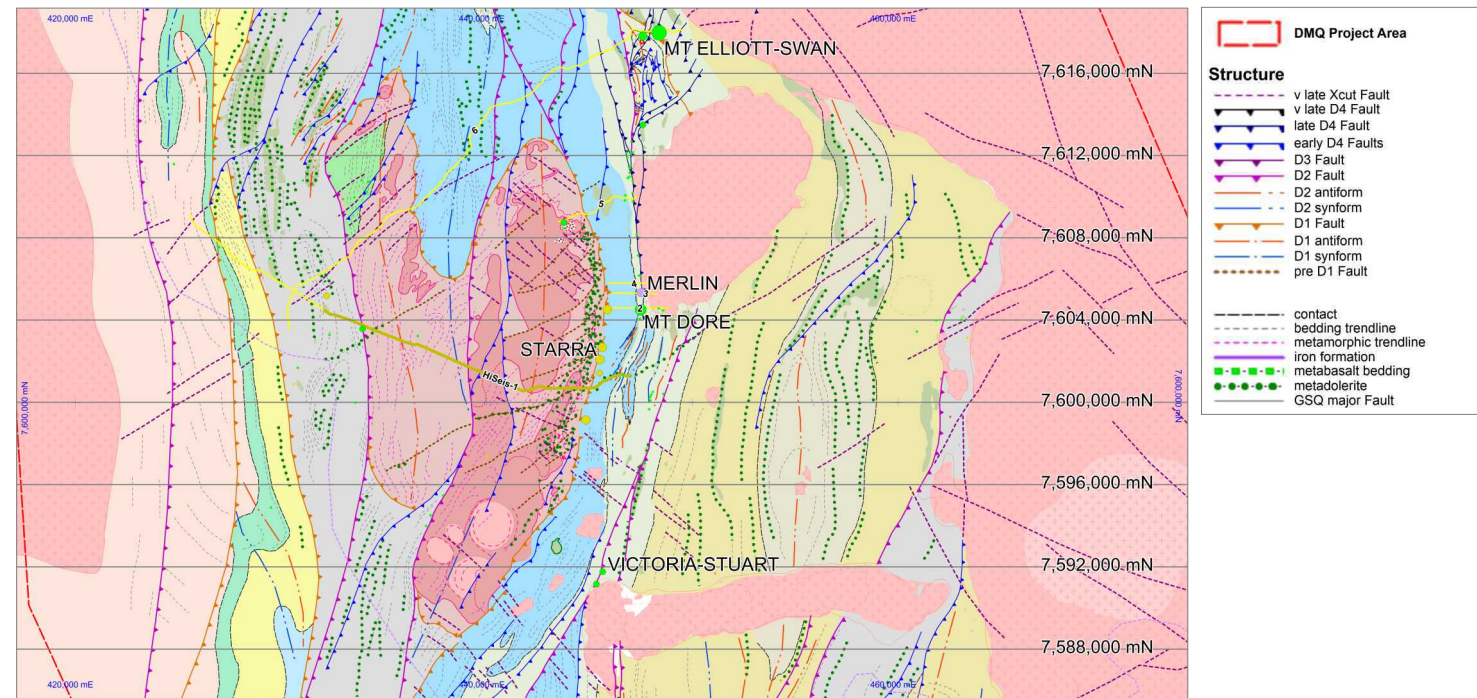


**Figure 4.3** Seismic line 06GA-M6 Interpretation showing seismic line trace and control points over Solid Geology, DMQ interpretation and migrated segy. Caution D1 Fault colour inconsistency between Section & Plan. DMQ Project Area in red.



## Serial Section Interpretation

Forth-seven 4km-spaced sections were interpreted using the constraints provided from the Solid Geology interpretation (Figures 3.6 & 4.1), the three seismic interpretations and some geophysical modelling on the dip of magnetic bodies. The section extents were designed to provide generous coverage of the DMQ Project area and to encompass important and/or interesting areas of adjacent geology.

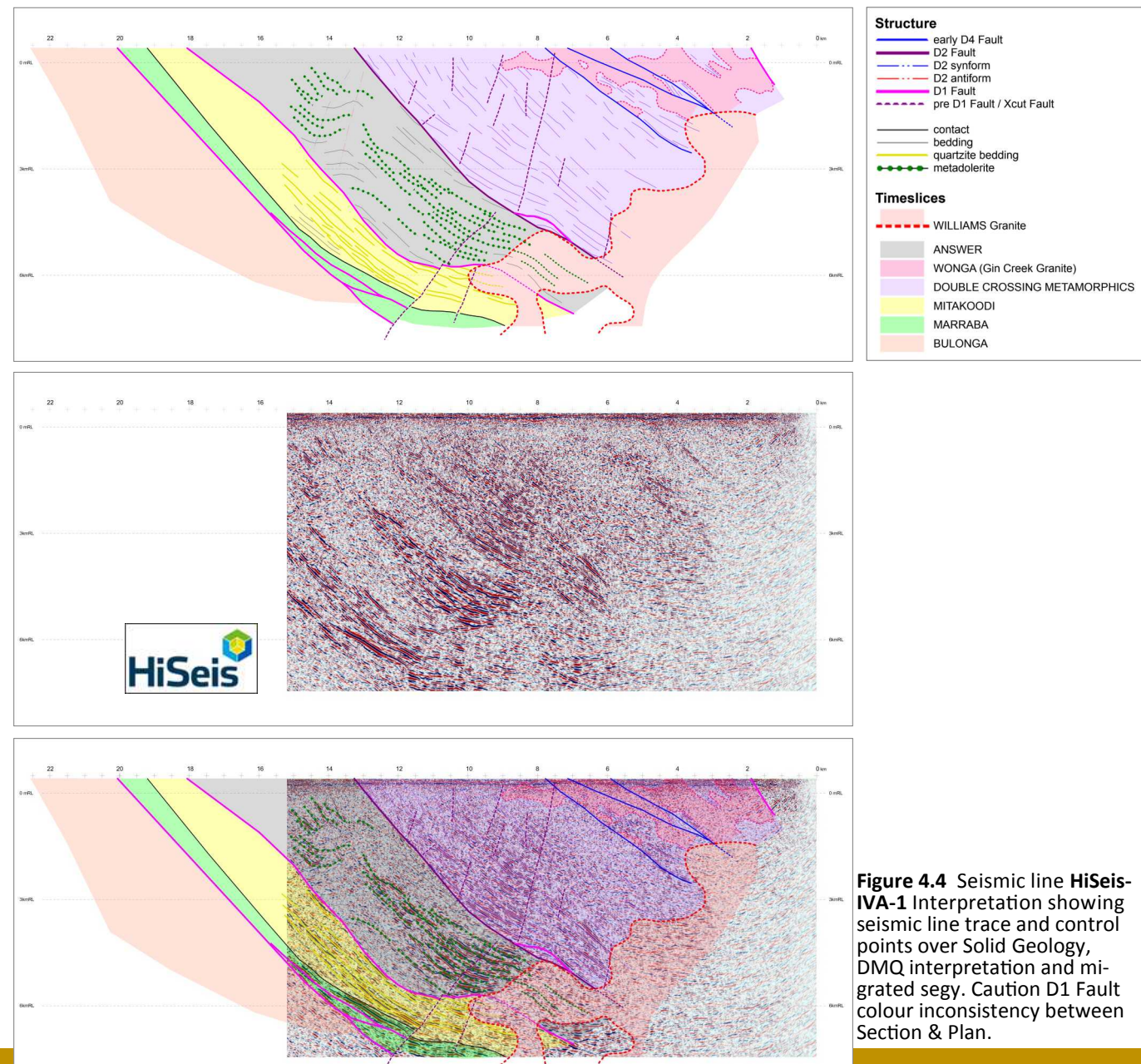
The full set of completed sections is presented in Appendix 5. These sections include granite geometries whose generation is discussed in the following sections of Chapter 4.

Fault architectures were interpreted first and then the timesliced stratigraphy (with thicknesses interpolated from the Solid Geology and the seismic interpretations) was interpreted into the fault-bounded block architecture. As in the Solid Geology interpretation, structures are flagged by their interpreted initiation event and the interpretation assumes

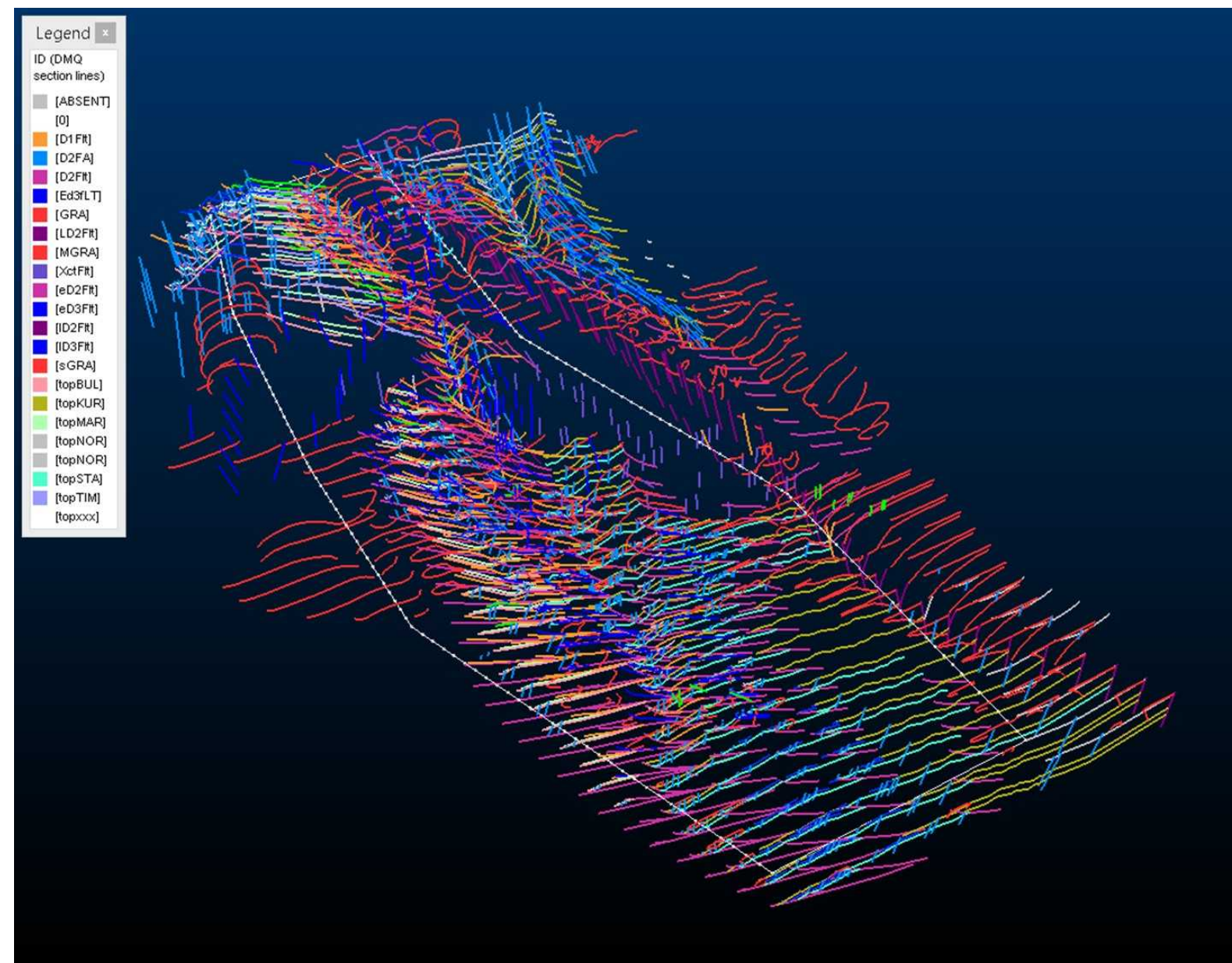
reactivation during subsequent deformation events where they are suitably oriented with respect to the evolving stress field. Additionally, as in the seismic interpretations, timeslice surfaces in the sectional interpretations also represent 'form surfaces' and a level of tighter D2 folding mapped at surface is not necessarily imaged in the sections.

Figure 4.5 presents an oblique view looking NNE of all the strings from the 47 sections colour coded by fault timing and stratigraphic position. The DMQ Project Area is represented by the white dashed polygon. Six selected sections from the forty-seven are presented in Figure 4.6.

**Figure 4.5** Oblique view looking NNE of stacked fault and stratigraphic strings from the 47 DMQ section interpretations. DMQ area is outlined by white polygon.



**Figure 4.4** Seismic line HiSeis-IVA-1 Interpretation showing seismic line trace and control points over Solid Geology, DMQ interpretation and migrated segy. Caution D1 Fault colour inconsistency between Section & Plan.



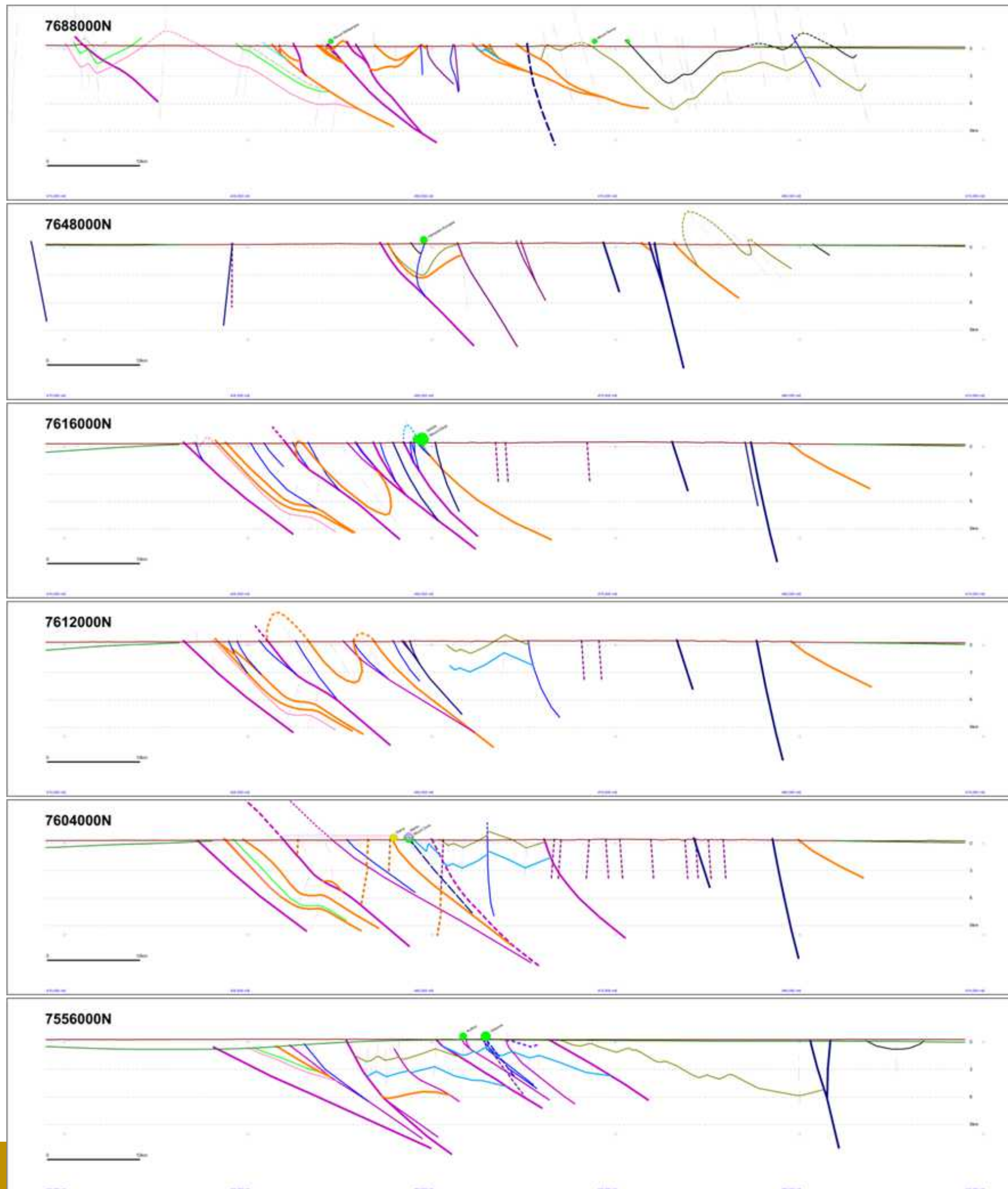
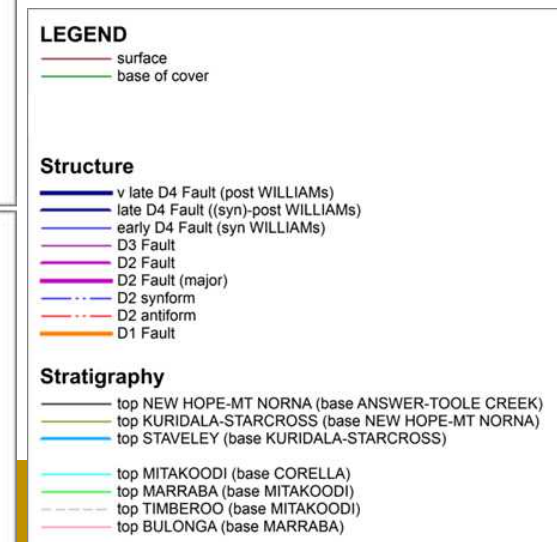


**Figure 4.6** Six selected section interpretations that demonstrate the DMQ focus on the upper crustal architecture and which highlight the east-dipping character of the geometries. These sections do not include granites subsequently interpreted at depth and presented in finalised form in Figure 4.27. The full set of sections are presented in Appendix 5.



## Southern Cloncurry Granite Morphology: Vpmg Gravity Inversion Modelling

Previous geophysical modelling work in the southern Cloncurry Belt (Mira, 2010) has interpreted granites (largely WILLIAMS) to have extents very largely confined to areas of outcrop and areas of interpreted granite exposure at the base of cover. DMQ has developed a significantly different view of granite geometry at depth that has very crucial implications for intrusion-driven, IOCG-style mineralising systems within the belt.

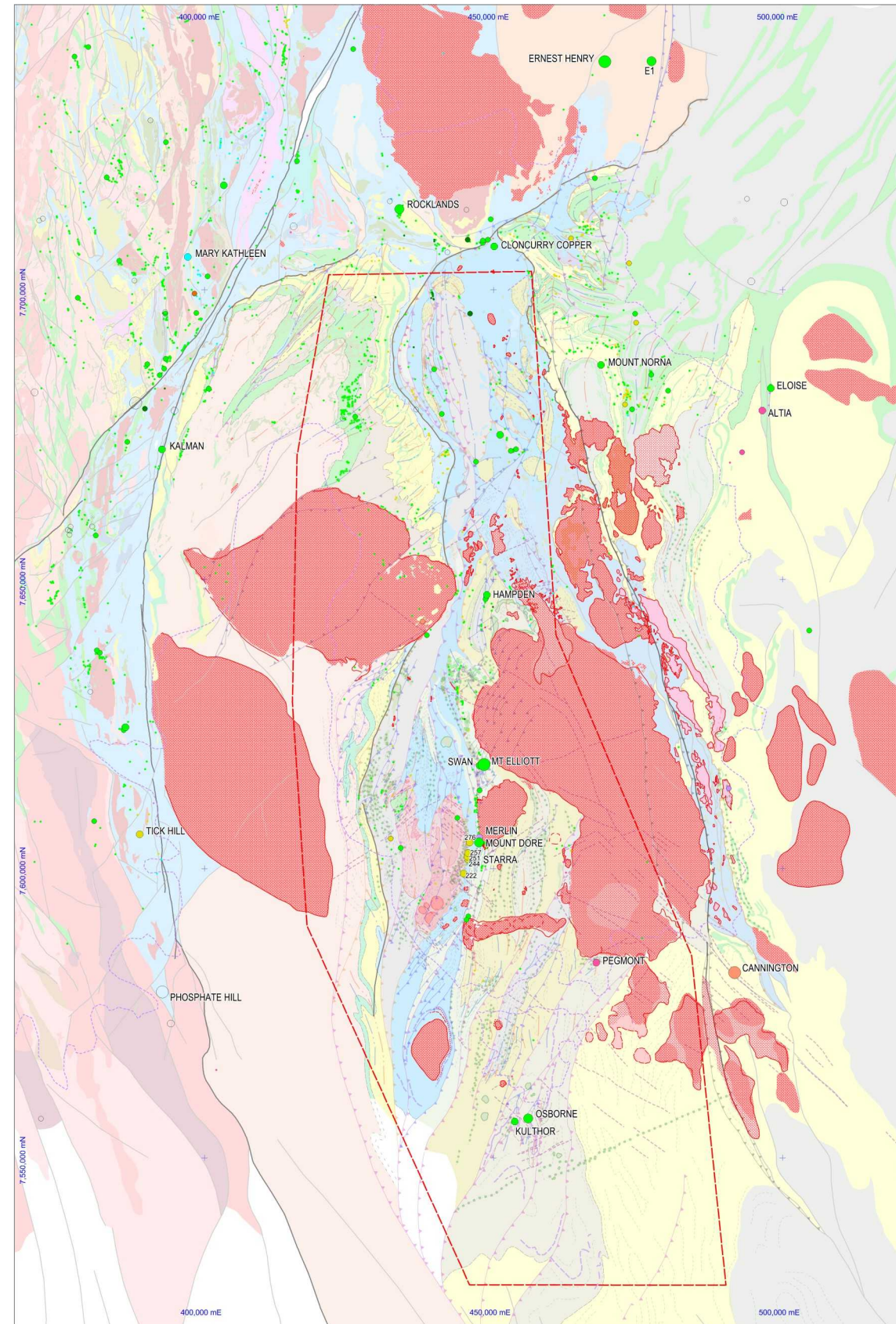
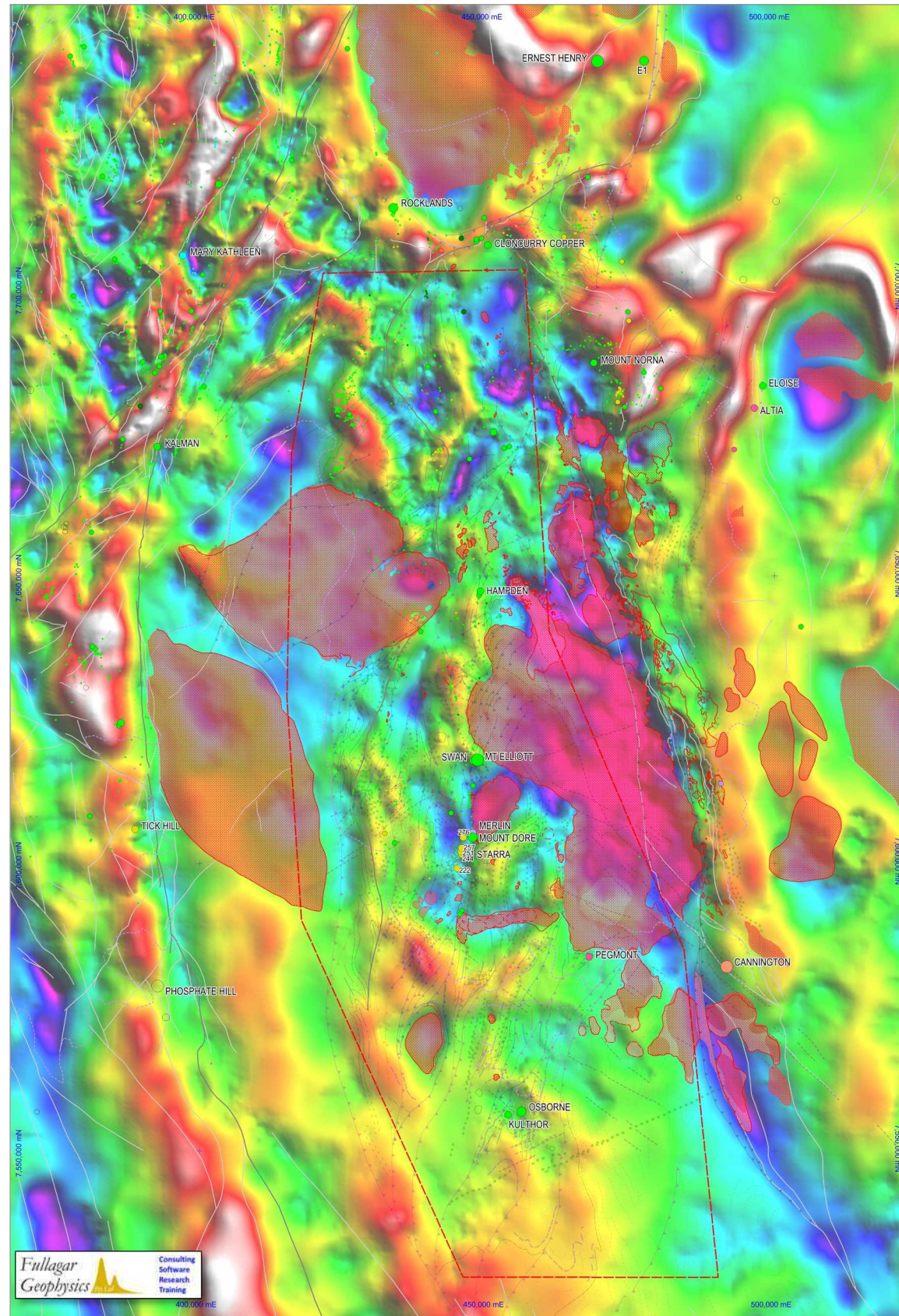
DMQ's thesis is that WILLIAMS intrusion geometry strongly influences the large-scale geometry of convective and magmatic fluid flow at WILLIAMS time. This high temperature fluid flow is further focussed in the mid to shallow crust where synchronous D4, brittle deformation of juxtapositioned, favourable (brittle) host packages provide permeable fluid pathways. These concepts are the essence of DMQ's targeting model within the belt that will come together in the Prospectivity Analysis in Chapter 5.

The granite morphology modelling has depended entirely on **Fullagar GeoPhysics Vpmg** potential field inversion software provided by Peter Fullagar to the DMQ project under a generous research license arrangement. Peter is gratefully acknowledged and thanked for the provision of the Vpmg software.

## Gravity Inversion of GA Bouguer Gravity

Figure 4.7 presents an Apparent Density Model derived from a Vpmg 'Basement only' inversion of the GA 2011 Isostatic Residual gravity Anomaly grid data. An apparent density model is constructed by establishing an input model of vertical prisms that extend from surface to a depth of 25 km. A single density value is assigned to each prism and the inversion process iteratively adjusts the density of each prism until a match between the model's gravitational response and the observed gravity data is achieved within some density range constraint. Prism dimensions were 900x900m. The apparent density model assumes no crustal architecture, but very usefully highlights density *deficits* and *surpluses* in relation to areas of known granite and Proterozoic outcrop. Because the density is allowed to vary freely in each prism within prescribed limits the apparent density model provides useful quantitative estimates for density contrasts throughout the model area.

Close comparison of the Apparent Density Inversion Model (Figure 4.7) with the DMQ Solid Geology (granite outcrop highlighted; Figure 4.8) suggests granitic rocks are far more



extensive at depth than the extent of mapped and interpreted granites. The Apparent Density Model also suggests significant extensions of mapped and interpreted granite at depth beneath outcropping Proterozoic. Importantly, density *deficit* trends in the Apparent Density Model are highly discordant with the Isan deformation-controlled, Proterozoic trends highlighted in the DMQ Solid Geology (Figures 3.6 & 4.8) suggesting their causative bodies are discordant in character as intrusives would be expected to be.

DMQ interprets that density *deficits* in the Apparent Density Model reflect significant volumes of granite at depth throughout the southern Cloncurry Belt and that these granite geometries at depth play a significant role in Isan D4, syn-WILLIAMS fluid convection geometry and the ultimate location of IOCG-style deposits in the belt.

Many deposits and occurrences show a close spatial relationship with what would be interpreted from the Apparent Density Model to be margins, shoulders or apophyses of granite at depth (compare Figures 4.7 & 4.8). Notable examples include Mount Norna, Cloncurry, Rocklands, Eloise, Greenmount, Hampden, Mount Elliott-SWAN and Osborne-Kulthor. Additionally and importantly, DMQ also highlights the lack of significant mineral resources and a scarcity of occurrences within what would be interpreted as the immediate roof zones above shallow bodies of granite. This implies that fluid flow/circulation along intrusive margins and extending vertically above intrusive shoulders, rather than simple magmatic exhalation from the roofs of intrusives, might be a more significant process ingredient in IOCG/ISCG-type mineralisation in the belt. This idea will be developed further later.

### Vpmg Gravity Inversion Modelling

DMQ has invested considerable effort into the generation of a geologically-reasonable granite model that honours known 3D and 2D geological constraints on the distribution of WILLIAMS-aged intrusions (from Solid Geology, seismic and drilling) and has attempted to satisfy the relationships that are implicit within the Apparent Density Model. Away from granite outcrop, interpretation of geophysical inversion models is complicated by the ubiquitous non-uniqueness problem where many combinations of volume and depth of additional low density material (granite) can be placed to satisfy the observed gravity signatures and density *deficits* highlighted in Figure 4.7. Small volumes of granite at shallower depths or larger volumes of granite at greater depths can equally explain the observed gravity data away from granite outcrop. Similarly, adjusting the Granite-Proterozoic density contrast has a

**Figure 4.7** Vpmg Apparent Density Model of GA Gravity ver1 (2011) including overlay of outcropping granites to highlight significant extension of low densities at depth beyond outcropping granite.

**Figure 4.8** DMQ Solid Geology with granite at surface and interpreted beneath cover highlighted.

significant bearing on the resultant 3D model volumes i.e. the lower the density contrast, the larger the volume of low density material generated to reproduce an observed gravity low signature. The application of carefully considered geological constraints from all known relationships and the testing of multiple different starting model geometries were used to ameliorate the inherent ambiguity problem and develop a geologically-reasonable 3D model of granite within the belt.

## Vpmg Inversion Modelling Fundamentals

The *Vpmg* 3D software has been developed specifically to incorporate a-priori geological information as surfaces into 3D inversion modelling and is the DMQ project's preferred choice of software for integrating geophysical and geological information. Geological constraints include physical property measurements, outcrop maps and drill hole data. Each cell in the *Vpmg* model is assigned a geological unit (Figure 4.9 left) in contrast to other common 3D geophysical modelling programs where a model cells can cross geological units. *Vpmg*, 'geometry inversion' allows for the geometry of a geological unit's contact to be manipulated during the inversion process while holding the geological unit's physical properties fixed (Figure 4.9 middle). Physical properties of the geological unit (eg. density or susceptibility) can be also adjusted by *Vpmg* 'homogeneous' or heterogeneous inversion while keeping unit contacts fixed (Figure 4.9 right). In homogeneous inversion a geological unit's physical property value is the same throughout the unit i.e. there is no internal variation permitted. In heterogeneous inversion the geological unit is sub-celled further allowing variations in physical proper-

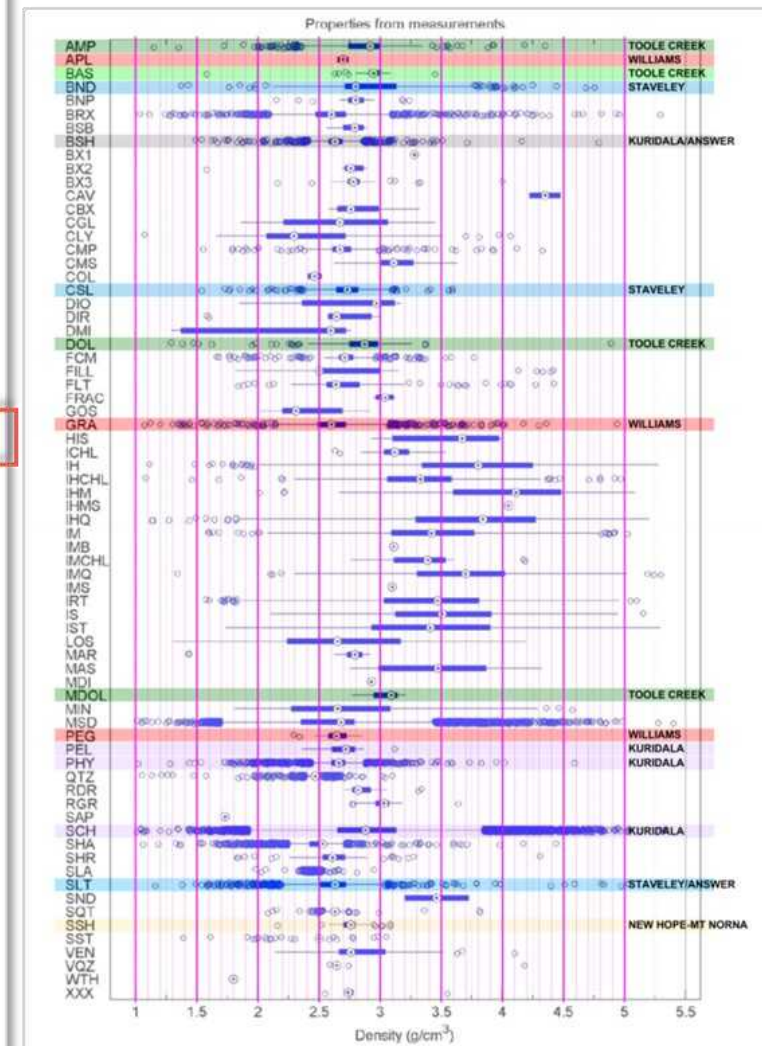
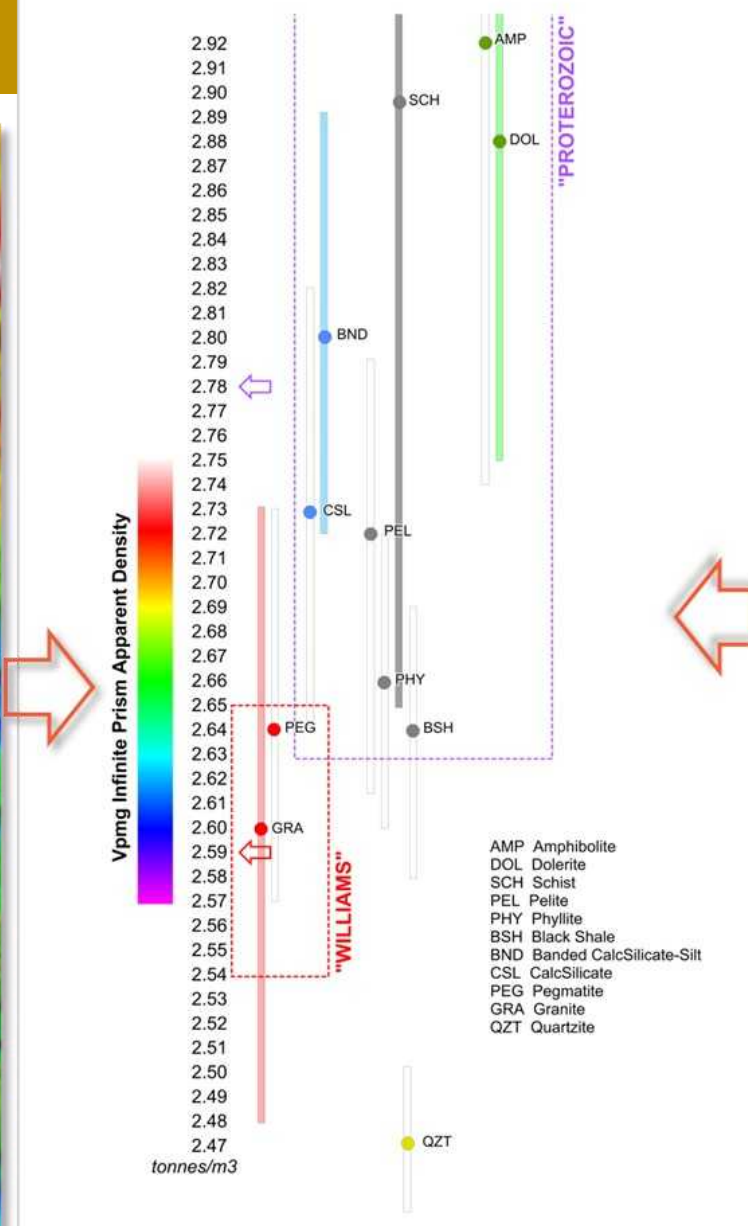
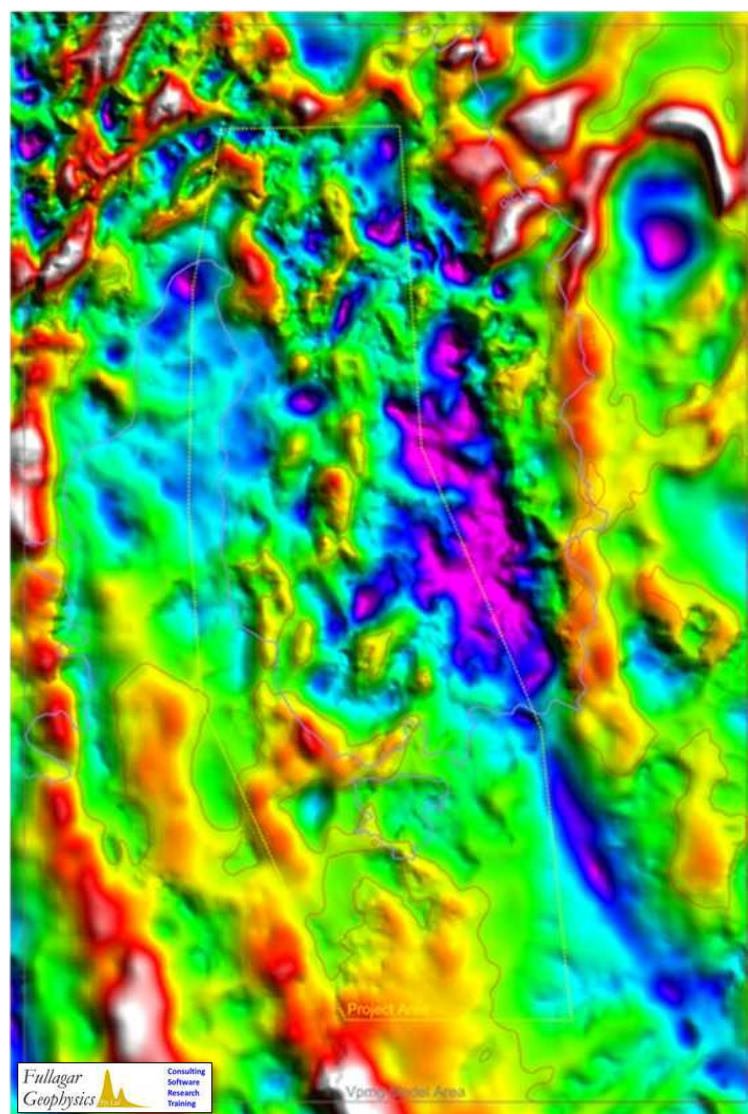


**Figure 4.11** *Vpmg* Apparent Density Model (left) suggests a density range from 2.57 to 2.75t/m3. Chinova drillcore densities (right) demonstrate wide ranges in density but a selection of dominant rock types (tagged by their TIMESLICE on right) suggest the choice of generic 'Granite' and 'Proterozoic' densities at 2.59t/m3 and 2.78t/m3 (arrows, centre) are consistent with available data.

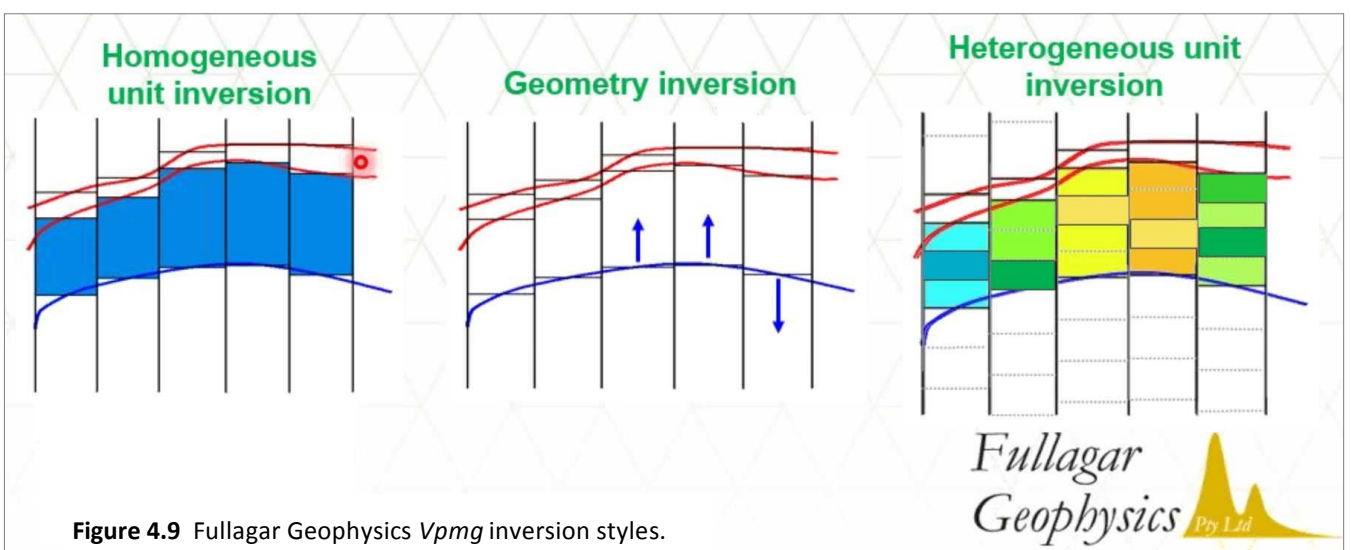


**Figure 4.9** Fullagar Geophysics *Vpmg* inversion styles.



**Figure 4.10** Cross section example of simple DMQ 3-component, 3 & 2-layer *Vpmg* input model.

ty values within the unit (Figure 4.9 right). Further details of 3D *Vpmg* inversion modelling investigated by DMQ can be found in the detailed Half Yearly Reports appended to this Report (Appendix 8). To reduce the complex geology into a manageable geophysical model space, and in the absence of a software package like Gocad, DMQ developed simple 3 and 4 component models for input into the *Vpmg* 3D inversions. The components are assigned 'Granite', 'Proterozoic', and 'Cover' (Figure 4.10).

## Density Data

Due to the non-uniqueness problem, gravity inversion models are highly sensitive to the densities and density contrasts ascribed to cells/elements/layers of the starting model. This is particularly crucial for *Vpmg* geometry inversion where unit densities are held constant while unit

contacts are adjusted to match the gravity data. The sensitivity of the data to the shape of a boundary is proportional to the physical property contrast (Fullagar, 2008) DMQ has been provided measured rock densities from the Chinova drillhole databases. This data is presented in Figure 4.11. It has been sorted and is coded by Ivanhoe-Chinova drillhole database Lithology CODES (left hand column) and has been selectively annotated with appropriate DMQ geology time slices (right hand column) to group lithologies that reflect granite (WILLIAMS) densities and background Proterozoic densities (STAVELEY, KURIDALA, MOUNT NORNA, TOOLE CREEK ...). The DMQ modelling has trialed various density combinations constrained by this data (see Appendix 8 for details). The central portion of Figure 4.11 highlights those lithologies that contribute significant proportions to the 'Granite' and 'Proterozoic' *Vpmg* geophysical units. Clearly all the lithologies (including the high density iron formation lithologies; IH., IM., etc, Figure 4.11

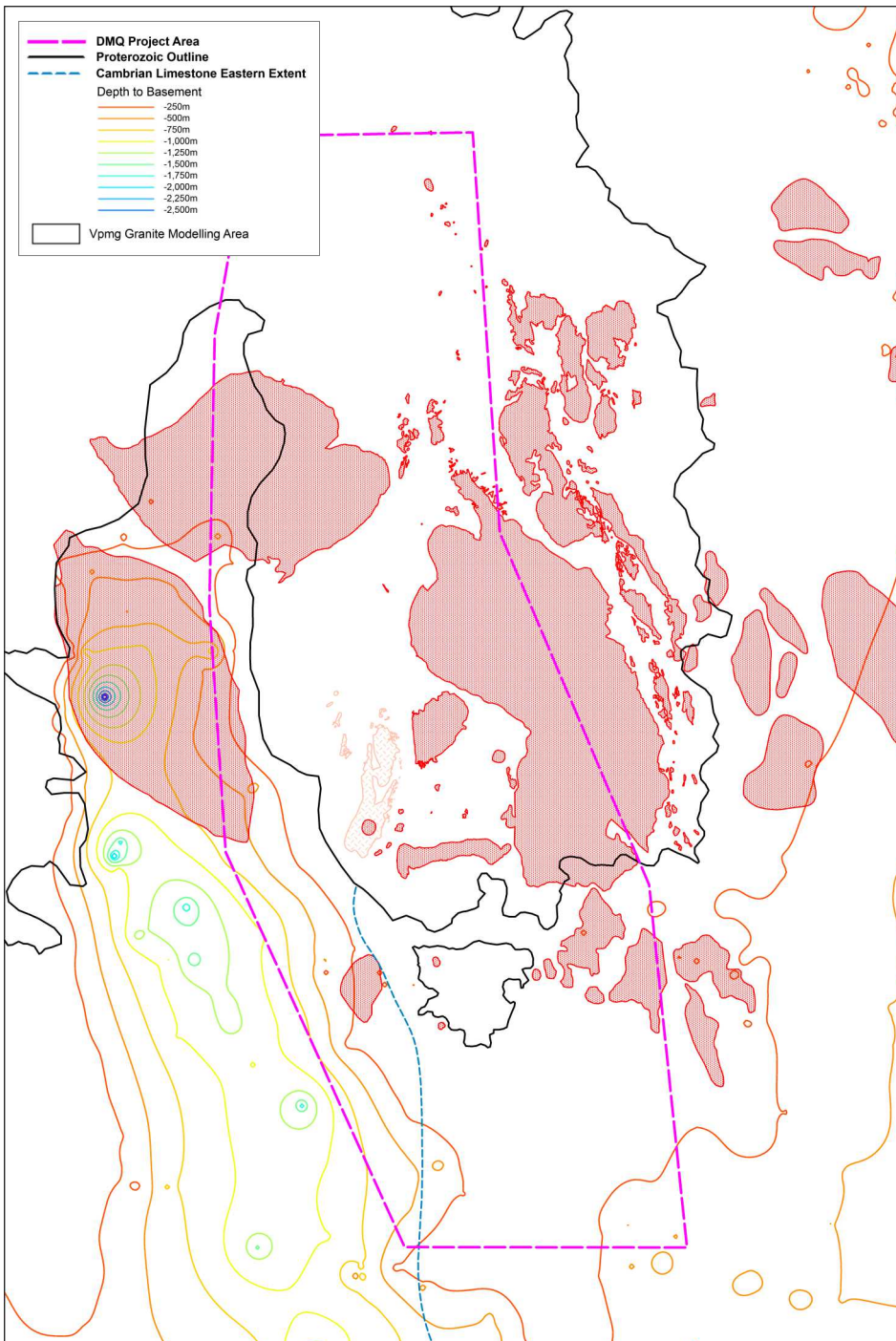


**Figure 4.12** Vpmg Modelling area showing Project Area, outcropping 'Granite' (including interpreted beneath 'Cover'), depth of 'Cover' contours, and eastern extent of Cambrian Limestone.

**Table 4.1** LOW, MEDIUM and HIGH density contrasts (tonnes/m<sup>3</sup>) used in trial Vpmg Inversion modelling before settling on HIGH contrast densities. Two different 'Cover' densities were used to handle domains of Mesozoic-only 'Cover' and Mesozoic over Cambrian limestone 'Cover'.

	LOW		MEDIUM		HIGH	
b/g	2.67	contrast	2.67	contrast	2.67	contrast
'Cover'	2.45	-0.22	2.45	-0.22	2.45	-0.22
'Cover LST'					2.54	-0.13
'Granite'	2.61	-0.06	2.61	-0.06	2.59	-0.08
'Proterozoic'	2.73	+0.06	2.79	+0.12	2.78	+0.11

right) are present but do not comprise significant proportions of the Proterozoic so have not been considered when assigning densities to the 'Proterozoic' volumes in the Vpmg starting models.

### Cover

Depth to basement data from the NWQMEP (2011) has been used to constrain cover thickness in the southern, western and eastern portions of the 3D inversion model space (Figure 4.12) which is considerable larger than the Project Area. Cover thicknesses from the seismic data have not been sufficiently well modelled with detailed seismic velocity data and so have not been incorporated into the cover thickness model. An average density contrast for 'Cover' was initially used (in line with that used by Mira Geoscience, 2010 for Mesozoic sedimentary cover. In the west of the Project Area, dense Cambrian limestone underlies the Mesozoic Cover. To manage the significant impact this shallow density variation in the 'Cover' has on the modelling, DMQ incorporated two 'Cover' volumes; one including limestone and one without. Figure 4.12 shows where the different 'Cover' densities have been applied in the inversion modelling. This two-fold 'averaged' density for the 'Cover' alleviated the need to establish a detailed cover stratigraphy. Cover thicknesses are, in any case, not well constrained (Figure 4.12) so this 'lumped' approach approximated the 'Cover' density structure sufficiently well. Table 4.1 summarises different density contrasts that were investigated before settling on the HIGH contrast densities for 'Granite' and 'Proterozoic' in all the later domained Vpmg modelling reported here (see following section).

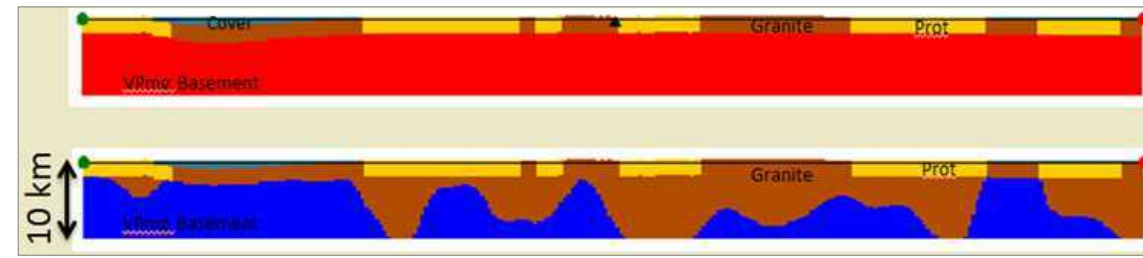


**Figure 4.13:** Series A geometry inversion starting (top) & output (bottom) models ... see text

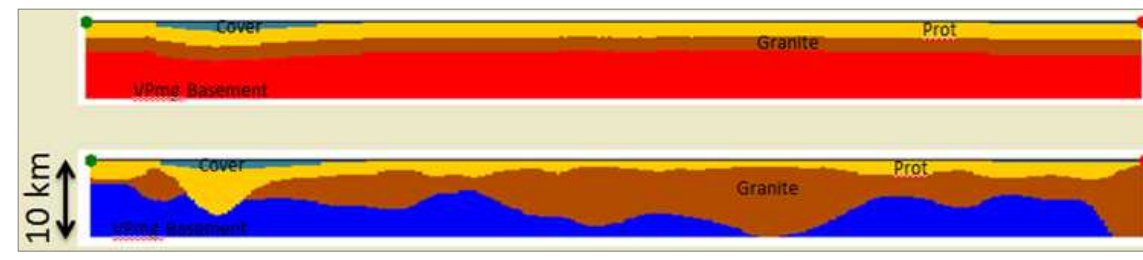


**Figure 4.14:** Series B geometry inversion starting (top) & output (bottom) models ... see text

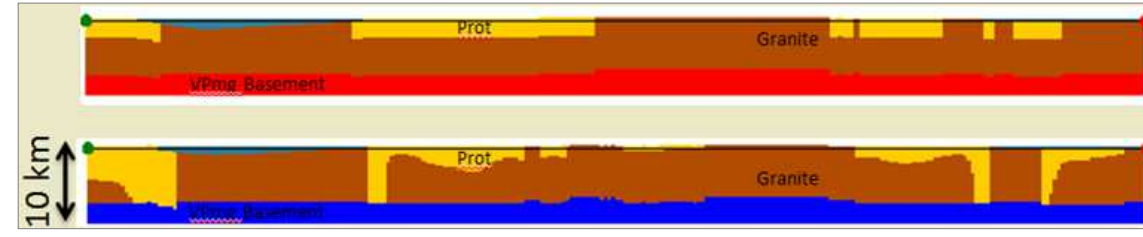


**Figure 4.15:** Series C geometry inversion starting (top) & output (bottom) models ... see text

### Vpmg Inversion Modelling Workflow

Initial and simplistic Vpmg geometry inversion modelling involved the generation of different series of multi-component layer-like (2, 3 and 4-layered) Vpmg models of 'Granite', 'Proterozoic' and 'Cover'. Away from granite outcrop, or granite outcrop under cover, Series 'A' models started with the 'Top-of-Granite' fixed at different depths (100m, 500m, 1km, 2km, 3km) beneath the 'Proterozoic' unit and the 'Granite' base free to expand downward to satisfy the gravity data (Figure 4.13).

Series B models are simple layer-cake models with the 'Granite' layer below 'Proterozoic' and 'Cover' and the top and base of the granite allowed to distort simultaneously (Figure 4.14). Granite outcrop is not able to be honoured in the Series B input models.

Series C models are fixed 'Base-of-Granite' models with the base at different depths (3km, 5km, 7km). The 'Granite' is only allowed to expand vertically upwards to satisfy the gravity data (Figure 4.15). All of these models were run with the different density contrast combinations tabulated in Table 4.1.

Further details of all these early, simple, slab-layered, modelling iterations, their setup and results can be found in DMQ Tech Report 4 presented in Appendix 8.

Any single one of these simple, slab-layered (start) models could not satisfy both the geological constraints and gravity data everywhere; however, different models provided insights in different areas where geological understanding

provided certain constraints on geometries at depth. Crucially this multiplicity of models did inform an interpretation method that ultimately lead to a successful Vpmg modelling methodology that input crude starting geometries that were geologically-constrained and allowed granites to 'grow' so as to satisfy the gravity data constraints.

It needs to be reiterated that there is no unique and accurate modelling solution to granite geometries from the gravity data. The DMQ models have incorporated interpretive geological controls and constraints gleaned from all the geological and geophysical information welded into the evolving 3D interpretation. Resulting granite geometries should be viewed with these limitations in mind. Based on wide spaced ( $\geq 2$  km) gravity data, these are regional-scale granite interpretations and will not stand up to prospect-scale scrutiny. The somewhat-crude, regional-scale granite geometries, however, remain critically important to the process models for Cu-Au-Mo mineralisation in the belt and the identification of Cu-Au-Mo prospective tracts.

The following sections outline the more-evolved DMQ Vpmg Modelling-interpretation workflow that has ultimately lead to the granite geometries presented in this Report, and which have formed the basis of the DMQ 4D Prospectivity Analysis.

The previous Mira Geoscience (2010) granite modelling work applied 2-layer Vpmg density modelling (granite over denser Proterozoic material) to an earlier pmd\*CRC (2008) geological model which restricted granite intrusion

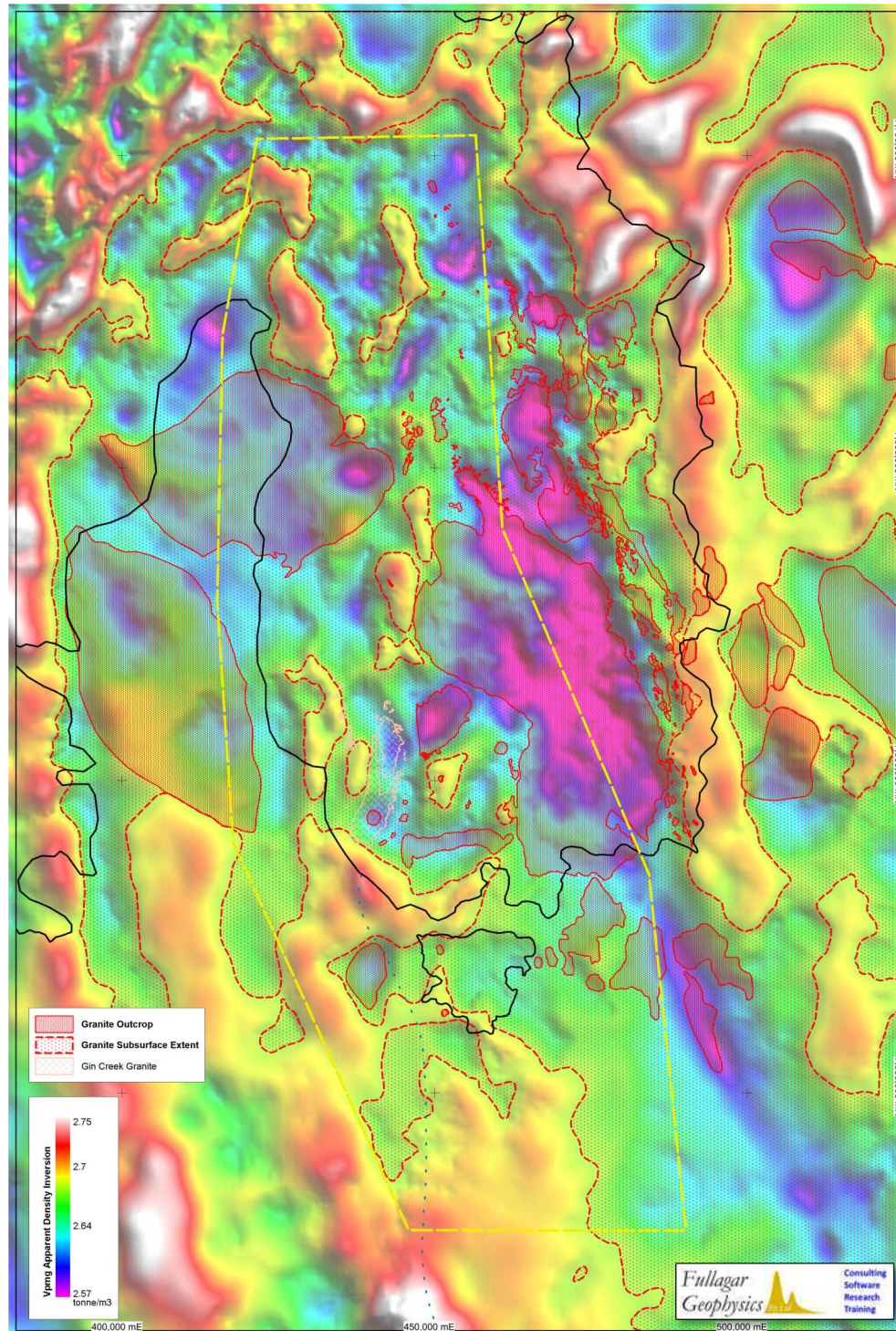


**Figure 4.16** *Vpmg* Apparent Density Model showing outcropping Granite (at surface and interpreted beneath cover) and the early, un-refined, version of DMQ's interpreted extent of significant granite at depth. Black outline is the limit of outcropping Proterozoic; yellow outline DMQ Project Area; red dashed line is Extent-of-Granite at depth

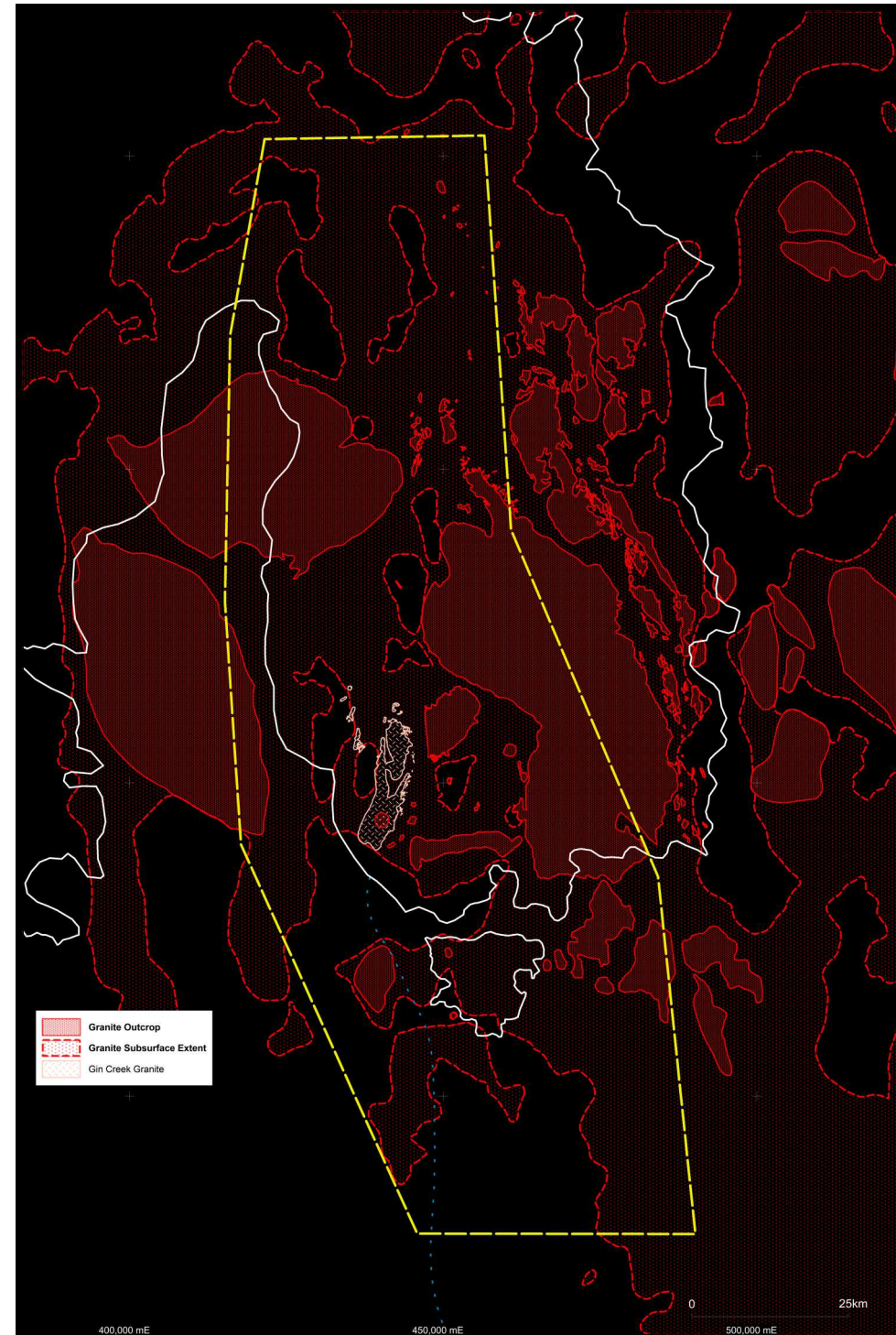


**Figure 4.17** *Vpmg* Inversion Modelling area highlighting the early, un-refined, extent of significant granite at depth compared with outcropping granite (at surface and beneath cover). Pale grey outline is the limit of outcropping Proterozoic; yellow outline DMQ Project Area; red dashed line is Extent-of-Granite at depth.

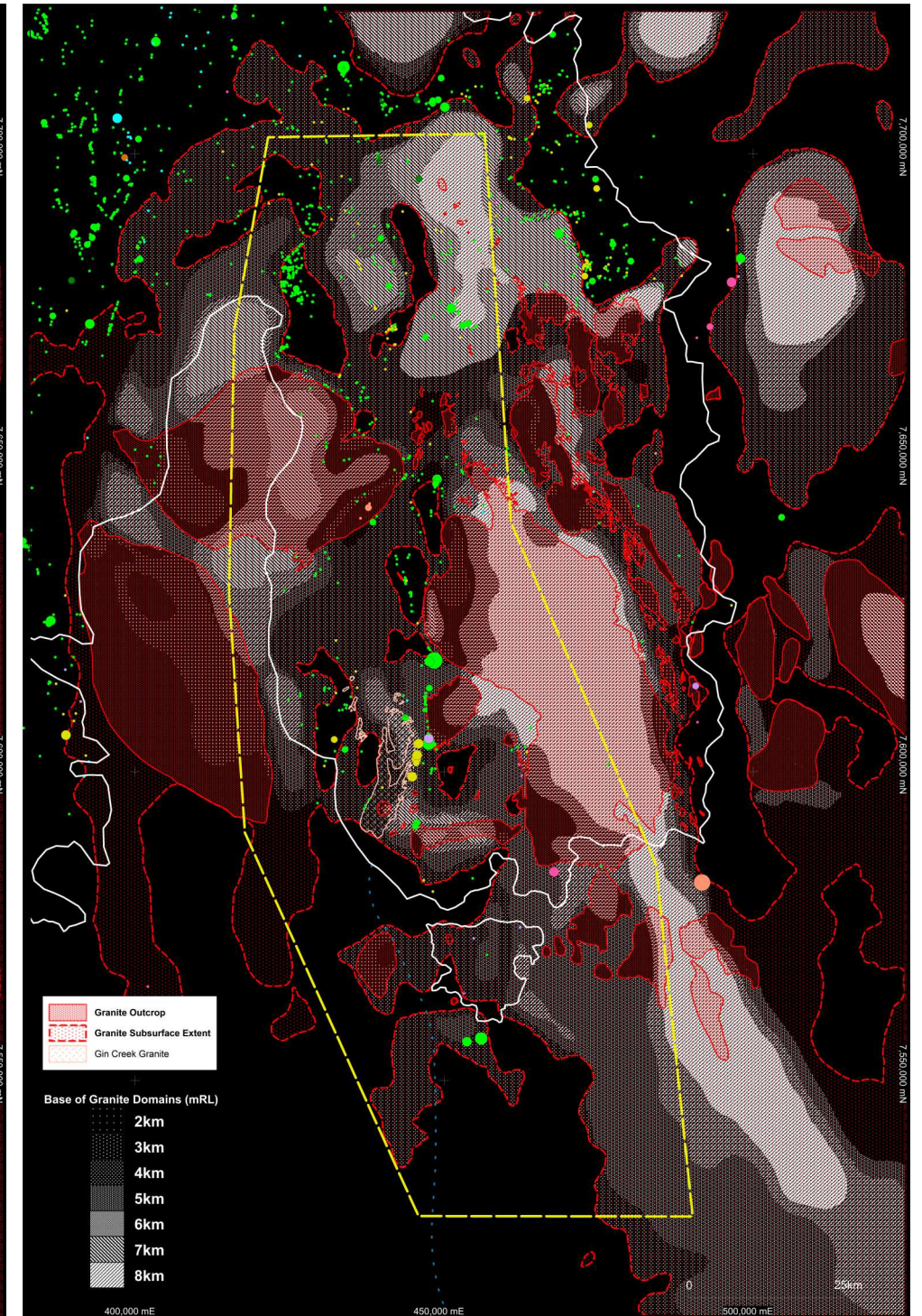


**Figure 4.18** DMQ Base-of-Granite RL Domains interpreted from known 3D geological relationships of depth to granite and the Apparent Density Model. Mineral Occurrences show a close spatial relationship with margins, shoulders and apophyses of granites at depth. Cu-Au: green-yellow. Other outlines as for Figure 4.17

to areas of outcropping granite (apart for a single buried granite body). This Mira modelling initially indicated that the pmd\*CRC volume of granite (with reasonable density attributes) was insufficient to explain the measured gravity response. The base of granite was then allowed to move (*Vpmg* 'Geometry' inversion), and lateral variations in Proterozoic density away from granite outcrop were allowed, to enable a better fit between the modelled and observed gravity data. However, both these Mira granite models

critically restricted granite to areas of granite outcrop and/or their interpretation beneath Mesozoic cover. As outlined, DMQ considers this to be a fundamentally flawed assumption.

### Base-of-Granite Domain *Vpmg* Modelling

While the simple layered *Vpmg* starting models could not generate geologically realistic granite geometries, the

accumulated results did suggest that domaining the model area into regions with different starting geometries might produce more realistic results. This series of geometry inversions set a Base-of-Granite start depth that was domained across the modelling area and allowed the *Vpmg* inversion to 'grow' the granite upwards to satisfy the gravity data. In areas of granite outcrop, the base of granite was free to 'move' in either vertical direction to satisfy the gravity data.

A critically-important additional constraint on the modelling was the definition of a region within which granite was expected to exist at depth, and outside of which the vertical profile was expected to be dominated by Proterozoic rocks .... at least within the crustal depth range of interest to the DMQ process models and the Prospectivity Analysis. This 'Extent of Granite' region was defined from the Apparent Density Model and a consideration of other low density lithologies (and their likely 3D geome-

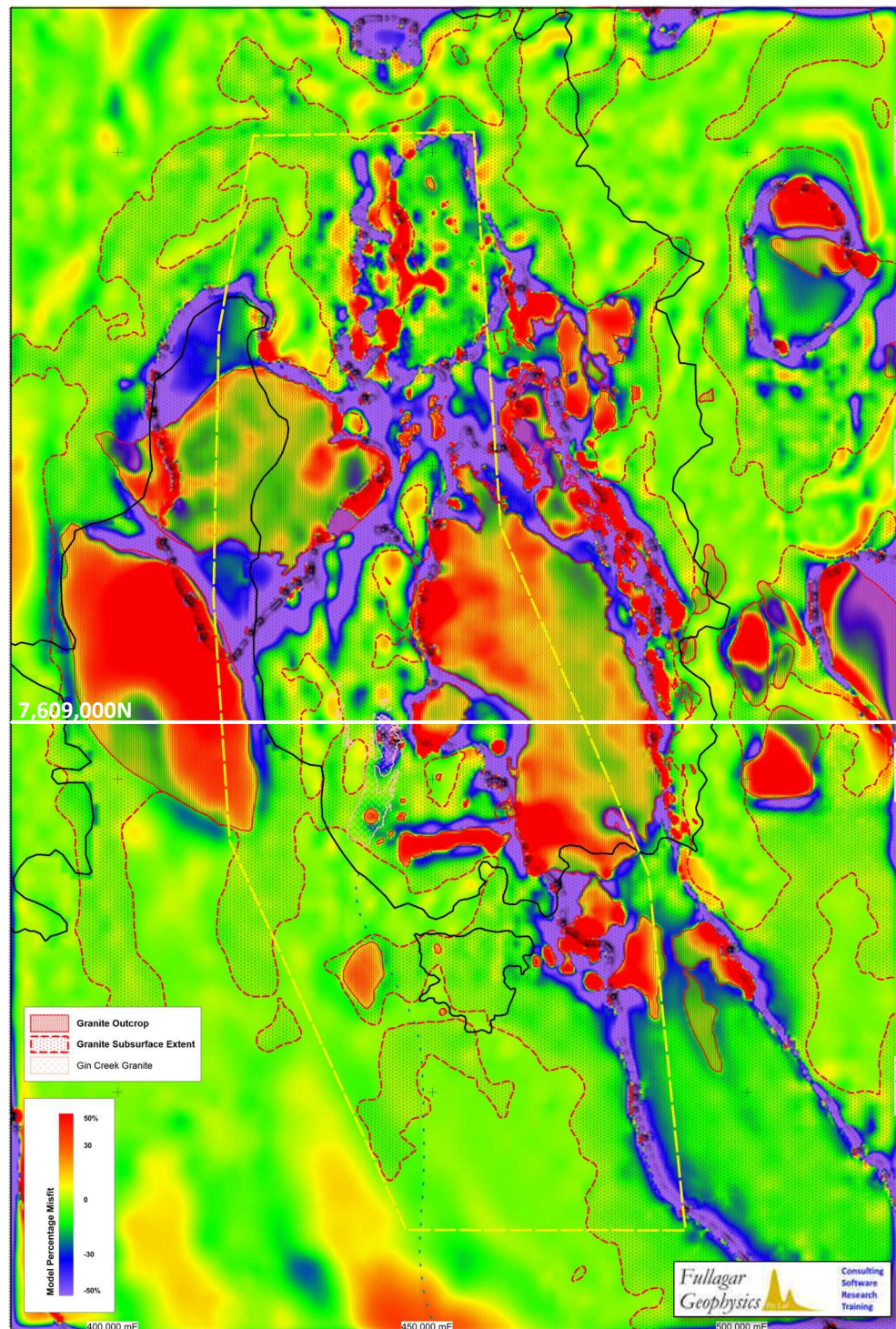


**Figure 4.19** Percentage misfit of Base-of-Granite RL Domain *Vpmg* Inversion model output highlighting very significant misfits around outcropping WILLIAM-aged granites. Note the reasonable fits within the interpreted Extent-of-Granite away from granite outcrop. Section 7,609,000N shown in Figure 4.20 is in the centre of the modelled area and is a representative section across the Wimberu, Mount Dore and Squirrel Hills Granites.

try) from the Solid Geology interpretation.

Figures 4.16 to 4.18 outline the domained constraints applied to this early set of Base-of-Granite Domain models. Figure 4.16 is the *Vpmg* Apparent Density Model with outcropping granite superimposed that highlights the significant additional extent of low density rocks at depth, in large part interpreted to reflect WILLIAMs-aged granites. Some low density domains in the west reflect MITAKOODI

relationship between Cu-Au(-Mo) occurrences with the margins and shoulders of the suggested granites at variable depth in the subsurface.

In these inversion models, in regions where granite was interpreted not to be present within the crustal volume of interest (ie. outside the Extent-of-Granite polygon) a thin, low density dummy unit was introduced ('Qzt') and allowed to 'grow' to accommodate the low density litholo-

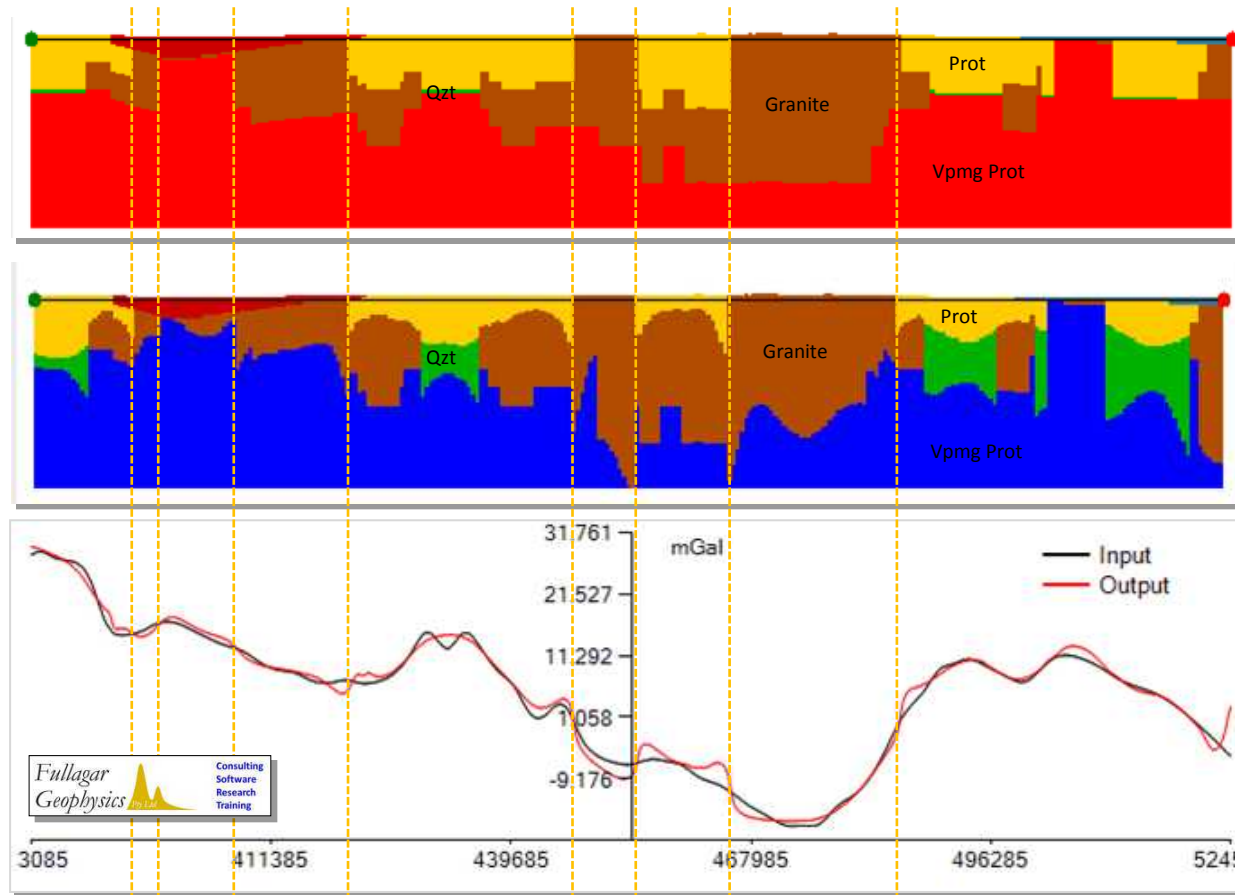


**Figure 4.20** Section 7,609,000N *Vpmg* Model starting Base-of-Granite RL Domains (top); Output geometries (middle) and Input and Output gravity profiles (bottom) through Wimberu, Mount Dore and Squirrel Hills Granites. Vertical yellow lines highlight the significant dipole misfits at the margins of outcropping granite bodies. This model section line is located on Figure 4.19. The model sections are 10km deep and have a V/H exaggeration of x2.

Quartzite and BULONGA Felsic Volcanics dipping east beneath the AN-SWER-STAVELEY-KURIDALA-MOUNT NORN packages and were excluded from later domained models (see following Sections). Figure 4.17 highlights the interpreted Extent-of-Granite at depth compared with outcropping granite (at surface and interpreted at the base of cover). Figure 4.18 presents the Base-of-Granite RL Domains that controlled the starting geometries for this series of *Vpmg* inversions. The figure also re-highlights the significant spatial

relationship between Cu-Au(-Mo) occurrences with the margins and shoulders of the suggested granites at variable depth in the subsurface. Quartzite and BULONGA Felsic Volcanics dipping east beneath the AN-SWER-STAVELEY-KURIDALA-MOUNT NORN packages and were excluded from later domained models (see following Sections). Figure 4.17 highlights the interpreted Extent-of-Granite at depth compared with outcropping granite (at surface and interpreted at the base of cover). Figure 4.18 presents the Base-of-Granite RL Domains that controlled the starting geometries for this series of *Vpmg* inversions. The figure also re-highlights the significant spatial

## Results

The Base-of-Granite RL Domain *Vpmg* Inversions also failed to produce realistic granite geometries. The inversions were unable to handle the steep, high frequency discontinuities along the margins of the outcropping granites in the starting model. Hoped-for, smooth transitions from outcropping granite to granite at depth were not achieved. Figures 4.19 and 4.20 highlight the very significant Observed vs Calculated misfits associated with the margins of outcropping granite in these Inversion models.

Imposing granite outcrops in the starting model of these inversion runs poses a problem for the modelling. The gravitational response across the vertical contact between outcropping Granite and Proterozoic will never

match the broad wavelength observed gravity data across the contact (Figures 4.19 & Figure 4.20). The geometry inversion is not able to adjust or smooth these vertical contacts of granite outcrop to improve the data mismatch, instead distorting the volumes adjacent and significantly corrupting the output model (Figure 4.20) in these contact regions.

The gravity response measured at surface of an outcropping vertical density contrast is inconsistent with the low frequency nature of the gridded regional gravity data being used. Given *Vpmg* geometry inversion can't modify the vertical contact and the constraint of needing to keep starting models simple, the challenge becomes how to honour the granite outcrop while appropriately adjusting the model geometry and maintaining consistency with the observed gravity data. Upward continuing the gravity data to overcome the problem diminished the data resolution too much.

## Mid-Granite 'PERT' Domain *Vpmg* Modelling

A number of innovative refinements and changes to modelling parameters and starting geometries were made to alleviate the issues that were manifest in the Base-of-Granite RL Domain and earlier models. Early stage (Series A) inversion modelling with constant thicknesses of 'Proterozoic' over 'Granite' that was allowed to 'grow' vertically returned good matches with the gravity data but failed to produce granite outcrop where required. This observation and the issues manifest in the Base-of-Granite RL Domain modelling suggested a new approach where granite mid-points would be setup (in domains) and the granite would be allowed to 'grow' from these starting depths. Shallower starting depths under outcropping granite would 'encourage' *Vpmg* to generate outcropping granite.

### Adjustment of *Vpmg* Inversion Parameters

The following adjustments were made to DMQ's modelling parameters to speed model run-time and turn-around and to drive granite growth uniformly from the assigned starting depths. Glenn Pears (Mira Geoscience) is thanked for his tips when the 'going got tough' in finessing the subsurface geometries of granite and honouring known outcrop geometries.

1. To reduce *Vpmg* computation times while solving the problem of honouring granite outcrop in the output models, model prisms were increased from 500x500m to 1500x1500m. This resulted in a reduction of prism numbers from ~119,000 to ~13,400. The larger prism sizes were used until reasonable granite geometries were achieved and then final runs used 1000x1000m prisms (~29,300 prisms) to gain finer fidelity of granite morphologies.

- To simplify model complexity, the gravitational response of the Cover was subtracted from the observed gravity data. Removing the response of the Cover increased the simplicity of the models by removal of the complex Mesozoic sedimentary and Cambrian limestone Cover units from the starting models. In areas of cover final model geometries were iteratively honed to geometrically fit to the base of cover surface and to honour the reduced gravity response resulting from the removal of the cover component of gravity response in these areas.
- In the southwest and far west of the modelling area, in regions beyond the DMQ Project area, strong positive gravity anomalism (see Figures 4.15 & 4.20) degraded the modelling effort (focused on gravity **low** modelling) because it diverted the iterative *Vp<sub>mg</sub>* inversion process away from refining the model in the area of prime interest. Allowing the model basement to accommodate positive heterogeneity in these areas by directing *Vp<sub>mg</sub>* to run a few iterations of Heterogeneous Inversion in this basement slab followed by as many Geometry Inversions as required in the upper Granite and Proterozoic volumes produced significantly better misfit results. (see details in Half Yearly Tech Report 4 in Appendix 8).
- To drive granite 'growth' equally (upward and downward) from starting surfaces, a *Vp<sub>mg</sub>*-controlling parameter, 'PERT' was activated. PERT determines the maximum relative change in interface depth allowable per iteration during a model run and is typically set to around 0.1 (10%). At a setting of 0.1, depth changes applied to shallow interfaces are significantly less than deeper interfaces. For example, with PERT = 0.1, an interface at 200m depth will change by 20m each iteration while an interface at 2 Km can change by 200m. Setting PERT to a large number, eg 10,000, overrides the differential depth change, resulting in the amount a shallow interface can change per iteration to asymptote towards the change applied to deeper interface. The PERT value is added to the layer interface depth for determining the amount of change. A PERT of 10,000 allows an interface at 200m depth to change by 1020m (10% x 10,200m) and an interface at 2km deep is able to change by a comparable 1200m (10% x 12,000m). (see further details in Half Yearly Tech Report 4 in Appendix 8).
- A modified Extent-of-Granite volume interpretation was produced to exclude volumes of low density rocks in the west that had previously been simplistically included within the previous Extent-of-Granite volume. Regions of MITAKOODI Quartzite and BULONGA Felsic Volcanics dipping east beneath the ANSWER-STAVELEY-KURIDALA-MOUNT NORNA packages were excluded from the updated Extent-of-Granite domain. Figure 4.21 highlights the extent of MITAKOODI Quartzite and BULONGA Felsic Volcanics in the west of the modelling volume and the modified Extent-of-Granite that was subsequently input into the Mid-Granite 'PERT' *Vp<sub>mg</sub>* modelling. Despite the relatively low densities of the MITAKOODI Quartzite and BULONGA Felsic Volcanics (see also Figure 4.8), the Apparent Density Model (Figures 4.6 & 4.10) suggests there may still be granite at depth north of the Wimberu Granite beneath the Mitakoodi Culmination. The modified Extent-of-Granite domain reflects this likelihood while excluding the volumes through which the MITAKOODI Quartzite and BULONGA Felsic Volcanics are interpreted to dip.

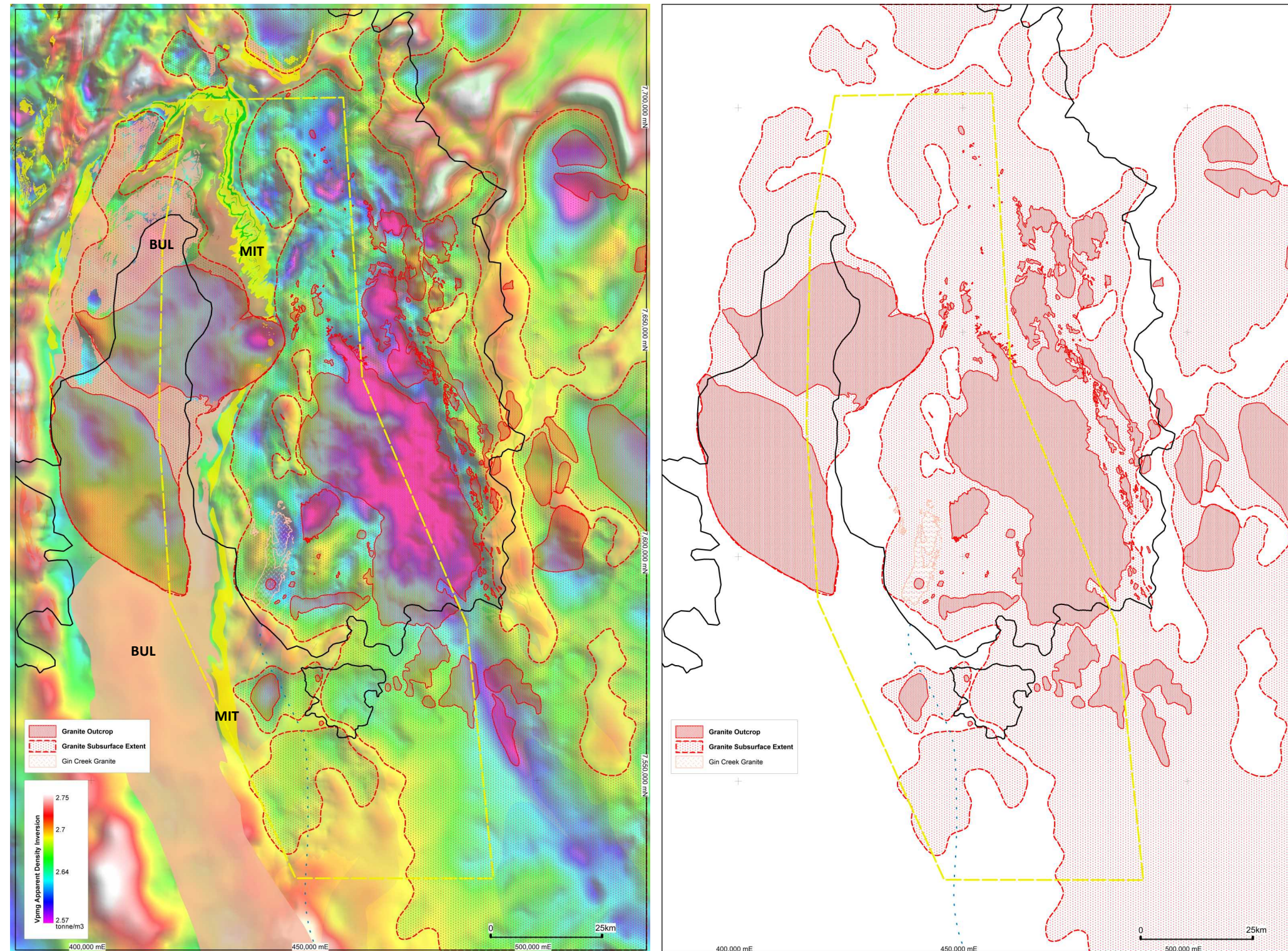


**Figure 4.21** Modified Extent-of-Granite to accommodate low density MITAKOODI quartzite (MIT) and BULONGA felsic volcanics (BUL) outcropping in the west within the *Vp<sub>mg</sub>* modelling volume plunging to the northeast within the Mitakoodi Culmination and dipping east into the DMQ Project Area over the Apparent Density Model (on left). Compare modified Extent-of-Granite with previous un-refined Extent-of-Granite in Figure 4.11.

### Mid-Granite 'PERT' Domain *Vp<sub>mg</sub>* Modelling Workflow

A new set of domains were defined that interpreted potential mid-Granite depths based on regional geological relationships informed by the sectional interpretations, seismic interpretation, the inferred proximity to surface of granite (sometimes based on drilling) and the *Vp<sub>mg</sub>* Apparent Density grid. This mid-Granite depth is

trivial to fix where granite outcrops, but inferences from geological and geophysical data need to be made to distinguish between regions of shallow (thin) Granite over Proterozoic and deep (thicker) Granite under Proterozoic as both will produce identical integrated Apparent Density and gravity responses.

An initial guesstimate of mid-Granite start depths was fashioned into a domain

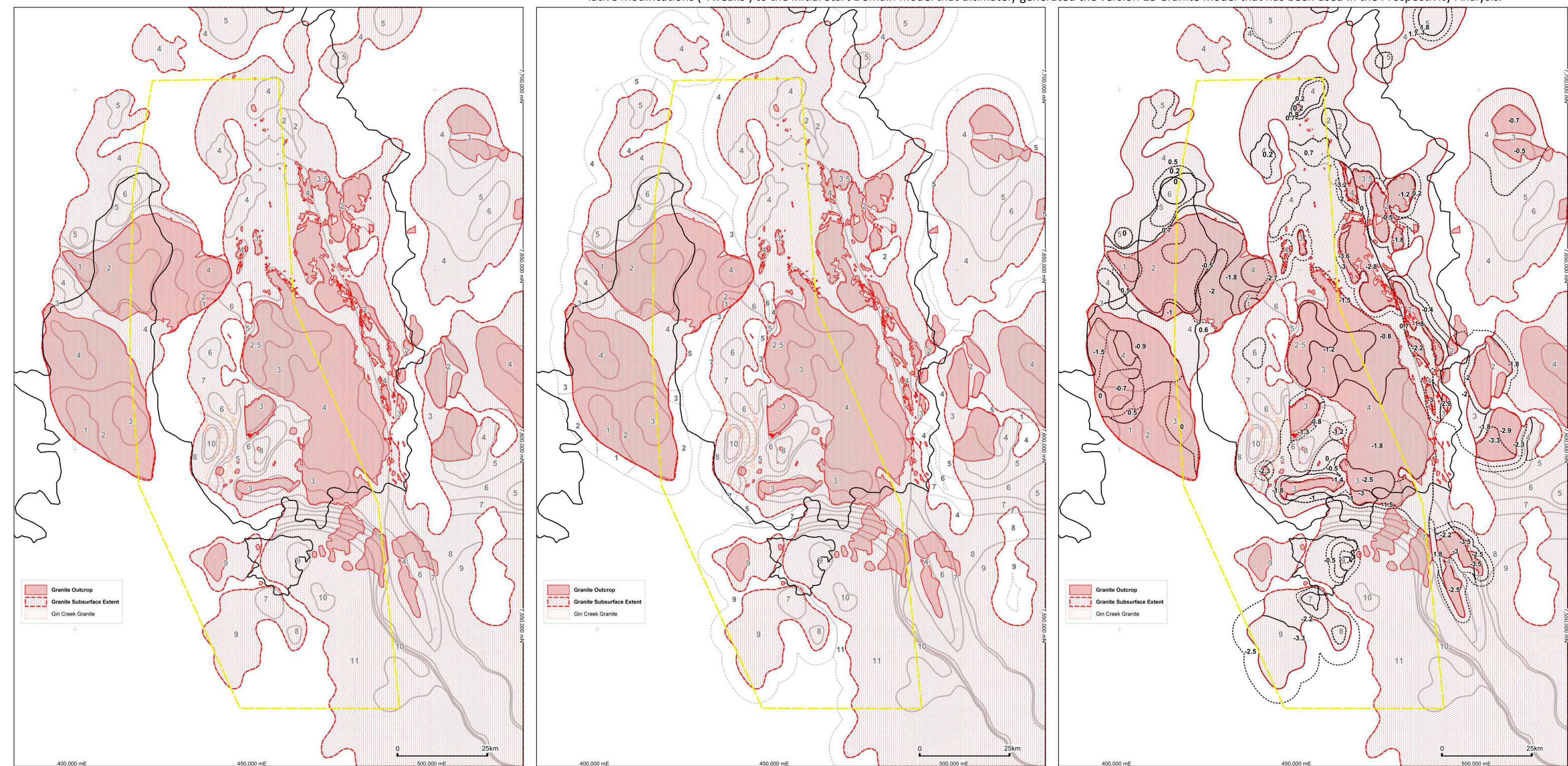
START MODEL Descriptions & Tweak Descriptions

SetUp	RunDate	Version	Tweak	GRID	Detail / Modifications to START DEPTHS
12-Jan-17	14-Jan-17	V1		1500m	Simple START DEPTH Domains
16-Jan-17	17-Jan-17	V2		1500m	Simple START DEPTH Domains with Heterogeneous Vp <sub>mg</sub> Prot Basement (+ve contrast only)
17-Jan-17	17-Jan-17	V3		1500m	V1 plus 1km TEST
17-Jan-17	17-Jan-17	V4		1500m	V2 output with top Granite free to grow; base fixed
18-Jan-17	19-Jan-17	V5	#1	1500m	V2 - Tweak #1 lift SqHG, MDG, YWG, OG; drop WG, LG, DBGs
19-Jan-17	20-Jan-17	V6	#2	1500m	V2 - Tweak #2 further lift & modify SqHG, MDG, YWG, OG; fix WG; further drop LG, DBGs
13-Jan-17	23-Jan-17	V7	#3	1500m	V2 - Tweak #3 further lift & modify SqHG, MDG, YWG, ESqH, WG, SCG
30-Jan-17	01-Feb-17	V8	#4	1500m	V7 - Tweak #4 lift & modify DBGs, ESqHG, MDG, YWG, MMG
02-Feb-17	03-Feb-17	V9	#5	1500m	V7 - Tweak #5 lift & modify SqHG, MDG, YWG, MMG, ESqHG, nWG
03-Mar-17	06-Feb-17	V10	#6	1500m	V9 - Tweak #6 lift & modify SqHG, MMG
06-Feb-17	08-Feb-17	V11	#7	1500m	V10 - Tweak #7 lift OG, HG
09-Feb-17	09-Feb-17	V12	#8	1500m	V11 - Tweak #8 lift & modify SqHG, WG, MD, YWH
10-Jan-17	10-Feb-17	V13	#9	1500m	V12 - Tweak #9 fix YWH, southern SqHG
10-Feb-17	10-Feb-17	V14	#9	500m	V12 - Tweak #9 500x500m TEST
14-Feb-17	14-Feb-17	V15	#9	1000m	V12 - Tweak #9 1000x1000m TEST
14-Feb-17	14-Feb-17	V16	#10	1500m	V12 - Tweak #10 further modifications YWG, southern SqHG
15-Feb-17	15-Feb-17	V17	#11	1000m	V15 - Tweak #11 fixes OG, nWG, CGs, DBGs
19-Feb-17	20-Feb-17	V18		1000m	V17 - added upper Houdini & southern Squirrel Hills flanges

SqHG=Squirrel Hills Granite, ESqHG=eastern Squirrel Hills Granites, MDG=Mt Dore Granite, YWG=Yellow Waterhole Granite, OG=Osborne Granite, HG=Houdini Granite, LG=Levuka Granite, DBG=Doherty Belt Granites, SCG=Snake Creek Granites, MMG=Maramungee Granites, WG=Wimberu Granites

Table 4.2 left Vp<sub>mg</sub> Mid-Granite 'PERT' Inversion Modelling Start Geometry Versions, Modifications and Run details that ultimately produced the final V18 Granite Model.

Figure 4.22 below (left) Initial simple domained mid-Granite Start Depths within the modified Extent-of-Granite. (middle) Addition of 4km buffer zone around the modified Extent-of-Granite with assigned Start Depths to conform with adjacent domains to prevent the generation of large vertical discontinuities that distress Vp<sub>mg</sub>. (right) Superimposed cumulative modifications ('Tweaks') to the initial Start Domain model that ultimately generated the version 18 Granite model that has been used in the Prospectivity Analysis.



map (Figure 4.22 left). The mid-Granite start domains were SQL-queried across the *Vpmg* starting model prisms to fix individual prism granite starting depths. In addition, a 4km buffer volume was defined beyond the defined Extent-of-Granite (Figure 4.22 middle) and its starting depth defined to conform to the adjacent start domain depth so as to not introduce wild discontinuities into the inversion starting model. Beyond the buffer domain an arbitrary

start depth was assigned. The 'dummy', low density 'Quartzite' was again placed on a fixed start depth everywhere outside the Extent-of-Granite to flag potential low density deficits adjacent to the output modelled Granite.

The V1 inversion model was run and an assessment of the resulting granite morphology with respect to granite outcrop and morphologies at depth was made. Subsequently

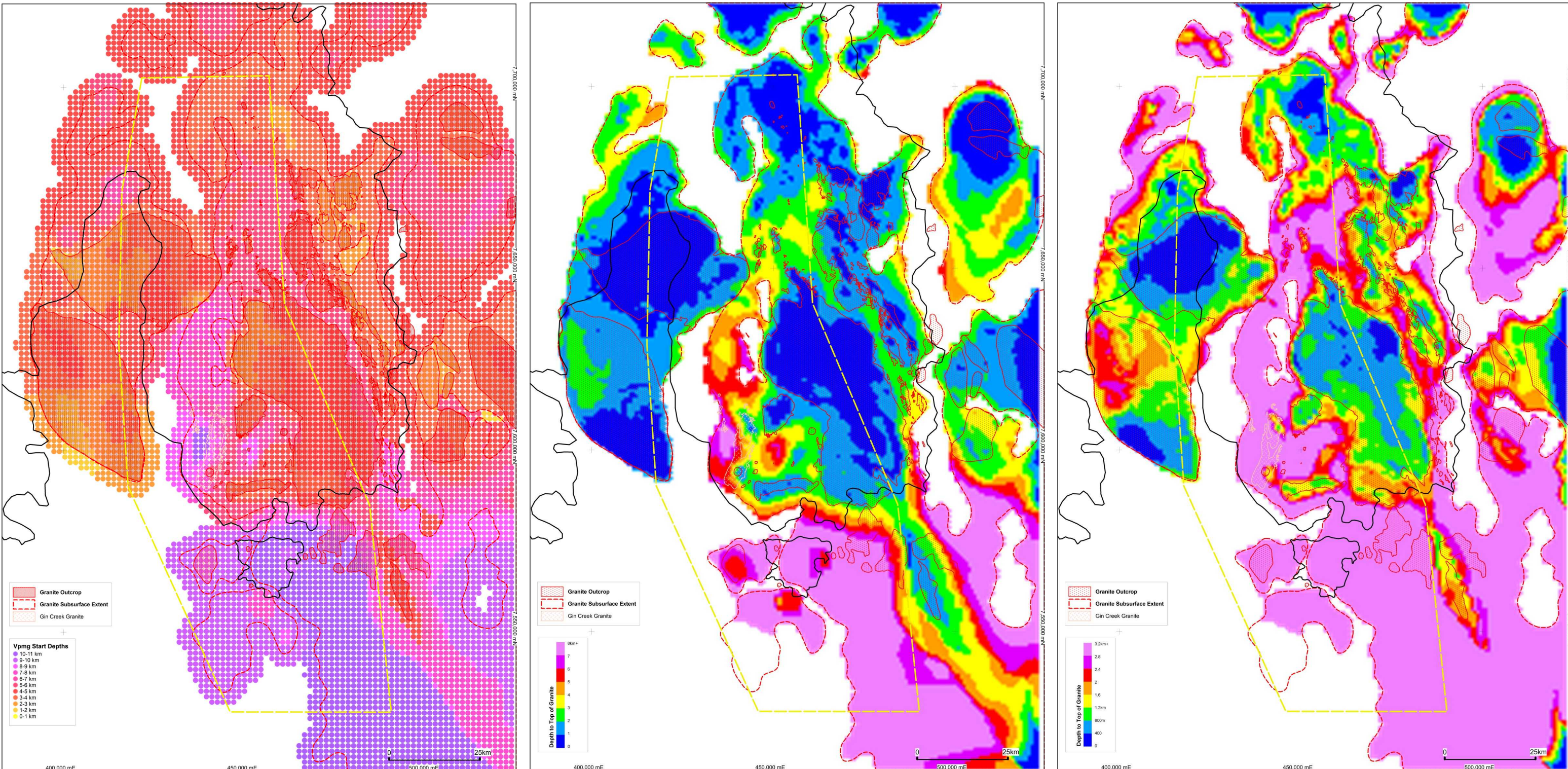
a series of modifications ('Tweaks') were made to each of the starting domain models and the cycle progressed iteratively until geologically reasonable granite morphologies were produced. Table 4.2 lists the various set-ups, run dates, prism sizes and tweaks that culminated in a final V18 Granite Model that has been fed into the 4D Geological Model and the Prospectivity Analysis. Figure 4.22 (right) superimposes on the initial start mid-Granite do-

main map an integration of all the start domain modifications that culminated in the V18 Granite Model.

### Results

Eighteen iterative modifications (Table 4.2) to the Inversion Start Model Domains ultimately produced the geologically-reasonable Version 18 Granite Model that DMQ has taken to its Prospectivity Analysis. Figures 4.23 and 4.24

**Figure 4.23** (left) Version 1 1500x1500m *Vpmg* prism Start Depths that include depths within a 4km buffer around the Extent-of-Granite but not showing Start Depths outside the Extent-of-Granite which were set at an average depth. (middle & right) *Vpmg* Output Depth-to-Granite gridded with colour stretch to 8km and 3.2km respectively. Model outputs show poor match with outcrop extents (Mount Dore, Yellow Waterhole, Squirrel Hills, Wimberu etc) compared with final iteration Model output (Figure 4.19)



present the initial simple Version 1 and the final Version 18 Domain Start Models and their Outputs (respectively) and demonstrate the convergence of the iterative modelling process towards a geologically-reasonable granite model for the belt. A fuller sequence of converging models is detailed in Tech Report 4 in Appendix 8. The output model matching of granite outcrop was progressively

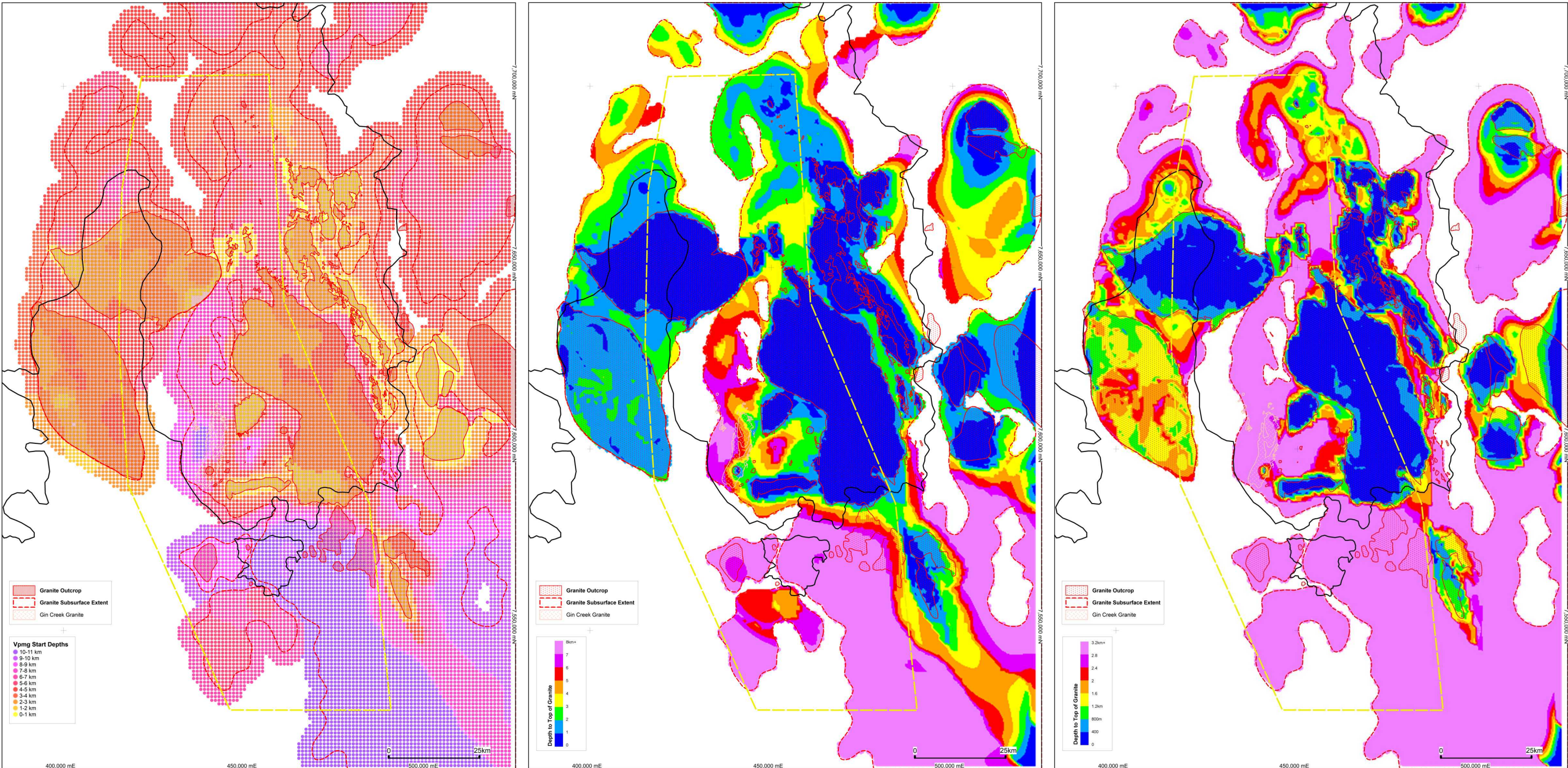
assessed via the generation of grids showing the depth below topography to the top of Granite (shown in Figures 4.23 and 4.24 for the initial and final models) in the progression of output models. Different grid colour stretches of this measure allowed the iterative refinement of the model granite outcrop geometries and the subsurface volumes of granite beneath them. These figures show a

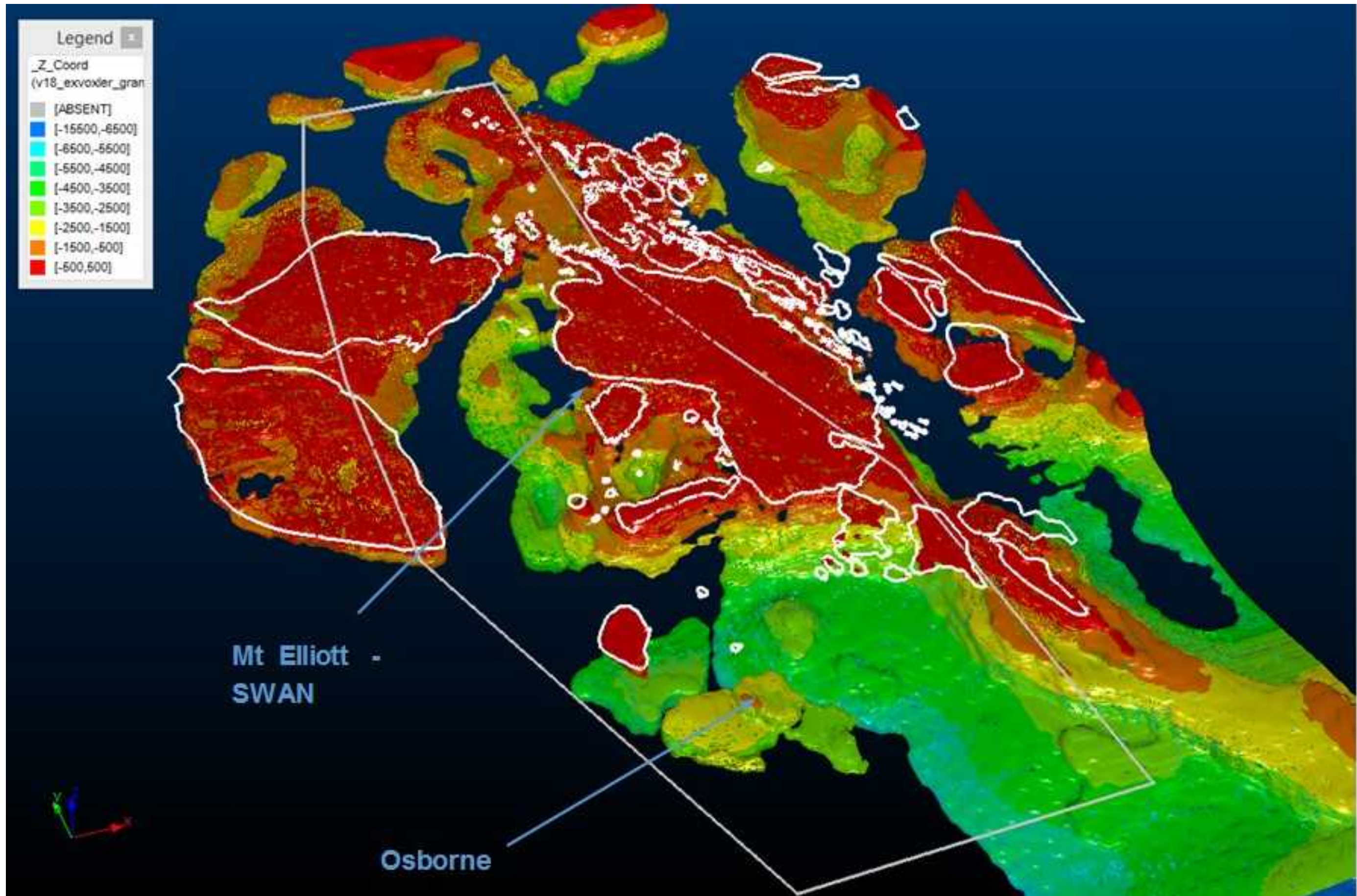
coarse and fine stretch of the Depth-to-Granite results used to constrain the iterative model Start Domain modifications.

Figure 4.25 presents the final V18 Granite model in 3D view. Figure 4.26 presents the Vpmg Model Section 7,609,000N (cf. Figure 4.20) and highlights the excellent fit to outcrop and the realistic sub-surface granite geometries

achieved in the V18 model version of the iterative modelling process.

**Figure 4.24** (left) Final Version 18 1000x1000m Vpmg prism Start Depths. Other details as for Figure 4.23. (middle & right) Vpmg Output Depth-to-Granite gridded with colour stretch to 8km and 3.2km respectively. Model outputs show an excellent match with outcrop extents (Mount Dore, Yellow Waterhole, Squirrel Hills, northern Wimberu etc) compared with early iteration Model output (Figure 4.23). Southern Wimberu remains only crudely resolved due to the complexity of matching the model to the base of cover.





**Figure 4.25** 3D view looking NNE of Final Version 18 Granite morphology. Coloured by RL and highlighting significant subsurface granite beyond outcropping granite outlined in white and locations of Mount Elliott-SWAN and Osborne-Kulthor relative to subsurface granite topography. DMQ Project Area shown on surface. Full 3D models presented in Appendix 7.

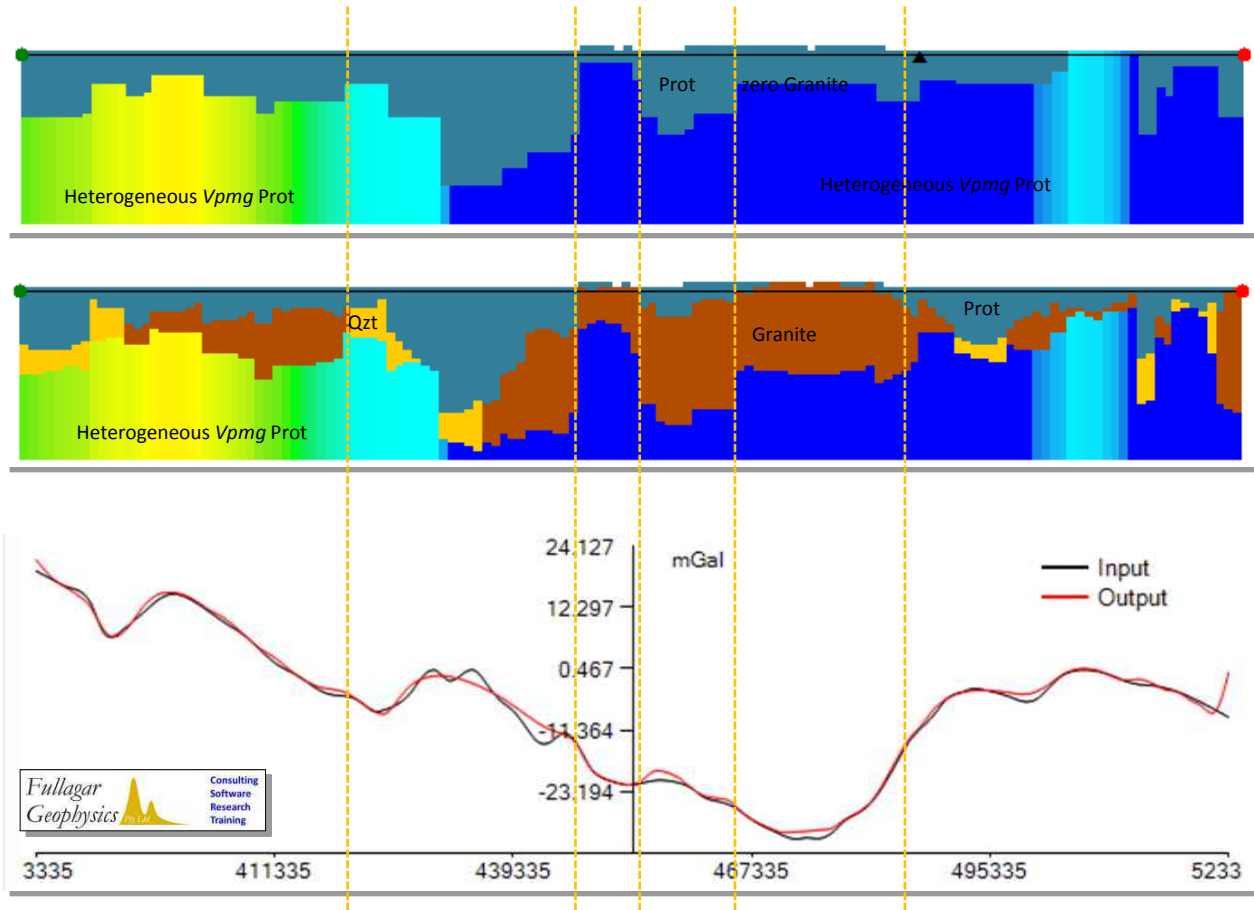


**Figure 4.26** Section 7,609,000N Final V18 Vpmg Mid-Granite Domained Starting Model (top) with ZERO thickness granite on the Proterozoic-Proterozoic contact. The higher density Heterogeneous Vpmg Proterozoic is shown (see text for discussion). Output granite geometry (middle) and Input & Output gravity profiles (bottom). Section 7,609,000N through southern Wimberu, Mount Dore and Squirrel Hills Granites to compare with Figure 4.20. Outputs highlight the good approximations to outcrop (marked by vertical yellow lines) and realistic subsurface morphologies. The model sections are 10km deep and have a V/H exaggeration of x2. The model section line is located on Figure 4.13.

## Finalised Section Interpretations

The forty-seven DMQ Section Interpretations built across the Project Area and adjacent areas of interest were finalised with the sectioning of the V18 Granite Model. Figure 4.27 presents a sample of six of the sections including the V18 granite with its correct overprinting relationships with pre-WILLIAMS architecture and the post-WILLIAMS structures that cut (and displace) the intrusives. A full set of the finalised 4km-spaced sections including the V18 Granite Model is presented in Appendix 5.

### Comparison with Seismic Sections

Where the Seismic sections transect and coincide with the sectional interpretations (Figures 4.28 & 4.29), a comparison between the two is possible and offers some support to the Vpmg V18 modelled granite morphologies at depth. Figure 4.28 presents granite margin line work from the

**LEGEND**

- surface
- base of cover
- granite

**Structure**

- v late D4 Fault (post WILLIAMS)
- late D4 Fault (syn-post WILLIAMS)
- early D4 Fault (syn WILLIAMS)
- D3 Fault
- D2 Fault
- D2 Fault (major)
- D2 synform
- D2 antiform
- D1 Fault

**Stratigraphy**

- top NEW HOPE-MT NORNA (base ANSWER-TOOLE CREEK)
- top KURIDALA-STARCROSS (base NEW HOPE-MT NORNA)
- top STAVELEY (base KURIDALA-STARCROSS)
- top MITAKOODI (base CORELLA)
- top MARRABA (base MITAKOODI)
- top TIMBEROO (base MITAKOODI)
- top BULONGA (base MARRABA)

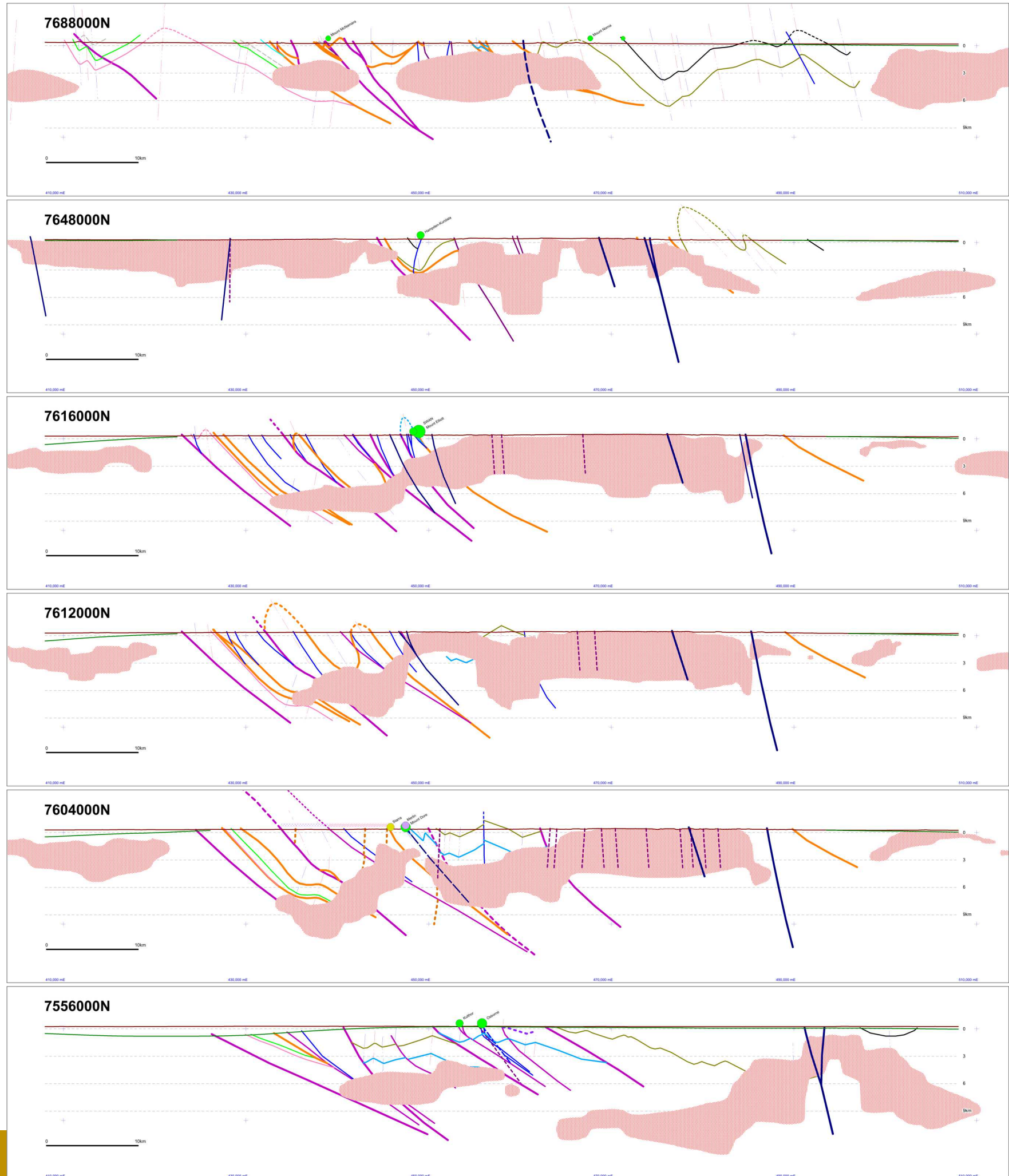
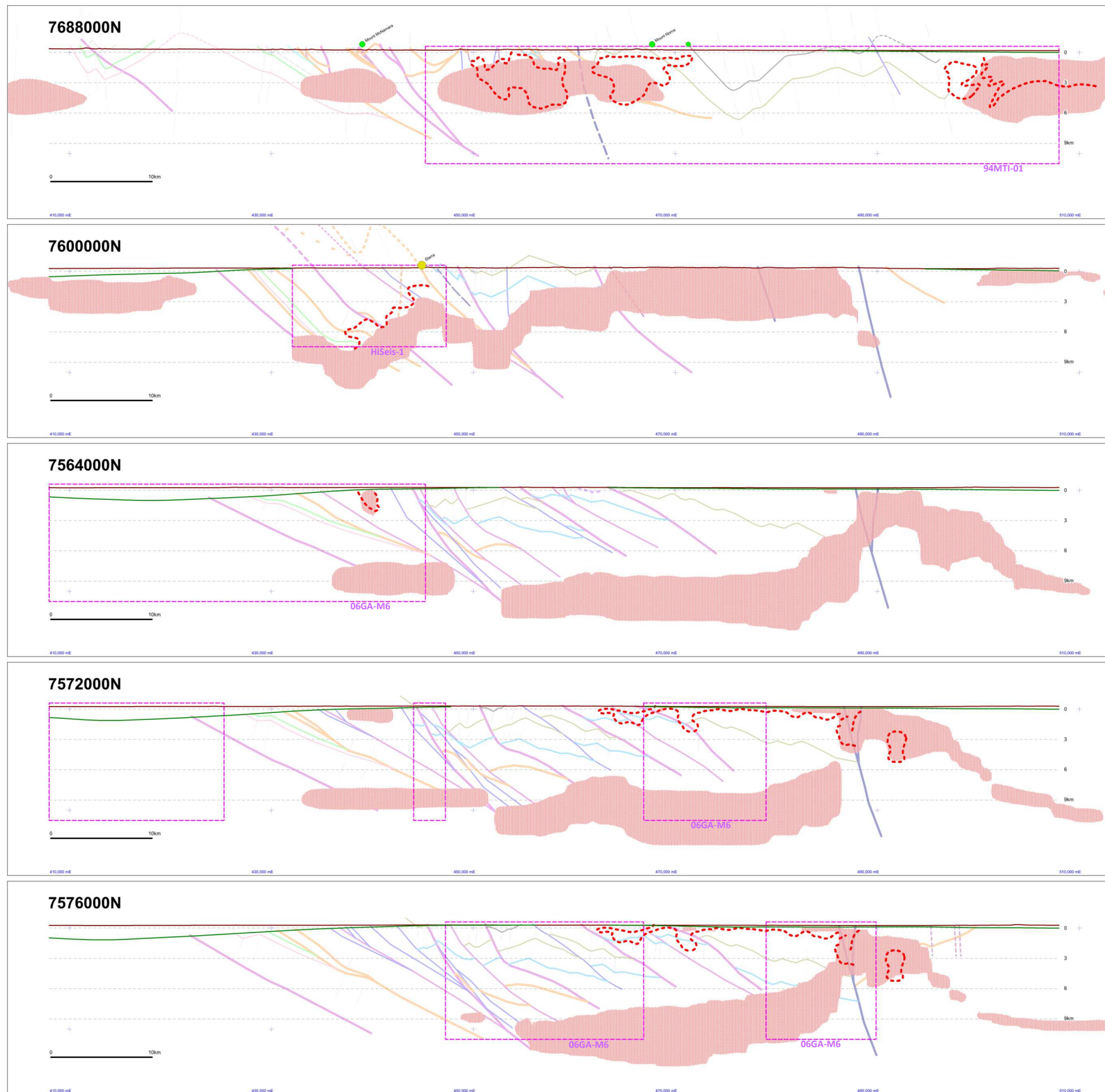
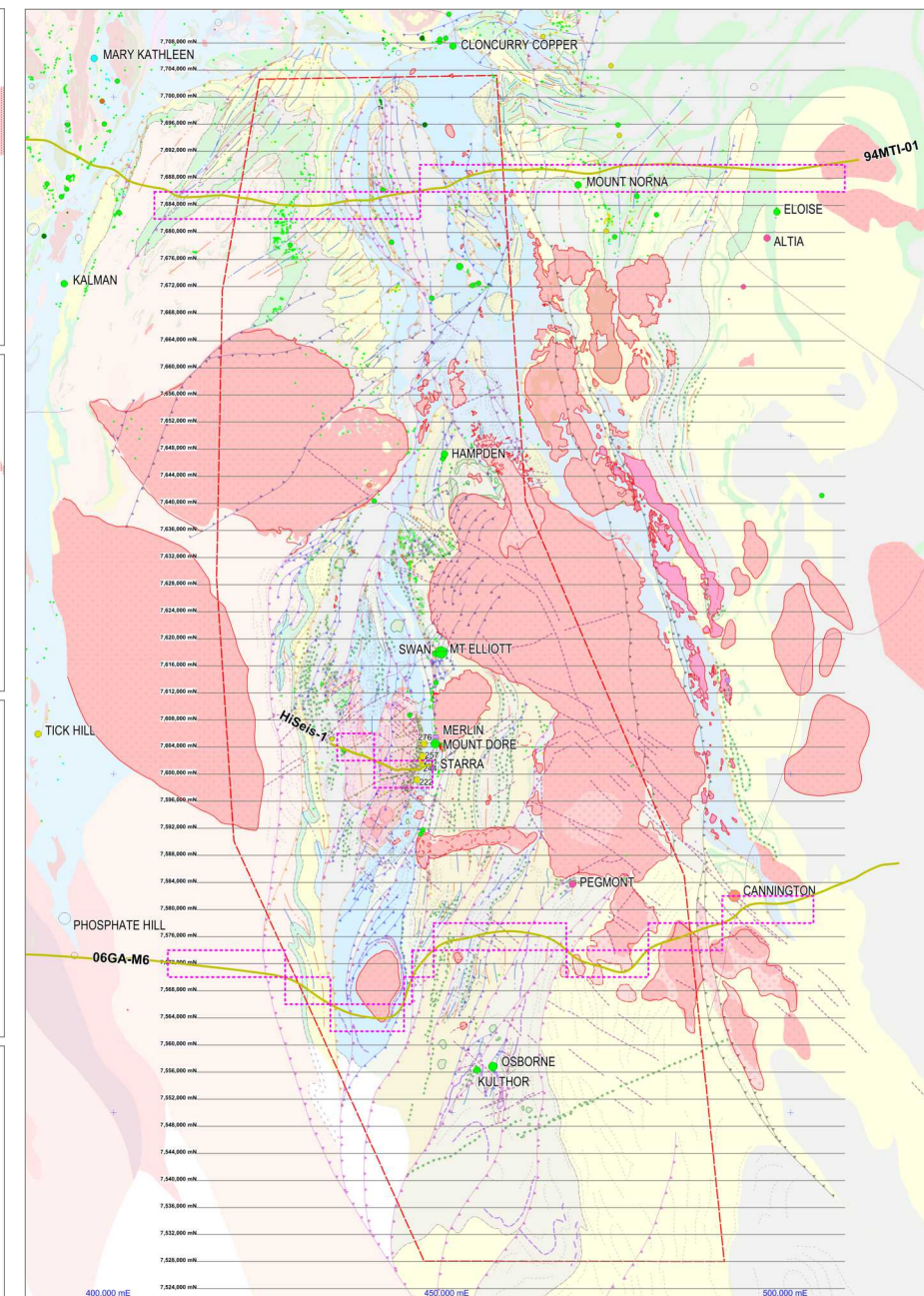


Figure 4.27 The same six selected section interpretations as presented in Figure 4.6 through some of the known resources and occurrences with the V18 Granite Model cut into the sections. The full set of sections are presented in Appendix 5.



**Figure 4.28** Five section interpretations that coincide with seismic lines and DMQ seismic interpretation showing a comparison of the two granite interpretation modes. The overlap (applying  $\pm 2$ km projections) are highlighted (purple boxes) with the seismic granite interpretations outlined in red. Crude conformity between modelled granites and seismically-interpreted granite is seen. The misfits suggests the degree of 'fuzziness' ( $\pm 1-2$ km) with which the *V<sub>pmg</sub>* inversion-modelled granite morphologies at depth should be handled.



**Figure 4.29** DMQ Solid Geology showing locations of projected Seismic Line coincidence with DMQ Sectional Interpretations.

DMQ seismic interpretations overlay on the immediately adjacent serial section for 5 sections where granite was intersected by the seismic lines. It should be remembered that these inversion granite models have a significant margin of error and are indicative only given the geological constraints placed upon the modelling. In the seismic interpretation comparison sections it should be noted that projections up to 2km from the seismic line will be present. The complete seismic section interpretations were presented in Figures 4.2 to 4.4. The portions that coincide with the sectional interpretations (where granite is present; purple dashed boxes, Figures 4.28 & 4.29) are highlighted on each of the comparative sections.

Despite the above issues, the comparisons are not too shabby and offer some degree of reassurance that the geologically-constrained inversion modelling has produced geologically-reasonable granite morphologies at depth. The degree of misfit between the modelled and seismic-interpreted granites is some indication of the fuzziness with which the inversion modelling should be handled. It clearly does not represent a prospect-scale rendition of granite morphology.

## Prospectivity for additional Cloncurry-style Cu-Au Deposits

### Geological Criteria Determining Prospectivity

To form the variety of deposit styles that are present within the Cloncurry Cu-Au belt, process parameters at two contrasting scales are believed to be essential.

At a regional scale, prospectivity is empirically linked with contacts (both structural and stratigraphic) between carbonate lithologies (Staveley & Corella Formations) and other (often reduced) packages (Kuridala Group, Answer Slate, Toole Creek Formation), as illustrated on Figure 5.1. Asymmetric buffering will be applied to these contacts (Figure 5.2).

At the camp scale, broadly-coherent structural brecciation processes of brittle hosts focusses fluid flux and mineral deposition. Different camps are characterised by different structural-kinematic (-lithological) controls making regional scale, fault architecture, structural-kinematic prediction ineffectual. A brittle host of sizeable continuity and depth connectivity is essential to produce significant permeability.

The interpreted most essential ingredient in Cloncurry Cu-Au deposit formation is the delivery of high-temperature Cu-Au-Mo - bearing brine. Interpretations developed as part of the DMQ project suggest a spatial relationship

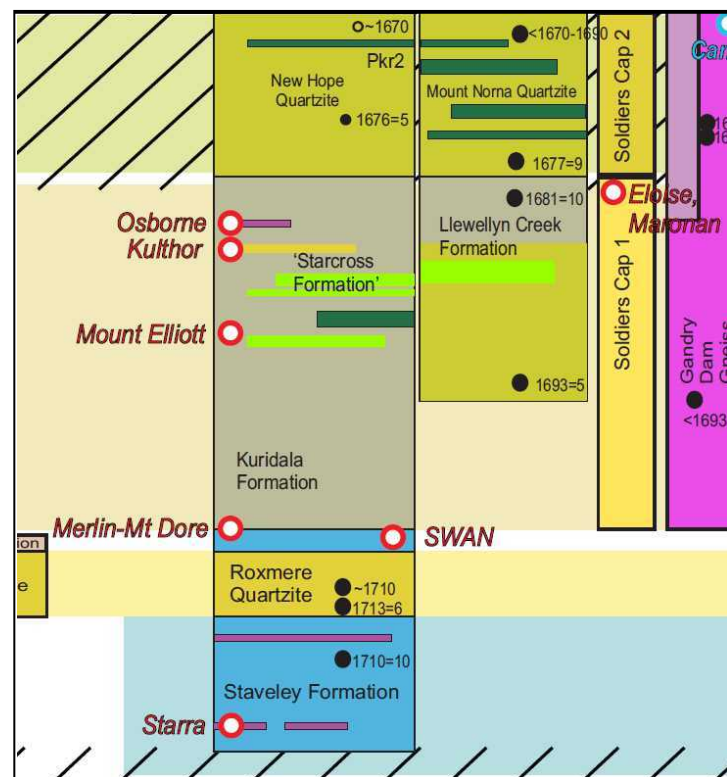


Figure 5.1 Excerpt of the Time-Space Chart (Figure 3.5) showing deposit localities relative to stratigraphy.

between Williams-age intrusion morphology, high temperature brine circulation and Cu-Au-Mo deposits and occurrences. Tracts along steep granite sidewalls, above granite shoulders at depth, and above tight apophyses at depth are considered prospective and will be buffered for targeting purposes (Figure 5.3).

### DMQ Project: Recognized Deposit Styles

As noted in previous DMQ reports, there is significant variability in the Cu-Au deposit style within the DMQ project area, and IOCG/ISCG deposits in general.

Regardless of differences in deposit-scale specific form/geometry, host-rock, sulphide-tenor, and FeO association; common to each deposit is the relative timing, favourable stratigraphic package comprising brittle host-rocks, and proximity to steeper gradients in granite-geometry/edges (Figure 5.1).

### Deposits Hosted Within the Upper Staveley/Lower Kuridala Stratigraphy.

- Rheological contrast between Calc-silicates, Roxmere Quartzite, and Kuridala schists seen as a focus for deformation and exploited during mineralization in late D3.
- 'Other' rigid bodies at this stratigraphic position, e.g. SWAN Diorite, offer further rheological contrast and focusses brecciation/secondary permeability and potential to host mineralization if within a fluid cell.
- Redox potential of Staveley in contact with overlying reduced rocks (Figure 5.2) inferred as an important ingredient.
- Presence of ironstones yields discrete targets within this broader stratigraphic package.
- Includes the Osborne-Kulthor, Mt Elliott-SWAN, and Merlin-Mt Dore deposits.

### Structural juxtaposition of Staveley with Other (Reduced) Packages.

- Not restricted to the upper Staveley prospective stratigraphy (Figure 5.2).
- Likely to be evidently structurally-controlled/

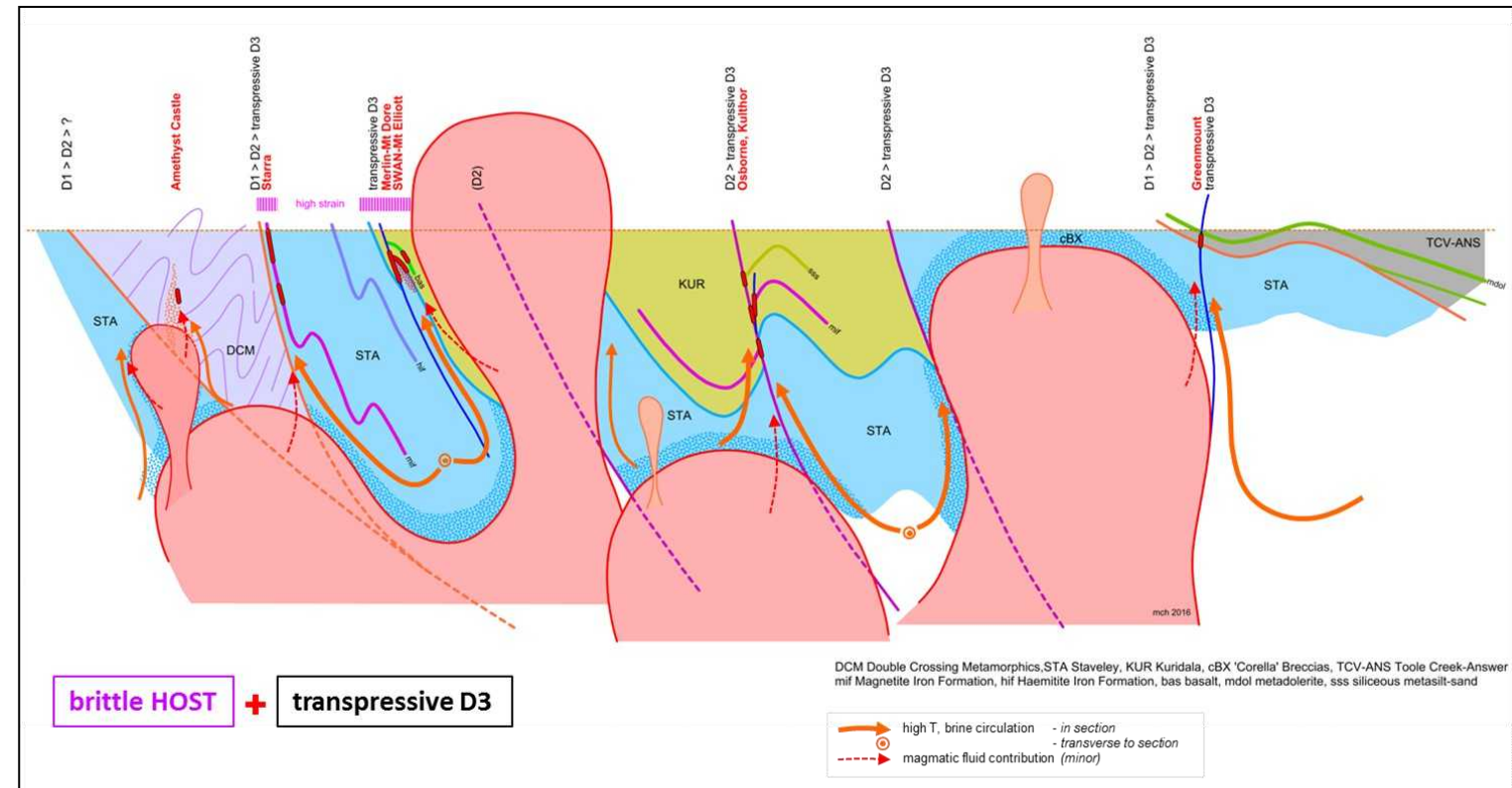


Figure 5.2 Schematic cross-section illustrating inferred controls on deposit styles in the DMQ project area. Essential ingredients required for each of the identified deposit styles. Orange arrows represent high temperature brine circulation, red arrow represent magmatic fluid contribution.

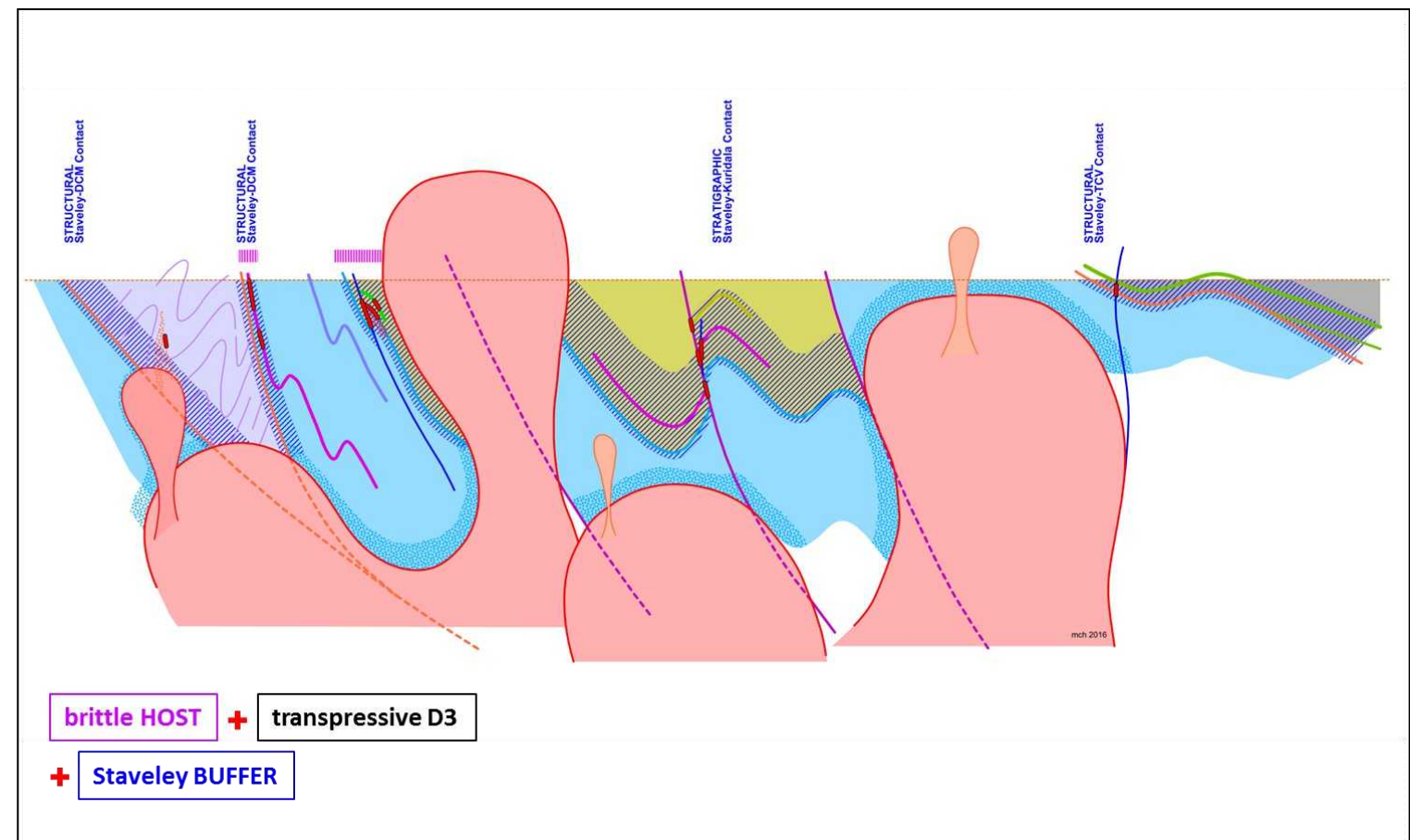
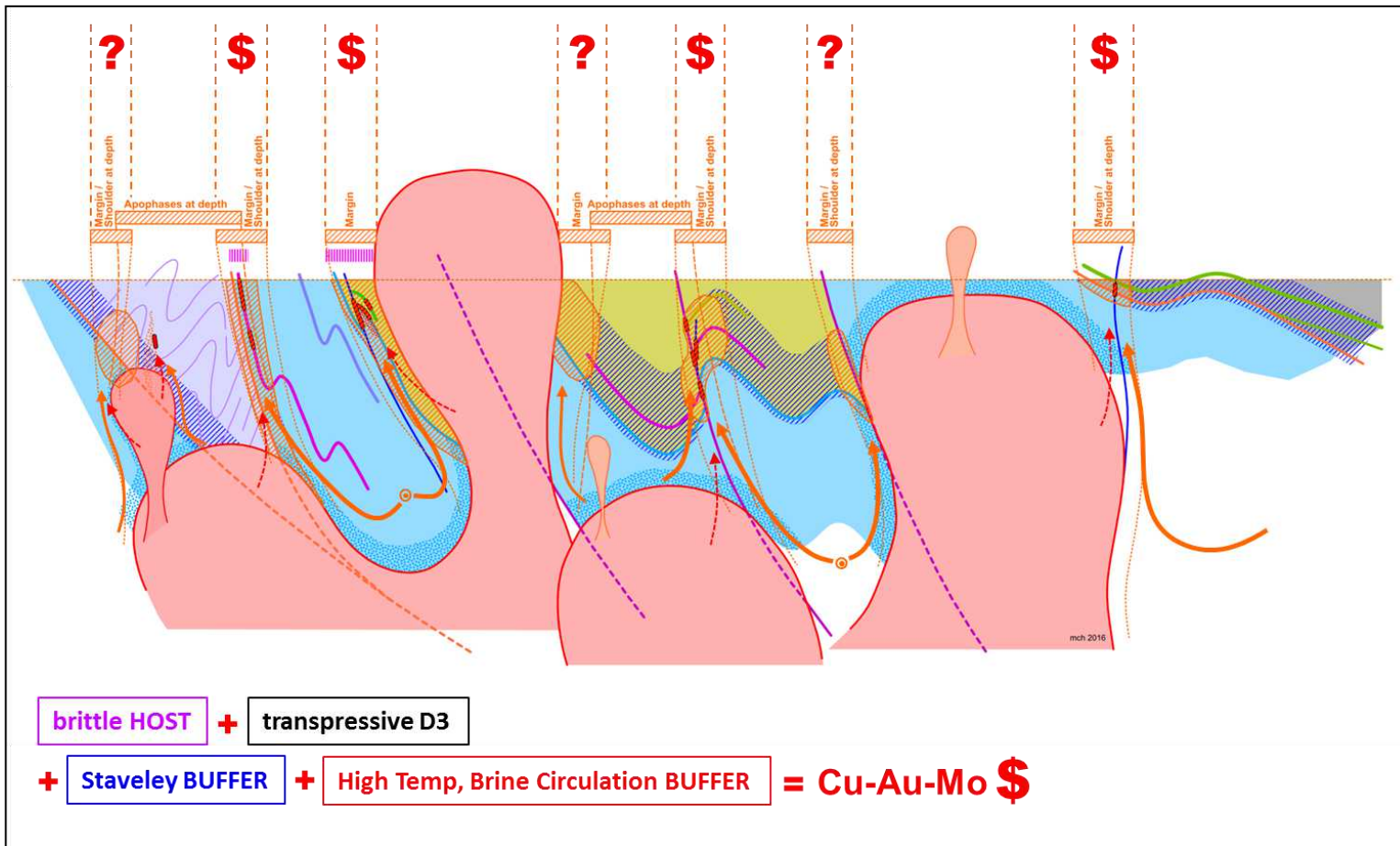


Figure 5.3 Schematic cross-section illustrating the asymmetric buffer around the upper Staveley stratigraphic contact, and buffering of structural juxtaposition of Staveley against other stratigraphy. These buffer zones conceptually encompass the bulk of deposit locations in the belt.



**Figure 5.4 Schematic cross-section illustrating buffers specific to the role of granite morphology in convective focussing of fluid into favourable litho-structural sites. Granite morphology is considered critical in driving convective fluid movement, and as such, will determine prospective corridors**

hosted.

- Greater potential expected where Staveley is in structural contact with reduced packages such as Answer Slate/ Toole Creek Formation.
- Focussing relationship of early structural features, likely reactivated basement structures.
- Includes the Starra line of deposits.

*Deposits hosted in Overlying Sequences, but Related to Staveley:Granite:Fault Association at Depth.*

- Highly variable deposit-style possible.
- Deposits may be structurally-focussed or within broader breccia bodies.
- Intrusion of granite into the Staveley calcareous sequence inferred as driver for brecciation (CO<sub>2</sub> release). Marshall (2003) interpreted brecciation in the Cloncurry district as related to magmatic-hydrothermal implosion brecciation, gas-streaming, and

fault-jog brecciation. The DMQ interpretation is a variant of this whereby granite intrusions whose top is within Staveley rocks, may cause sufficient gas release to promote brecciation of overlying sequences. These breccia zones, and discrete faults, will not all be mineralized, unless located within the favourable convective cell driven by subsurface granite geometry (Figure 5.3).

- This type of deposit may include Eloise (hosted in Toole Creek Formation) situated well above interpreted Staveley position and in a very discrete structural setting; and the Amethyst Castle prospect in the Gin Creek Inlier, interpreted as a large-scale CO<sub>2</sub> release breccia related to granite intrusion into Staveley formation at depth, and the Ernest Henry deposit located proximal to interpreted subsurface granite margins and within an enigmatic structural position (see Chapter 3).

The range of deposit-styles embodied in the three 'classes' above is manifest in the variability of known deposits and prospects in the Cloncurry district. No two mining-fields in

the Cloncurry Cu-Au district are the same, a function of the inherent structural control on mineralization and multiple suitable host-rocks.

### 3D Representation of Prospectivity Inputs through Buffering

Buffering, in this instance, refers to volume creation around a 3D stratigraphic or structural surface, or other volumetric domains of significance (proximity to granite margins).

The schematic sections in Figure 5.3 and 5.4 indicate the concept of building buffers around the Staveley-Kuridala stratigraphic boundary, major faults as fluid focussing macro-permeability zones, and the inferred influence of granite margins. Orange polygons in Figure 5.4 represent the conceptual resultant target domains through this process of intersection of additive volumetric models.

#### Intrusive Buffer

Observations that mineral occurrences and deposits were located proximal to inferred granite margins (see Chapter 3) as defined by steep gradients in the apparent density data, indicated that capturing a 3D volume associated with steep edges and margins would be an important inclusion in a prospectivity equation. A 3D volume for the interpreted felsic intrusions has been constructed and is shown in Figure 5.5.

Buffering of the granite bodies so as to capture the inferred upwelling of fluid associated with convection at/ above margins/shelves/apophyses has been approximated by applying a vertically extended buffer where the dip of granite surface exceeds a threshold.

Those areas of the 3D intrusive geometry where dip is greater than 50° have been highlighted in Figure 5.6, and are converted into an anisotropic 3D buffer volume by application of an elliptical search volume, with greater vertical extent than horizontal (Figure 5.7). The buffer incorporates a 4km:1km height to diameter aspect ratio (Figure 5.7).

#### Stratigraphic Buffer

For the purposes of 3D prospectivity analysis, only the 'Top of Staveley Formation' (Figure 5.8) is utilised in the buffering (Figure 5.9) and target generating exercise. As shown in Figure 5.1, and incorporated into the schematic diagrams 5.2 - 5.4, the Staveley-Kuridala contact zone is

captured as the preferential host-sequence by an asymmetrical buffer which includes the top of the Staveley Formation (300m) and well into the Kuridala Formation (1500m). The asymmetry of the buffer captures the bulk of known deposits in the project area.

#### Structural Buffer

3D representation of the respective deformation events, and major structures formed during each, has seen construction of surfaces honouring, where possible, cross-cutting relationships with other structural elements, stratigraphy and intrusives. These are illustrated in Figure 5.10. Other structural features representing inferred basement faults, reactivated during later deformation; and younger faults which cross-cut the granite intrusives are also captured, but not displayed below.

A buffer is applied to modelled faults that pre-date D4 (interpreted timing of Cu-Au mineralization). This is not indicating that all faults of a certain age are mineralized, but identifies domains within which smaller-scale faults may occur, which influence sites of Cu-Au mineralization. Often, D3 faults are short strike-length and have small displacements, rendering these difficult to interpret outside of areas of intensive mapping (mines) or areas with little cover that have had detailed magnetics acquired.

It is interpreted that the later faulting is initiated on, and propagates from earlier major fault networks, and as such the D1-D2 fault system underpins this element of the prospectivity analysis. It is intended that the buffers on the earlier faults capture the likely domain within which younger daughter faults will be located.

For the purposes of prospectivity analysis, any structures pre-syn- early-D4 have the potential to focus fluid/ mineralization dependent on their location with respect to granite geometry and favourable host-rocks. Late-D4 faults include the Cloncurry Fault system (Figure 5.10) which cross-cut the granite bodies and are considered largely post-mineralization. The early, D1 thrust spatially proximal to the Cloncurry Fault in the northern part of the project area is included in the prospectivity analysis.

### Prospectivity Analysis Workflows

#### Prospectivity for Deposits Hosted Within the Upper Staveley/Lower Kuridala Stratigraphy.

The identification of additional Staveley contact zone style targets requires intersection of the intrusive buffer (Figure

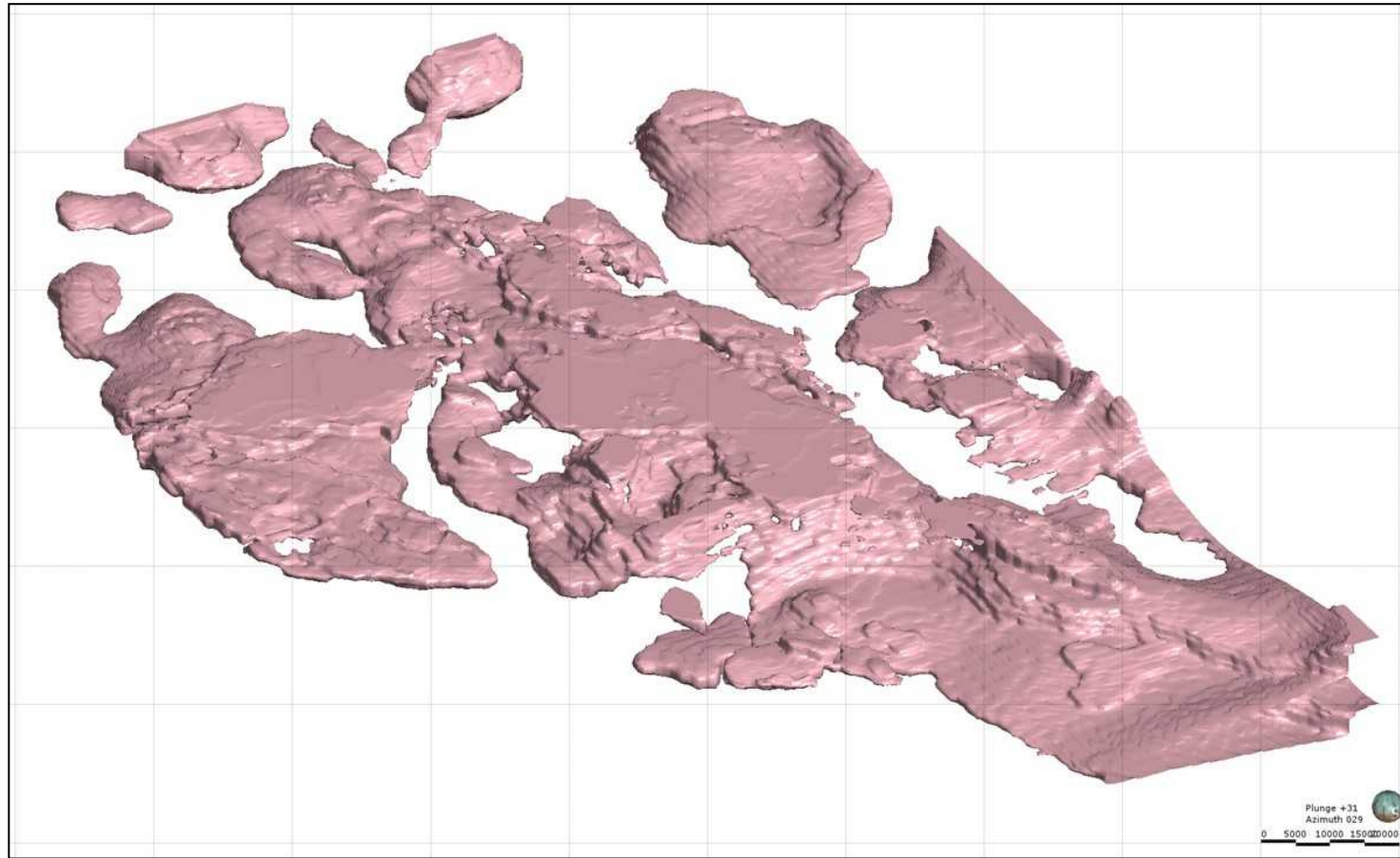


Figure 5.5 3D view of the Williams-age felsic intrusions in the study area, as determined through geologically-constrained gravity inversion. Looking northeast.

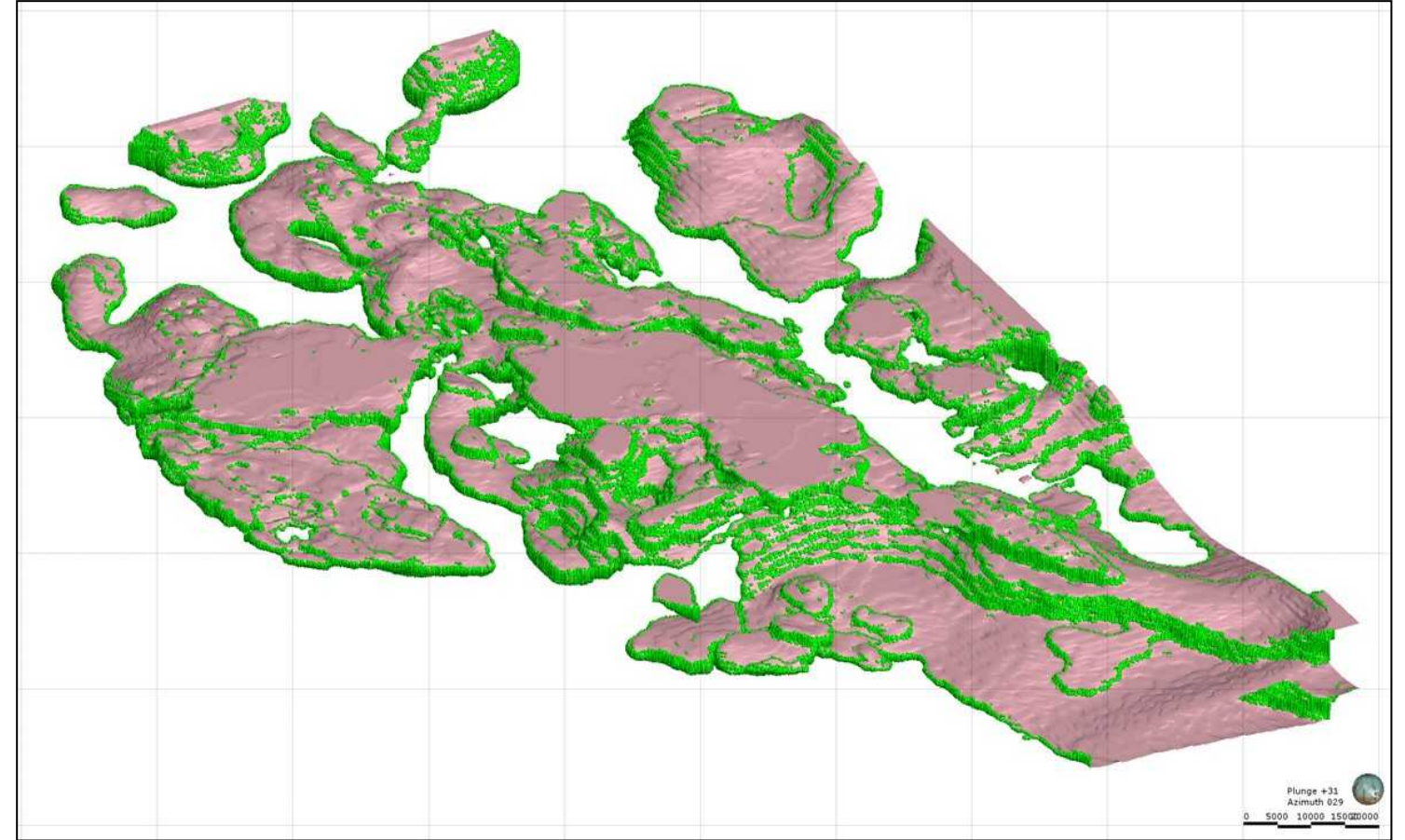


Figure 5.6 Edges of intrusive bodies with higher dip (>50°) identified in green.

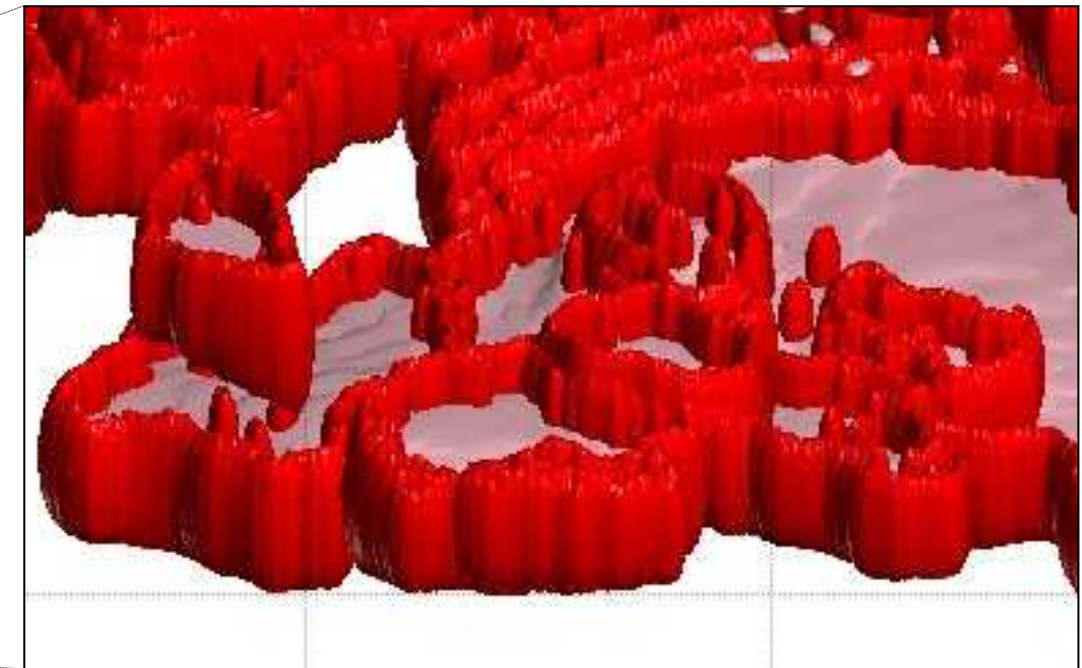
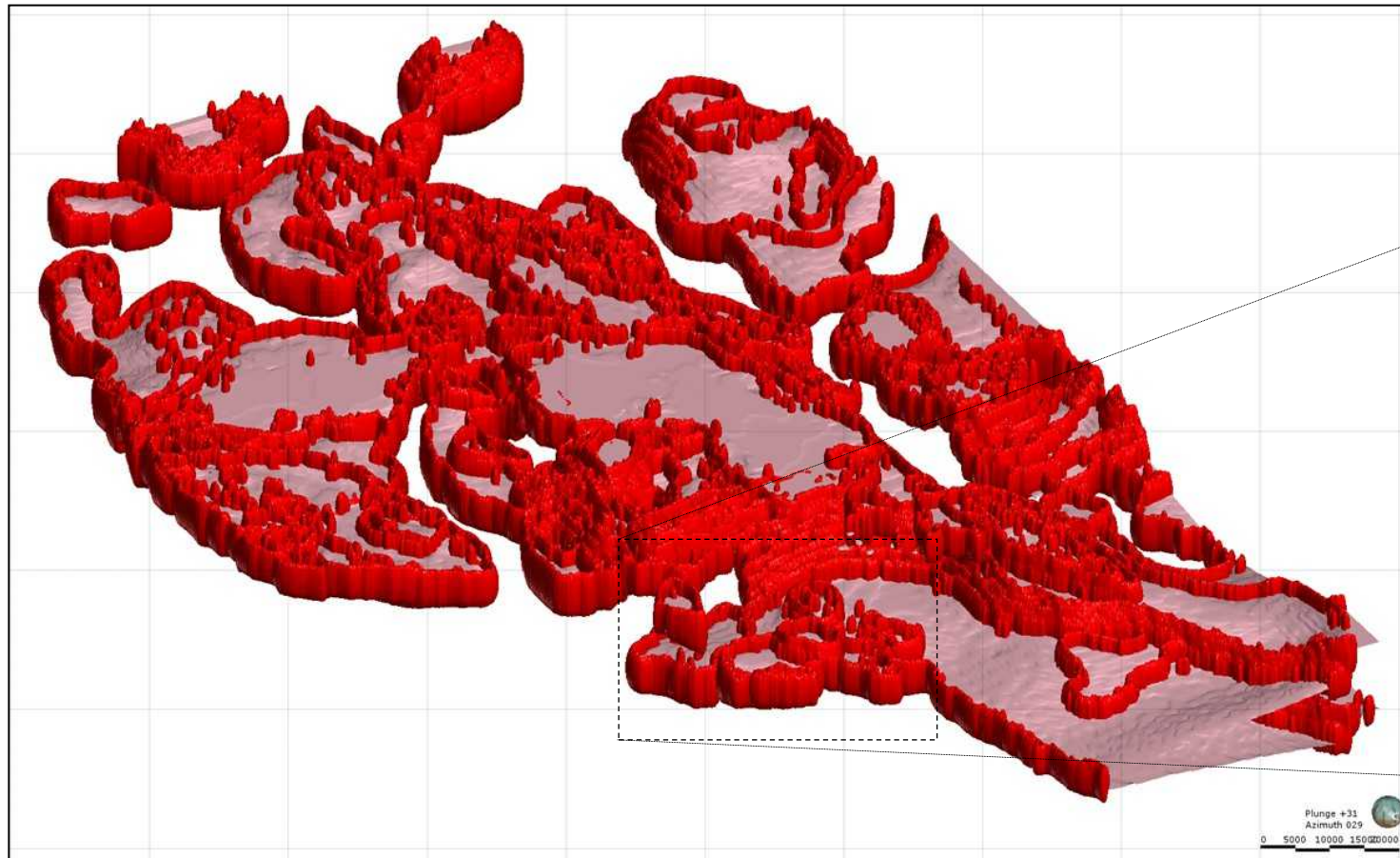


Figure 5.7 Anisotropic buffer applied to the 3D felsic intrusive geometry. Inset enlarged image highlights the elliptical search volume applied to edges identified in Figure 5.6.

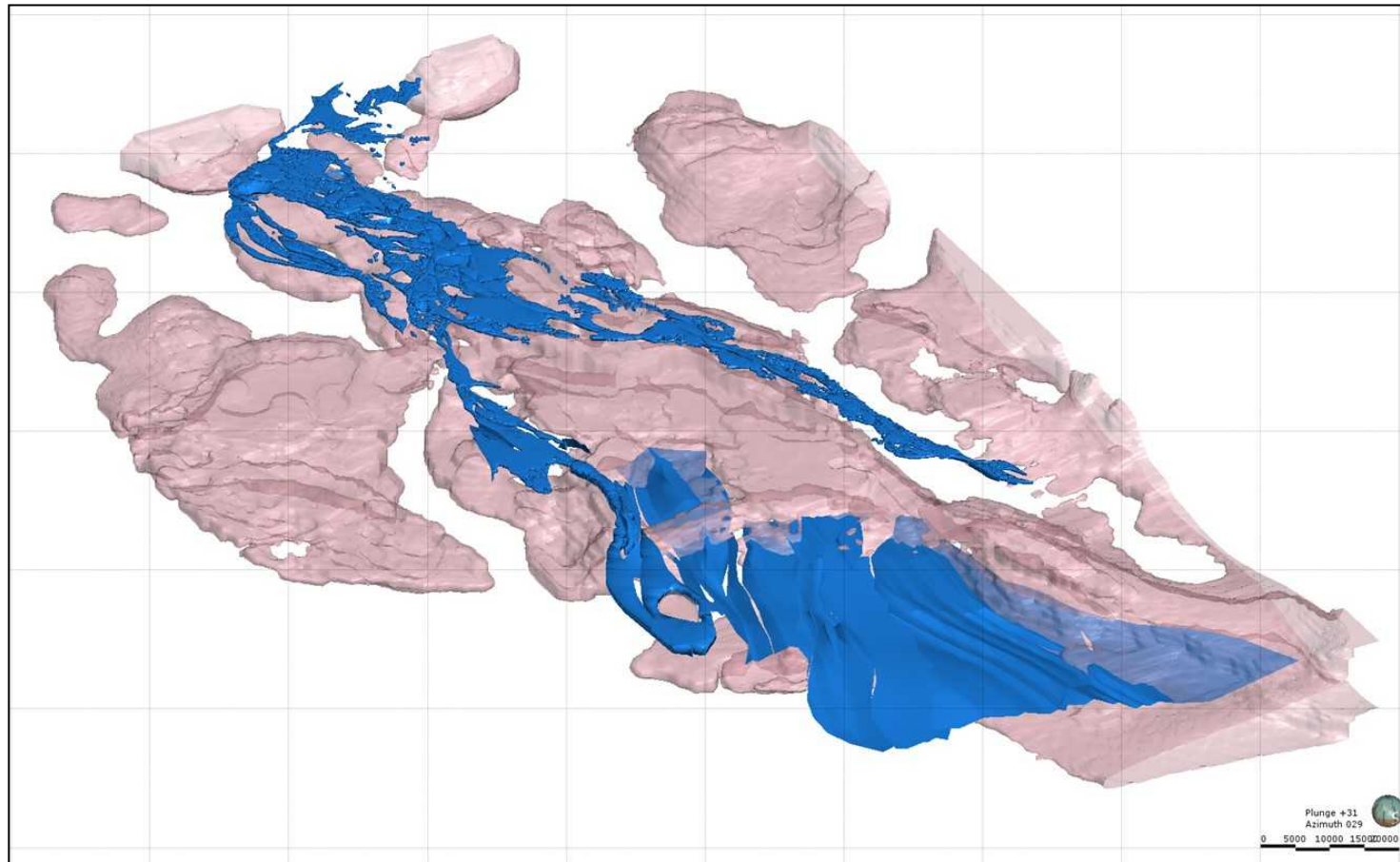


Figure 5.8 Top of Staveley Formation stratigraphic surface (blue) in bottom right hand corner of image (south), and outcropping Staveley Formation and equivalents represented by blue solid in the top left of image (north).

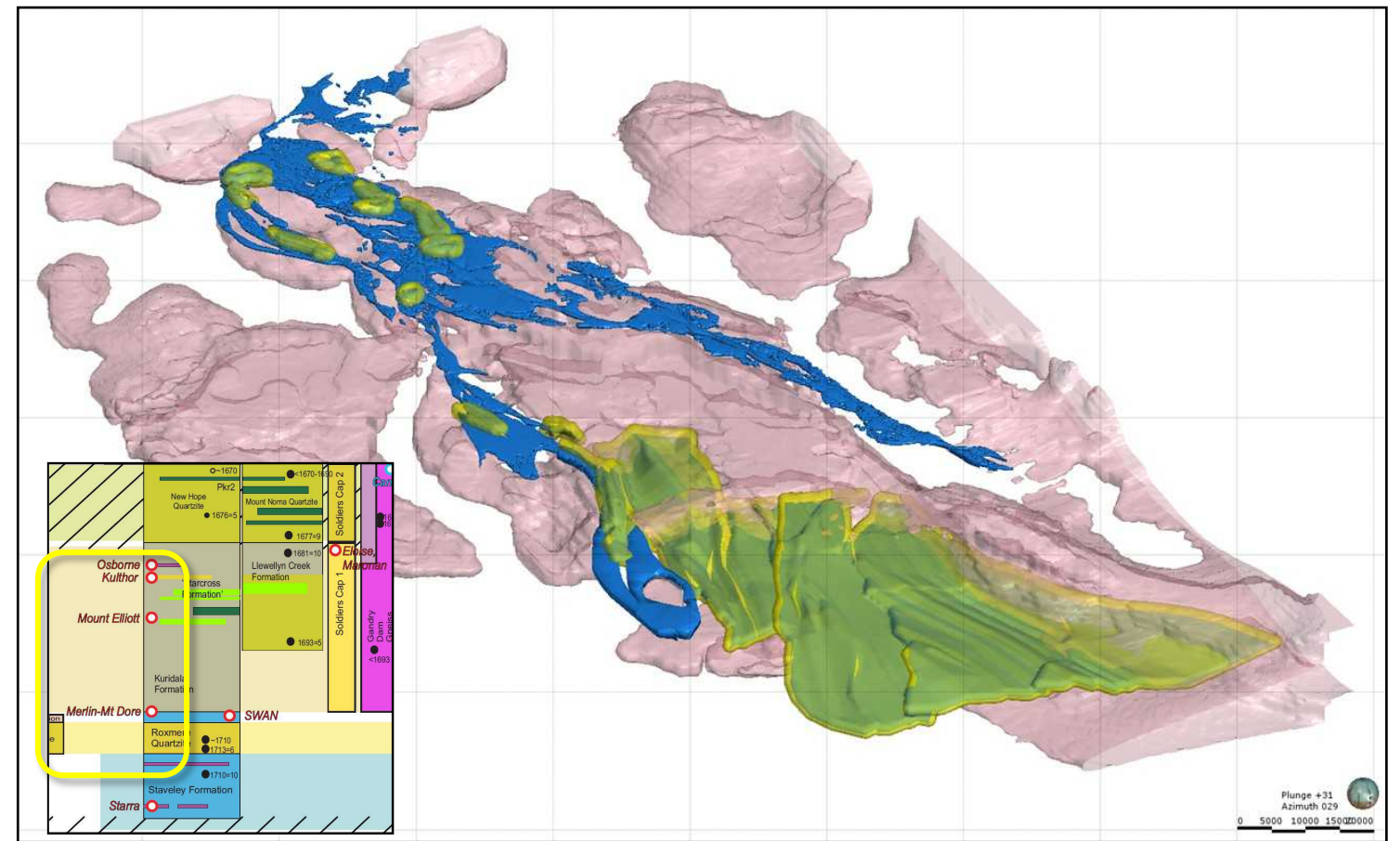


Figure 5.9 Asymmetric buffering (yellow) of the Top of Staveley Formation stratigraphic surface (-300m/+1500m).

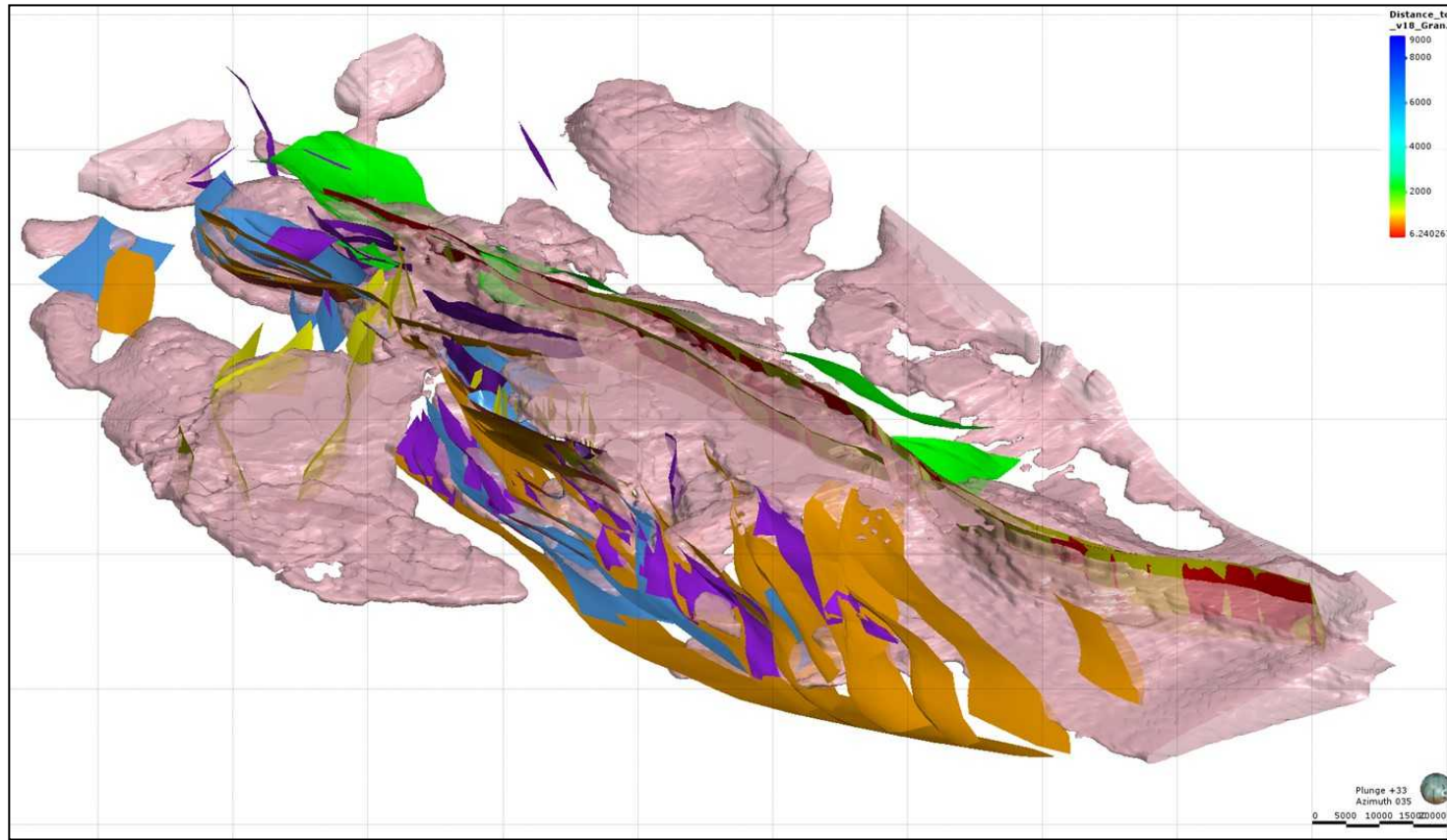


Figure 5.10 Modelled faults displayed as coloured surfaces. D1 faults: blue, D2 faults: orange, D3 faults: navy, early-D4 faults: purple, late-D4 faults: red/yellow.

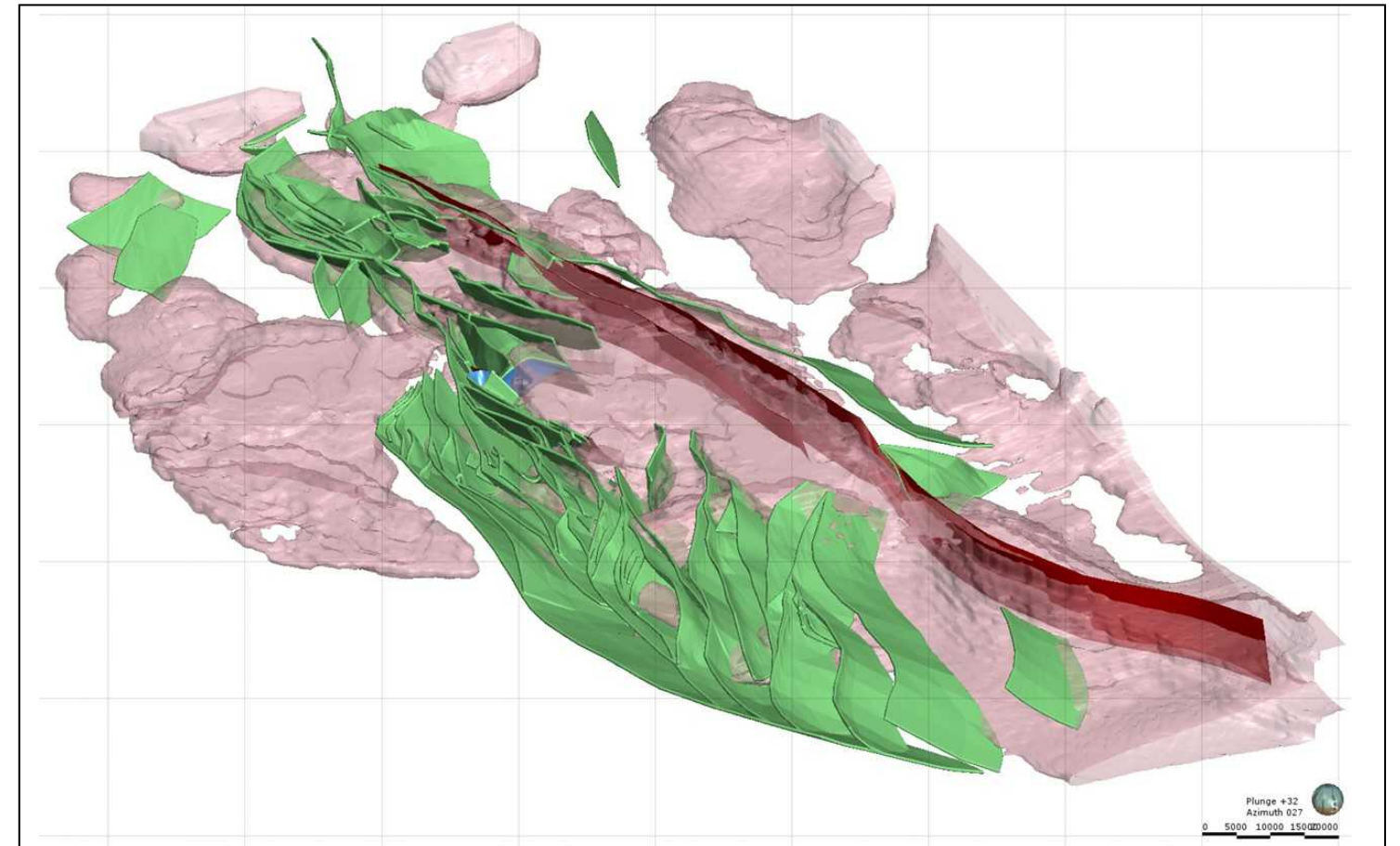


Figure 5.11 Buffered faults (green) where interpreted to predate the latter stages of D4. The green buffer is  $\pm 250\text{m}$  each side of the modelled faults illustrated in Figure 5.10.

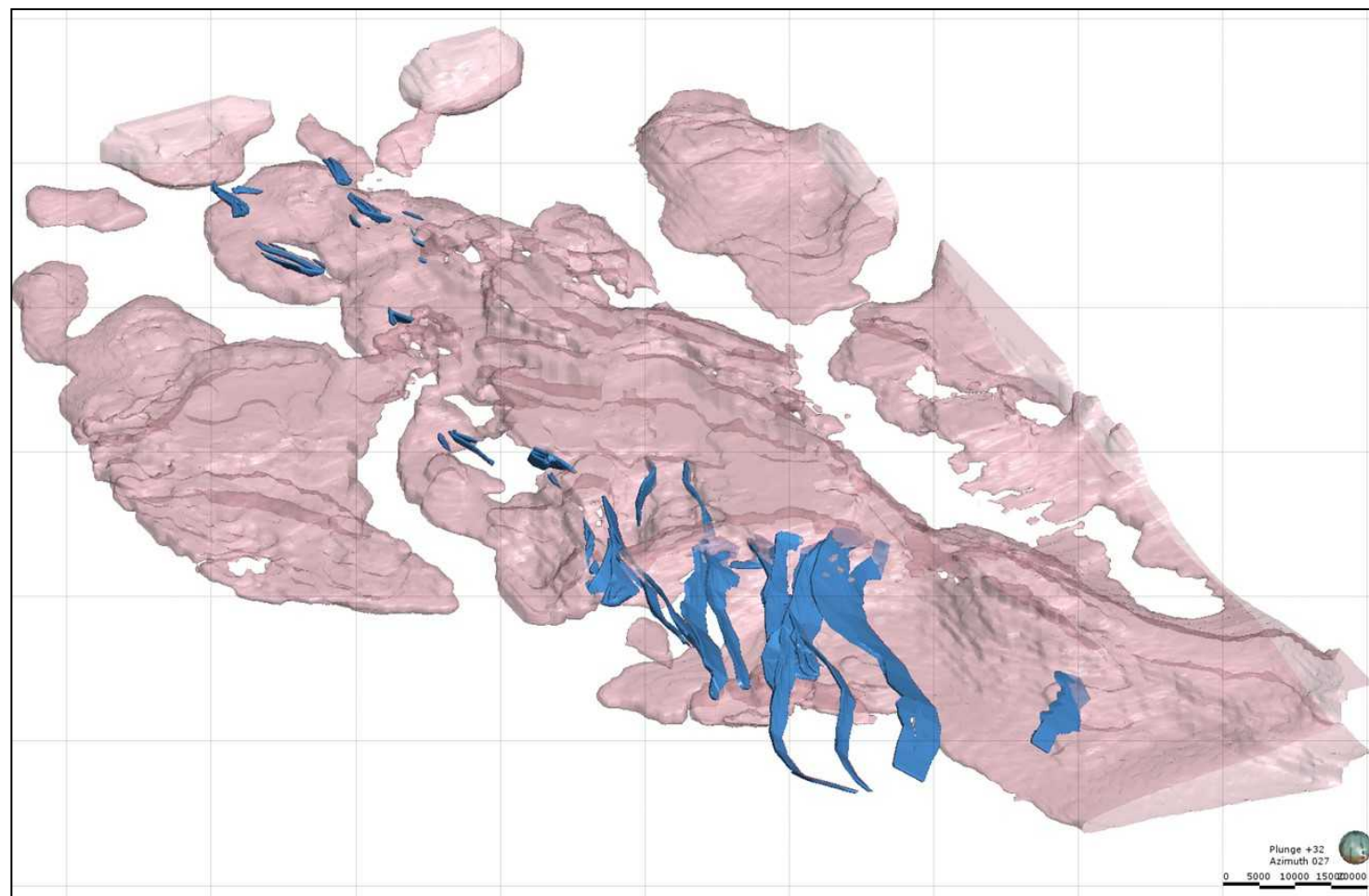


Figure 5.12 Resultant volumes after intersection of structural and stratigraphic buffer domains.

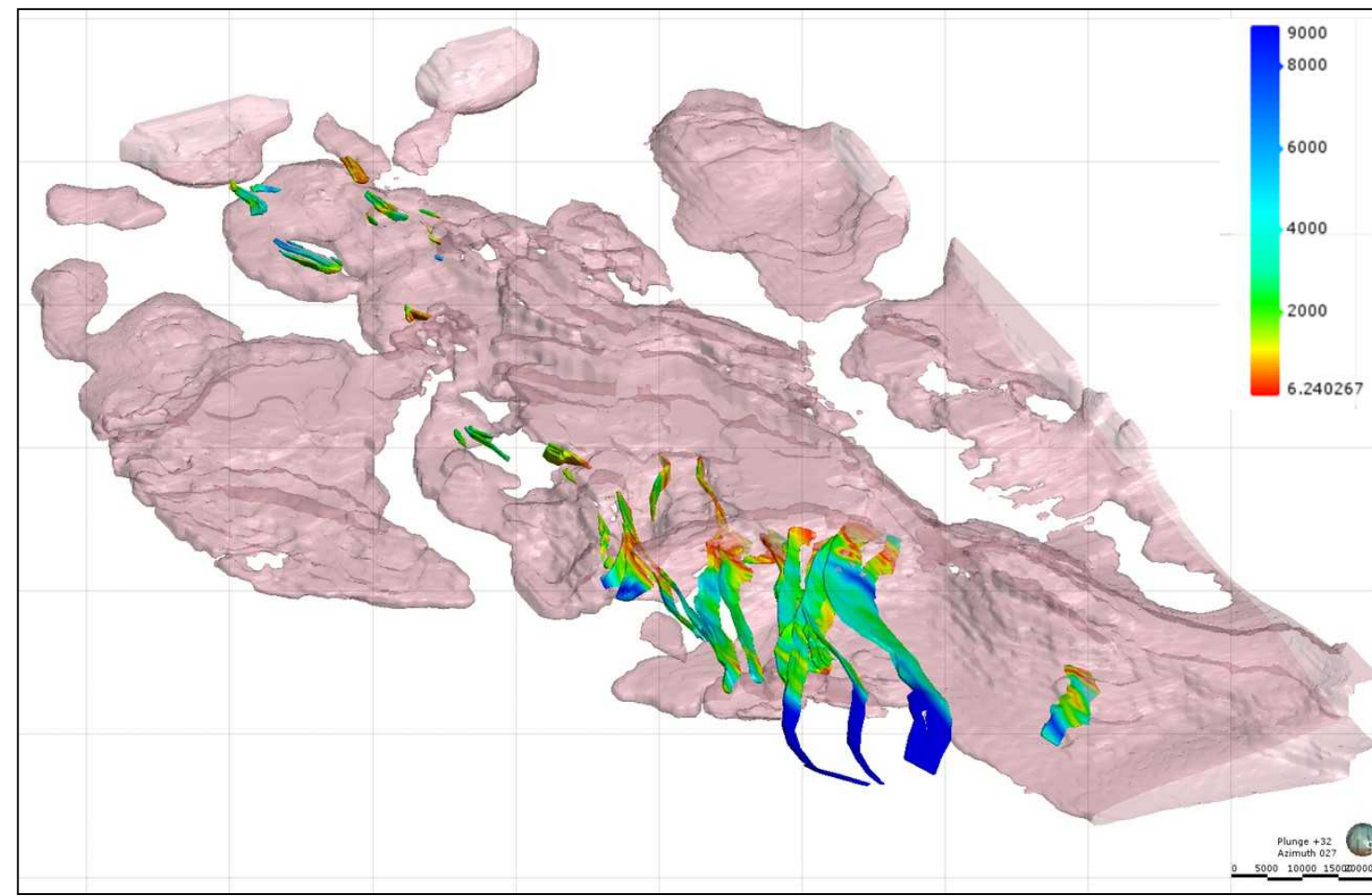


Figure 5.13 As per Figure 5.12, but coloured by proximity to intrusive buffer zones (as per legend).

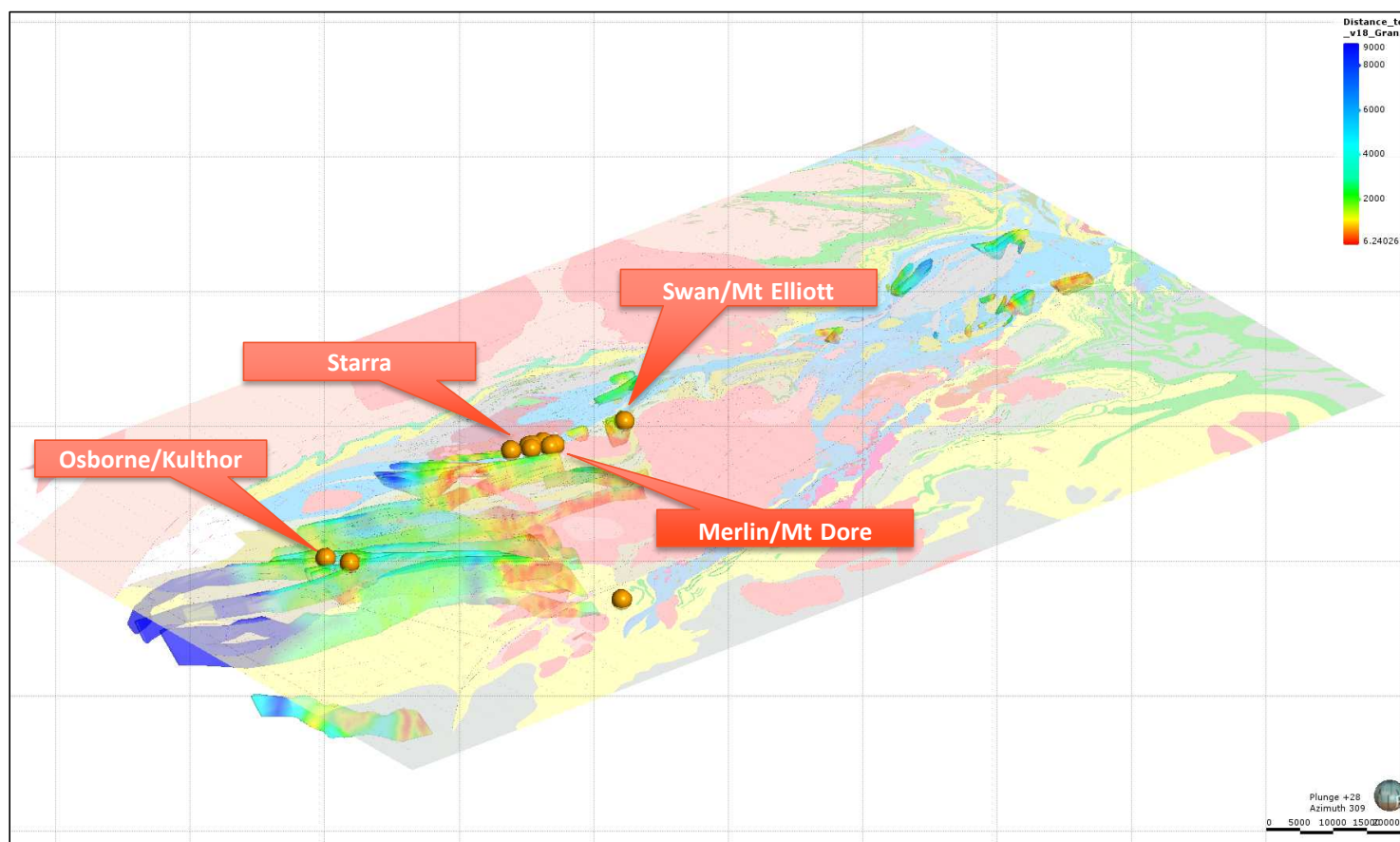


Figure 5.14 Location of significant deposits and mines relative to the inferred areas of enhanced prospectivity for Mt Dore-SWAN style mineralization.

5.7), Staveley-Kuridala buffer (Figure 5.9), structural buffer (Figure 5.11).

The resulting intersection as illustrated on Figure 5.12 and coloured by proximity to intrusive margins (Figure 5.13) and represents localities of enhanced prospectivity for Mt Elliott-SWAN and Merlin-Mt Dore deposits.

### *Prospectivity for Structural Juxtaposition of Staveley with Other (Reduced) Packages.*

Identification of additional Starra-style targets is determined by intersection of the intrusive buffer (Figure 5.7), Staveley solid volume (Figure 5.8) and the structural buffer (Figure 5.11). The intersection and prospective tracts are illustrated in Figure 5.15.

The structural juxtaposition with reduced rocks is preferred.

### *Prospectivity for Deposits Hosted in Overlying Sequences, but Related to Staveley:Granite:Fault Association at Depth.*

While these deposits may be captured in the Staveley buffer targeting, expansion of the area influenced by the effect of intrusive margins may indicate prospective zones in disparate stratigraphy such as Toole Creek Formation (e.g. Eloise) and Mt Fort Constantine Volcanics (e.g. Ernest Henry).

To capture the prospective areas for this style of mineralization, the structural buffer was queried for those regions above the Staveley buffer. These volumes were then coloured to represent proximity to intrusive margins as illustrated in Figure 5.16.

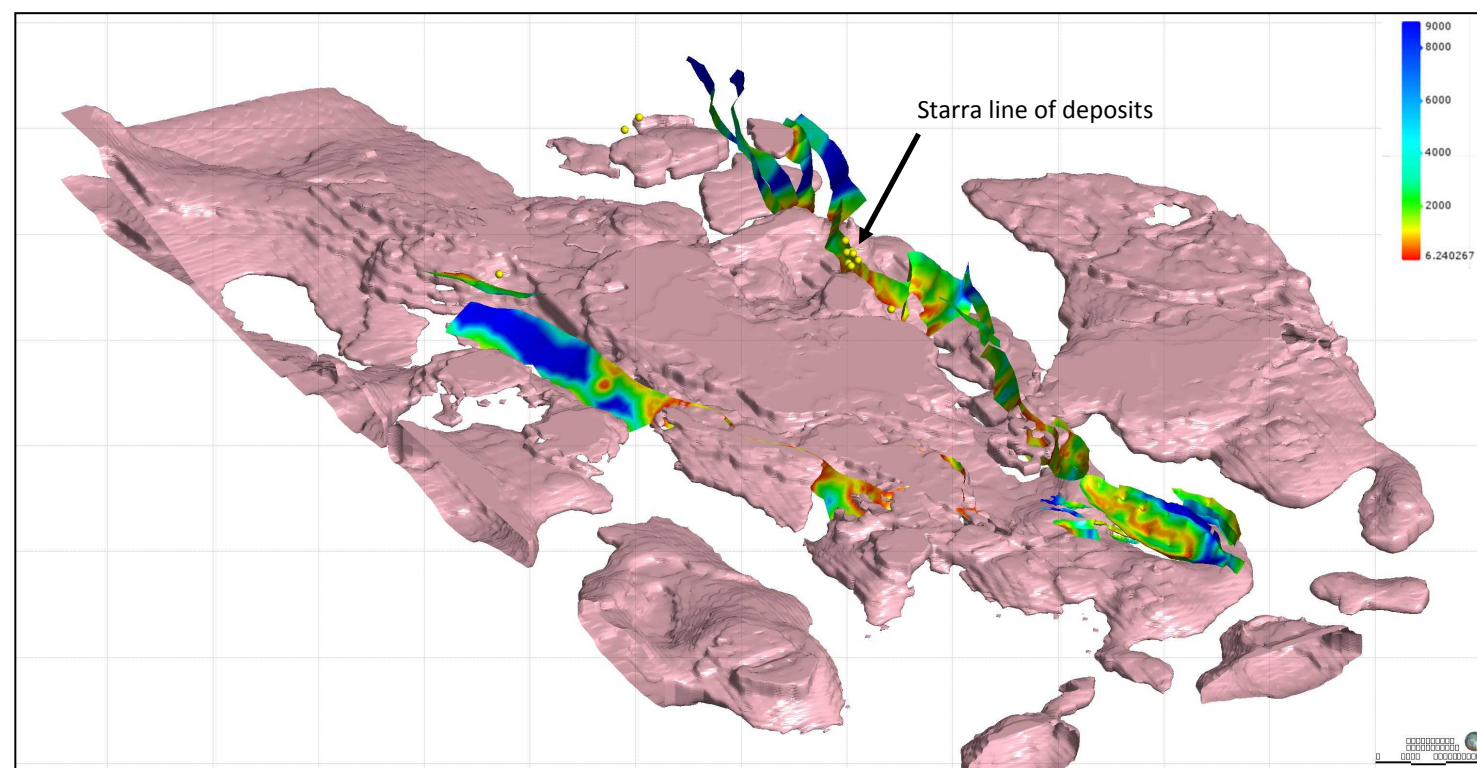


Figure 5.15 Staveley Structural juxtaposition targets coloured by granite edge proximity, looking SW.

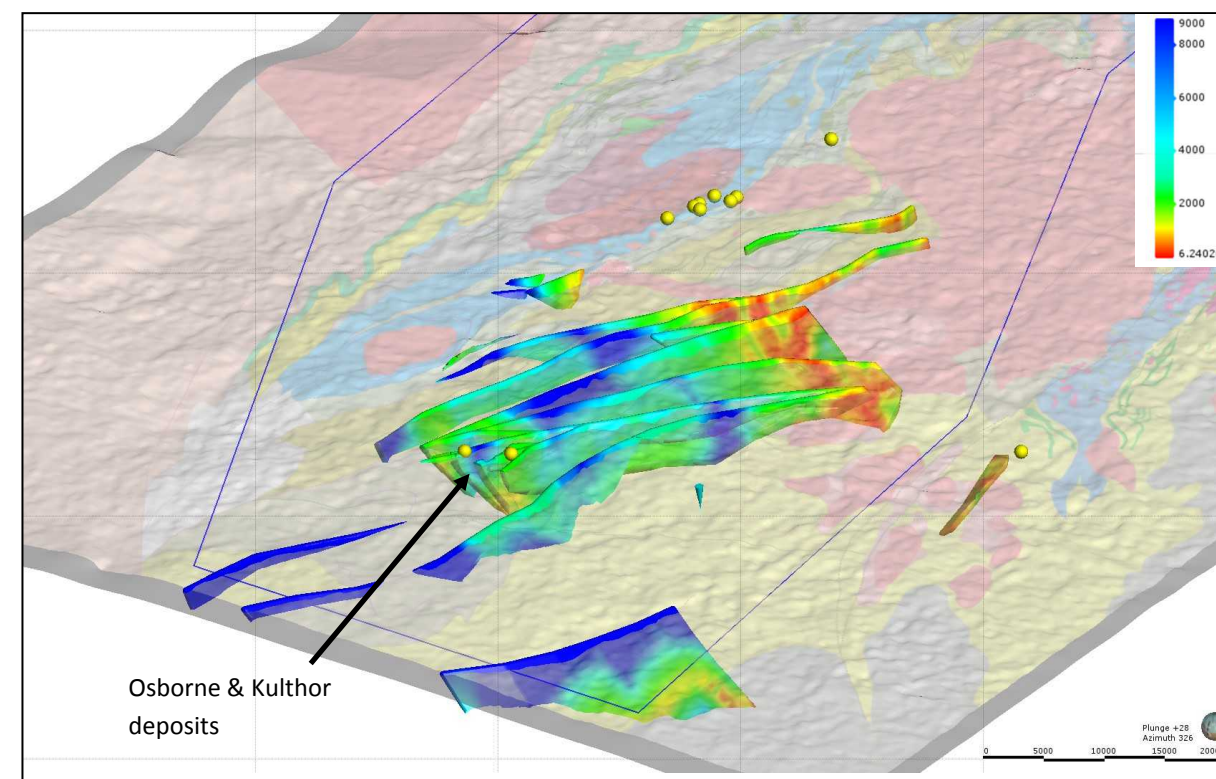


Figure 5.16 Higher stratigraphy targets—structurally focussed prospective zones above the Staveley buffer, looking NW.

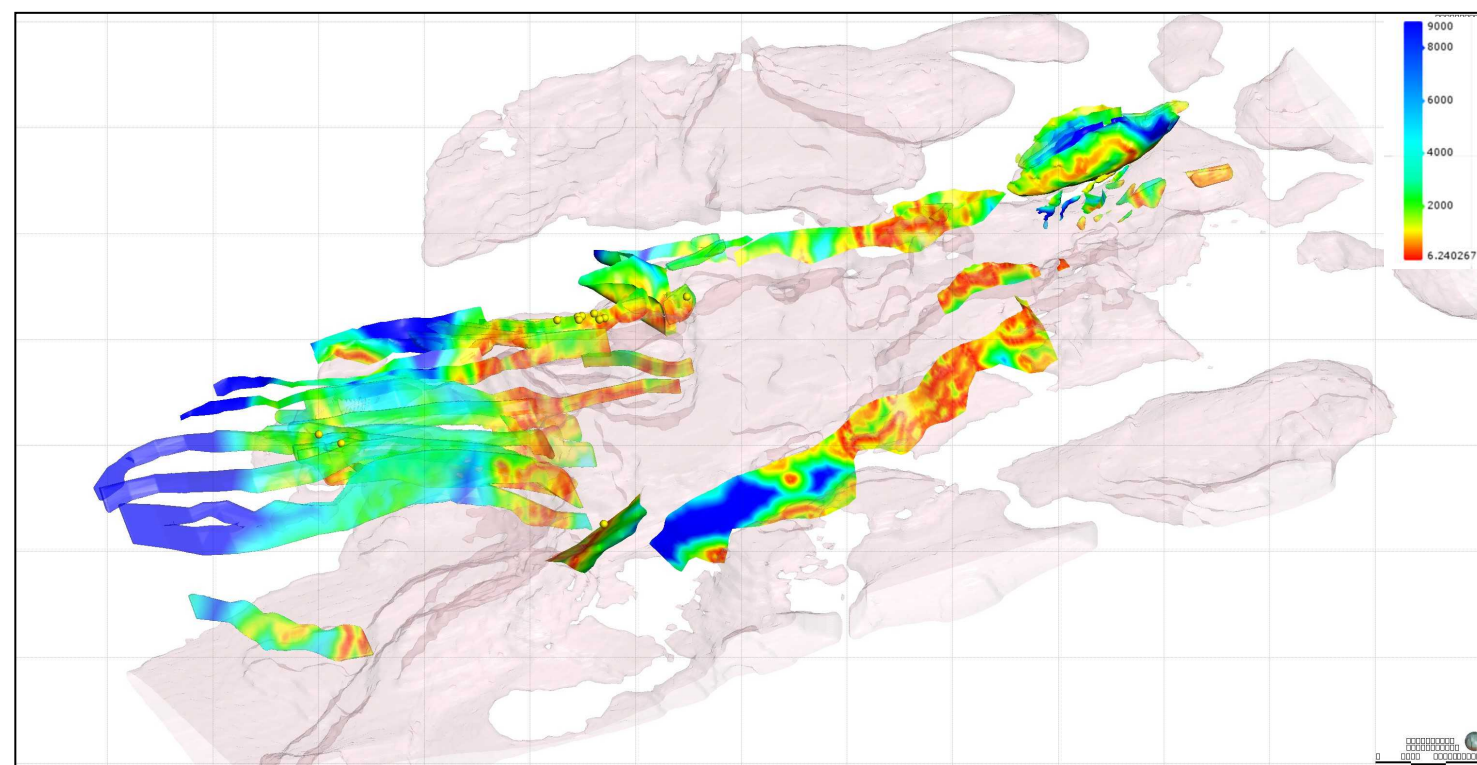


Figure 5.17 Combined Starra-type structural juxtaposition and Mt Dore-SWAN style prospective zones, looking WNW.

## Synthesis of 3D Prospectivity in the Southern Cloncurry Cu-Au district.

Use of 3D geological surfaces, buffered to produce volumes, has enabled delineation of domains of enhanced prospectivity for the three defined mineralization styles. The input criteria for these deposit-styles has been determined through geological investigation of deposit controls, from the district-scale to the ore-shoot scale. Given that the known mineral deposits were used to inform the process, the resultant prospectivity models identify the known deposits and mines as having enhanced 'prospectivity'. This confirms that the spatial inputs into the prospectivity analysis (structure, stratigraphy, intrusives) have an appropriate resolution and accuracy, where sufficient data is present.

The 3D prospectivity process identifies prospective domains, in addition to known deposits, for each of the deposit-styles in question. Significant additional prospectivity is recognised (Figure 5.17). Collation of prospective domains by deposit-type (Figure 5.18) reveals the distribution of areas of potential for 'Starra-style', 'SWAN/Mt Dore-style', and 'Osborne/Eloise/Ernest Henry-style' deposits.

Note the correlation of the Starra-line of deposits with the structural-juxtaposition targets, SWAN-Mt Elliott spatial correlation with Staveley-buffer domains, and the spatial coincidence of the Osborne and Kulthor mined deposits, with prospective domains for structural focussing above the Staveley buffer.

These 3D models of geology and prospectivity are made available in Appendix 7.

Although the colouring for proximity to granite-margins gives the impression of equal prospectivity, and therefore mining-potential; there are distinctions in mineability of the different deposit-types as determined by their geometry, contained value, and amenability for underground mining. Further evaluation of the delineated prospective domains will be discussed in Chapter 6.

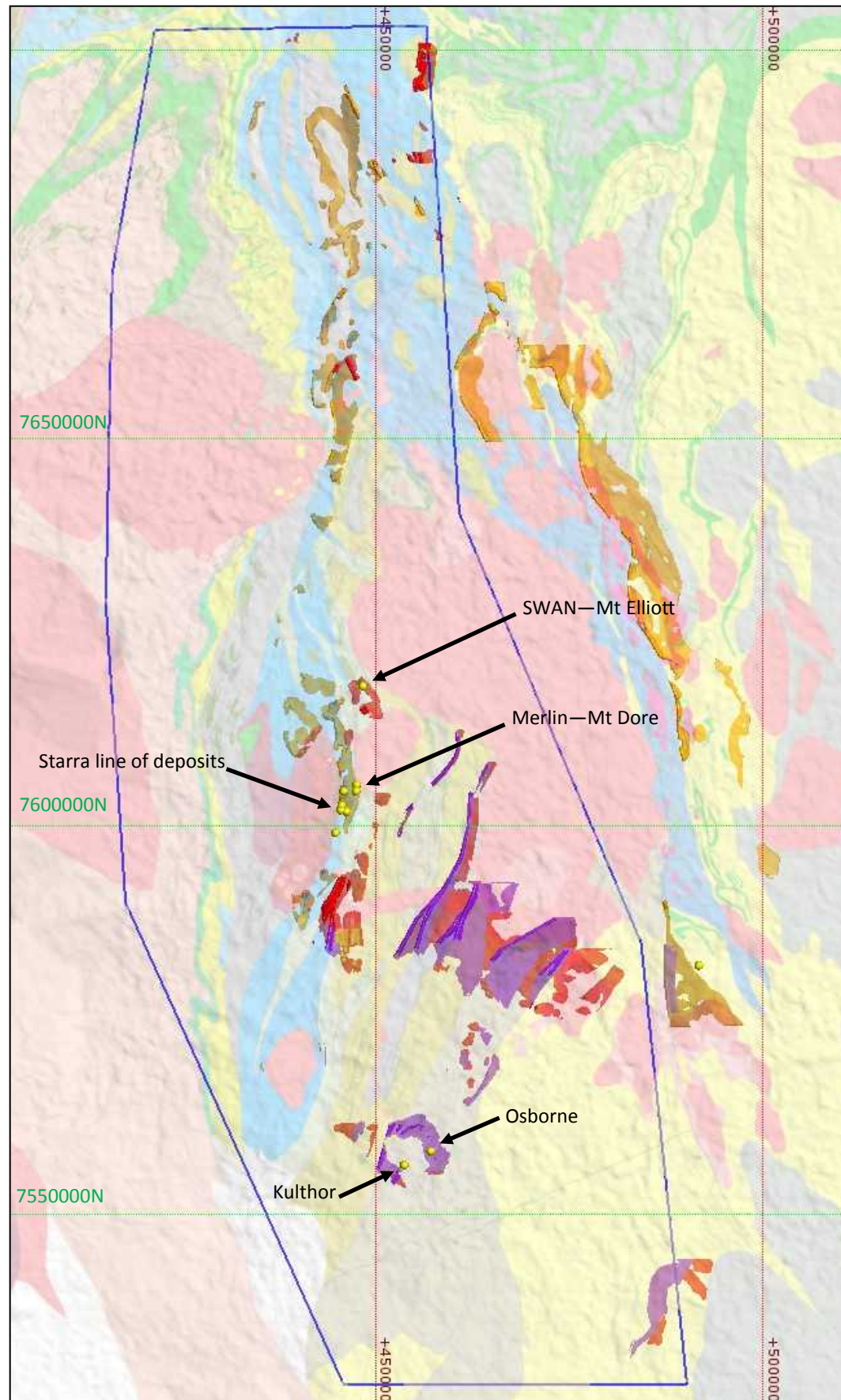


Figure 5.18 Geological map and prospective zones identified in the DMQ project. Staveley (buffer) contact domain targets, or 'SWAN/MT Dore-style' (red); Staveley structural juxtaposition targets, or 'Starra-style' (orange); and deposits structurally focussed above the Staveley buffer, or 'Osborne/Eloise/Ernest Henry-style' (magenta).

## Quantitative Target and Prospect Evaluation

### Introduction

In order to assess for mineability and viability, mining constraints, both technical and cost-related; must be incorporated into measures of prospectivity.

Exploring under significant cover impacts on discovery through higher uncertainty in geological interpretations and higher cost of exploration drilling deeper. Traditional exploration techniques and 'workflows' must be modified for exploring undercover as the usefulness of standard exploration geochemistry practices (e.g. soil sampling, stream-sediment sampling) is diminished.

More reliance on geophysical techniques results but the ambiguity/non-uniqueness of outputs adds to the geological uncertainty.

The approach of the DMQ project in taking geological and context from exposed terrain to covered areas helps to reduce uncertainty but does not reduce the cost associated with deep exploration. Knowing what constitutes a viable target is key to optimising the exploration spend, particularly at depth.

The significant deposits, particularly of the Cu-Au variety, that have progressed to development in the Eastern Fold Belt; are largely constrained in-board of the 100m depth of cover contour as illustrated on Figure 6.1. These mines are predominantly open-cut, progressing to underground operations e.g. Starra mines, Osborne, Ernest Henry. The stripping ratio and/or depth of overburden required to be removed due to cover, is prohibitive at deeper than 100m of cover material. At 100m of barren cover, tonnages of material to be removed are significant, based on existing pit geometries; and determine the size of deposit required to be discovered to warrant removal of significant cover. While the depth of cover at both Osborne and Ernest Henry is in the order of 40-60m, below 100m, it is assumed that underground extraction is the more economically and technically feasible option.

Significant depth to the top of any deep discovery poses both economic and technical challenges. Some aspects of the economic drivers constraining deep exploration and discovery were discussed in Chapter 1. It is well accepted that prospective geology continues under cover off the outcropping Mt Isa Inlier and that discovery and mining has clearly focussed on those parts of the Inlier which are outcropping or under very shallow cover. This both increases the probability of exploration success and economic return of mining at shallow depth. The 500m

depth of cover contour (Figure 6.1) may be an approximate limit to underground mining viability of EFB Cu-Au deposits. Assuming that the only cost-effective means to mine these deposits at depth will be via a lower cost, mass-mining method; technical factors affecting caving operations (see also Murphy et al., 2015) at significant depth (ca. >500m) must be considered, and include:

- Successful propagation of a mining-induced cave through the cover sequence to surface
- Interaction between groundwater flow and the subsidence column.
- Significant stresses that may be present in an extraction level and associate mine capital development at ca. 1500m depth.

Again, while not impossible, mining of an IOCG in the Cloncurry district where the top of the orebody is 500m below surface is, thus far, uncharted territory.

One of the impediments to viable mining of Cloncurry-style Cu-Au deposits as standalone underground operations, is the low unit-value of this ore (Figure 1.3).

### Early-stage Economic Analysis of Cu-Au Targets and Prospects

The purpose of this evaluative framework is to enable exploration professionals to direct their work with due regard to scale and value required for a deposit to merit considerations as a reasonable candidate to support a commercially viable mining operation. The insight provided by this evaluation is expected to allow exploration professionals to confidently and quickly assess, and rank prospects within their portfolio. This process is intended to support discussion and decision making with respect to the allocation of time, resources and ultimately funding for exploration projects.

A method of assessing what 'success looks like' for discovery in a given geological terrane, is warranted. This should answer 'What constitutes discovery in terms of grade, tonnage, footprint, depth, and preliminary estimate of financial outcome of a mining operation?'. Inputs would incorporate deposit-descriptive data such as dimensions, geometry, grade, depth, but also include potential mine scale (tonnage), mining rates, processing rates, scale and cost of capital infrastructure and access to power, water,

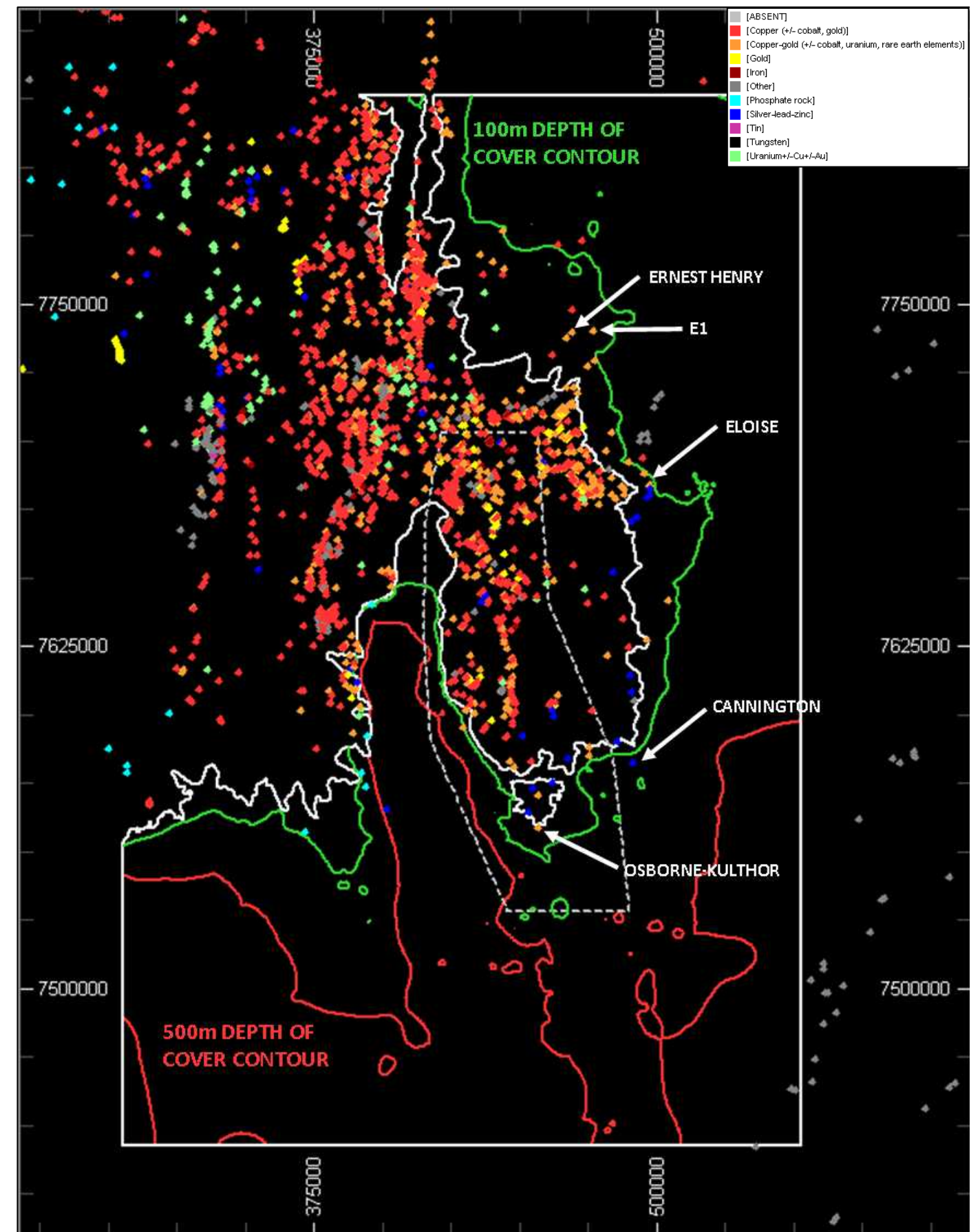


Figure 6.1 Mineral occurrence map of the Mt Isa Inlier showing the DMQ project area (grey dashed polygon), 100m and 500m depth of cover contours, and the key mines that have been developed under-cover in the EFB are annotated. White boundary is the limit of the outcropping Mt Isa Inlier.

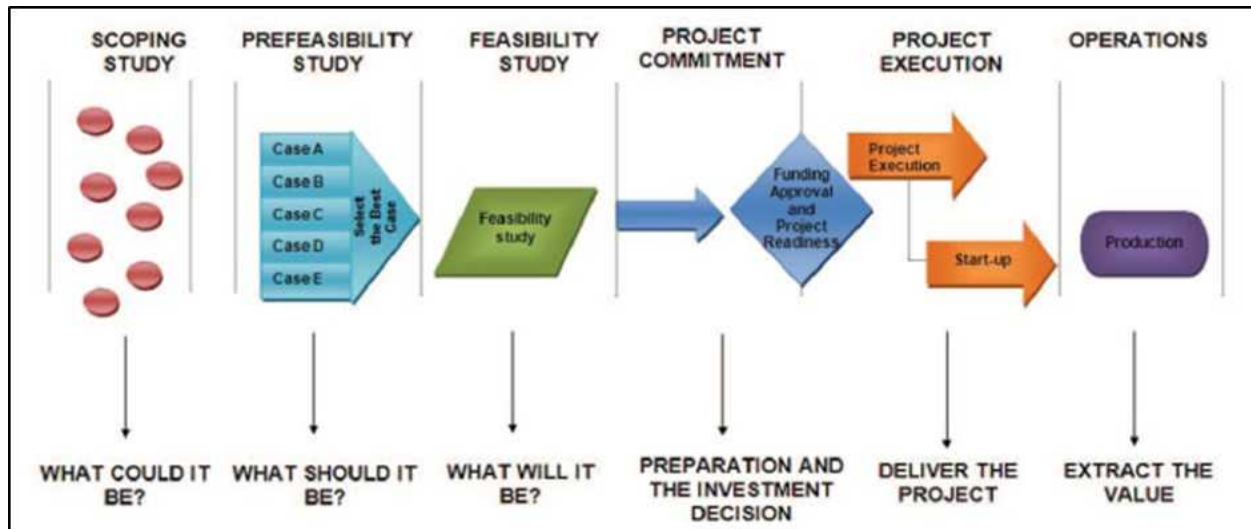


Figure 6.2 The progress of studies for mineral projects (Source: AusIMM Cost Estimation Handbook, Second Edition)

and transport routes. An insight into this type of information offers a measure of viability for a 'discovery' going well beyond the intercepted width and grade. It is anticipated that an interactive 'tool/model' as outlined in this report could be used not only to indicate what may be economic in development of an exploration strategy, but also be useful as a means to rank viability amongst a selection of targets and/or prospects, utilising pre-concept stage data.

The evaluations prepared using the framework described here are not intended to provide a definitive evaluation or valuation of exploration or mining projects. The chronological placement of the evaluation approach described in this report and enabled in an associated spreadsheet model in the continuum of project knowledge, the progress of studies and their associated decision making, is prior to a scoping study (Figure 6.2).

The focus of the work is on mineral deposits between 300 and 1,500m deep. The prospectivity of the area South Cloncurry toward the Osborne mine is considered as being mature for near surface deposits, down to 300m. Therefore, there is a reasonable expectation that deposits of sufficient scale and commercial value, based on a reasonable range of currently relevant metal price assumptions, have all been identified.

The evaluative process used for the work reported here is, at best, consistent with the level of work associated with conceptual level studies for mineral project evaluations. For this reason, its use is limited to supporting decision making around the merits of further work over potential mineral prospect or for comparative purposes within an exploration portfolio. The nature of future work typically entails collection of additional data and its evaluation to

build confidence in understanding a prospect's potential, reduce risk and enable assessment of alternative development paths.

## Prospect Evaluation Tool

The Prospect Economic Evaluation Tool for Underground (PEET-UG) is designed as an interactive, spreadsheet-based tool (included in Appendix 12), for prospect/target evaluation at a project stage considered pre-'Concept-level'. The tool evaluates only for underground mining options (consistent with 'Deep Mining Queensland') and assumes no existing infrastructure or pre-existing mine access.

The tool serves three main purposes:

- **Input into area selection during exploration strategy development.** (Where should I be exploring?) Are there mining constraints due to geography, climate, groundwater, orebody ground conditions, orebody grade distribution (e.g. vein vs massive vs disseminated)
- **Ranking of targets and prospects** to determine which has higher likelihood of sustaining a viable mining operation.
- **Stage-gating of the exploration process.** At what point can we determine that a given prospect no longer has the potential to evolve into a mining operation? Iterative model runs through the course of exploration of a prospect can assist tracking it's progress/trajectory as knowledge builds

with time.

### Inputs and Assumptions

The workings of PEET-UG are described in detail by Adrian Pratt in Murphy et al. (2016). The following is a summary of key inputs and outputs of the tool.

The Prospect Economic Evaluation Tool for Underground (PEET-UG) utilizes input information pertaining to:

- Deposit grade, grade distribution, geometry, orientation, depth below surface
- Mining and processing recovery estimates
- Mining method and materials handling options, and associated costs
- Minerals processing costs
- Site infrastructure costs
- Geographical factors (transport, access to power and water)
- Metal prices and exchange rate
- Discount rate, income tax rate, and government royalties.

While it is recognized that stress-field, geothermal gradient, and rock-mass characteristics impact on mine design and operation, these are not included in the early-stage evaluation. It is considered that insufficient information, or required accuracy of data, would be available at the target/prospect stage and these variables are better assessed at scoping-study/pre-feasibility stage.

Derived information from these inputs include: tonnage, in-ground value, mining-rate potential, estimates of the diluted mill feed, recovered metal, mine operating life, calculated inputs for capital (CapEx) and operating (OpEx) expenditure estimates.

The intention is for the evaluative framework to be utilised at early-stage or as a conceptual target evaluation tool, and it is therefore fitting that geological knowledge of the prospect/target is emerging and not yet definitive. To that end, the definition of a deposit's geology is limited in the spreadsheet model to its inferred:

- Basic geometry; strike length, width and depth extension
- Depth of cover
- Value and its mineralization distribution characteristics.

The user can complete a model run with this minimum descriptive information, and setting the metal price and

exchange rate thresholds.

### Outputs

The selection of a mining method, or methods, for a particular deposit is dependent on the ability of a mining method to accommodate or exploit the physical properties of the deposit. The physical properties include its size, geometric configuration, orientation, geomechanical features, distribution of value within the deposit, and relationship with the environment beyond the boundaries of the deposit itself. These properties, all influence how the economically viable material intended for processing, ore, is identified, liberated from a deposit and transported for processing. The PEET-UG process assigns a 'most appropriate' mining-method based on the simplistic inputs pertaining to deposit geometry and grade, both absolute and distribution. The selection of a mining method is rarely this straightforward and it is the role of the pre-feasibility study (Figure 6.2) to test the applicability of multiple mining scenarios. For the purposes of early-stage assessment, the mining method selection is dominantly influenced by the following governing questions:

1. Is there enough potential in-ground value, to suggest compatibility with the potential mining methods and their associated operating expenditure? It is either possible or not.
2. Does the geometry meet or exceed the minimum dimensions nominated for each of the mining methods?
3. Does the amount of material potentially available to mine meet or exceed the minimum dimensions nominated for each of the mining methods?

The models will select, by preference, the method with the lowest operating expenditure from those determined as possibly applicable.

The mining options assessed in PEET-UG (and described in detail in Murphy et al., 2015) include:

- Sub-Level Open Stopping (SLOS)
- Sub-Level Caving (SLC)
- Block Caving (BC)

The derivation of potential mine/mill feed estimates in the spreadsheet model considers only a basic set of modifying factors for mining and processing. These are applied to the estimated size, tonnage, of the potential deposit (Mineral Resource surrogate) to derive estimates for the:

- potential mine / mill feed estimate (Ore Reserve); and

- recovered metal.

Likely/potential project and production schedule for the hypothetical mining project is determined, as is the revenue schedule for concentrate sales and smelting. This facilitates development of annualized capital and operating expenditure estimates, and evaluation of cash-flow for the life of the operation. The estimated financial measures output by PEET-UG include:

- Net Present Value (NPV)
- Internal Rate of Return (IRR)
- Time to payback
- Revenue
- Maximum negative cash position
- Earnings before interest, taxes, depreciation, and amortization (EBITDA)
- Net cashflow, or profit.
- Net Direct Cash Cost (C1 Cost)

The financial evaluation is not intended for use in feasibility studies or to value deposits in the context of corporate transactions, as the intent is to utilize information from the pre-scoping study stages of exploration, discovery, and initial testing of deposit extents and tenor. Instead, the tool should be utilized to rank exploration opportunities ('targets') and provide guidance as to the potential to establish a mining operation around any discovered mineralization. An outcome may be that economic evaluation suggests a prospect is mothballed, or abandoned; dependent on the forward-looking estimates of commodity prices.

Application of PEET-UG, in developing an exploration programme, may focus activity on exploration above a specific depth, a minimum resource size, and/or combined grade (Figure 2). Initial holes drilled into a prospect can be critically analyzed in terms of the potential viability of a mining operation, with this expanded insight; and inform the decision process accordingly.

The evaluation tool is only for use in assessment of potential underground extraction options, consistent with the parent 'Deep Mining Queensland' research project. The tool therefore does not take into account any resources which may be extracted via open-cut mining. It is recognized that open-cut mining, particularly for lower unit-value orebodies, covers the costs for site-infrastructure and access and may provide some capital toward underground mine development. In this sense, the underground mine is an incremental extension to the existing operation, with a processing facility in place. The

PEET-UG assessment measures relative viability of initiating a new, stand-alone mining operation, where the underground resource and mine must cover all costs borne by the operation.

## Orebody Simulations as Input to PEET-UG

PEET-UG is designed to handle actual and/or hypothetical data. Data from actual operations has been used to calibrate/validate the tool (see Murphy et al., 2016).

As starting models from which to determine relative value, and incentive for which to explore; a series of 3D volumes have been input into PEET-UG, and are illustrated in Figure 5.

The geometries are based on both mining methods and representative orebody shapes. The shapes represent the following mining scenarios:

- Block cave scenario. A 400mx400m volume is used which corresponds to a shape slightly larger than the Ernest Henry orebody.
- Block cave/Sub-level cave scenario. 250mx250m in plan section.
- Sub-level cave scenario. 500m strike length and 100m across-strike. This is similar to the SWAN deposit within the Mt Elliott Cu-Au system.
- Sub-level cave/Large open-stope scenario. 625m of strike and 50m across-strike.
- Sub-level open-stope scenario. 750m strike length and 25m across-strike. This is most similar to the Osborne orebody.
- Small sub-level open-stope scenario. 400m strike length and 15m across-strike. This is more similar to the Kulthor, Starra.
- Small selective stoping scenario. 200m strike length and 15m across-strike. This geometry is a representation of the Eloise orebody.

The geometries used are for comparative purposes only and any permutation of geometry can be tested in PEET-UG, as defined by the user.

Other assumptions or 'locked' variables in the analysis presented here include the 'depth below surface', dip, and price assumptions. These can all be changed according to the target volume required to be tested.

Copper equivalence (CuEq [%]) (Figure 6.4) is used to represent the data in the accompanying diagrams. Copper

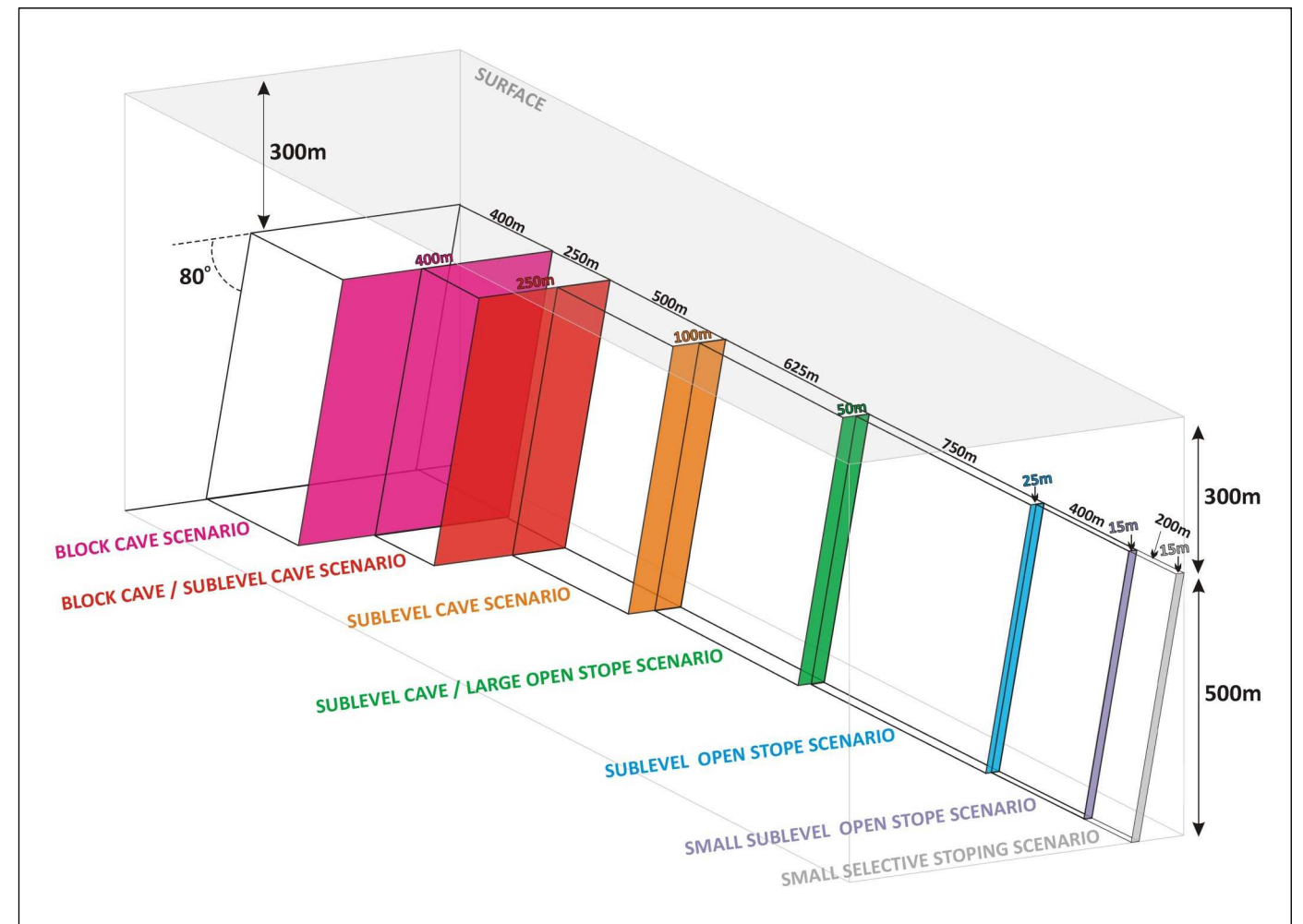


**Figure 6.3** Diagrammatic representation of the orebody/mining-block geometries used in the PEET-UG analysis. For each of the following analyses, a mining-block height of 500m is used. Depth to the top of this block (300m in the above illustration) is varied accordingly.

contributes approximately 75% of the value at a 20,000:1 ratio (Cu:Au) of w/w concentration (2% Cu:1g/t Au). The gold contribution is therefore incorporated into a Cu-Equivalent value (curves of Cu equivalence illustrated as orange lines on Figure 6.4). The inputs to PEET-UG are Cu (%) and Au (ppm), not CuEq, and this has been derived separately. In the context of this study Copper equivalence is calculated as follows:

$$\text{CuEq (\%)} = (\$ \text{value contributed from both Cu and Au}) / \text{Cu price.}$$

The following scenarios are set at \$5,500/t Cu and \$1,200/oz Au; considered reasonable average values for the past three years (2014-2017). Again, these can be adjusted by the user to be consistent with metal price fluctuations or forecast estimates.

The various orebody/mining-block geometries have been analysed in terms of varying Cu and Au grade (reported as Cu equivalence), depth of cover, and dip. The impact of these variables is assessed in terms of financial measures

IRR and NPV (Figure 6.5) and production rate (Figure 6.6).

As expected, the higher tonnage and lower cost mining methods achieve greater IRR, NPV, and profit at the same grades as more selective stoping operations, and can achieve profitability at grades where stoping is not viable (Figures 6.5).

As illustrated in Figure 6.6, steepening of orebody dip erodes NPV through reduction of footprint (access for extraction) and reducing metal content in the 500m vertical high mining block. An 80deg imposed threshold on Block Caving limits its application, but arrests the reduction in NPV and production rate. An interesting phenomenon in Figure 6.5 is that NPV is maximised where these mining methods are at their technical limit, i.e. the lowest dip achievable.

Geometry, and its impact on mining method selection, is a more important driver of value than depth alone. Orientation/attitude also has been shown, through PEET-UG analysis, to have a measurable effect on method

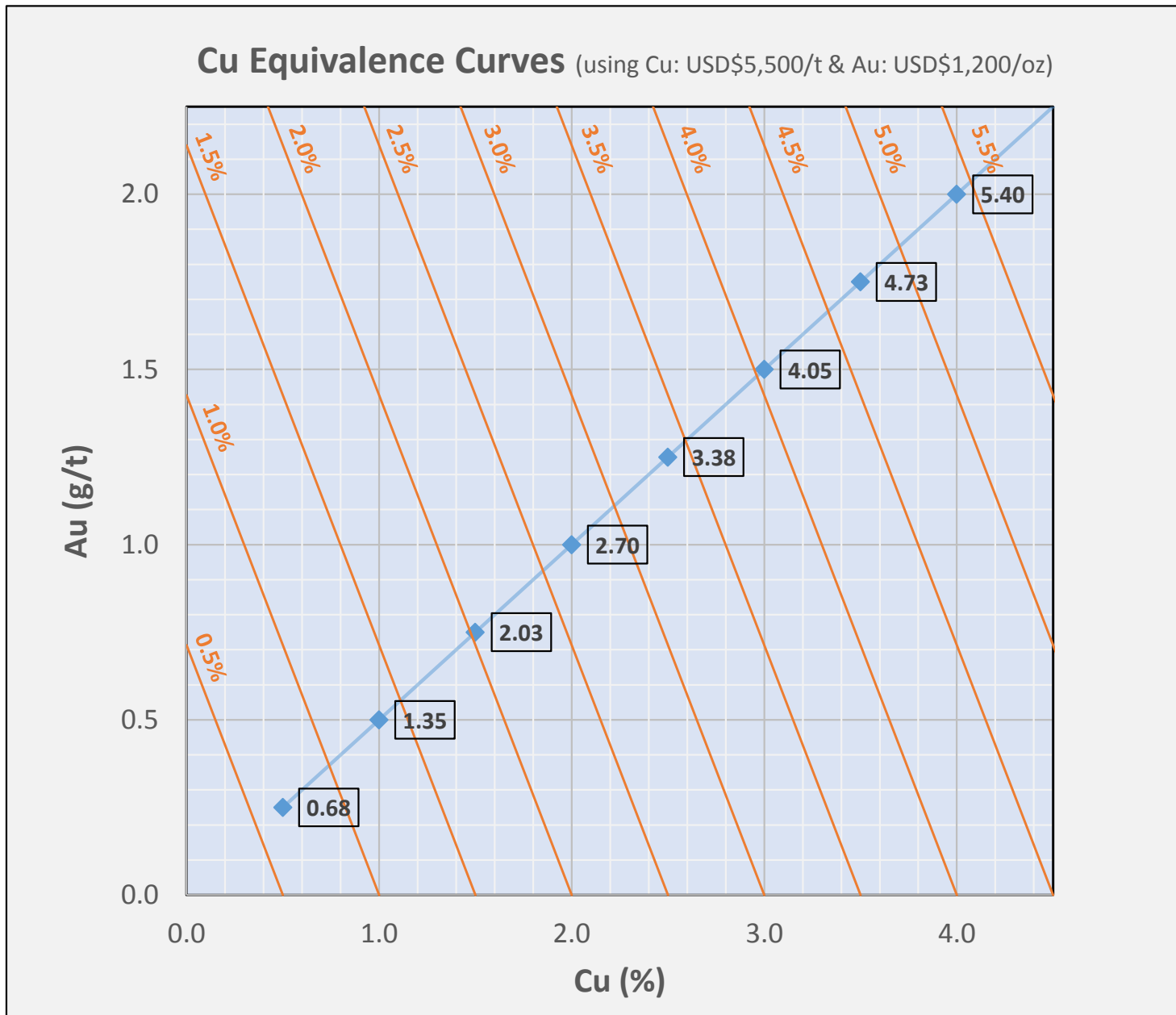


Figure 6.4 Graphical representation of Copper Equivalence thresholds used in this analysis. Cu:Au ratio, defining the gradient of the blue line; is 20,000:1, an 'average' ratio recognised in many IOCG systems. Copper equivalence values (boxed) are used in the following graphs comparing economic outcomes.

selection, production rate, and NPV.

The effect of dip on horizontal area ('footprint') available for extraction has also been resolved through PEET-UG analysis. Production rate is higher at gentler dips because more of the orebody is exposed on intersection with the horizontal plane of the extraction level. NPV is maximised where the orebody has greater 'footprint'. Other technical challenges affect mining orebodies with lower dips or plunges. These relate to flow of material in the cave and how stresses impact on mineability, but are deposit-specific and not dealt with at this early stage assessment.

Other economic measures such as total cash-flow and unit

cash-flow have been reported in Murphy et al. (2016b). Similarly, the trajectories of total cash-flow are significantly enhanced for the mass-mining methods which are able to see more ore extracted, and metal recovered; compared to more selective means. This is also reported out from PEET-UG as a 'net' cash-flow (or profit) per tonne. The caving scenarios generate higher profit per tonne than the more selective stopping methods, at the same grades (Murphy et al., 2016b).

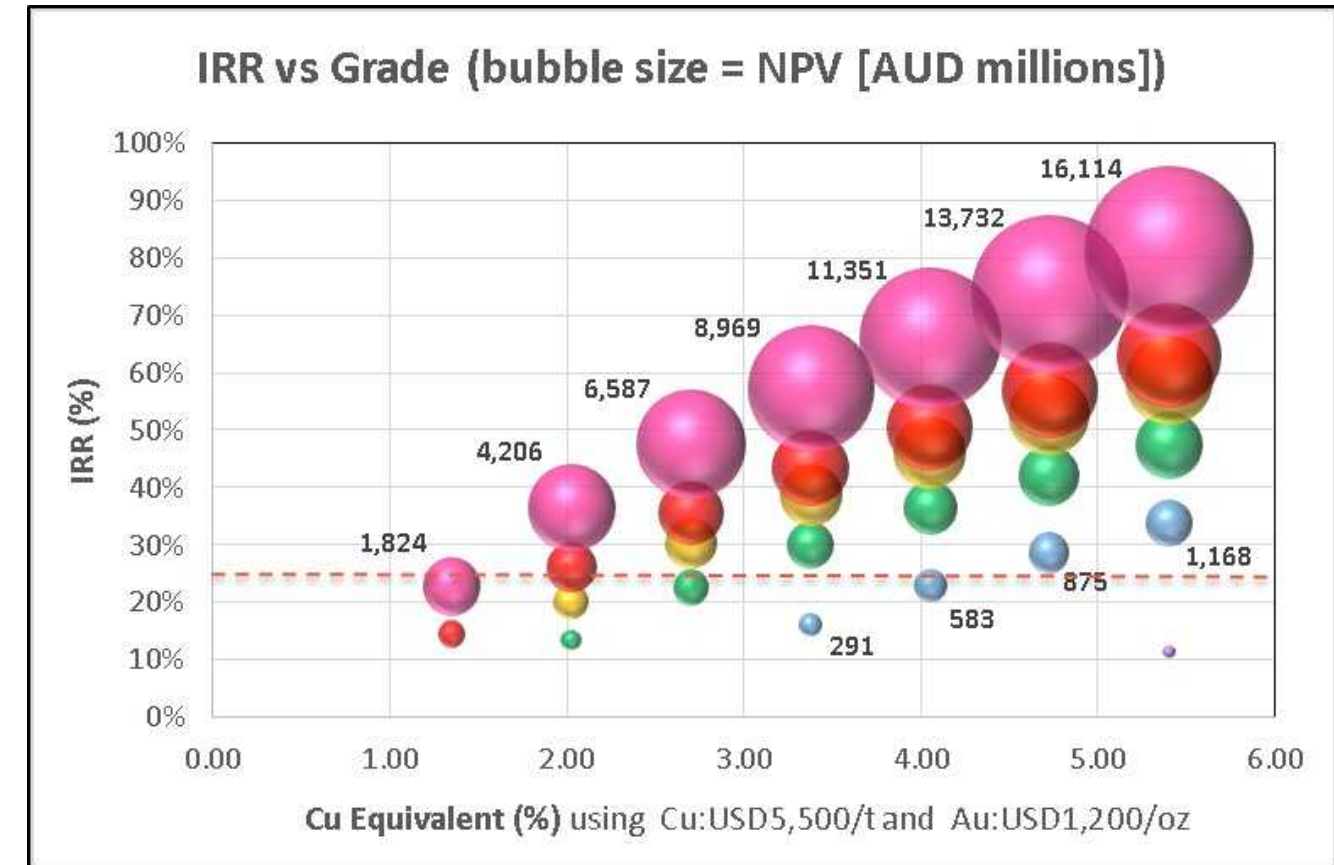


Figure 6.5 Internal Rate of Return (IRR) vs grade for each of the orebody/mining-block geometries. Dashed line represents a 'target' 25% IRR. Colours correspond to orebody/mining-block shapes illustrated in Figure 6.3.

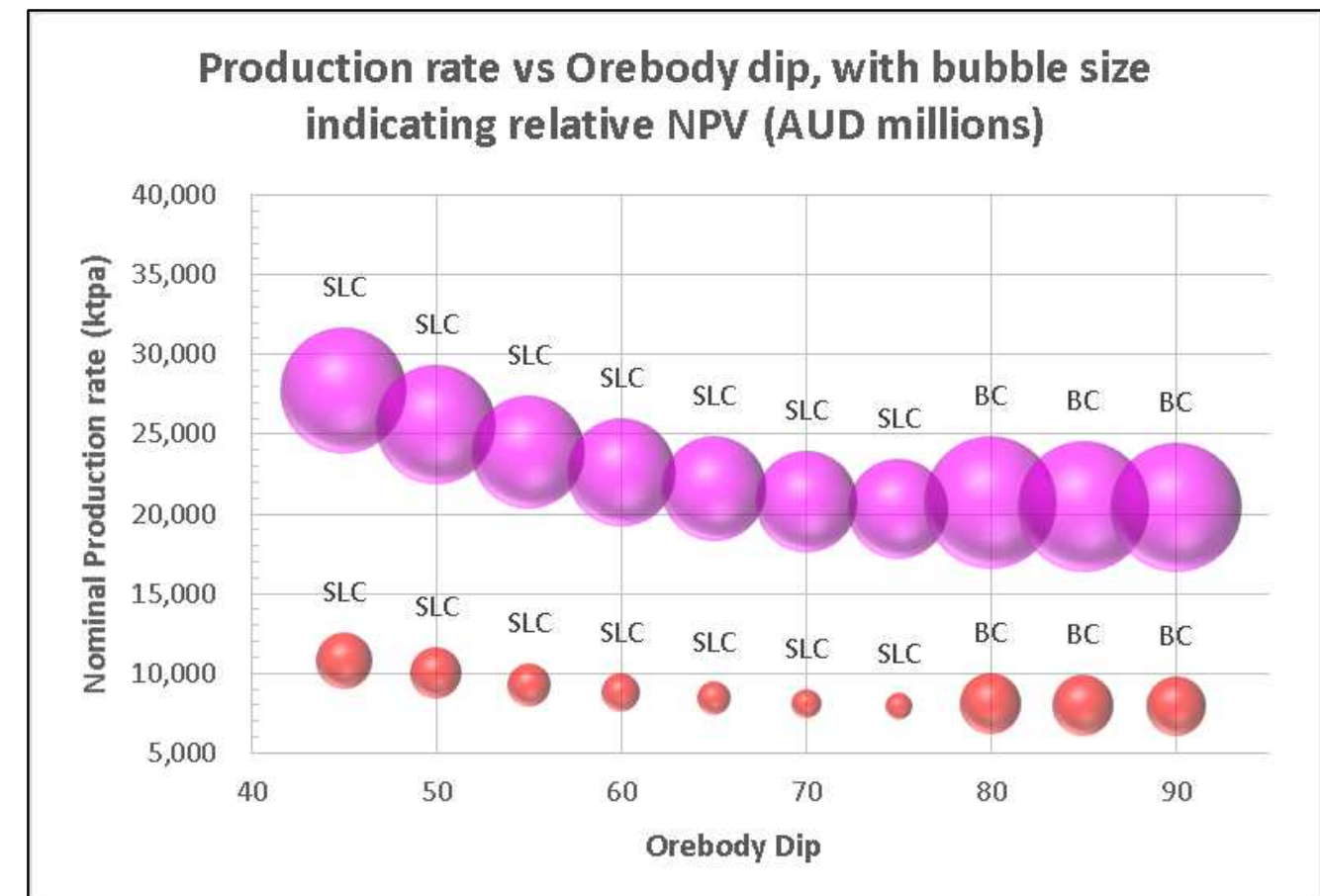
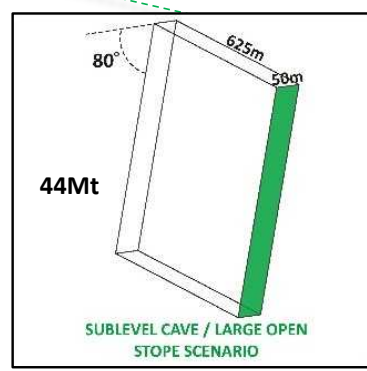
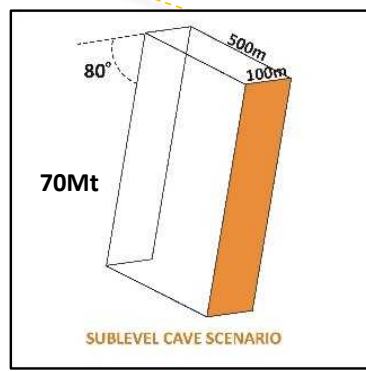
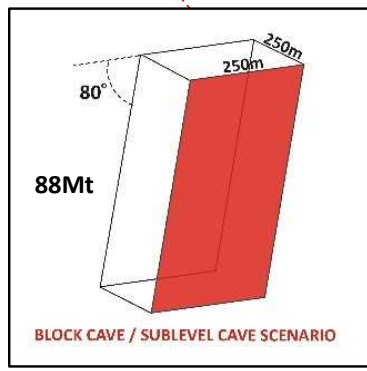
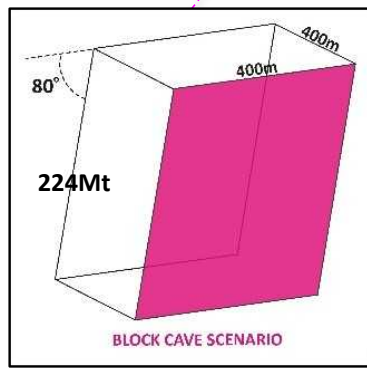
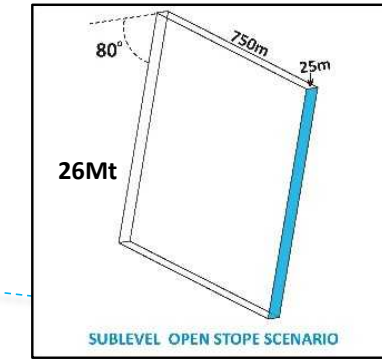
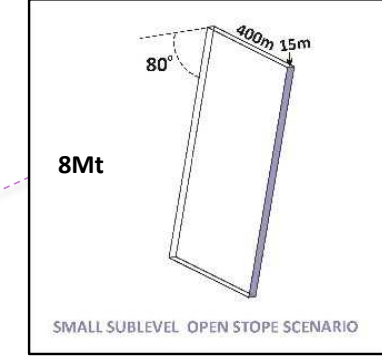
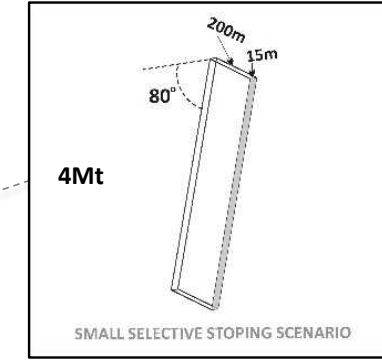
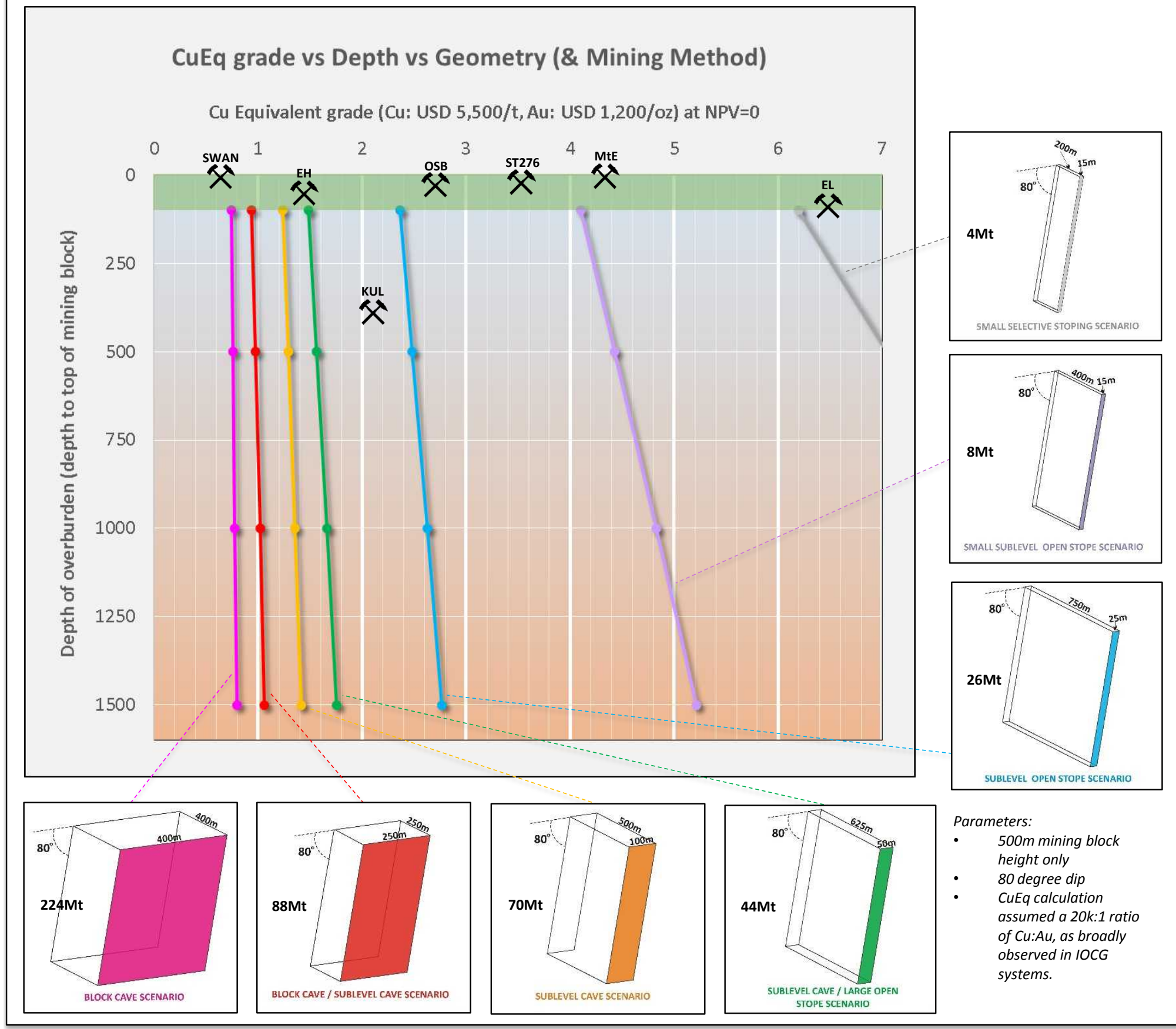
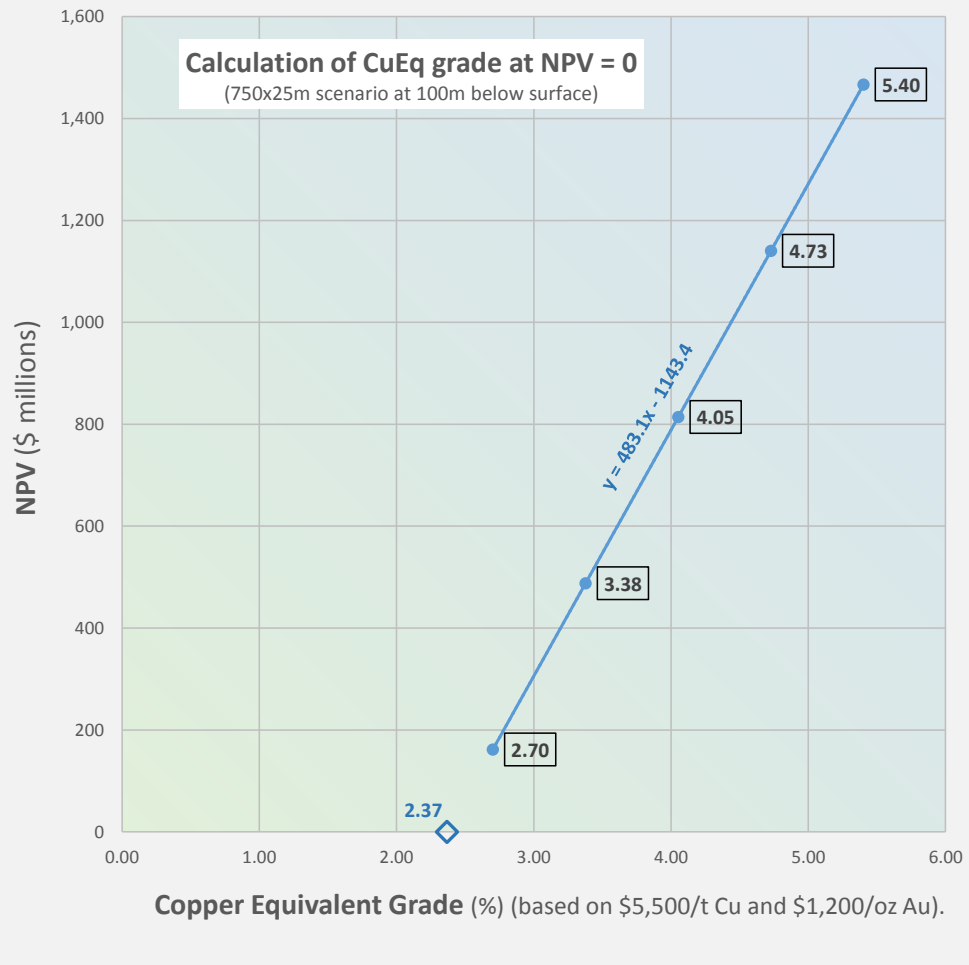


Figure 6.6 Production rate (and mining method) as a function of dip. Bubble size equates to relative NPV. Red = Sub-Level Cave scenario, magenta = Block Cave scenario. Dip overrides geometry control on mining method selection.



- Parameters:
- 500m mining block height only
  - 80 degree dip
  - CuEq calculation assumed a 20k:1 ratio of Cu:Au, as broadly observed in IOCG systems.

Figure 6.8 Graph displaying the relationship between orebody geometry (and therefore mining method), depth of cover, and the required CuEq grade to achieve NPV=0 (see text for discussion). Mining symbols represent the approximate depth to top vs CuEq grade for SWAN, Ernest Henry, Kulthor, Osborne, Starra 276, Mt Elliott, and Eloise. The green band at the top of the chart represents 0-100m below surface, the domain within which any discovered resource is likely to be mined via open-cut means, initially, rather than

Figure 6.7 Graphical representation of calculating NPV=0 for the 750mx25m mining scenario at 100m depth to the top of the mining block. The result of 2.37% corresponds to the first point on the blue curve in Figure 6.8.

### Implications for discovery at depth in the Cloncurry District

With scenarios capturing most of the known orebody geometries (amenable to underground mining) in the Cloncurry field, an assessment of the depth sensitivity of these geometries is required in order to determine the case for deep exploration and, more importantly, what constitutes ore at depth in the Cloncurry field.

The assessment compares each mining geometry scenario based on the CuEq grade required to achieve NPV equal to zero. This was calculated by determining NPV at various CuEq grades and using a regression to derive NPV=0, as shown on Figure 6.7. This does not mean that the project has no value, but implies that it offers no greater realisation of value than other investment options, or benefits outweighing the cost of capital. At NPV=0, project risk would be a determining factor in investment choice.

As expected, large projects generate larger NPVs than their smaller counterparts. At NPV=0, there is a tipping point in the investment decision process which is common for each mining method. To the left of each curve (mining method/geometry) the NPV is negative and the project, based on orebody geometry/grade, is therefore non-viable at the given depth below

surface.

Some of the key observations from Figure 6.8 include:

- Depth insensitivity of Block and Sub-level Caving scenarios. This is a function of the bottom-up mining sequence whereby the significant capital infrastructure is established at the base of the mining block, particularly in the case of Block-caving, and the increment of additional cost in deepening this horizon is insignificant compared to the overall cost. The 'cut-off' CuEq grade is, as a result, less sensitive to depth compared to other mining methods. Also, these mines have significantly higher metal production and a lower cost-base, and will therefore operate at a lower cut-off grade, particularly once established.
- SWAN occurs left of its corresponding geometry curve (orange) and is uneconomic in the assumed rice environment.
- Kulthor is well to the left of its corresponding geometry curve (purple) and was economically extracted as it was an incremental expansion of an existing mine and utilized existing processing facility. Discovery of a Kulthor-analogue away from this infrastructure would likely be sub-economic.
- Eloise, despite being significantly higher grade, would likely be sub-economic if the top of the ore-reserve was 250m below surface. The economics of Eloise are restrictive due to the short strike length and relatively narrow orebody.
- The more selective and development intensive (per tonne of mined ore) stoping methods have a shallower gradient to their CuEq vs Depth curve. Extensions to these mines with depth, carries additional costs; and these costs are amortised across fewer tonnes mined and metal produced.

The significance of this chart to explorers in the Cloncurry district is that it provides a guide for what is required to be discovered to sustain a new mining operation, at depth. For example, intersection of 15m @ 3% CuEq from 300m depth is likely unviable. The chart indicates that at this width, and with some assumptions around strike length informed by adjacent drillholes or geophysics, that an operation from 300m would require resource grades greater than 4.25% CuEq. However, at this depth, a larger

volume target (ca. 50m wide), need only be greater than 1.55% CuEq.

While nothing reported here precludes discovery of a viable orebody at depth and/or undercover in the Eastern Fold Belt, PEET-UG can be used by explorationists to put their drilling results and geophysical interpretations into context of what might be an extractable ore deposit. The prospectivity aspect of the DMQ project will more inform as to the right geological conditions or ingredients for discovery, PEET-UG provides the framework to compare economic outcomes of any identified target geometries at this early stage and/or during drill-testing.

It is apparent that the successful mining of Cloncurry Cu-Au deposits as underground mines has largely been possible due to precursor open-cut mines at the same operation. In other words, the initial extraction method was via open-cut mining and this has covered costs of site access and infrastructure (processing plant, power, water, offices, camp, and tailings storage facility). The underground mine has been an incremental expansion or evolution of the mining operation (e.g. Starra line, Osborne, Ernest Henry). In the event that there is no open-cut resource available to get the operation started, PEET-UG indicates the requirements for a viable underground operation.

## Implications for the DMQ Project Area and Generated Target Domains

The known deposits in the EFB are constrained by unit-value of ore constituents Cu and Au; and this is clear on Figure 3 where various deposit-styles are compared based on their contained value per tonne of ore. Cloncurry Cu-Au deposits are amongst the lower unit-value and lower total resource tonnage deposits (Figure 6.5) and their exploitation at depth requires lower cost mining methods so as to maintain sufficient operating margin.

The average value per tonne for Cloncurry Cu-Au deposits is \$161, with larger deposits (>10Mt) averaging \$85/t. The smaller deposits have average contained value of \$236/t.

This equates to CuEq of 1.5% for the >10Mt deposits and 4.1% for the remainder of deposits, which are generally <5Mt.

This information informs the applicable mining methods, on a cost basis. For example, it is not feasible to apply open-stopping as a mining method to extract ore that comprises value of \$70/t, remembering that additional

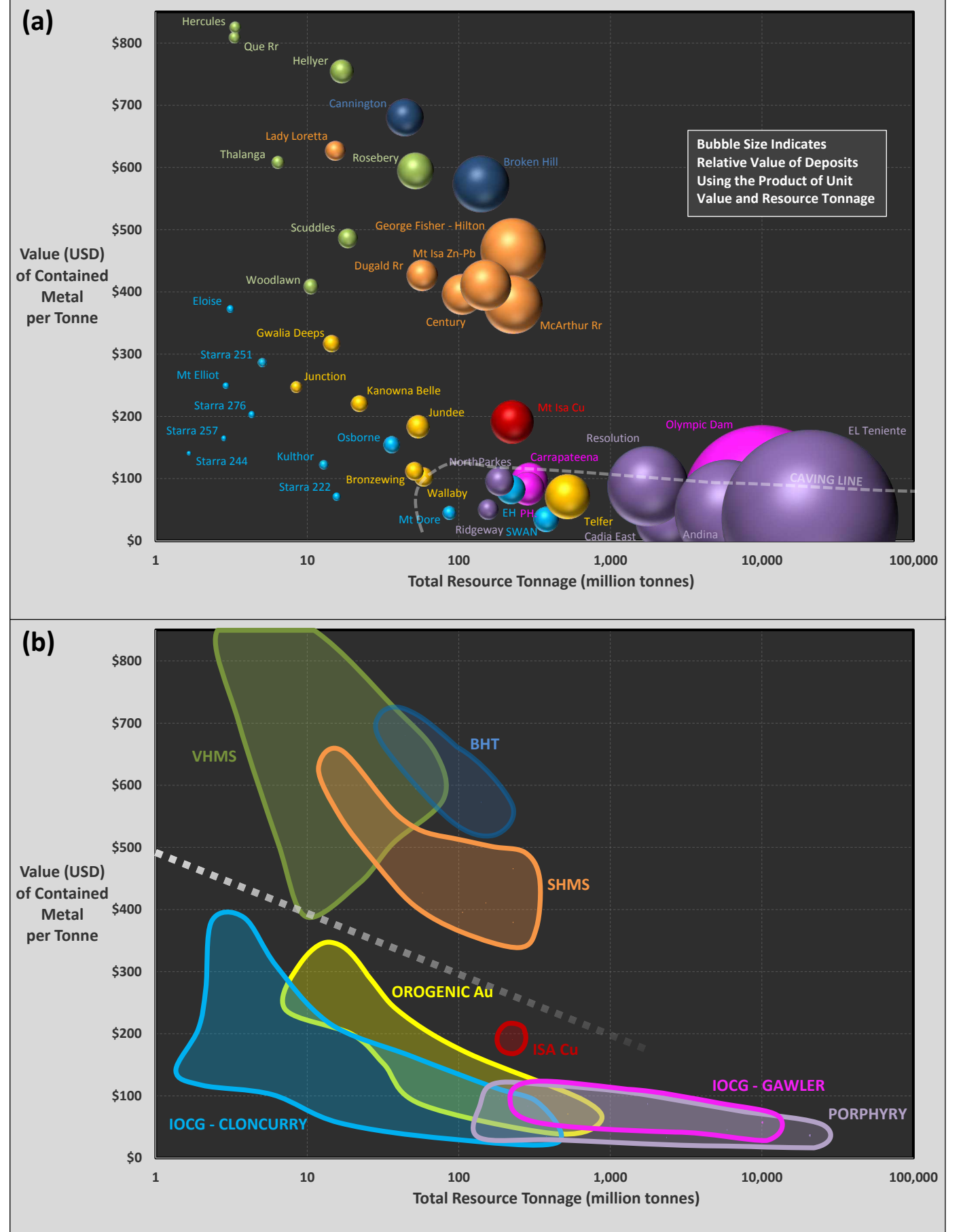


**Figure 6.9** (a) Contained value (USD) of selected mineral deposits. Bubble size indicates relative, pre-mining, total contained value. 'Caving line' indicates a field within which 'mass-mining' methods may be required to facilitate economic extraction. Metal prices and exchange rate as at 14th March, 2017. (b) Grouped by deposit type. Dotted line emphasises the significant value divide between 'massive' ores and disseminated/vein-hosted/discrete-structural deposit styles.

costs relating to processing and admin/exploration/geology are in addition to the mining costs (shown in the graph in Chapter 1, Figure 1.4).

Similarly, discovery of ore with \$300/t contained value in the Cloncurry Cu-Au district is likely to be low resource tonnage (Figure 6.5), lower tonnes per vertical metre, and shorter mine-life. This type of deposit, if discovered, is unlikely to be amenable to lower cost mining methods due to its geometry and volume, but can be economically extracted using open-stopping or other selective methods.

As shown in Figure 6.5a, the total value of the deposits (size of bubble) is significantly greater in the larger deposits of low-grade ore compared to the smaller deposits of higher grade ore. In fact, using the same 10Mt demarcation as in above analyses, the larger deposits, on average, comprise 10x the value of the smaller deposits.

There is a spectrum of Cu-Au deposits in the district ranging from low-tonnage and high-grade, to high-tonnage and low grade (Figure 6.10, Table 6.1). According

to the groupings on Figure 6.10, Starra-style structural-juxtaposition targets are discrete moderate value deposits, Staveley/Kuridala contact domain deposits are generally high-tonnage and low to moderate grade, but the real contenders for sustained underground mining operations are those deposits situated well-above the Staveley contact, hosted in Kuridala/Toole Creek/Mt Fort Constantine Volcanics whereby structural focussing of fluid has facilitated incrementally higher-value deposits but over a wide range of tonnages (Figure 6.10).

Depth sensitivity for a given mining method varies from the large scale (low sensitivity) to the narrow mining methods (high sensitivity) driven by costs associated with capital development and haulage. The mass-mining methods (LH side of Figure 6.8) such as block-caving, require development of key capital infrastructure at the base of the mining block prior to production (bottom-up mining method). As such, this method is less sensitive, in economic terms, to depth. Other factors affect block-cave mine viability at depth and include high-stress

environments affecting the longevity of development, and the greater distance of overburden to cave to facilitate propagation to surface (see Murphy et al., 2015).

Stoping methods (RH side of Figure 6.8), on the other hand, are typically top-down mining and capital development (decline etc) is an incremental cost for each additional mining block at depth. The required cut-off grade increases with depth incrementally with mine expansion.

Focussing on those deposits within the magenta polygon in Figure 6.10, the mining methods employed range from selective, smaller longitudinal stoping at Eloise, longitudinal stoping and longitudinal SLC at Osborne, and Sublevel Caving at Ernst Henry. This indicates that no single mining method is the panacea to enable

economic extraction of Cloncurry-style Cu-Au deposits, however, the economics of narrow, short strike-length mining at depth does not compete with the economies of scale achieved with a long-lived, large tonnage, large footprint operation; even at significantly lower grade.

Although based on few data-points, the relationships observed in Figure 6.10 could be used as a guide to the deposit-style with the highest propensity for sustaining a new, standalone mining operation.

### Rationalization of DMQ-generated Prospective Tracts

Identification of prospective locales and tracts as part of the 3D prospectivity exercise has resulted in a spatial domains of prospectivity by deposit-type (Figure 6.11). This depiction of the prospective volumes is limited to a maximum of 2.5km below surface. This is to allow sufficient radius around a mineralised system to be identified within the anticipated 2km depth limit to underground mining.

These target-types have demonstrated contrasting value. Starra-style targets can be expected to have high unit-value but lower overall deposit value (Table 6.1), whereas the Staveley-buffer (SWAN/Mt Dore) style and Structural

Deposit	Tonnes	Cu (%)	Au (ppm)	Cu_Eq (%)	Value/t (\$AUD)	Total Value (\$m)
Ernest Henry	220,000,000	1.1	0.5	1.4	\$83	\$18,280
Osborne	36,000,000	2.0	1.0	2.7	\$155	\$5,565
Kulthor	12,800,000	1.5	1.0	2.1	\$122	\$1,566
Eloise	3,100,000	5.5	1.4	6.4	\$373	\$1,156
SWAN (resource)	375,000,000	0.4	0.3	0.6	\$35	\$13,189
Mt Elliott	2,900,000	3.3	1.5	4.3	\$250	\$725
Mt Dore (resource)	86,500,000	0.6	0.1	0.8	\$45	\$3,879
Starra 222	15,500,000	0.6	1.0	1.2	\$72	\$1,109
Starra 244	1,650,000	0.7	2.6	2.4	\$141	\$232
Starra 251	5,040,000	2.3	3.9	4.9	\$286	\$1,443
Starra 257	2,800,000	0.7	3.3	2.8	\$165	\$461
Starra 276	4,300,000	2.7	1.2	3.5	\$203	\$874

**Table 6.1 Comparative resource and value details for the deposits plotted in Figure 6.10. 'Deposit' name colouring corresponds to the groupings in Figure 6.10 also. Cells coloured by maximum (hot) to minimum (cold) values. Value calculations utilised 14th March 2017 metal prices.**

focus type (EH, Osborne) have higher total value. This information should guide the ranking of target areas derived from Figure 6.11.

Based on approximate size and Cu-equivalent grade, Starra-type targets are less likely to be economically viable if not initiated with an open-cut. This is shown in Figure 6.8 where a Starra-style deposit would need to be in the order of 5% Cu-Eq at top-of-deposit 250m below surface.

By contrast, Osborne/Ernest Henry-type deposits are viable targets even where the top of the target is at depths of 500m to 1,000m (Figure 6.8).

SWAN/Mt Dore-style targets, while comprising significant total value (Table 6.1), are of low unit-value. Mining-method selection, if open-cut mining is not feasible, is driven toward low-cost underground mining methods such as block-caving. Feasibility of block-cave mining of such deposits is constrained largely by orebody geometry and orientation.

Findings derived from use of Figure 6.8 inherently assume that the deposit is standalone and must cover all capital costs associated with the operation (including processing plant). Naturally, if a cluster of deposits occurs such that a common processing plant can be utilised, then the incremental project economics by deposit changes significantly. This, however, requires sufficient capacity in

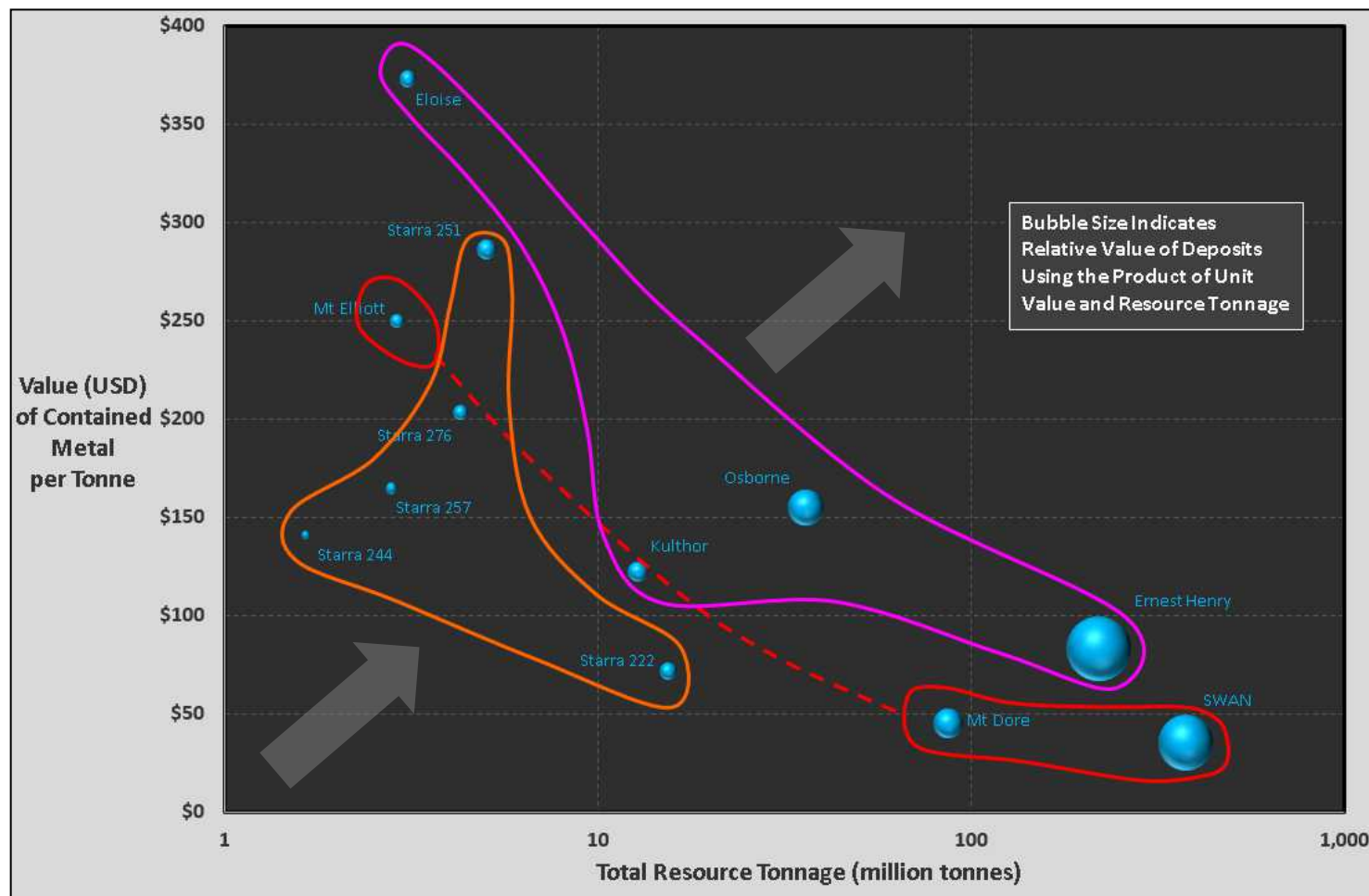


**Figure 6.10 Unit-value per tonne of ore for Cloncurry Cu-Au deposits grouped by deposit-style. Polygons represent grouping of Cloncurry Cu-Au deposits based on the following deposit-styles: Orange polygon: Structural juxtaposition with Staveley Fmn; red polygon: Staveley/Kuridala contact domain, magenta polygon: deposits well into the hangingwall of the Staveley Fmn. Grey arrow indicates the preferred direction, i.e. higher value and higher tonnage. Modified from Murphy et al., 2017.**

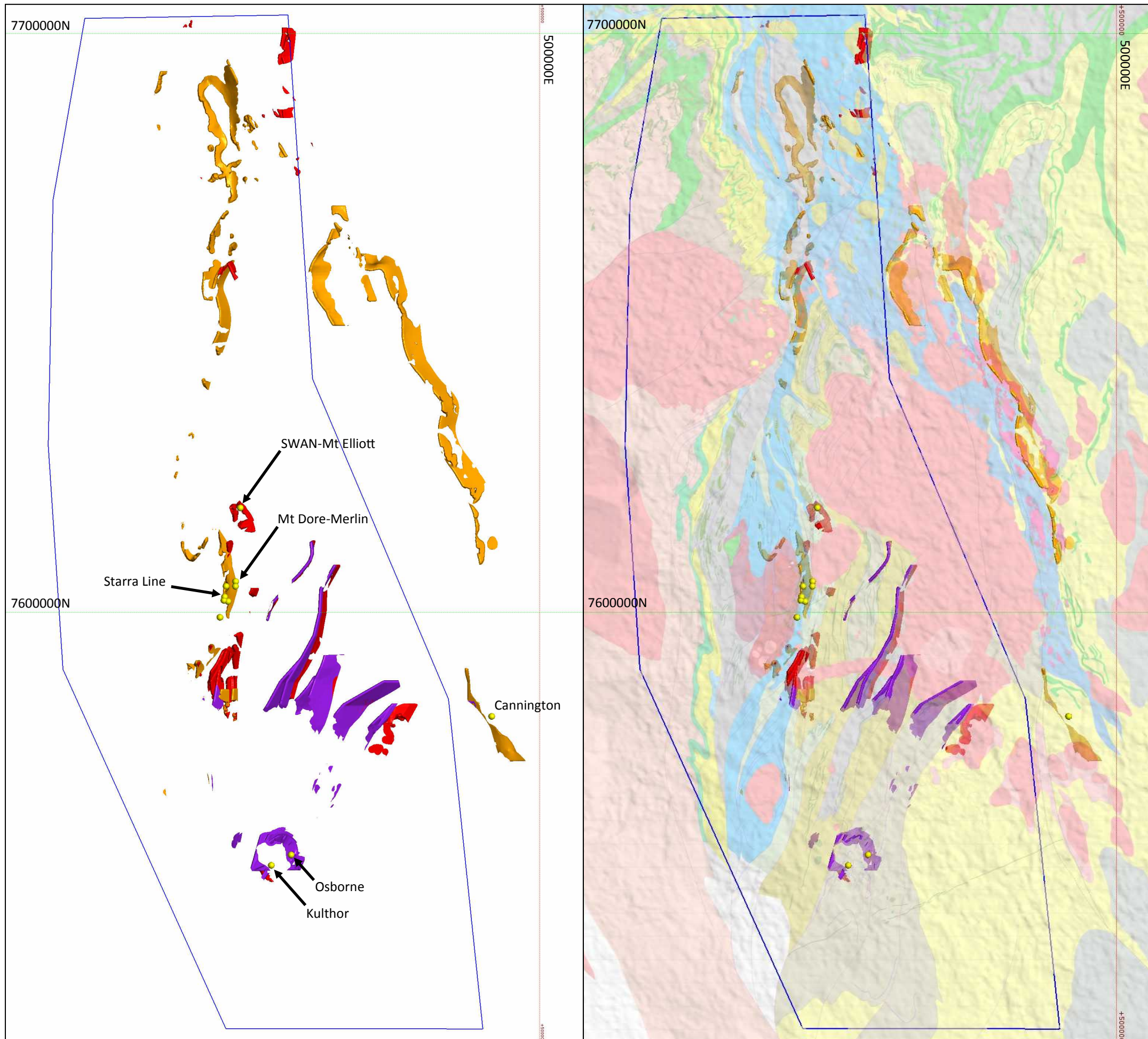


**Figure 6.11 DMQ-generated target domains in the Southern Cloncurry district. Rights hand image with surface/base of cover geology appended. Both images display depth-limiting to 2.5km below surface. Magenta: Hangingwall Structural focus type (e.g. Ernest Henry, Eloise, Osborne), Red: SWAN-Mt Dore style, and Orange: Starra-style target domains.**

the plant, and the associated capital to build a larger scale processing facility.

Discovery of a larger system, such as SWAN, requires mining at a higher rate than available in existing processing facilities (e.g. Osborne), and the costs associated with building a higher capacity plant must be incorporated in the economic assessment of the project.

Likewise, any significant target amongst the portfolio must be treated similarly, that is, there may not be a suitable existing processing option for a discovered deposit.

For these reasons, the utilisation of PEET-UG is recommended as a comparative process to aid in early-stage decisions around prioritisation of exploration targets, and it is not intended for definitive pre-feasibility and feasibility level analysis. More so, the intent of PEET-UG is to provide geologists with engineering parameters and constraints with the aim of progressing those targets and prospects which have a higher likelihood of developing to a point where a scoping study can be conducted. With this in mind, use of the PEET-UG tool may actually suggest that certain prospects are not likely to warrant a scoping-study level of analysis, as it fails at certain hurdles. This itself should indicate that exploration expenditure is better redirected to alternative prospects.

The tool also gives the user the ability to assess sensitivity to recovery, both mining and minerals processing, metal prices, and changes to any of the input costs if these are considered to have a material effect on the economic result.

Sensitivity analysis through simulation in the tool will provide the project geologist with a measure of robustness of a mineral deposit, but also provide common language in terms of engineering, minerals processing, and financial assessment measures; to initiate discussion early in the life of a project. This may justify deposit-knowledge/geometallurgical programmes of work in order to determine the variability and distribution of those parameters affecting key drivers of profitability and viability.

PEET-UG is designed to meet the needs of the DMQ project and has limitations in terms of commodities available to the user, and processing paths. A list of potential modifications is provided in Appendix 12, recommended as improvements to the existing PEET-UG platform.

- Adshead, N. D., and Keogh, D. 1993. Mineralisation and Alteration styles at the Osborne Cu-Au Deposit: *AIG Bulletin 14*
- Adshead, N. D. 1995. Geology, alteration and geochemistry of the Osborne Cu-Au deposit, Cloncurry district, NW Queensland: *Unpublished Ph.D. thesis, Townsville, Queensland, James Cook University, 382 p.*
- Adshead, N. D., Voulgaris, P., and Muscio, V. N. 1998. Osborne copper-gold deposit: *Australasian Institute of Mining and Metallurgy Monograph 22, p. 793–798.*
- Adshead-Bell, N. S. 1998. Evolution of the Starra and Selwyn high strain zones, Eastern Fold Belt, Mount Isa Inlier: Implications for Au-Cu mineralization: *Economic Geology, 93, p. 1450–1462.*
- Almasi, A., Jafarirad, A., Kheyrollahi, H., Rahimi, M., and Afzal, P. 2014. Evaluation of structural and geological factors in orogenic gold type mineralisation in the Kervian area, north-west Iran, using airborne geophysical data. *Exploration Geophysics, Vol. 45, pp 261 – 270.*
- [AMC Consultants, 2012. Preliminary Economic Assessment of the Mt Elliott Project Queensland, Australia, May 2012. NI 43-101 Technical Report, \(SEDAR website http://www.sedar.com\)](http://www.sedar.com)
- [AMC consultants, 2013. Technical Report on the Lookout Hill Property, Ömnögovi, Mongolia; Entrée Gold Inc. \[ONLINE\] Available at: data/1271554/000119907313000399/exh99\\_1.htm. \[Accessed 23 August 15\].](http://www.avancoresources.com/content/investor-centre/annual-reports/)
- [Anglo American Annual Report. 2014. \[ONLINE\] Available at: http://www.angloamerican.com/~media/Files/A/Anglo-American-PLC-V2/report-builder-2014/annual-report/aa-ar14-interactive-final.pdf.](http://www.angloamerican.com/~media/Files/A/Anglo-American-PLC-V2/report-builder-2014/annual-report/aa-ar14-interactive-final.pdf)
- Atlas Copco. 2007. Mining Methods in Underground Mining (2<sup>nd</sup> ed).
- AusIMM, 2012. Cost estimation Handbook, Second Edition (Monograph 2), Section 6.2.2 Mining feasibility studies pp233-249, (The Australasian Institute of Mining and Metallurgy: Melbourne)
- [Avanco. 2014 Annual Reports | Avanco Resources Website. 2015. Annual Reports | Avanco Resources Website. \[ONLINE\] Available at: http://www.avancoresources.com/content/investor-centre/annual-reports/.](http://www.avancoresources.com/content/investor-centre/annual-reports/)
- Babo, J., Spandler, C., Oliver, N. H. S., Brown, M., Rubenach, M. J. and Creaser, R. A. 2017. The High-Grade Mo-Re Merlin Deposit, Cloncurry District, Australia: Paragenesis and Geochronology of Hydrothermal Alteration and Ore Formation. *Economic Geology, 112, pp. 397-422.*
- Barton, M. D., and Johnson, D. A. 2000. Alternative Brine Sources for Fe-Oxide (-Cu-Au) Systems: Implications for Hydrothermal Alteration and Metals. In: Porter, T.M. (Ed.), *Hydrothermal Iron Oxide Copper-Gold and Related Deposits: A Global Perspective, Volume 1; PGC Publishing, Adelaide, pp 43-60*
- Barton, M. D., and Johnson, D. A. 1996. Evaporitic-source model for igneous-related Fe oxide-(REE-Cu-Au-U) mineralization. *Geology, 24, no. 3, p. 259–262*
- Barton, M. D., and Johnson, D. A. 2004. *Footprints of Fe oxide(-Cu-Au) systems: University of Western Australia Special Publication 33, p. 112–116.*
- Bastrakov, E. N., Skirrow, R. G., and Davidson, G. J. 2007. Fluid Evolution and Origins of Iron Oxide Cu-Au Prospects in the Olympic Dam District, Gawler Craton, South Australia; *Economic Geology, v. 102, pp. 1415-1440.*
- Bates, R. L., and Jackson, J. A. (eds.). 1987. *Glossary of geology (3<sup>rd</sup> ed.): Alexandria, Va., American Geological Institute, 788 p.*
- Bell, T. H. 1983. Thrusting and duplex formation at Mount Isa, Queensland, Australia. *Nature, 304, 493-497.*
- Bell, T. H. 1983. The Role of Thrusting in the Structural Development of the Mount Isa Mine and Its Relevance to Exploration in the Surrounding Region. *Economic Geology, 86, pp.1602-1625.*
- Bell, T. H. and Hickey, K. A. 1998. Multiple Deformations with Successive subvertical and Subhorizontal Axial Planes in the Mount Isa Region: Their Impact on Geometric Development and Significance for Mineralisation and Exploration. *Economic Geology, 93, pp. 1369-1389.*
- Benavides, J., Kyser, T. K., Clark, A., Stanley, C., and Oates, C. 2008a. Exploration guidelines for copper-rich iron oxide-copper-gold deposits in the Mantoverde area, northern Chile: the integration of host-rock molar element ratios and oxygen isotope compositions. *Geochemistry: Exploration, Environment, Analysis, Vol. 8, pp. 343-367.*
- Benavides, J., Kyser, T. K., Clark, A., Stanley, C., and Oates, C. 2008b. Application of molar element ratio analysis of lag talus composite samples to the exploration for iron oxide-copper-gold mineralization: Mantoverde area, northern Chile. *Geochemistry: Exploration, Environment, Analysis, Vol. 8, pp. 369-380.*
- Benavides, J., Kyser, T. K., Clark, A. H., Oates, C. J., Zamora, R., Tarnovschi, R., and Castillo, B. 2007. The Mantoverde iron oxide-copper-gold district, III Región, Chile: The role of regionally derived, nonmagmatic fluids in chalcopyrite mineralization: *Economic Geology, Vol. 102, p. 415–440.*
- [BHP Billiton | Annual Reporting 2014 . 2015. BHP Billiton | Annual Reporting 2014 . \[ONLINE\] Available at: http://www.bhpbilliton.com/investors/annualreporting2014.](http://www.bhpbilliton.com/investors/annualreporting2014)
- Blackthorn Resources. 2013. *Commercial Potential of Kitumba Copper Project Demonstrated in Prefeasibility Study. ASX Announcement.*
- Blakely, R. 1995. *Potential theory in gravity and magnetic applications. Cambridge University Press, 441p.*
- Boric, R., Holmgren, C., Wilson, N. S. F., and Zentilli, M. 2002. The Geology of the El Soldado Manto Type Cu (Ag) Deposit, Central Chile. In: Porter, T. M. (Ed.), *Hydrothermal Iron Oxide Copper-Gold & Related Deposits: A Global Perspective, Volume 2; PGC Publishing, Adelaide, pp 163-184.*
- Briggs, D. F. 2014. *History of the San Manuel – Kalamazoo Mine, Pinal County, Arizona. Arizona Geological Survey - Contributed Report CR-14-A.*
- Brown, E. T. 2003. *Block Caving Geomechanics, Julius Kruttschnitt Mineral Research Centre, Brisbane, p. 516.*
- Brown, J. G., and Favor, B. (eds). 1996. *Hydrology and Geochemistry of Aquifer and Stream Contamination Related to Acidic Water in Pinal Creek Basin Near Globe, Arizona. US Geological Survey Water-Supply Paper 2466.*
- Brown, M., and Porter, T. M. 2010. The Mount Elliott IOCG System, Eastern Fold Belt, Mount Isa Inlier, Northwest Queensland. In: Porter, T. M., (ed.), *Hydrothermal Iron Oxide Copper-Gold & Related Deposits: A Global Perspective, v. 3 - Advances in the Understanding of IOCG Deposits; PGC Publishing, Adelaide, pp. 219-232.*
- Brown, E. T., and Chitombo, G. P. 2007. Underground Mass Mining by Caving – The Way of the Future, pp6, (Sustainable Minerals Institute, University of Queensland),
- Bullock, R. 2011. Comparison of Underground Mining Methods. In: SME Mining Engineering Handbook (3rd Edition) (ed P Darling) Society for Mining, Metallurgy, and Exploration (SME).
- Carter, P. G. 2011. *Selection Process for Hard-Rock Mining. In: SME Mining Engineering Handbook (3rd Edition) (ed P Darling) Society for Mining, Metallurgy, and Exploration (SME).*
- Castle Resources Inc. 2013. *Castle Resources Announces Positive Preliminary Economic Assessment for the Granduc Copper Project. TSX announcement.*
- Chen, H. Y. 2008. The Marcona-Mina Justa district, south-central Perú: implications for the genesis and definition of the iron oxide-copper (-gold) ore deposit clan; Unpublished PhD Thesis, *Queen’s University, Kingston, Ontario, Canada, 266p.*
- Chen, H.Y. 2010. Mesozoic IOCG Mineralisation in the Central Andes: an Updated Review; in Porter, T.M., (ed.), *Hydrothermal Iron Oxide Copper-Gold & Related Deposits: A Global Perspective, v. 3 - Advances in the Understanding of IOCG Deposits; PGC Publishing, Adelaide, pp. 259-272.*
- Chen, H. Y., Clark, A. H., Kyser, T. K., Ullrich, T. D., Baxter, R., Chen, Y., and Moody, T. C. 2010. Evolution of the Giant Marcona-Mina Justa Iron Oxide-Copper-Gold District, South-Central Peru *Economic Geology, v.105, pp. 155-185*
- Cheyney, S., Hill, I., and Linford, N. 2011. Advantages to Using the Pseudogavity Transformation to Aid Edge Detection of Total Field Archaeomagnetic datasets. *Archaeological Prospection, Vol. 18 pp. 81 – 93.*
- Chieftain Metals Corp. 2014. *Chieftain Reports Strong Feasibility Optimization. [ONLINE] Available at: http://www.chieftainmetals.com/2014/10/20/chieftain-reports-strong-feasibility-optimization/. [Accessed 27 August 15].*
- China Gold International Resources Corp. Ltd. 2012. *Pre-Feasibility Study for the Phase II Expansion of the Jiama Project.*
- Chitombo, G. P. 2010. *Cave mining – 16 years after Laubscher’s 1194 paper ‘Cave mining – state of the art’. Proceedings of Caving 2010, Perth, Australia (ed Y Polvin).*
- Conor, C., Raymond, O., Baker, T., Teale, G., Say, P., and Lowe, G. 2010. Alteration and Mineralisation in the Moonta-Wallaroo Copper-Gold Mining Field Region, Olympic Domain, South Australia; in Porter, T.M., (ed.), *Hydrothermal Iron Oxide Copper-Gold and Related Deposits: A Global Perspective, v. 3 - Advances in the Understanding of IOCG Deposits; PGC Publishing, Adelaide, pp. 147-170.*
- Davidson, G. J., Paterson, H. L., Meffre, S., and Berry, R. G. 2007. Characteristics and Origin of the Oak Dam East Breccia-Hosted, Iron Oxide Cu-U-(Au) Deposit: Olympic Dam Region, Gawler Craton, South Australia; *Economic Geology, v. 102, pp. 1471-1498*
- de Haller A., Zúñiga A. J., and Fontboté L. 2001. Geology of the Raul-Condestable IOCG deposit, central coast of Peru: Geological Society of America, Annual Meeting, Boston, November 5–8, <[http://gsa.confex.com/gsa/2001AM/finalprogram/abstract\\_25106.htm](http://gsa.confex.com/gsa/2001AM/finalprogram/abstract_25106.htm)>.
- de Haller, A., and Fontboté, L. 2009. The Raúl-Condestable Iron Oxide Copper-Gold Deposit, Central Coast of Peru: Ore and Related Hydrothermal Alteration, Sulfur Isotopes, and Thermodynamic Constraints *Economic Geology, v 104. pp. 365-384*
- de Haller, A., Corfu, F., Fontboté, L., Schaltegger, U., Barra, F., Chiaradia, M., Frank, M., and Alvarado, J. Z. 2006. Geology, geochronology, and Hf and Pb isotope data of the Raúl-Condestable iron oxide-copper-gold deposit, central coast of Perú; *Economic Geology, v. 101, pp. 281-310.*
- [DMITRE. 2013. South Australia's Major Operating/Approved Mines Resource Estimates and Production Statistics. \[ONLINE\] Available at: https://www.google.com.au/#q=South+Australia%27s+Major+Operating%2FApproved+Mines.](https://www.google.com.au/#q=South+Australia%27s+Major+Operating%2FApproved+Mines)

[Dominion Diamond Corp. 2013. Ekati Diamond Mine NI 43-101 Technical Report. \[ONLINE\] Available at: <http://www.sec.gov/Archives/edgar/data/841071/000106299313002759/exhibit99-1.htm>. \[Accessed 28 August 15\].](http://www.sec.gov/Archives/edgar/data/841071/000106299313002759/exhibit99-1.htm)

Drummond, B. J., MacCreedy, T., Lister, G., Goncharov, v A., Goleby, B., Page, R., and Wyborn, L. 1995. *AGRC Mount Isa Transect Workshops, Brisbane & Mt Isa*.

Duncan, R. J., Hitzman, M. W., Nelson, E. P., and Togtokhbayar, O. 2014. Structural and Lithological Controls on Iron Oxide Copper-Gold Deposits of the Southern Selwyn-Mount Dore Corridor, Eastern Fold Belt, Queensland, Australia *Economic Geology* v. 109, pp. 419-45

Duncan, R. J., Stein, H. J., Evans, K. A., Hitzman, M. W., Nelson, E. P., and Kirwin, D. J. 2011. A new geochronological framework for mineralization and alteration in the southern Cloncurry district, Eastern fold belt, Mount Isa inlier, Australia: Genetic implications for iron oxide-copper-gold deposits: *Economic Geology*, v. 106, p. 169–192.

Dundee Precious Metals Inc. 2005. *Chelopech Mine Feasibility Study. ASX Release*.

Duplancic, P., and Brady, B. H. 1999. Characterisation of caving mechanisms by analysis of seismicity and rock stress, in Proceedings 9th Congress International Society for Rock Mechanics, G. Vouille and P. Berest (eds), 25–28 August, Paris, France, Balkema, Rotterdam, Vol. 2, pp. 1049–1053.

Ebbels, A-M., Fairfield, P., Horton, J., and Munro, P. 2012. Starra 276 NI 43-101 Technical report located in northwest Queensland Region of Australia. *Unpublished Consultants Report (SRK & Golder Assoc.)*.

Ehrig, K. 2014. Olympic Dam: 11<sup>th</sup> SA Exploration and Mining Conference presentation

[Ernest Henry Mining. 2015. Hoisting underway. \[ONLINE\] Available at: \[http://www.ernesthenry.com.au/hoisting-underway.aspx\]\(http://www.ernesthenry.com.au/hoisting-underway\). \[Accessed 26 Aug 15\].](http://www.ernesthenry.com.au/hoisting-underway)

European Goldfields. 2011. *Skouries Cu/Au Project, Greece - NI 43-101 Technical Report*.

Fabris, A. J., Halley, S., van der Wielen, S., Keeping, T., and Gordon, G. 2013. IOCG-style mineralisation in the central eastern Gawler Craton, SA; characterisation of alteration, geochemical associations and exploration vectors. *Report Book 2013/00014. Department of Innovation, Manufacturing, Trade, Resources and Energy, South Australia, Adelaide*.

Fairhead, J., Salem, A., Cascone, L., Hammil, M., Masterton, S., and Samson, E. 2011. New developments of the magnetic tilt-depth method to improve structural mapping of sedimentary basins. *Geophysical Prospecting, Vol. 59, pp. 1072 – 1086*.

Fantin, M. 2011. *Ridgeway Gold Mine: Surveying in a Sub-Level and Block Cave Mine. Unpublished company presentation*.

Fisher, L. A., and Kendrick, M. A. 2008. Metamorphic fluid origins in the Osborne Fe oxide-Cu-Au deposit, Australia: evidence from noble gases and halogens; *Mineralium Deposita*, v. 43, pp. 483-497.

Flores, G. 2014. *Future Challenges and Why Cave Mining Must Change. Proceedings of Caving 2014, Santiago, Chile*

Fortowski, D. B., and McCracken, S. 1998. Mount Elliott copper-gold deposit; in Berkman D.A. and Mackenzie D.H., (eds.), *Geology of Australia and Papua New Guinean Mineral Deposits, The Australasian Institute of Mining and Metallurgy, Melbourne, Monograph 22, pp. 775-782*.

Fortune Minerals [Limited](http://www.fortuneminerals.com/news/press-releases/press-release-details/2014/Fortune-Minerals-announces-positive-updated-Micon-Feasibility-Study--updated-reserves-for-the-NICO-project/). 2014. *Fortune Minerals announces positive updated Micon Feasibility Study & updated reserves for the NICO project. [ONLINE] Available at: <http://www.fortuneminerals.com/news/press-releases/press-release-details/2014/Fortune-Minerals-announces-positive-updated-Micon-Feasibility-Study--updated-reserves-for-the-NICO-project/default.aspx>. [Accessed 27 August 15].*

Fullagar, P. K., Pears, A., and McMonnies, B. 2008. *Constrained Inversion of geologic surfaces – pushing the boundaries. The Leading Edge, Vol 27 pp. 98-105*

Gallegos, T. J., and Varela, B. A. 2014. *Trends in Hydraulic Fracturing Distributions and Treatment Fluids, Additives, Proppants, and Water Volumes Applied to Wells Drilled in the United States from 1947 through 2010—Data Analysis and Comparison to the Literature. USGS Scientific Investigations Report 2014–5131*.

Gauthier, L., Hall, G., Stein, H., and Schaltegger, U. 2001. The Osborne deposit, Cloncurry district: A 1595 Ma Cu-Au skarn deposit: James Cook University, Economic Geology Research Unit Contribution 59, p. 58–59.

Gazley, M., and Collins, K. 2016. Multivariate analyses of geochemical data from Cloncurry deposits. Integrated Petrophysical and Geochemical analyses. *CSIRO Mineral Resources Report EPXXXXXX*.

GBS Gold International Inc. 2008. *GBS Gold's Cosmo Deeps Project Feasibility Study and Mineral Reserve Estimate. [ONLINE] Available at: <http://www.reuters.com/article/2008/03/27/idUS109254+27-Mar-2008+MW20080327>. [Accessed 27 August 15].*

Geological Survey of Queensland. 2011. *North-West Queensland Mineral and Energy Province Report. Queensland Department of Employment, Economic Development and Innovation, Brisbane*

Gibson, G. M. 2016. Geodynamic evolution of the Mount Isa

region and its bearing on mineralisation: clues from basin architecture and deep seismic reflection profiling. GSQ Workshop Presentation.

Gibson, G. M., Meixner, A. J., Withnall, I. W., Korsch, R. J., Hutton, L. J., Jones, L. E. A., Holzschuch, R. D., Henson, P. A., and Saygin, E. 2015. Basin architecture and evolution in the Mount Isa mineral province, northern Australia: Constraints from deep seismic reflection profiling and implications for ore genesis. *Ore Geology Reviews* v76, pp 414-441

[Glencore. 2015. Glencore Resources & Reserves at 31 Dec 2014. \[ONLINE\] Available at: \[http://www.glencore.com/assets/investors/doc/reports\\\_and\\\_results/2014/GLEN-2014-Resources-Reserves-Report.pdf\]\(http://www.glencore.com/assets/investors/doc/reports\_and\_results/2014/GLEN-2014-Resources-Reserves-Report.pdf\).](http://www.glencore.com/assets/investors/doc/reports_and_results/2014/GLEN-2014-Resources-Reserves-Report.pdf)

Golder Associates. 2012. *Pre-feasibility Block Cave Mine Design - Iron Cap Deposit. Consultants report to Seabridge Gold Inc.*

Gow, P. A., Wall, V. J., Oliver, N. H. S., and Valenta, R. K. 1994. Proterozoic iron oxide (Cu-U-Au-REE) deposits: Further evidence of hydrothermal origins: *Geology*, v. 22, p. 633–636.

Groves, D. I., and Vielreicher, N. M. 2001. The Phalaborwa (Palabora) carbonatite-hosted magnetite-copper sulfide deposit, South Africa: An endmember of the iron oxide-copper-gold-rare earth element deposit group?: *Mineralium Deposita*, v. 36, p. 189–194.

Guidelines for the Technical Economic Evaluation of Mineral Industry Projects. 2012. Published with The AusIMM's Mine Managers Handbook (Monograph 26)

Gunter, J. 2015. Mt Elliott-SWAN 3D Modelling and Target Generation: *unpublished Virga Report to Chinova Resources*

Guyana Goldfields Inc. 2013. *Aurora Gold Project - Key Findings Technical Presentation. TSX Release*.

Harmer, R. E. 2000. Mineralisation of the Phalaborwa Complex and the Carbonatite Connection in Iron Oxide-Cu-Au-U-REE Deposits; in Porter, T.M. (Ed.), *Hydrothermal Iron Oxide Copper-Gold and Related Deposits: A Global Perspective, Volume 1; PGC Publishing, Adelaide, pp. 331-340*.

Hawkes, N., Clark, A. H., and Moody, T. C. 2002. Marcona and Pampa de Pongo: Giant Mesozoic Fe-(Cu, Au) Deposits in the Peruvian Coastal Belt; in Porter, T.M. (Ed.), *Hydrothermal Iron Oxide Copper-Gold & Related Deposits: A Global Perspective, Volume 2; PGC Publishing, Adelaide, pp 115-130*.

Haynes, D. W. 2000. Iron Oxide Copper (-Gold) Deposits: Their Position in the Ore Deposit Spectrum and Modes of Origin; in Porter, T.M. (Ed.), *Hydrothermal Iron Oxide Copper-Gold and Related Deposits: A Global Perspective, Volume 1; PGC Publishing, Adelaide, pp 71-90*.

Haynes, D. W., Cross, K. C., Bills, R. T., and Reed, M. H. 1995.

Olympic Dam ore genesis: A fluid mixing model: *Economic Geology*, v. 90, p. 281–307.

Hayward, N., and Skirrow, R. G. 2010. Geodynamic Setting and Controls on Iron Oxide Cu-Au (±U) Ore in the Gawler Craton, South Australia; in Porter, T.M., (ed.), *Hydrothermal Iron Oxide Copper-Gold and Related Deposits: A Global Perspective, v. 3 - Advances in the Understanding of IOCG Deposits; PGC Publishing, Adelaide, pp. 119-146*.

Heron Resources Limited. 2015. *Preliminary Economic Assessment Delivers Strong Business Case for the Woodlawn Zinc-Copper Project. ASX/TSX release*.

Hinman, M. C. 2012. Merlin-Mt Dore Structure: *unpublished ppt Report to Ivanhoe Australia, Mar 2012*

Hinman, M. C. 2012. Regional mineralisation controls at Starra: *unpublished ppt Report to Ivanhoe Australia, Mar 2012*

Hinman, M. C. 2012. Structure, mineralisation controls, shoots & targeting at Kulthor: *unpublished ppt Report to Ivanhoe Australia, Aug 2012*

Hinman, M. C. 2013. 3D Mine structure, ore geometry & targeting in- & near-mine at Kulthor: *unpublished ppt Report to Ivanhoe Australia, May 2013*

Hinman, M. C. 2013. MIF convergence, near-mine targeting, late deformation at Kulthor: *unpublished ppt Report to Ivanhoe Australia, May 2013*

Hinman, M. C. 2015. *Kulthor-Osborne Regional Interpretation-2: Analysis & Targeting: unpublished ppt Report to Chinova, March 2015*

Hinman, M. C. 2016. New Insights into the Architectural Development of the southern Cloncurry IOCG Terrain-Controls and Timing of Mineralisation, DMQ Presentation to QEC 'Exploring Outside the Box' seminar, Brisbane.

[HiSeis. 2016. <http://www.hiseis.com.au/>](http://www.hiseis.com.au/)

Hitzman, M. W., and Valenta, R. K. 2005. Uranium in iron oxide-copper-gold (IOCG) systems; *Economic Geology*, v. 100, pp. 1657-1661.

Hitzman, M. W. 2000. Iron Oxide-Cu-Au Deposits: What, Where, When and Why; in Porter, T.M. (Ed.), *Hydrothermal Iron Oxide Copper-Gold and Related Deposits: A Global Perspective, Volume 1; PGC Publishing, Adelaide, pp 9-25*.

Hitzman, M. W., Oreskes, N., and Einaudi, M. T. 1992. Geological characteristics and tectonic setting of Proterozoic iron oxide (Cu-U-Au-REE) deposits: *Precambrian Research*, v. 58, p. 241–287.

Huhn, S. R. B., Soares, A. D. V., Souza, C. I. J., Albuquerque, M. A. C., Leal, E. D., Vieira, E. A. P., Masotti, F. S., and Brustolin, V.

2000. The Cristalino copper–gold deposit, Serra dos Carajás, Pará. IUGS, Intern Geol Congr, 31
- Huston, D. 2016. Metallogenesis of the Mount Isa Province – links to basin and tectonic evolution. *Mount Isa Stratigraphy, Geodynamics, and Mineral Systems Symposium. Brisbane, February 2016.*
- Hutton, L. J. 2015. The Mount Isa Inlier - An Introduction to its Geodynamic Setting, Stratigraphic Succession and Mineral Systems focussing on the Western Fold Belt, QEC Seminar, Brisbane
- Idnurm, M. 2000. Towards a high resolution Late Palaeoproterozoic–earliest Mesoproterozoic apparent polar wander path for northern Australia, *Australian Journal of Earth Science*, v47, pp405–429
- Jakubec, J., and Esterhuizen, G. S. 2007. Use of the Mining Rock Mass Rating (MRMR) classification: Industry Experience Proceedings of the International Workshop on Rock Mass Classification in Underground Mining, pp73–79, (Department of Health and Human Services, Centers for Disease Control and Prevention, National Institute for Occupational Safety and Health, Pittsburgh Research Laboratory, Pittsburgh, PA)
- [Jeffrey, R. G. 2011. Hydraulic fracturing in mining. \[ONLINE\] Available at: http://www.csiropedia.csiro.au/display/CSIROPedia/Hydraulic+fracturing+in+mining. \[Accessed 26 August 15\].](http://www.csiropedia.csiro.au/display/CSIROPedia/Hydraulic+fracturing+in+mining)
- Johnson, D. B. 2015. *Biomining goes underground. Nature Geoscience*, vol 8.
- Jungmann, D. 2013. Osborne Environs Exploration Review, unpublished *Inova Resources Report*
- Kendrick, M. A., Baker, T., Fu, B., Phillips, D., and Williams, P. J. 2008. Noble gas and halogen constraints on regionally extensive mid-crustal Na-Ca metasomatism, the Proterozoic Eastern Mount Isa Block, Australia; *Precambrian Research*, v. 163, pp. 131–150.
- King, S. 2001. Structural Mapping at the Osborne Cu-Au mine, Queensland: unpublished *Solid Geology Report to Osborne Mines Pty Ltd*
- Kirwin, D. 2009. Merlin: A new Mo-Re Discovery in the Cloncurry District, SMEDG-SEG unpublished ppt presentation, *Ivanhoe Australia*
- Laing, W. P. 1993. Structural/metamorphic controls on ore deposits in the east Mount Isa Block: the key to tonnes and grade: *AIG Bulletin 14*
- Lancaster, J. A., Fanton, J., Almeida, A. J., Leveille, R. A., and Vieira, S. 2000. Discovery and geology of the Sossego copper–gold deposit, Carajás District, Pará State, Brazil. IUGS, Intern Geol Congr, 31
- Landmark, J. 1992. *Gunpowder Copper Ltd: in-situ leaching at Mammoth mine, NW Queensland. AulMM Bull.* 6: 12–13.
- Laubscher, D. H. 1990. *A geomechanics classification system for the rating of rock mass in mine design. J. S. Afr. Inst. Min. Metall.* 90(10).
- Laubscher, D. H. 2000. *A practical manual on Block caving. Prepared for the International Caving Study (1997–2000).*
- Lawrance, L. 1999. Multi-Element Dispersion in Mesozoic Basement Sediment over the Osborne Deposit, Northern Queensland, Australia: Implications for Regional Geochemical Exploration in Buried Terrain, 73–81. In: Lewis, P. C. 1999. Exploration Under Cover '99. Australian Institute of Geoscientists Bulletin 28, 127pp.
- Lazo, F., and Pal, T. 2009. The Merlin Mo-Re zone, a new discovery in the Cloncurry District, Australia; in *Williams, P.J. et al., (eds.), Smart Science for Exploration and Mining, Proceedings of the 10th Biennial SGA Conference, 17–20 August, 2009, Townsville, Australia, Extended abstracts*, v. 1 pp. 56–58.
- [Lundin Mining Corporation - Reserves & Resources - Fri Aug 28, 2015. 2015. Lundin Mining Corporation - Reserves & Resources - Fri Aug 28, 2015. \[ONLINE\] Available at: http://www.lundinmining.com/s/Reserves.asp.](http://www.lundinmining.com/s/Reserves.asp)
- [M3 Consultants. 2012. Escobal Guatemala Project, NI 43-101 Preliminary Economic Assessment, Prepared for Tahoe Resources Inc.](http://www.m3consultants.com.au)
- M3 Consultants. 2013. *Florence Copper Project, NI 43-101 Technical Report Pre-Feasibility Study. Prepared for HDI Curis.*
- M3 Consultants. 2014. *Gunnison Copper Project, NI 43-101 Technical Report Prefeasibility Study. Prepared for Excelsior Mining Corp.*
- MaCready, T. 2006. Structural cross-section based on the Mt Isa deep seismic transect. *Australian Journal of Earth Sciences* v53:1 pp5–26
- Maksaev, V., and Zentilli, M. 2002. Chilean Strata-bound Cu-(Ag) Deposits: An Overview; in *Porter, T.M. (Ed.), Hydrothermal Iron Oxide Copper-Gold & Related Deposits: A Global Perspective, Volume 2; PGC Publishing, Adelaide, pp 185–205.*
- Manca, L., and Flores, G. 2013. *Modern Planning Practices for Cave Mining. Proceedings of 3<sup>rd</sup> International Seminar on Mine Planning, Santiago, Chile (Eds: J Beniscelli, C Bottinelli, J Cardenas, H Constanzo, H Gopfert, and E Henriquez).*
- Mark, G., Oliver, N. H. S., Williams, P. J., Valenta, R. K., and Crookes, R. A. 2000. The Evolution of the Ernest Henry Fe-Oxide-(Cu-Au) Hydrothermal System; in *Porter, T.M. (Ed.), Hydrothermal Iron Oxide Copper-Gold and Related Deposits: A Global Perspective, Volume 1; PGC Publishing, Adelaide, pp 123–136.*
- Marschik, R., and Fontboté, L. 1996. Copper(-iron) mineralization and superposition of alteration events in the Punta del Cobre belt, northern Chile: *Society of Economic Geologists Special Publication 5*, p. 171–189.
- Marschik, R., and Fontboté, L. 2001. The Candelaria-Punta del Cobre iron oxide Cu-Au(-Zn-Ag) deposits, Chile: *Economic Geology*, v. 96, p. 1799–1826.
- Marschik, R., Chiaradia, M., and Fontboté, L. 2003. Implications of Pb isotope signatures on rocks and iron oxide Cu-Au ores in the Candelaria-Punta del Cobre district, Chile: *Mineralium Deposita*, v. 38, p. 900–912.
- Marschik, R., Leveille, R. A., and Martin, W. 2000. La Candelaria and the Punta del Cobre District, Chile: Early Cretaceous Iron-Oxide Cu-Au(-Zn-Ag) Mineralisation; in *Porter, T.M. (Ed.), Hydrothermal Iron Oxide Copper-Gold and Related Deposits: A Global Perspective, Volume 1; PGC Publishing, Adelaide, pp 163–175.*
- Marschik, R., Singer, B. S., Munizaga, F., Tassinari, C., Moritz, R., and Fontboté, L. 1997. Age of Cu(-Fe)-Au mineralization and thermal evolution of the Punta del Cobre district, Chile: *Mineralium Deposita*, v. 32, p. 531–546.
- Marshall, L. 2003. Brecciation within the Mary Kathleen Group of the Eastern Succession, Mt Isa Block, Australia: Implications of district-scale structural and metasomatic processes for Fe-oxide-Cu-Au mineralisation. PhD thesis, James Cook University.
- McLean, G., and Benjamin, P. 1993. The geology and development of the Mount Elliott Copper-Gold Deposit: *SMEDG publication?*
- McLellan, J. G., Mustard, R., Blenkinsop, T., Oliver, N. H. S., and McKeagney, C. 2010. Critical Ingredients of IOCG Mineralisation in the Eastern Fold Belt of the Mount Isa Inlier: Insights from Combining Spatial Analysis with Mechanical Numerical Modelling; in *Porter, T.M., (ed.), Hydrothermal Iron Oxide Copper-Gold & Related Deposits: A Global Perspective, v. 3 - Advances in the Understanding of IOCG Deposits; PGC Publishing, Adelaide,*
- Metanor Resources Inc. 2011. *Bachelor Lake Gold Project's Pre-feasibility Study Confirms profitability with an 85% IRR. [ONLINE] Available at: http://www.metanor.ca/en/index.php/press-releases/article/bachelor-lake-gold-projects-pre-feasibility-study-confirms-profitability. [Accessed 27 August 15].*
- Metminco. 2015. *Presentation - Los Calatos Mining Study.*
- Meyer, C. 1988. Ore deposits as guides to geologic history of the Earth: *Annual Reviews of Earth and Planetary Science*, v. 16, p. 147–171.
- [Mincon Limited. 2013. Technical Report on the Mineral Reserves and Mineral Resources of the Salobo Copper-Gold Mine Carajás, Pará State, Brazil. \[ONLINE\] Available at: http://www.silverwheaton.com/files/doc\\_maps/Salobo%20TR%20final%2019%20Mar%202013.pdf](http://www.silverwheaton.com/files/doc_maps/Salobo%20TR%20final%2019%20Mar%202013.pdf)
- MIRA Geoscience (Authors unknown). 2010. Geophysical modelling and 3D mineral potential mapping for Iron Oxide Copper Gold mineralisation over the Mount Dore region, Queensland. *GSQ Research Report.*
- Mira Geoscience. 2010. Geophysical Modelling and 3D Mineral Potential Modelling for Iron Oxide Copper Gold mineralisation over Mount Dore Region, Queensland. *GSQ Report*
- Monteiro, L. V. S., Xavier, R. P., Carvalho, E. R., Hitzman, M. W., Johnson, C. A., Souza, Filho C. R., and Torresi, I. 2008. Spatial and temporal zoning of hydrothermal alteration and mineralization in the Sossego iron oxide–copper–gold deposit, Carajás Mineral Province, Brazil: parageneses and stable isotope constraints. *Mineralium Deposita*, v. 43, pp. 129–159
- Montreuil, J. F., Corriveau, L., and Grunsky, E. C. 2013. Compositional data analysis of hydrothermal alteration in IOCG systems, Great Bear magmatic zone, Canada: to each alteration type its own geochemical signature. *Geochemistry: Exploration, Environment, Analysis*, 13, pp. 229–247.
- Mudd, G. M. 2007. An analysis of historic production trends in Australian base metal mining: *Ore Geology Reviews*, v.32, pp. 227–261
- Murphy, T., Hinman, M., Pirlo, M., Donohue, J., and Jones, M. 2015. Deep Mining Queensland: Prospectivity for underground, mass-mineable IOCG deposits in the Cloncurry district, Queensland. *First Technical Report. August 2015. Confidential to GSQ & DMQ Sponsors.*
- Murphy, T., Hinman, M., Pirlo, M., Donohue, J., Jones, M. and Pratt, A. 2016. Deep Mining Queensland: Prospectivity for underground, mass-mineable IOCG deposits in the Cloncurry district, Queensland. *Second Technical Report. February 2016. Confidential to GSQ & DMQ Sponsors.*
- Murphy, T., Hinman, M., Pirlo, M., Donohue, J., Jones, M., and Pratt, A. 2016. Deep Mining Queensland: Prospectivity for underground, mass-mineable IOCG deposits in the Cloncurry district, Queensland. *Third Technical Report. August 2016. Confidential to GSQ & DMQ Sponsors.*
- Newcrest Mining Limited. 2007. *2007 Mineral Resource & Ore Reserve Explanatory Notes. ASX Release.*
- Newcrest Mining Limited. 2012. *Golpu Pre-Feasibility Study and Reserve Announcement. ASX Release.*
- O’Dea, M. G., Betts, P. G., MacCready, T., and Ailleres, L. 2006.

- Sequential development of a mid-crustal fold-thrust complex: evidence from the Mitakoodi Culmination in the eastern Mt Isa Inlier, Australia: *Australian Journal of Earth Sciences*, v53, pp69-90.
- O’Gorman, G., von Michaelis, H., and Olson, G. J. 2004. *Novel In-Situ Metal and Mineral Extraction Technology. Report to US Govt prepared by Little Bear Laboratories Inc.*
- Oliver, N. H. S., Mark, G., Pollard, P. J., Rubenach, M. J., Bastrakov, E., Williams, P. J., Marshall, L. C., Baker, T., and Nemchin, A. A. 2004. The role of sodic alteration in the genesis of iron oxide-copper-gold deposits: Geochemistry and geochemical modeling of fluid-rock interaction in the Cloncurry district, Australia: *Economic Geology*, v. 99, p. 1145–1176.
- Oreskes, N., and Einaudi, M. T. 1990. Origin of rare earth element-enriched hematite breccias at the Olympic Dam Cu-U-Au-Ag deposit, Roxby Downs, South Australia: *Economic Geology*, v. 85, p. 1–28.
- [OZ Minerals Annual Report. 2015. Annual Reports . \[ONLINE\] Available at: http://www.ozminerals.com/news/reports/annual-reports.html.](http://www.ozminerals.com/news/reports/annual-reports.html)
- OZ Minerals. 2014. *Ore Reserve for Carrapateena underpins low operating cost, long life operation. ASX Announcement.*
- [OZ Minerals. 2015. Carrapateena Pre-Feasibility Study. \[ONLINE\] Available at: http://www.ozminerals.com/Media/docs/ASX-20140818-Carrapateena-Pre-Feasibility-Study-Presentation-37d37987-a586-4e3a-8e3f-9d6e11f652c9-0.pdf.](http://www.ozminerals.com/Media/docs/ASX-20140818-Carrapateena-Pre-Feasibility-Study-Presentation-37d37987-a586-4e3a-8e3f-9d6e11f652c9-0.pdf)
- [OZ Minerals. 2015. OZ Minerals website, \[ONLINE\] Available at: http://www.ozminerals.com/.](http://www.ozminerals.com/)
- PanAmerican Silver Corp. 2014. *Technical Report for the Dolores Property, Chihuahua, Mexico - Preliminary Economic Assessment of a Pulp Agglomeration Treatment and Underground Option.*
- Parsons, A., and Withnall, I. 2008. The tectono-stratigraphic framework of the Cloncurry-Selwyn Zone: working towards a resolution, Queensland Department of Employment, Economic Development and Innovation presentation, Brisbane
- [Parsons, P. 2011. Premier Mine, South Africa. \[ONLINE\] Available at: https://en.wikipedia.org/wiki/Premier\\_Mine#/media/File:South\\_Africa-Cullinan\\_Premier\\_Mine02.jpg. \[Accessed 24 August 15\].](https://en.wikipedia.org/wiki/Premier_Mine#/media/File:South_Africa-Cullinan_Premier_Mine02.jpg)
- Perkins, C., and Wyborn, L. A. I. 1998. Age of Cu-Au mineralization, Cloncurry district, Mount Isa inlier, as determined by <sup>40</sup>Ar/<sup>39</sup>Ar dating: *Australian Journal of Earth Sciences*, v. 45, p. 233–246
- Perring, C. S., Pollard, P. J., Dong, G., Nunn, A. J., and Blake, K. L. 2000. The Lightning Creek sill complex, Cloncurry district, north-west Queensland: a source of fluids for Fe-oxide-Cu-Au mineralization and sodic-calcic alteration; *Economic Geology*, v. 95, pp. 1067-1069.
- Pilkington, M. 2007. Locating geologic contacts with magnitude transforms of magnetic data. *Journal of Applied Geophysics*, Vol. 63, pp. 80 - 89.
- pmd\*CRG. 2008. Mineral System Analysis of the Mt Isa-McArthur Region, northern Australia. Project 17 Final Report, April 2005-July 2008
- Pollard, P. J. 2000. Evidence of a Magmatic Fluid and Metal Source for Fe-Oxide Cu-Au Mineralisation; in Porter, T.M. (Ed.), *Hydrothermal Iron Oxide Copper-Gold and Related Deposits: A Global Perspective, Volume 1; PGC Publishing, Adelaide*, pp 27-41.
- Pollard, P. J. 2006. An intrusion-related origin for Cu-Au mineralization in iron oxide-copper-gold (IOCG) provinces; *Mineralium Deposita*, v. 41, pp. 179-187.
- Porter, T. M. 2010. Current Understanding of Iron Oxide Associated-Alkali Altered Mineralised Systems: Part I, An Overview; in Porter, T.M., (ed.), *Hydrothermal Iron Oxide Copper-Gold and Related Deposits: A Global Perspective*, v. 3 - *Advances in the Understanding of IOCG Deposits*; PGC Publishing, Adelaide, pp. 5 -32.
- Porter, T. M. 2010. The Carrapateena Iron Oxide Copper Gold Deposit, Gawler Craton, South Australia: a Review; in Porter, T.M., (ed.), *Hydrothermal Iron Oxide Copper-Gold and Related Deposits: A Global Perspective*, v. 3 - *Advances in the Understanding of IOCG Deposits*; PGC Publishing, Adelaide, pp. 191-200.
- Pratt, A. G. L., and Ellen, P. J. 2005. Selection of an Ore Haulage System for Telfer Deeps, The AusIMM Hoist and Haul 2005 Conference Proceedings, pp 131-140, (the Australasian Institute of Mining and Metallurgy)
- Puko, T. 2013. *Starra Review, unpublished Inova Resources Report*
- Queensland Department of Mines & Energy, Taylor Wall & Assoc., SRK Consulting, ESRI Australia. 2000. *North-West Queensland Mineral Province Report.*
- [Queensland Mineral Resources Act 1989, Mineral Resources Regulation 2013, https://www.legislation.qld.gov.au/LEGISLTN/CURRENT/M/MineralReR13.pdf, pp 88-90 \[access 21 February 2016\]](https://www.legislation.qld.gov.au/LEGISLTN/CURRENT/M/MineralReR13.pdf)
- Ramírez, L. E., Palacios, C., Townley, B., Parada, M. A., Sial, A. N., Fernandez-Turiel, J. L., Gimeno, D., Garcia-Valles, M., and Lehmann, B. 2006. The Mantos Blancos copper deposit: an upper Jurassic breccia-style hydrothermal system in the Coastal Range of Northern Chile: *Mineralium Deposita*, v.41, pp 246-258
- Rashidi-Nejad, F., Suorineni, F. T., and Asi, B. 2014. *Open pit or block caving? A numerical ranking method for selection. The Southern African Institute of Mining and Metallurgy, 2014 SOMP Annual Meeting*
- Rawlings, D. E., and Johnson, B. D. (eds). 2007. *Biomining. Springer (ISBN 10 3-540-34909-X)*
- Reeve, J. S., Cross, K. C., Smith, R. N., and Oreskes, N. 1990. Olympic Dam copper-uranium-gold-silver deposit, in Hughes, F. E., ed., *Geology of the mineral deposits of Australia and Papua New Guinea: Melbourne, Australasian Institute of Mining and Metallurgy*, p. 1009–1035.
- Resolute Mining Limited. 2015. *Revised PFS Delivers Major Boost for Underground Development at Syama. ASX Announcement.*
- [Resolution Copper Mining. 2015. Underground Mining. \[ONLINE\] Available at: http://resolutioncopper.com/the-project/underground-mining/. \[Accessed 26 August 15\].](http://resolutioncopper.com/the-project/underground-mining/)
- [Rex Minerals. 2015. Hillside Project – Mineral Resource and Ore Reserve Update. \[ONLINE\] Available at: http://www.rexminerals.com.au/-/rex/Lib/Docs/20150525\\_Mineral%20Resources%20and%20Ore%20Reserves\\_Hillside\\_Statement%20and%20Table%201.pdf.](http://www.rexminerals.com.au/-/rex/Lib/Docs/20150525_Mineral%20Resources%20and%20Ore%20Reserves_Hillside_Statement%20and%20Table%201.pdf)
- Rieger, A. A., Marschik, R., and Díaz, M. 2010. The Mantoverde District, Northern Chile: an Example of Distal Portions of Zoned IOCG Systems; in Porter, T.M., (ed.), *Hydrothermal Iron Oxide Copper-Gold and Related Deposits: A Global Perspective*, v. 3 - *Advances in the Understanding of IOCG Deposits*; PGC Publishing, Adelaide, pp. 273-284.
- Rieger, A. A., Marschik, R., Díaz, M., Hölzl, S., Chiaradia, M., Akker, B., and Spangenberg, J. E. 2010. The Hypogene Iron Oxide Copper-Gold Mineralization in the Mantoverde District, Northern Chile: *Economic Geology*, v.105, pp. 1271-1299
- Rigon, J. C., Munaro, P., Santos, L. A., Nascimento, J. A. S., and Barreira, C. F. 2000. Alvo 118 copper– gold deposit—geology and mineralization, Serra dos Carajás, Pará, Brazil. 31 Intern Geol Congr
- Robertson, I. D. M., and Shu, L. 2002. Surficial geology around the Eloise Cu-Au mine and dispersion into Mesozoic cover from the Eloise mineralisation, N.E. Queensland. *CRC LEME Open File Report 135.*
- Robertson, I. D. M., and Shu, L. 2003. Eloise Cu-Au Deposit, Cloncurry District, Queensland. In: Butt, C. R. M., Cornelius, M., Scott, K. M. & Robertson, I. D. M. *Regolith Expressions of Australian Ore Systems. A compilation of geochemical case histories and conceptual models. CRC LEME (http://www.crclme.org.au/Pubs/Monographs/RegExpOre.html)*
- Robertson, I. D. M., Shu, L., and Wildman, J. E. 2002. Geochemical dispersion around the Maronan Cu-Au prospect, N.E. Queensland. *CRC LEME Open File Report 134.*
- Ronzê, P. C., Soares, A. D. V., Santos, M. G. S., and Barreira, C. F. 2000. Alemão Copper-Gold (U-REE) Deposit, Carajas, Brazil; in Porter, T.M. (Ed.), *Hydrothermal Iron Oxide Copper-Gold and Related Deposits: A Global Perspective, Volume 1; PGC Publishing, Adelaide*, pp 191-202.
- Rotherham, J. F., Blake, K. L., Cartwright, I., and Williams, P. J. 1998. Stable isotope evidence for the origin of the Starra Au-Cu deposit, Cloncurry district: *Economic Geology*, v. 93, p. 1435–1449.
- RPA Inc. 2015. *NI 43-101 Report - Technical Report on the Cerro Bayo Project, Region XI (Aisen), Chile. Prepared for Mandalay Resources Corporation.*
- Rubenach, M., Adshead, N., Oliver, N., Tullemans, F., Esser, D., and Stein, H. 2001. The Osborne Cu-Au Deposit: Geochronology and Genesis of Mineralisation in relation to Host Albitites and Ironstones: *A Hydrothermal Odessey, EGRU Publication, James Cook University*
- Rubenach, M. J., Foster, D. R. W., Evins, P. M., Blake, C. M., and Fanning, C. M. 2008. Age constraints on the tectonothermal evolution of the Selwyn Zone, Eastern Fold Belt, Mount Isa Inlier, Precambrian Research, v163, pp81-107
- Rusk, B. G., Oliver, N. H. S., Cleverley, J. S., Blenkinsop, T. G., Zhang, D., Williams, P. J., and Habermann, P. 2010. Physical and Chemical Characteristics of the Ernest Henry Iron Oxide Copper Gold Deposit, Australia; Implications for IOCG Genesis; in Porter, T.M., (ed.), *Hydrothermal Iron Oxide Copper-Gold and Related Deposits: A Global Perspective*, v. 3 - *Advances in the Understanding of IOCG Deposits*; PGC Publishing, Adelaide, pp. 201-218.
- Rutherford, N. F., Lawrance, L. M. and Sparks, G., 2005. Osborne Cu-Au Deposit, Cloncurry, North West Queensland. In: Butt, C. R. M., Cornelius, M., Scott, K. M. & Robertson, I. D. M. *Regolith Expressions of Australian Ore Systems. A compilation of geochemical case histories and conceptual models. CRC LEME (http://www.crclme.org.au/Pubs/Monographs/RegExpOre.html)*
- Schodde, R. 2014. Challenges and opportunities for under-cover exploration in Australia. *UNCOVER Summit 2014, 31st March, 2014, Adelaide.*
- [Schodde, R. C. 2014. MinEx Consulting - The Global Shift to Undercover Exploration – “How fast? How effective?”. \[ONLINE\]](http://www.minexconsulting.com.au/undercover-exploration-how-fast-how-effective/)

- Available at: <http://www.minexconsulting.com/publications/sep2014b.html>. [Accessed 28 August 15].
- Schodde, R.C. 2015. MinEx Consulting - "A review of Australia's discovery performance over the last 40 years", [ONLINE] Available at: <http://www.minexconsulting.com/publications/jul2015.html>. [Accessed 28 Aug 15].
- Searl, R. A. 1952. Geology of the Mount Elliott Copper Mine, Selwyn, Queensland: *BMR Record 1952/27*
- Selwyn Resources Ltd. 2012. *Selwyn Updates Revised Mine Development Plan for the Selwyn Project - News Release*.
- Sillitoe, R. H. 2003. IOCG deposits: An Andean view: *Mineralium Deposita*, v. 38, p.787–812.
- Singer, D. A., Berger, V. I., and Moring, B. C. 2015. *Porphyry Copper Deposits of the World: Database, Map, and Grade and Tonnage Models*. [ONLINE] Available at: <http://pubs.usgs.gov/of/2005/1060/>
- Skirrow, R. G., and Walshe, J. L. 2002. Reduced and oxidised Au-Cu-Bi deposits of the Tennant Creek inlier, Australia: An integrated geologic and chemical model: *ECONOMIC GEOLOGY*, v. 97, p. 1167–1202.
- Sleigh, D. W. 2001. *Selwyn Mines : Digesting Data To Put On Weight*. 2015. *Selwyn Mines : Digesting Data To Put On Weight*. [ONLINE] Available at: <http://www.smedg.org.au/shadsleighab.htm>.
- Smith, P. 2012. *Cadia Valley. Newcrest Mining Limited Presentation*. ASX Release.
- Souza, L. H., and Vieira, E. A. P. 2000. Salobo 3 Alpha Deposit: Geology and Mineralisation; in Porter, T.M. (ed.), *Hydrothermal Iron-Oxide Copper-Gold and Related Deposits: A Global Perspective*, PGC Publishing, Adelaide, v. 1, pp. 213-224.
- SRK Consulting. 2014. *Technical Report for the Compañía Minera Candelaria and Compañía Minera Ojos del Salado Copper Projects, Atacama Province, Region III, Chile*. SRK Report for LundinMining, [ONLINE] Available at: [http://www.lundinmining.com/i/pdf/2014-10-06\\_NI43-101\\_CandelariaOjosDelSalado.pdf](http://www.lundinmining.com/i/pdf/2014-10-06_NI43-101_CandelariaOjosDelSalado.pdf).
- Stewart, A. J. 1987. Fault reactivation and superimposed folding in a Proterozoic sandstone-volcanic sequence, Davenport Province, central Australia, *Journal of Structural Geology*, v9-4, pp441-455
- Tallarico F. H. B., Figueiredo, B. R., Groves, D. I., Kositcin, N., McNaughton, N. J., Fletcher, I. R., and Rego, J. L. 2005. Geology and SHRIMP—Pb geochronology of the Igarapé Bahia Deposit, Carajás Copper–Gold Belt, Brazil: an Archean (2.57 Ga) example of iron–oxide Cu–Au–(U–REE) mineralization. *Econ Geol* 100:7–28
- Torresi, I., Xavier, R. P., Bortholoto, D. F., and Monteiro, L. V. 2012. Hydrothermal alteration, fluid inclusions and stable isotope systematics of the Alvo 118 iron oxide–copper–gold deposit, Carajás Mineral Province (Brazil): Implications for ore genesis. *Mineralium Deposita*, v. 47(3), pp. 299-323.
- Twining, M., and Burgess, J. 2013. *Hillside, South Australia: Rex Minerals presentation AUSIMM Meeting*. [ONLINE] Available at: [https://www.ausimm.com.au/Content/docs/branch/2013/adelaide\\_2013\\_04\\_presentation.pdf](https://www.ausimm.com.au/Content/docs/branch/2013/adelaide_2013_04_presentation.pdf)
- TWP Sudamerica S.A. 2013. *NI 43-101 Technical Report - Pulacayo Project Feasibility Study. Prepared for Apogee Silver Ltd*.
- Ullrich, T. D., and Clark, A. H. 1997. Paragenetic sequence of mineralization in the main orebody, Candelaria copper-gold deposit, Chile: Phoenix, Arizona, Phelps Dodge Exploration Corporation, *unpublished internal report 3*, 36 p.
- Vale Annual Report. 2014. [ONLINE] Available at: [http://www.vale.com/EN/investors/Quarterly-results-reports/20F/20FDocs/Vale%2020-F%202014\\_i\\_novo.pdf](http://www.vale.com/EN/investors/Quarterly-results-reports/20F/20FDocs/Vale%2020-F%202014_i_novo.pdf).
- van As, A. 2003. *Subsidence definitions for block caving mines. Technical Report, Rio Tinto Technical Services*, 59 pp.
- Vielreicher, N. M., Groves, D. I., and Vielreicher, R. M. 2000. The Phalaborwa (Palabora) Deposit and its Potential Connection to Iron-Oxide Copper-Gold Deposits of Olympic Dam Type; in Porter, T.M. (Ed.), *Hydrothermal Iron Oxide Copper-Gold and Related Deposits: A Global Perspective, Volume 1; PGC Publishing, Adelaide*, pp 321-329.
- VMS Ventures Inc. 2012. *Reed Copper Project Positive Pre-Feasibility Study Completed*. [ONLINE] Available at: <http://www.vmsventures.com/news/news-details/2012/VMS-Ventures-Inc-Reed-Copper-Project-Positive-Pre-Feasibility-Study-Completed/default.aspx>. [Accessed 27 August 15].
- Wang, S., and Williams, P. J. 1996. The alteration and mineralization styles of a skarn hosted Mount Elliott deposit and adjacent SWAN prospect, Cloncurry district: *MIC'96: New Developments in Metallogenic Research, The McArthur-Mt Isa-Cloncurry Mineral Province*
- Webster, T., Murphy, T., Puscasu, R., and Muhlhaus, H. 2015. Geology and Mass Mining (GMM) Project – Final Report. *Report to sponsors of the SMI-BRC GMM project*.
- Wildman, J. E. 2002. The geochemical discrimination of mineralised and barren ironstones from the Selwyn Au-Cu deposit, N.W. Queensland. *CRC LEME Open File Rep*
- Williams, P. J. 1994. Iron mobility during syn-metamorphic alteration in the Selwyn Range area, NW Queensland: Implications for the origin of ironstone-hosted Au-Cu deposits: *Mineralium Deposita*, v. 29, p. 250–260.
- Williams, P. J., Adshead, N. D., Blake, K. L., de, J. G., Mark, G., and Rotherham, J. F. 1995. Magnetite-Cu-Au deposits in deeply eroded magmatic arcs; lessons from Proterozoic terrains: Australasian Institute of Mining and Metallurgy, 1995 PACRIM Congress Exploring the Rim, Parkville, Victoria, Australia, 1995, Proceedings, p. 631–636.
- Williams, P. J., Barton, M. D., Johnson, D. A., Fontboté, L., de Haller, A., Mark, G., Oliver, N. H. S., and Marschik, R. 2005. Iron Oxide–copper–gold deposits: geology, space–time distribution, and possible modes of origin. *Economic Geology. 100th Anniversary Volume*, 371–405.
- Williams, P. J., Dong, G., Ryan, C. G., Pollard, P. J., Rotherham, J. F., Mernagh, T. P., and Chapman, L. H. 2001. Geochemistry of hypersaline fluid inclusions from the Starra (Fe oxide) Au-Cu deposit, Cloncurry district, Queensland: *Economic Geology*, v. 96, p. 875–884.
- Williams, P. J., Kendrick, M. A., and Xavier, R. P. 2010. Sources of Ore Fluid Components in IOCG Deposits; in Porter, T.M., (ed.), *Hydrothermal Iron Oxide Copper-Gold and Related Deposits: A Global Perspective, v. 3 - Advances in the Understanding of IOCG Deposits; PGC Publishing, Adelaide*, pp.
- Withnall, I. 2007. Progress towards resolving the Corella-Staveland-Doherty conundrum, GSQ Queensland the Smart State presentation
- Withnall, I., Parsons, A., and Carson, C. 2007. Eastern Succession-Stratigraphy and New Dating, Queensland Mines & Energy Presentation
- Woo, K., Eberhardt, E., and van As, A. 2009. *Characterization and empirical analysis of block caving induced surface subsidence and macro deformations. Proceedings of the 3rd CANUS Rock Mechanics Symposium, Toronto (Ed: M.Diederichs and G. Grasselli)*.
- Wood, D., Chitombo, G. P., and Bryan, S. 2011. *Mass Underground Mining and the Role of the Exploration Geologist. SEG Newsletter Number 83*.
- Xavier, R. P., Monteiro, L. V. S., Souza Filho, C. R., Torresi, I., Carvalho, E. R., Dreher, A. M., Wiedenbeck, M., Trumbull, R. B., Pestilho, A. L. S., and Moreto, C. P. N. 2010. The Iron Oxide Copper-Gold Deposits of the Carajás Mineral Province, Brazil: an Updated and Critical Review; in Porter, T.M., (ed.), *Hydrothermal Iron Oxide Copper-Gold and Related Deposits: A Global Perspective, v. 3 - Advances in the Understanding of IOCG Deposits; PGC Publishing, Adelaide*, pp. 285-306.
- Xavier, R. P., Wiedenbeck, M., Trumbull, R. B., Dreher, A. M., Monteiro, L. V. S., Rhede, D., de Araújo, C. E. G., and Torresi, I. 2008. Tourmaline B-isotopes fingerprint marine evaporites as the source of high-salinity ore fluids in iron oxide copper-gold deposits, Carajás Mineral Province (Brazil); *Geology*, v. 36, pp 743-746.